

University of Southampton Research Repository ePrints Soton

Copyright © and Moral Rights for this thesis are retained by the author and/or other copyright owners. A copy can be downloaded for personal non-commercial research or study, without prior permission or charge. This thesis cannot be reproduced or quoted extensively from without first obtaining permission in writing from the copyright holder/s. The content must not be changed in any way or sold commercially in any format or medium without the formal permission of the copyright holders.

When referring to this work, full bibliographic details including the author, title, awarding institution and date of the thesis must be given e.g.

AUTHOR (year of submission) "Full thesis title", University of Southampton, name of the University School or Department, PhD Thesis, pagination

UNIVERSITY OF SOUTHAMPTON

**FACULTY OF ENGINEERING, SCIENCE AND
MATHEMATICS**

SCHOOL OF ELECTRONICS AND COMPUTER SCIENCE

**DESIGN AND DEVELOPMENT OF A SITE
SPECIFIC PROTEIN PATTERNING TECHNIQUE
FOR USE IN A MICROFLUIDIC ANTIBODY
SEPARATION DEVICE**

by Christopher W.A. Johnson

A thesis submitted for the degree of Doctor of Philosophy

April 2010

UNVIERSITY OF SOUTHAMPTON

ABSTRACT

FACULTY OF ENGINEERING, SCIENCE AND MATHEMATICS

SCHOOL OF ELECTRONICS AND COMPUTER SCIENCE

Doctor of Philosophy

DESIGN AND DEVELOPMENT OF A SITE SPECIFIC PROTEIN PATTERNING
TECHNIQUE FOR USE IN A MICROFLUIDIC ANTIBODY SEPARATION
DEVICE

by Christopher Johnson

The rapid quantification of the concentration of different immunoglobulins classes from patient serum is required to diagnose patients in the early stages of sepsis. Microfluidic point of care technology can improve diagnostics by decreasing the analysis time, and integrating parallel analysis in a single portable device. The design of a novel method to fabricate surfaces presenting multiple micron scale protein motifs, for integration within a microfluidic channel device, is described in this thesis.

Initial research focussed on conjugating protein motifs on silicon <100> substrates in micron and submicron scale patterns. A method involving the UV-initiated conjugation of a heterobifunctional linker, undecylenic acid *N*-Hydroxysuccinimide ester (UANHS), to a hydrogen terminated silicon surface was investigated. A photolithographic mask and phase mask were used to form micron and submicron UANHS motifs respectively, on silicon. The conjugation of protein with UANHS motifs was investigated to determine how reproducible the patterns were. The conjugation of streptavidin, streptavidin-FITC, NeutrAvidin, single domain protein L and multidomain protein L to silicon surfaces, upon reaction with UANHS, were investigated. Fluorescently labelled probes that associated with the protein motifs were used to confirm successful conjugation of protein to the silicon. Micron scale motifs of streptavidin, streptavidin-FITC, NeutrAvidin and single domain protein L could be formed reproducibly on silicon. Using a phase mask 140 nm motifs of streptavidin-FITC, conjugated to silicon, were achieved.

Also an alternative method to pattern multiple proteins onto glass surfaces was investigated. A 500,000 MW dextran was modified to incorporate an aryl azide moiety, which was subsequently immobilised on glass surfaces. A method to synthesise and characterise the aryl azide conjugated dextran was investigated, as well as methods to characterise and improve the reproducibility of the aryl azide conjugated dextran layer immobilised on the glass surface. Two photolithographic masks and glass surfaces with alignment marks were fabricated. The masks were used to form micron scale protein motifs, via a photoinitiated conjugation reaction, on the aryl azide conjugated dextran surface. An in-house alignment system was built and a method to produce adjacent protein motifs was investigated. Two adjacent micron scale patterns of multidomain protein L and protein A were achieved. The surface density of conjugated protein L was investigated and a density of $\sim 1.16 \times 10^{11}$ molecules/cm² was confirmed. This approach offers a method to attach high density micron scale protein motifs, aligned with micron scale resolution, which is vital to the realisation of a microfluidic point of care device.

Contents

Abstract	i
Contents	ii
List of Figures	vii
List of Tables	xviii
Declaration of Authorship	xx
Acknowledgments	xxi
List of Abbreviations and Symbols	xxii
1 Introduction	1
1.1 Background and Motivations	1
1.2 Aims and Scope of Work	6
1.3 Summary of Main Achievements	6
1.4 Organisation of Thesis	7
2 Biomolecule Patterning for Microfluidic Applications	9
2.1 Introduction	9
2.2 Association of Immunoglobulins with Antibody Binding Proteins	10
2.2.1 Immunoglobulin Structure	11
2.2.2 Protein A	13
2.2.2.1 The Fc Binding Interaction with Protein A	13
2.2.2.2 The Fab Binding Interaction with Protein A	14
2.2.3 Protein G	15
2.2.3.1 The Fc Binding Interaction with Protein G	16
2.2.3.2 The Fab Binding Interaction with Protein G	16
2.2.4 Protein L	17
2.2.4.1 The Fab Binding Interaction with Protein L	18
2.2.4.2 The Site 1 Fab Binding Site of Protein L	19
2.2.4.3 The Site 2 Fab Binding Site of Protein L	20

2.2.4.4	Evaluation of the Binding Properties of Wild Type and Mutant Protein L by Stopped Flow Analysis -----	20
2.3	Current Methods Applied to Conjugate Biomolecules onto Surfaces -----	22
2.3.1	Biomaterials Suitable for Protein Patterning -----	23
2.3.1.1	Methods to Modify Silicon Surfaces -----	23
2.3.1.2	Methods to Modify Silicon Oxide Surfaces -----	27
2.3.1.3	Methods to Modify Polymer Surfaces -----	28
2.3.1.4	Evaluation of Substrates for Application to Protein Patterning -----	29
2.3.2	Prevention of Non Specific Protein Adsorption -----	30
2.3.3	Immobilising Proteins on Surfaces -----	34
2.3.3.1	Physical Adsorption as a Method to Conjugate Proteins to Surfaces -----	34
2.3.3.2	Covalent Attachment as a Method to Conjugate Proteins to Surfaces -----	35
2.3.3.3	Affinity Immobilisation as a Method to Conjugate Proteins to Surfaces -----	40
2.3.3.4	Evaluation of Methods to Conjugate Proteins -----	42
2.4	Microfabrication for Protein Patterning Applications -----	42
2.4.1	Contact Lithography -----	43
2.4.1.1	Micro Contact Printing for Patterning Surfaces -----	43
2.4.1.2	Microfluidic Channel Patterned Surfaces -----	46
2.4.1.3	Stencil Lithography Patterned Surfaces -----	47
2.4.1.4	Nanoparticle Lithography Patterned Surfaces -----	49
2.4.1.5	Dip Pen Nanolithography Patterned Surfaces -----	50
2.4.2	Non Contact Lithography -----	51
2.4.2.1	Using Photoresists for Biomolecule Patterning -----	52
2.4.2.2	Patterning of Surfaces Conjugated with Photoactive Caged Groups -----	53
2.4.2.3	Photodegradation of Surfaces to Generate Biomolecule Patterns -----	54
2.4.2.4	Photoinitiated Conjugation of Biomolecule Patterns -----	55
2.4.2.5	Electron-Beam Lithography Patterned Surfaces -----	57
2.4.2.6	Printing Patterned Surfaces -----	57
2.4.3	Protein Patterning Rationale -----	58
2.5	Summary -----	59
3	Materials and Methods -----	61
3.1	Conjugation of Proteins on Silicon Surfaces -----	61

3.1.1	Synthesis of the Bifunctional Linker Undecylenic Acid <i>N</i> -Hydroxysuccinimide Ester	61
3.1.2	Photolithographic Mask Fabrication	62
3.1.3	Photopatterning of NHS-ester Terminated Alkene on Silicon Surfaces	64
3.1.4	SEM of Photopatterned Alkene Surfaces	65
3.1.5	X-ray Photoelectron Spectroscopy of Photopatterned Alkene and Protein Conjugated Surfaces	65
3.1.6	Conjugation of Protein to Photopatterned Alkene Surfaces	66
3.1.7	Submicron Photopatterning of Alkene on Silicon and Subsequent Protein Conjugation	67
3.2	Conjugation of Proteins on Glass Surfaces	68
3.2.1	Surface Cleaning and Silanisation of Glass Surfaces	68
3.2.2	Conjugation of Dextran to an Epoxy Functionalised Glass Surface	69
3.2.3	Water Contact Angle Measurements	70
3.2.4	Protein Conjugation to Carboxymethyl Dextran Surfaces	71
3.2.5	Aryl Azide Conjugated Dextran Synthesis	72
3.2.6	Attenuated Total Reflectance Fourier Transform Infrared Spectroscopy	74
3.2.7	Elemental Analysis	74
3.2.8	UV-Vis Spectrophotometry	75
3.2.9	Conjugation of Aryl Azide Conjugated Dextran to Silanised Glass Surfaces	75
3.2.10	X-ray Photoelectron Spectroscopy of Aryl Azide Conjugated Dextran Surfaces	76
3.2.11	Mask Fabrication for Multiple Alignment Patterning	76
3.2.12	Single Protein Patterning on Aryl Azide Conjugated Dextran Surfaces	78
3.2.13	Purification and Characterisation of IgG Fragments Prior to Conjugation with a Fluorescent Probe	78
3.2.14	Multiple Protein Patterning on Aryl Azide Conjugated Dextran Surfaces	80
3.2.15	Protein Surface Concentration Analysis	83
4	Bioconjugation of Micron and Submicron Protein Motifs on Silicon Surfaces	85
4.1	Introduction	85
4.2	The Fabrication of Photolithographic Masks for Silicon Patterning	86
4.3	Photopatterning of Alkene Patterns on Silicon	87
4.3.1	Synthesis of Undecylenic Acid <i>N</i> -Hydroxysuccinimide ester	87
4.3.2	Scanning Electron Microscopy of Photopatterned Silicon	87
4.3.3	X-ray Photoelectron Spectroscopy of Photopatterned Silicon	88
4.4	Immobilisation of Proteins on Alkene Patterned Silicon	92
4.4.1	Conjugation of Streptavidin	92
4.4.2	Conjugation of Single Domain Protein L	94
4.4.3	Conjugation of Multidomain Protein L	97

4.4.4	Conjugation of NeutrAvidin -----	98
4.4.5	Conjugation of Biotinylated Protein A-----	100
4.5	Submicron Patterning of Protein -----	101
4.6	Summary-----	102
5	Bioconjugation of Multiple Micron Sized Protein Patterns on Glass Surfaces	104
5.1	Introduction -----	104
5.2	Protein Patterning on Glass Surfaces -----	105
5.2.1	Evaluation of Methods used to Silanise Glass -----	105
5.2.2	Conjugating Protein to Dextran Surfaces -----	106
5.3	Optimisation of Conditions to Immobilise Dextran on Glass-----	108
5.3.1	Water Contact Angle Measurements of Glass Surfaces Immobilised with Dextran -----	111
5.4	Synthesis and Characterisation of an Aryl Azide Conjugated Dextran ----	112
5.4.1	Characterisation of the Reactants and Product of Aryl Azide Conjugated Dextran Synthesis by Attenuated Total Reflection Fourier Transform Infrared Spectroscopy-----	112
5.4.2	Characterisation of Aryl Azide Conjugated Dextran by Elemental Analysis-----	116
5.4.3	Characterisation of the Reactants and Product of Aryl Azide Conjugated Dextran Synthesis by Absorption Spectroscopy-----	118
5.5	Characterisation of Aryl Azide Conjugated Dextran Immobilised on Glass	119
5.5.1	Water Contact Angle Measurements -----	119
5.5.2	X-Ray Photoelectron Spectroscopy-----	120
5.6	Masks and Alignment Mark Fabrication for Aligned Protein Patterning -	124
5.6.1	Alignment Features-----	124
5.6.2	Photolithographic Mask 1 -----	125
5.6.3	Photolithographic Mask 2 -----	128
5.7	Protein Attachment to Dextran Surfaces-----	130
5.7.1	Conjugation of Protein Carboxymethyl Dextran surfaces -----	130
5.8	Patterning Proteins on Aryl Azide Conjugated Dextran Surfaces -----	131
5.8.1	Photochemical Coupling of Single Proteins -----	134
5.8.2	Motifs Produced by Aligning Multiple Proteins on Glass Surfaces	137
5.9	Study of Protein L Surface Density Conjugated to Glass Surfaces -----	141
5.10	Summary-----	143
6	Conclusions and Suggestions for Future Work	146
6.1	Thesis Summary and Conclusion -----	146
6.2	Future Work -----	150
6.2.1	Microfluidic device fabrication -----	151
	Appendix A Protein L Sequence Alignment	153

Appendix B Protein L Mutants	154
Appendix C Photolithographic Mask Layouts	160
C.1 Photolithographic Mask 1-----	160
C.2 Photolithographic Mask 2-----	161
Appendix D X-Ray Photoelectron Spectra	162
D.1 X-Ray Photoelectron Spectra of Modified Silicon Surfaces-----	162
D.1.1 Undecylenic Acid N-hydroxysuccinimide ester Modified Silicon --	162
D.1.2 NeutrAvidin Modified Silicon -----	167
D.2 X-Ray Photoelectron Spectra of Modified Glass Surfaces -----	172
D.2.1 3-Glycidoxypropyltrimethoxysilane Modified Glass -----	172
D.2.2 Aryl Azide Conjugated Dextran Modified Glass -----	177
D.2.3 NeutrAvidin Modified Glass-----	182
References	187

List of Figures

- Figure 1-1 Immunologic progression in sepsis over time. Both pro- and anti-inflammatory responses are activated early in sepsis; the pro-inflammatory response predominates. As sepsis progresses the anti-inflammatory response becomes predominant, leading to the suppression of the immune response. In the early stage of sepsis deaths are due to cytokine storm-mediated events produced as part of the pro-inflammatory response. Later deaths are caused by the suppression of the immune system, during the anti-inflammatory response, causing a failure to control pathogenic infection (Reprinted with permission from [12]). 2
- Figure 1-2 Cross section of a proposed microfluidic affinity chromatography device. The channel surface is patterned with a bifunctional linker and conjugated with proteins to the surface. As the two analytes are transported by convection and diffusion they associate with surface immobilised protein. When the analytes are eluted depends on the size of the device, the size of the protein motif and the association constant of the interaction. 5
- Figure 2-1 Ig variation – (a) Immunoglobulin components can be isolated as fragments, each of which have specific properties. Transgenic organisms have been developed specifically to produce defined regions of the Ig molecule. Possible fragments include F(ab')₂, Fab, ScFv, and diabodies. (b) Igs are Y-shaped heteromeric protein complexes composed of two light chains (MW = 25 kilodaltons (kDa)) and two heavy chains (MW = 55 kDa). Light chains form disulfide bridges with the N-terminus of the heavy chains to form two arms (the Fab portion), which contain the antigen-binding sites. The Fc domain has the capacity to interact with molecules such as complement or Fc receptors. Mammals have five different Ig classes (IgA, IgD, IgE, IgG and IgM), the class being dependent on the heavy chain type. Reprinted with permission from [67, 68]. 12
- Figure 2-2 Structural representation of the complex between domain D of protein A and Fab'2A2 from human IgM. (a) Ribbon diagram of the V_H region of Fab showing the residues of interest that interact with domain D. (b) Structure diagram detailing the residues of domain D and Fab 2A2 involved in the interaction. Kabat numbering is used for the V_H residues (blue); domain D is numbered (in brown). Contact residues are identified if 20 Å² or more of their surface are buried in the interface and if they make at least one van der Waals contact. Figures were reprinted with permission from [87]. 15
- Figure 2-3 Dual interface – This figure shows a ribbon diagrammatic representation of the two binding sites of PpL₃₃₁₆ with the V_L domain. (Reprinted with permission from [110]). 18
- Figure 2-4 Kinetic model – This model shows the kinetics which govern κ-chain binding to PpL₃₃₁₆, complex formation is dependent on the K_d of each of the sites. Image reproduced with permission from [114]. 22
- Figure 2-5 Modification of a) silicon <100> and b) silicon <111> by radical initiated alkene hydrosilylation. 24

- Figure 2-6 Chemical structure of silicon taken at (a) $\langle 100 \rangle$ plain and (b) $\langle 111 \rangle$ plain (adapted from [136]) (c) after the covalent attachment of biomolecules (R) on silicon $\langle 100 \rangle$ with an undecene (left) and decene (right) bifunctional linker. 25
- Figure 2-7 Structure representation of silanisation depicting condensation reactions between (a) surface hydroxyls prior to reaction between surface bound silanol's and (b) free silanol's prior to reaction with surface bound hydroxyl groups. 27
- Figure 2-8 UV radical initiated graft polymerisation reaction scheme on a PDMS surface a) Formation of radicals on PDMS by UV light b) Initial step of radical initiated polymerisation (adapted from [163]) 29
- Figure 2-9 Polyelectrolyte brush coating exhibiting neutral collapsed (a) and ionised expanded state (b) (Reprinted with permission from [168]) 31
- Figure 2-10 Illustration of protein adsorption at surfaces carrying PEG brushes, which may occur via three modes: (a) Primary adsorption involving an attractive contact with the surface. Here, this case is illustrated for a partially inserted protein shaped as a triangular wedge as suggested by recent models of BSA. (b) Secondary adsorption at the outer edge of the brush due to van der Waals attraction to the surface. (c) Ternary adsorption of protein within the brush itself as a result of weak PEG-protein attraction. This is illustrated for a small globular protein of spherical shape. (Reprinted with permission from [180]) 33
- Figure 2-11 Chemical structure of the repeating polymeric units of a) PEG and b) Dextran..... 33
- Figure 2-12 Chemical illustration of the amide bond formed by the reaction between an NHS-ester and an amino group. 35
- Figure 2-13 Structural illustration of the Schiff base formed by the reaction between an aldehyde and amine moiety. 36
- Figure 2-14 Structural illustration of the thioether bond formed by the chemical reaction between a maleimide group and thiol chemistry..... 37
- Figure 2-15 Structural illustration of the thioether bond formed by the chemical reaction between an active halogen and a thiol group. 37
- Figure 2-16 Chemical structure diagram showing the potential reaction mechanisms exhibited by phenylnitrene photochemistry (Reprinted with permission from [210])...... 38
- Figure 2-17 Strategy for the biotinylation of protein using the intein-fusion system for immobilisation of protein on to avidin derivatised glass slides (Reprinted with permission from [222]). 41
- Figure 2-18 Diagram illustrating the fabrication of a PDMS stamp (Reprinted with permission from [235]). 44
- Figure 2-19 Diagram illustrating different microcontact printing failure events. (a) PDMS stamp with features of height h , width w , and gap distance d . (b) Lateral collapse occurs when adjacent structures make contact and remain adherent. (c) Collapse happens when the features buckle under the weight of the stamp. (d) Sagging occurs when the roof of the stamp collapses against the substrate (Reprinted with permission from [235]). 45
- Figure 2-20 Liquid flows between the filling pad and flow-promoting pad by capillary action filling the channels and introducing biomolecules to the channel surface (Reprinted with permission from [242]). 46
- Figure 2-21 Fabrication and selective patterning process using a patterned ParyleneTM sheet and a microfluidic system. (a) ParyleneTM is patterned by oxygen plasma using an

- aluminium layer as a mask. (b) Microchannel patterns are transferred from the SU-8 mold to PDMS. (c) The PDMS sheet with microchannels is aligned and placed on the patterned Parylene™ layer for the protein patterning. After the solution is introduced and the PDMS/Parylene™ sheet removed, the samples are selectively patterned on the planar glass surface (Reprinted with permission from [250]). 48
- Figure 2-22 Scheme of the process for the creation of the nanotemplate: (a) nanosphere monolayer of polystyrene, is deposited on a silicon substrate; (b) plasma etching of the polystyrene beads, reduction of the size; (c) plasma enhanced chemical vapour deposition of a SiO_x layer; and (d) mechanical removal of the beads (Reprinted with permission from [255]). 50
- Figure 2-23 Writing mechanism of the Nano Fountain Pen. Molecular ink fed from the reservoir forms a liquid–air interface at the annular aperture of the volcano tip. Molecules are transferred by diffusion from the interface to a substrate and a water meniscus is formed by capillary condensation (Reprinted with permission from [233]). . 50
- Figure 2-24 Illustration of relief structures formed after the patterning and development of a positive or negative photoresist. 52
- Figure 2-25 His-tagged YFP bound to photodegraded NTA-functionalised PEO-terminated films: (a) confocal microscopy image of a micrometre scale pattern of YFP formed by exposure through a mask; (b) tapping mode AFM image of the same pattern, reprinted with permission from [265]. 55
- Figure 2-26 Images reproduced from [276] illustrating the conjugation of photobiotin micropatterns on a silanised glass surfaces..... 56
- Figure 2-27 Illustration of the covalent patterning of proximal biomolecules upon BP modified surfaces by illumination with 365 nm light (Reprinted with permission from [278])...... 57
- Figure 2-28 Diagram illustrating the type of apparatus used for laser printing protein microarrays. A fluid jetting mechanism enables the efficient transfer of high-resolution droplets of protein solution to microarray substrates (Reprinted with permission from [284])...... 58
- Figure 3-1 Chemical structure of the EDC/NHS coupling reaction showing the reactants (A-Undecylenic Acid, B-EDC, and C-N-Hydroxysuccinimide), the unstable O-acylisourea intermediate (D) and the amine reactive product UANHS (E) and the urea by-product (F)..... 62
- Figure 3-2 Screenshot of an L-edit software design used for mask plate manufacture. The features in pink represent transparent regions on the mask plate and consist of 10 μm wide lines with a periodicity of 40 μm. 63
- Figure 3-3 Equipment setup used for the UV illumination of silicon samples to conjugate the bifunctional linker UANHS to the H-terminated silicon surface. 65
- Figure 3-4 Illustration of the silanisation reaction between the glass surface and GOPS used to form an epoxide terminated surface. 69
- Figure 3-5 Illustration of the oxirane ring opening reaction between the epoxide terminated glass surface and dextran (500,000 MW). 70
- Figure 3-6 Chemical structure of surface modifications depict (a) dextran immobilised on the silanised surface, (b) the introduction of a carboxyl group by the reaction of the dextran surface with bromoacetic acid. The chemical process illustrated in (d) is the EDC mediated coupling of NHS to the carboxyl terminated dextran resulting in the formation of an NHS-ester terminated dextran shown in (c). 72

- Figure 3-7 Chemical structure diagrams of the two reactants used to synthesise an aryl azide conjugated dextran, (a) dextran and (b) 4-azidobenzoic acid. The chemical groups highlighted react to form an ester bond, as illustrated in Figure 3-8..... 73
- Figure 3-8 Illustration of the Steglich esterification reaction used to form an ester bond between the carboxylic acid moiety of R (4-azidobenzoic acid) and the hydroxyl group of R₁ (dextran). The DCC is a coupling agent and DMAP is a catalyst. 73
- Figure 3-9 Images of alignment setup containing a) XY translation stages and 360° sample rotation stage (Newport), and b) chrome/gold mask XY and Z translation stages (Newport) and a tilt control (Thorlabs). 80
- Figure 3-10 Image of complete alignment setup with alignment mark and mask image capture system (Gene Snap software), CCD camera (LW135M, Framos), lens (Comar, UK), 5x objective (Carl Zeiss, UK), dichroic mirror (Comar, UK), and white light source (Thorlabs, UK) shown over the sample holder/mask platform system used for surface alignment. 81
- Figure 3-11 Image of the illumination setup. The 500W Hg(Xe) UV lamp (Oriel-Newport, UK) has a digital shutter (Oriel-Newport, UK), which when opened illuminates the 45° mirror (Comar, UK), which reflects light through the 280 nm longpass filter (Comar, UK) onto the aligned mask/sample below..... 82
- Figure 4-1 Transmission image of 10 μm features of the Chrome/Gold Photolithography mask captured at (a) EC Plan-Neofluar 10x objective and (b) a LD A-Plan 63x objective. 86
- Figure 4-2 NMR spectra assignment of undecylenic acid *N*-hydrosuccinimide (UANHS) 87
- Figure 4-3 SEM image of UANHS derivatised surfaces with 10 μm features. Captured at (a) 350x magnification and (b) 800x magnification. 88
- Figure 4-4 Illustration of the two surface modifications involved in conjugating protein with silicon including: (a) Conjugation of UANHS with silicon and (b) Immobilisation of NeutrAvidin on the UANHS conjugated surface..... 89
- Figure 4-5 Peak fitting of data from XPS experiments (see §3.1.5) carried out on UANHS conjugated surfaces showing a) peaks assigned to carbon bonds and b) peaks assigned to nitrogen bonding..... 90
- Figure 4-6 Peak fitting of data from XPS experiments (see §3.1.5) of NeutrAvidin conjugated silicon surfaces showing a) peaks assigned to carbon bonds and b) peaks assigned to nitrogen bonding. 91
- Figure 4-7 Chemical structures of the surface modifications used to produce the images in Figure 4-8 (see overleaf) including: (a) Conjugation of UANHS to silicon and (b) Conjugation of streptavidin-FITC. 92
- Figure 4-8 Epifluorescence images of streptavidin-FITC (10 μM) captured using (a) an LD A-Plan 20x objective, 5 second image capture and (b) an EC Plan-Neofluar 10x objective , 3 second image capture..... 93
- Figure 4-9 Chemical structures of the surface modifications used to produce the images in Figure 4-10 (see overleaf) including: (a) Conjugation of UANHS to silicon, (b) Immobilisation of streptavidin and (c) Incubation of the streptavidin immobilised surface with biotin-FITC..... 93
- Figure 4-10 Epifluorescence image of biotin-FITC (1 μM) bound to streptavidin (10 μM) derivatised surfaces captured with (a) an EC Plan-Neofluar 10x objective, 3 second image capture and (b) an LD A-Plan 20x objective, 5 image capture. 94

Figure 4-11 Chemical structures of the surface modifications used to reveal the immobilisation of PpL ₃₃₁₆ on silicon, including: (a) Conjugation of UANHS to silicon, (b) Immobilisation of PpL ₃₃₁₆ and (c) Incubation of the PpL ₃₃₁₆ immobilised surface with IgG-FITC.	95
Figure 4-12 Epifluorescence image of IgG-FITC (500 nM) bound to PpL ₃₃₁₆ (10 µM) derivatised surfaces incubated after (a) no BSE pre-wash and (b) a 1 % BSA pre-wash. Both images were captured using an EC Plan-Neofluar 10x objective with a 4 second image capture.	95
Figure 4-13 Images of IgG-FITC (500 nM) bound to PpL ₃₃₁₆ (10 µM) derivatised surfaces that have been (a) over and (b) under exposed. Images were captured with an EC Plan-Neofluar 10x objective, 5 second image capture.	97
Figure 4-14 Images of IgG-FITC (500 nM) bound to PpL ₃₃₁₆ (10 µM) derivatised surfaces captured with an EC Plan-Neofluar 10x objective, 5 second image capture.	97
Figure 4-15 Images of IgG-FITC (500 nM) bound to protein L (10 µM) derivatised surfaces captured with an EC Plan-Neofluar 10x objective with a 1 second image capture.	98
Figure 4-16 Chemical structures of the surface modifications used to produce the images in Figure 4-15 including: (a) Conjugation of UANHS to silicon, (b) Immobilisation of multidomain protein L and (c) Incubation of the protein L immobilised surface with IgG-FITC.	98
Figure 4-17 Chemical structures of the surface modifications used to produce the images in Figure 4-18 including: (a) Conjugation of UANHS to silicon, (b) Immobilisation of NeutrAvidin and (c) Incubation of the NeutrAvidin immobilised surface with biotin-FITC.	99
Figure 4-18 Epifluorescence images of biotin-FITC (1 µM) bound to a NeutrAvidin (10 µM) conjugated surface captured at LD A-Plan 20x objective with (a) a 5 second image capture and (b) a 4 second image capture.	99
Figure 4-19 Epifluorescence images of IgG-FITC (500 nM) bound to a protein-A biotin (1 µM) , which is associated to a NeutrAvidin (10 µM) immobilised surface taken using a) an EC Plan-Neofluar 10x objective, 3 second image capture and b) an LD A-Plan 20x objective, 5 second image capture.	100
Figure 4-20 Chemical structures of the surface modifications used to produce the images in Figure 4-19 including: (a) Conjugation of UANHS to silicon, (b) Immobilisation of NeutrAvidin, (c) Incubation of the NeutrAvidin surface with biotin-protein A and (d) Incubation of the protein A terminated surface with IgG-FITC.	100
Figure 4-21 The phase mask uses a +1/-1 order principle, where light is diffracted equally into the plus first and minus first orders. Self-interference between these two orders creates an interference pattern with half the pitch of the Phase mask pitch (Reprinted with permission from Ibsen Photonics).	101
Figure 4-22 SEM image of UANHS derivatised surfaces with 140 nm features (magnification x15,000)	102
Figure 4-23 Epifluorescence image of streptavidin-FITC (1 µM) conjugated surfaces. Imaged using a Plan-Apochromat 100x oil immersion objective, 11.2 millisecond image capture.	102
Figure 5-1 Illustration of a gold surface modified with CMD, Reprinted with permission from [323].	107

- Figure 5-2 Illustration of the process envisaged to conjugate protein motifs on glass surfaces. Bare glass (a) is silanised with GOPS (b), which when incubated with AACD conjugates the dextran photolinker with the surface (c). Upon illumination with UV light a photoinitiated reaction forms a covalent attachment with protein in solution (d). Using a photolithographic mask the site of illumination can be controlled to produce protein motifs (e)..... 108
- Figure 5-3 Graph showing the average greyscale of surfaces incubated with different concentrations of dextran-FITC, captured by epifluorescence microscopy (Axio Observer, Carl Zeiss, UK). Each image was taken using an EC Plan-Neofluar 10x objective and captured with an exposure time of 2 seconds. The average grey scales of 3 images were taken and the standard deviation between the averages calculated. 111
- Figure 5-4 ChemDraw image of the glucose units that make up dextran, and the bonds present in the polymeric structure. 113
- Figure 5-5 FTIR spectrum showing the main IR absorption peaks of dextran (500 kDa). The prominent bands are the O-H stretch at 3200 cm^{-1} and the valent C-O and C-C vibrations at 1149 and 998 cm^{-1} 113
- Figure 5-6 ChemDraw image of 4-azidobenzoic acid, showing the carboxylic acid and azide moieties attached to a benzyl ring. 114
- Figure 5-7 FTIR spectrum showing the main IR absorption peaks of 4-azidobenzoic acid). The peak of interest is the azide peak at 2102 cm^{-1} 115
- Figure 5-8 ChemDraw image of the aryl azide conjugated dextran showing the modification of the glucose units to conjugate the aryl azide moiety. 115
- Figure 5-9 FTIR spectrum showing the main IR absorption peaks of aryl azide conjugated dextran. The O-H stretch at 3200 cm^{-1} and the valent C-O and C-C vibrations at 1149 and 998 cm^{-1} from the dextran and the N=N and ester group are introduced at 2127 cm^{-1} and 1714 cm^{-1} respectively from the conjugated aryl azide. 116
- Figure 5-10 UV absorption spectra of dextran and AACD solution in water and 4-azidobenzoic acid solution in methanol (a.u. denotes arbitrary units). 119
- Figure 5-11 Illustration of the three surface modifications involved in conjugating protein with glass surfaces including: (a) Silanisation with GOPS, (b) Immobilisation of AACD, and (c) Photoinitiated conjugation of NeutrAvidin. 121
- Figure 5-12 Peak fitting of data from XPS experiments (see §3.2.10) of NeutrAvidin conjugated silicon surfaces showing peaks assigned to carbon bonds. 121
- Figure 5-13 Peak fitting of data from XPS experiments (see §3.2.10) of GOPS modified glass surfaces showing a) peaks assigned to carbon bonds and b) peaks assigned to nitrogen bonding. 122
- Figure 5-14 Peak fitting of data from XPS experiments (see §3.2.10) of NeutrAvidin conjugated glass surfaces showing a) peaks assigned to carbon bonds and b) peaks assigned to nitrogen bonding. 123
- Figure 5-15 Alignment features formed using a design created using L-edit ((a) and (d)), where purple is representative of chrome and white of transparent UV fused silica. The bright field images, captured using an EC Plan-Neofluar 10x objective, in (b) and (c) are surfaces patterned using the feature design in (a) using S1813. While (e) and (f) are patterned using the feature design in (d) using SU8-10. The two photoresists form an inverse pattern compared with one another, due to the different properties of the resists and were processed using the protocol described in §3.2.11. 125

- Figure 5-16 Images of the Mask 1 design produced in L-edit. The left image shows the orientation of the mask for the first protein illumination. The mask is then rotated 90°anti-clockwise, to the orientation shown in the right image, for the second illumination..... 126
- Figure 5-17 Mask features formed using a design created in L-edit ((a) and (d)), where purple is representative of chrome and white of transparent UV fused silica. The bright field images, captured using an EC Plan-Neofluar 10x objective, in (b) and (e), are features patterned in S1813. The transmission images taken with the same 10x objective, in (c) and (f) are the features transferred into chrome/gold after etching. Images b,c,e and f were taken during the process described in §3.2.11..... 127
- Figure 5-18 Bright field images, taken using an EC Plan-Neofluar 10x objective, of S1813 photoresist patterned on chrome/gold surfaces developed for (a) 60 s, (b) 75 s and (c) 90 s. 127
- Figure 5-19 Design of mask and alignment features produced using L-edit. The features are representative of (a) the surface alignment features and (b) the mask alignment features. The features in (b) and (c) are square windows ranging in size from 4-100 µm. 128
- Figure 5-20 Design of mask and alignment features designed using L-edit. The features enhance the horizontal (a) and vertical (b) alignment tolerance of the mask. The squares without numbers in are parallel to one-another. The squares with numbers have a deviation from a central square of ±10 µm. 129
- Figure 5-21 Design of vertical alignment tolerance features that, in these features, are - 9.5 and 10 µm below the plain of the ideal alignment pattern (zero). 130
- Figure 5-22 Bright field images of S1813 patterned chrome/gold surfaces (a and b) and features etched into the chrome/gold layer (c and d). The images were taken during the fabrication process described in §3.2.11..... 130
- Figure 5-23 Epifluorescence images of IgG-FITC (500 nM) associated on a protein L (10 µM)-dextran surface. Image (a) shows IgG-FITC is restricted to the spot of protein L on the surface. Image (b) shows protein L is restricted to the area where the EDC/NHS solution was incubated. Both images show immobilisation and excellent contrast between the protein and dextran surface (EC Plan-Neofluar 10x objective, 2 second image capture). 131
- Figure 5-24 Power output spectra from the 500W Hg(Xe) UV lamp system supplier (Oriel, Newport). 132
- Figure 5-25 Absorption spectra of UV fused silica used in the fabrication of the photolithographic mask and three filters that absorb different wavelengths of UV light. The absorption spectra were taken using the protocol described in §3.2.8. 133
- Figure 5-26 Absorption spectra of aryl azide conjugated dextran (AACD), protein L (28 µM), UV fused silica and a 280 nm longpass filter measured between 250-400 nm. The absorption spectra were taken using the protocol described in §3.2.8. 133
- Figure 5-27 Graph of average fluorescence intensity of features patterned using the methods described in §3.2.12 against changes to the protein concentration used in the patterning process. All the images analysed were captured with an EC Plan-Neofluar 10x objective with a 2 second image capture time. 134
- Figure 5-28 Graph of average fluorescence intensity of streptavidin/biotin-FITC motifs patterned using the methods described in §3.2.12 against changes to the illumination time of the patterning process. All the images used to determine the intensity were captured with an EC Plan-Neofluar 10x objective with a 2 second image capture time. 135

- Figure 5-29 Images (a) and (b) show line profiles taken from an image of the mask (a) and the subsequent protein pattern produced using the mask (b). The graph (c) shows the combined line profiles from the two images. The full width half maximum of each feature was compared to determine the resolution of the patterns. Images (a) and (b) were taken using an EC Plan-Neofluar 10x objective using bright field and 3 second image capture respectively. 136
- Figure 5-30 Illustration showing (a) Overlapping image of the surface (cross) and mask (squares) alignment features with a 5 μm gap, which could cause a potential $\pm 10 \mu\text{m}$ translation error. Overlapping features in (b) represents the Mask 2 features designed to counter translation error. The patterns represents a -10 μm error pattern (left), a 0 μm error pattern (centre) and a +10 μm error pattern (right). The green squares represent the first protein illuminated and the white the second protein. 137
- Figure 5-31 Image (a) shows a bright field transmission image of the smallest features found on Mask 2 (4 x 4 μm). The epifluorescence images in (b) and (c) show patterns of IgG-FITC (500 nM) bound to protein L (10 μM) immobilised surfaces captured using (b) an LD Plan-Neofluar 63x objective and (c) an LD A-Plan 20x objective, with (b) a 6 second and (c) a 2 second image capture. The images show features as small as 4 x 4 μm can be successfully transferred onto the surface. 138
- Figure 5-32 Epifluorescence images of IgG-FITC (500 nM) bound to protein A (14 μM) and protein L (10 μM) patches immobilised on aryl azide dextran surfaces. Images (a) and (b) show a column of protein L patches on the left and a column of protein A patches on the right. Concurrently images (c) and (d) show a column of protein A patches on the left and protein L on the right. All images were captured using an EC Plan-Neofluar 10x objective, with a 3 second image capture. 139
- Figure 5-33 Illustration of the protocol used to show the site specific conjugation of proteins that retain specific recognition properties. The first illumination (a) activates the AACD forming the reactive cyclic ketenimine, which reacts with amine groups present on protein L. The second illumination (b) activates the remaining aryl azide groups leading to protein A conjugation. When the protein patterned surface is incubated with rhodamine labelled F(ab')₂ (c) binding should be observed with protein L only. 140
- Figure 5-34 Epifluorescence images of protein modified glass surfaces. Images (a)/(b) and (c)/(d) were taken with Carl Zeiss filter set 15 and 9 respectively. Images (a)/(b) show a tetramethylrhodamine labelled F(ab')₂ (excitation wavelength 552 nm, emission wavelength 578 nm, 2.2 μM) associated with surface conjugated protein. Images (c)/(d) show background fluorescence images taken with filter set 9. The fluorescence images were captured in the same location using the different filter sets where images (a)/(c) and (b)/(d) correspond to each other. In (a) and (b) the protein A patterns show no fluorescence, but the protein L shows strong fluorescence. Both the protein L and A patches can be visualised when imaging with filter set 9, as observed in (c) and (d). Images (a)/(c) and (b)/(d) were captured with an EC Plan-Neofluar 10x objective and an LD A-Plan 20x objective respectively. Images (a)/(c) and (b)/(d) were captured with a 4 and 2 second image capture respectively. 141
- Figure 5-35 Normalised fluorescent intensity emission spectra of a range of IgG-FITC concentrations, using an excitation wavelength of 494 nm. The characteristic emission of IgG-FITC can be seen at 517 nm. The experimental protocol used to determine the absorption is detailed in §3.2.15. 142
- Figure 5-36 Standard curve of IgG-FITC concentration against total fluorescence intensity using the area under the curve between 510 and 550 nm. The experimental protocol used to determine the absorption is detailed in §3.2.15. 143

- Figure 6-1 Illustration of (a) alignment inaccuracies and (b) a potential mechanism to solve the problem. 151
- Figure 6-2 Top view of an affinity separation device taken at three time intervals. The surface receptors (green) have an affinity for the red molecules and no affinity for the blue molecules. As the molecules flow through the channel the red molecules are separated from the blue molecules as they spend an increased amount of time associating and dissociating with the surface. 152
- Figure A-1 Sequence alignment of single domains from *Peptostreptococcus magnus* strains 312 and 3316. The yellow highlighted residues display sequence variations between strains. Residues emboldened in red are those shown by NMR studies to have major chemical shifts on complex formation [107]. Residues emboldened in blue and pink have been shown by X-ray crystallographic studies [112] to be key residues involved in complex formation at the site 1 and site 2 binding sites respectively. The Arginine (R) of strain 3316, emboldened in purple, is believed to be involved in interactions at both binding sites. The residues highlighted in blue are those implicated by X-ray crystallography to form hydrogen bonds with the antibody V_L domain. The numbering systems used are found in Wikstrom [111], Baker [341], Gore [295], and the protein databank (PDB) files 2PTL and 1HEZ (www.pdb.org). 153
- Figure B-1 Lys residues present in Strain 312 of protein L. Image of protein L created using SwissProt PDB viewer (PDB:2PTL), the red residues indicate Lys residues. These residues display amines which can be used for the covalent immobilization to a surface. 154
- Figure B-2 Binding site residues and Lys present in Strain 312 of protein L. Image of protein L created using SwissProt PDB viewer (PDB:2PTL) The red residues indicate Lys residues not involved in antibody V_L domain binding. Yellow residues are those involved in antibody V_L domain binding. 154
- Figure B-3 Lys residues present in protein L from strain 3316. Image of protein L created using SwissProt PDB viewer (PDB:2PTL), the red residues indicate Lys residues. These residues display amines which can be used for the covalent immobilization to a surface. 157
- Figure B-4 Binding site residues and Lys residues present in protein L strain 3316. The image of protein L was created using SwissProt PDB viewer (PDB:1HEZ) The red residues indicate Lys residues not involved in the antibody V_L domain binding. Yellow residues are those that make up Site 1 of the V_L binding domain. Pink residues are those that make up Site 2 of the V_L binding domain. The purple amino acid is Arg-52, believed to be involved in both site 1 and 2 of the V_L binding domain. 157
- Figure C-1 Layout of mask 1, taken from L-edit, illustrating the features of interest (alignment features and protein patterning mask) designed for preparation of surfaces used in the investigation of surface patterning. 160
- Figure C-2 Layout of mask 2, taken from L-edit, illustrating the features of interest designed for the preparation of surfaces used in the investigation of multiple protein patterning. 161
- Figure D-1 Expanded X-ray photoelectron spectra peaks from likely oxygen moieties on UANHS modified silicon surfaces. Surfaces were prepared and analysed using the methods described in §3.1.5. 162
- Figure D-2 Expanded X-ray photoelectron spectra peaks from likely nitrogen moieties on UANHS modified silicon surfaces. Surfaces were prepared and analysed using the methods described in §3.1.5. 163

Figure D-3 Expanded X-ray photoelectron spectra peaks from likely carbon moieties on UANHS modified silicon surfaces. Surfaces were prepared and analysed using the methods described in §3.1.5.	164
Figure D-4 Expanded X-ray photoelectron spectra peaks from likely silicon moieties on UANHS modified silicon surfaces. Surfaces were prepared and analysed using the methods described in §3.1.5.	165
Figure D-5 Complete X-ray photoelectron spectra peaks from likely chemical moieties on UANHS modified silicon surfaces. Surfaces were prepared and analysed using the methods described in §3.1.5.	166
Figure D-6 Expanded X-ray photoelectron spectra peaks from likely oxygen moieties on NeutrAvidin conjugated silicon surfaces. Surfaces were prepared and analysed using the methods described in §3.1.5.	167
Figure D-7 Expanded X-ray photoelectron spectra peaks from likely nitrogen moieties on NeutrAvidin conjugated silicon surfaces. Surfaces were prepared and analysed using the methods described in §3.1.5.	168
Figure D-8 Expanded X-ray photoelectron spectra peaks from likely carbon moieties on NeutrAvidin conjugated silicon surfaces. Surfaces were prepared and analysed using the methods described in §3.1.5.	169
Figure D-9 Expanded X-ray photoelectron spectra peaks from likely silicon moieties on NeutrAvidin conjugated silicon surfaces. Surfaces were prepared and analysed using the methods described in §3.1.5.	170
Figure D-10 Complete X-ray photoelectron spectra peaks from likely chemical moieties on NeutrAvidin conjugated silicon surfaces. Surfaces were prepared and analysed using the methods described in §3.1.5.	171
Figure D-11 Expanded X-ray photoelectron spectra peaks from likely oxygen moieties on GOPS modified glass surfaces. Surfaces were prepared and analysed using the methods described in §3.2.10.	172
Figure D-12 Expanded X-ray photoelectron spectra peaks from likely nitrogen moieties on GOPS modified glass surfaces. Surfaces were prepared and analysed using the methods described in §3.2.10.	173
Figure D-13 Expanded X-ray photoelectron spectra peaks from likely carbon moieties on GOPS modified glass surfaces. Surfaces were prepared and analysed using the methods described in §3.2.10.	174
Figure D-14 Expanded X-ray photoelectron spectra peaks from likely silicon moieties on GOPS modified glass surfaces. Surfaces were prepared and analysed using the methods described in §3.2.10.	175
Figure D-15 Complete X-ray photoelectron spectra peaks from likely chemical moieties on GOPS modified glass surfaces. Surfaces were prepared and analysed using the methods described in §3.2.10.	176
Figure D-16 Expanded X-ray photoelectron spectra peaks from likely oxygen moieties on aryl azide conjugated dextran modified glass surfaces. Surfaces were prepared and analysed using the methods described in §3.2.10.	177
Figure D-17 Expanded X-ray photoelectron spectra peaks from likely nitrogen moieties on aryl azide conjugated dextran modified glass surfaces. Surfaces were prepared and analysed using the methods described in §3.2.10.	178

Figure D-18 Expanded X-ray photoelectron spectra peaks from likely carbon moieties on aryl azide conjugated dextran modified glass surfaces. Surfaces were prepared and analysed using the methods described in §3.2.10.....	179
Figure D-19 Expanded X-ray photoelectron spectra peaks from likely silicon moieties on aryl azide conjugated dextran modified glass surfaces. Surfaces were prepared and analysed using the methods described in §3.2.10.....	180
Figure D-20 Complete X-ray photoelectron spectra peaks from likely chemical moieties on aryl azide conjugated dextran modified glass surfaces. Surfaces were prepared and analysed using the methods described in §3.2.10.....	181
Figure D-21 Expanded X-ray photoelectron spectra peaks from likely oxygen moieties on NeutrAvidin conjugated glass surfaces. Surfaces were prepared and analysed using the methods described in §3.2.10.	182
Figure D-22 Expanded X-ray photoelectron spectra peaks from likely nitrogen moieties on NeutrAvidin conjugated glass surfaces. Surfaces were prepared and analysed using the methods described in §3.2.10.....	183
Figure D-23 Expanded X-ray photoelectron spectra peaks from likely carbon moieties on NeutrAvidin conjugated glass surfaces. Surfaces were prepared and analysed using the methods described in §3.2.10.	184
Figure D-24 Expanded X-ray photoelectron spectra peaks from likely silicon moieties on NeutrAvidin conjugated glass surfaces. Surfaces were prepared and analysed using the methods described in §3.2.10.	185
Figure D-25 Complete X-ray photoelectron spectra peaks from likely oxygen moieties on NeutrAvidin conjugated glass surfaces. Surfaces were prepared and analysed using the methods described in §3.2.10.	186

List of Tables

Table 2-1 Characteristics of Igs in human serum [66].....	11
Table 2-2 Table listing the amino acid residues from the V _L domain of IgG and the C domain of PpL ₃₃₁₆ that form hydrogen bonds in the site 1 interface, including the distance between interacting residues [110]	20
Table 2-3 Table listing the amino acid residues from the V _L domain of IgG and the C domain of PpL ₃₃₁₆ that form hydrogen bonds and salt bridges in the site 2 interface, including the distance between interacting residues [110]	20
Table 2-4 Table showing reported densities of biomolecules on silicon, glass and gold substrates.....	26
Table 2-5 Table showing the isoelectric point of different amino acids	31
Table 2-6 Functional groups, found in proteins, exploited to conjugate proteins to surfaces.....	34
Table 5-1 Table depicting the fluorescent edge of spots of dextran-FITC (5-20 μM) incubated with silanised glass surfaces. Glass surfaces were prepared with a 1 % GOPS solution incubated with the glass for between 5 minutes and 24 hours. All images were captured using an EC Plan-Neofluar 10x objective with a 2 second image capture (Axio Observer, Carl Zeiss, UK) for comparison.	109
Table 5-2 Table depicting the fluorescent edge of spots of dextran-FITC (5-20 μM) incubated with silanised glass surfaces. Glass surfaces were prepared with a 0.1 % GOPS solution incubated with the glass for between 5 minutes and 24 hours. All images were captured using an EC Plan-Neofluar 10x objective with a 2 second image capture (Axio Observer, Carl Zeiss, UK) for comparison.....	110
Table 5-3 Table of contact angle measurements taken at different stages of surface processing. All images were taken of a 1 μL droplet on the surface, in a humid chamber, using the same contact angle measurement equipment (Krüss DSA100). Drops were fitted using the sessile drop fitting software (Krüss) and an average contact angle was determined from 5 images.....	112
Table 5-4 Table showing the mass contributions of the four elements within the synthesised AACD compound.	117
Table 5-5 Table containing the mass and mol contributions of the 4 elements that make up the aryl azide moiety conjugated to the dextran.	117
Table 5-6 Table containing the remaining mass and mol contributions, after removing contributions from the conjugated aryl azide, which are attributed to the elements found in the dextran.	118
Table 5-7 Mass of AACD compound constituents calculated using elemental analysis data.....	118
Table 5-8 Table of contact angle measurements of an AACD layer immobilised on a glass surface. All images were taken of a 1 μL droplet on the surface, in a humid chamber, using the same contact angle measurer (Krüss DSA100). Drops were fitted using the sessile drop fitting software (Krüss) and an average contact angle was determined from 5 images.....	120

Table B-1 Mutants produced by the Bakers group taken from [341]. The residue assignments are base on PDB file 2PTL and the apparent dissociation rates were measured by surface plasmon resonance.....	155
Table B-2 Mutants produced by the Bakers group taken from [341]. The residue assignments are base on PDB file 2PTL and the apparent dissociation rates were measured by surface plasmon resonance.....	156
Table B-3 Table showing the dissociation constants of IgG with different protein L mutants [113, 114, 343, 344].....	158
Table B-4 Table showing the dissociation constants of IgG with different protein L mutants [113, 114, 343, 344].....	159

Declaration of Authorship

I, Christopher William Andrew Johnson

declare that the thesis entitled

Design and development of a site specific protein patterning technique for use in a microfluidic antibody separation device

and the work presented in it are my own. I confirm that:

- this work was done wholly or mainly while in candidature for a research degree at this University;
- where any part of this thesis has previously been submitted for a degree or any other qualification at this University or any other institution, this has been clearly stated;
- where I have consulted the published work of others, this is always clearly attributed;
- where I have quoted from the work of others, the source is always given. With the exception of such quotations, this thesis is entirely my own work;
- I have acknowledged all main sources of help;
- where the thesis is based on work done by myself jointly with others, I have made clear exactly what was done by others and what I have contributed myself;
- none of this work has been published before submission.

Signed:.....

Date: 04/2010

Acknowledgments

Firstly, I would like to thank my supervisor, Dr. Tracy Melvin, for her continuous support and guidance throughout this work and for her exceptional advice and assistance in completing my thesis. It has been an incredible experience working in a multi-disciplinary environment, and I could not thank her more for providing this opportunity throughout my PhD studies. Thanks must also go to my second supervisor Prof. Mike Gore for helping to guide me during the first two years of the PhD. I am also indebted to Dr. Eleanor Tarbox and Dr. Lucy Braddick for their helpful comments and critical feedback in proof reading some of the chapters of this thesis.

After the fire, I have spent almost 6 months at the University of Cambridge using the facilities at the Institute of Biotechnology. For this, I must thank Prof. Chris Lowe for accommodating me during this difficult period, for his support throughout my work at Cambridge, and not forgetting his hospitality during my stay. My thanks also go to Prof. Roland Zengerle for accommodating me during a 1 month stay at the University of Freiburg, especially for the helpful training I gained in the cleanroom facilities. I really enjoyed and appreciated the friendly environment working in the cleanroom across the campus at Southampton. In addition, my gratitude for the technical support and assistance from Dave Sager, Neil Sessions and Neil Fagan at the ORC Dairybox temporary cleanroom, and Zondy Webber at the Nanomaterials Rapid Prototyping Facility over at Physics.

Special thanks to Dr. Lucy Braddick for the preparation and purification, by HPLC, of F(ab)₂ and Fc fragments. These were prepared by the cleavage of murine IgG with papain. The IgG fragments (both prepared in house and purchased from Pierce) were then labelled with FITC NHS ester, Cy 5.5 NHS ester or tetramethylrhodamine-5-maleimide. The labelled fragments were then incubated with protein A and L patterned surfaces to visualise patterns to enable imaging. For her continual support I am extremely grateful.

Particular thanks go to Dr. Huabing Yin for her help and support during my first year of study and to Dr. Steve Harrison for providing me with single domain protein L. To Dr. Nic Perney for his help in building an optical alignment setup and to Dr. Sakellaris Mailis for his guidance in using the frequency-quadrupled Nd:YAG laser. I would like to thank Dr. David Morgan for carrying out XPS characterisation of surfaces produced in this thesis and to Daniel Friedrich for his discussions on the practical applications and theoretical proof that helped to direct my work. People at the School of Chemistry, in particular Prof. Tom Brown and his team past and present – Principally Dr. Simon Gerrard for his help in the synthesis and characterisation of the UANHS linker presented here and for his discussions on NMR assignment and chemical characterisation. Thanks also to James Richardson for showing me the spectrofluorimeter, Dr. Liz Tull for showing me how to measure water contact angles and to Rachel and Dorcas for helping with the freeze drying of protein samples. I must also thank Dr. Bob Greef and Dr. Owain Clark for their help in using and understanding ellipsometry and to Greg Ayre for his help with using the AFM.

My gratitude to the members in Tracy's group, especially graduates Ben, Andy, Chien and Mukhzeer for their invaluable discussion on topics not limited to the project; the post-docs, Suzanne, Samson, Liqin, Patrick, and Matt for their help and support; and fellow PhD candidates Tim, and Katrin. It has been a pleasant learning experience working with all of you.

Thank you to the Biotechnology and Biological Sciences Research Council for funding my PhD studies, the Nano research group who has supported me all the way through and the ORC who has allowed me to use their facilities and offices after the fire. I would also like to thank the many good friends that I've met here, to name a few, Stuart, Tristan, Gareth, Hamish, Julian, Charlie, Petros, Mehdi, and Badin. Above all, I would like to thank my parents and friends for their understanding, endless encouragement and support when it was most required.

List of Abbreviations and Symbols

Chemicals

AACD	aryl azide conjugated dextran
APTES	(3-aminopropyl)triethoxysilane
BP	benzophenone
CMD	carboxymethyl dextran
DCC	dicyclohexylcarbodiimide
DCM	dichloromethane
DMSO	dimethyl sulfoxide
EDTA	ethylenediaminetetraacetic acid
EDC	1-ethyl-3-(3-dimethylaminopropyl)carbodiimide
HF	hydrofluoric acid
ANB-NOS	<i>N</i> -5-azido-2-nitrobenzoyloxysuccinimide
NHS	<i>N</i> -hydroxysuccinimide
NVOC	nitroveratryloxycarbonyl
PBS	Phosphate buffer saline
PEG	poly(ethylene glycol)
PMMA	poly(methyl methacrylate)
Si	silicon
UANHS	undecylenic acid <i>N</i> -hydroxysuccinimide ester

Units and symbols

Å	Ångstrom
a.u.	arbitrary units
K_a	affinity constant
dL	decilitre
K_d	dissociation constant
fL	femtolitre
kDa	kilodalton

μg	microgram
μL	microlitre
mbar	millibar
mJ	millijoule
μm	micrometre
μM	micromolar
mM	millimolar
mW	milliwatt
M	molar
mol	moles
MW	molecular weight
nL	nanolitre
nM	nanomole
nm	nanometre
w/v	percent weight per volume
v/v	percent volume per volume
pL	picolitre
rpm	revolutions per minute
UV	ultra violet
W	Watt
wt%	weight percentage

Biological

ATP	adenosine-5'-triphosphate
Ala	alanine
Arg	arginine
Asn	asparagine
Asp	aspartic acid
BSA	bovine serum albumin
C _L	constant light domain of immunoglobulin
Cys	cysteine
DNA	deoxyribonucleic acid
Fc	Fragment, crystallisable
Fab	Fragment, antigen binding
Glu	glutamic acid

Gln	glutamine
Gly	glycine
C _H	heavy chain of the constant domain of immunoglobulin
V _H	heavy chain of the variable domain of immunoglobulin
His	histidine
Ig	immunoglobulin
pI	isoelectric point
κ	kappa light chain of immunoglobulin
Ile	isoleucine
λ	lambda light chain of immunoglobulin
Leu	leucine
V _L	light chain of the variable domain of immunoglobulin
Lys	lysine
Met	methionine
Phe	phenylalanine
Pro	proline
His-tag	series of several his-units at the C or N-terminus of a recombinant protein
Ser	serine
ScFv	single-chain variable fragment
PpL	single domain of <i>Peptostreptococcal</i> protein L
SpA	<i>Staphylococcal</i> protein A
SpG	<i>Streptococcal</i> protein G
Thr	threonine
Trp	tryptophan
Tyr	tyrosine
Val	valine
<i>General</i>	
AFM	atomic force microscopy
ATR-FTIR	attenuated total reflectance infrared spectroscopy
e-beam	electron beam
ELISA	enzyme linked immunosorbance assay
IR	infrared
LOC	lab-on-a-chip

μ CP	micro-contact printing
NMR	nuclear magnetic resonance
PDB	protein databank
POC	point-of-care
SNOM	scanning near-field optical microscopy
SAM	self assembled monolayer
SEM	scanning electron microscopy
SDS-PAGE	sodium dodecyl sulfate polyacrylamide gel electrophoresis
XPS	X-ray photoelectron spectroscopy

1

Introduction

1.1 Background and Motivations

Immunoglobulins (Igs), also known as antibodies, are a major part of the immune response. The number of different Igs produced by an individual in their lifetime is estimated in excess of 10^9 [1]. Igs, as part of the immune system, are fundamental indicators in the diagnosis of many diseases and have been for decades [2]. They can be used in diagnostic tests to detect a protein associated with disease or as an endogenous biomarker for an underlying pathology. Quantification of Igs is relevant specifically in the diagnosis of autoimmune disease [3], cancer [4], and immunodeficiency [5].

More generally changes in serum Ig levels, compared with standard age related levels, can be a signal of primary immunodeficiency disorders including X-linked Agammaglobulinemia [5] and Hyper Ig-M syndrome [6]. The disruption to normal levels of serum Ig is also a major indication of the onset of sepsis and the systemic inflammatory response. Sepsis is a condition characterised by a whole body inflammation state and is associated with severe injury, including those sustained from burns [7], trauma [8] and major surgery [9]. Sepsis has an estimated mortality of between 30 and 50 deaths per 100,000 population, regardless of age, and ranks in the top 10 causes of death globally [10]. In the United States alone approximately 500,000 people develop sepsis and 150,000 people die each year from the condition [11]. The failure to find effective therapies for sepsis is partly due to a lack of understanding of the pathogenic mechanism that drives the condition [12]. There is

a need for fresh diagnostic techniques to quantify the progression of immunosuppression in sepsis.

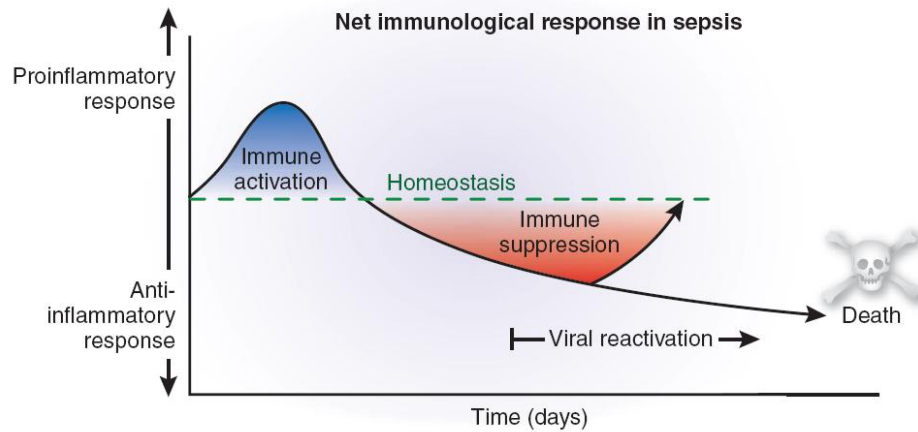


Figure 1-1 Immunologic progression in sepsis over time. Both pro- and anti-inflammatory responses are activated early in sepsis; the pro-inflammatory response predominates. As sepsis progresses the anti-inflammatory response becomes predominant, leading to the suppression of the immune response. In the early stage of sepsis deaths are due to cytokine storm-mediated events produced as part of the pro-inflammatory response. Later deaths are caused by the suppression of the immune system, during the anti-inflammatory response, causing a failure to control pathogenic infection (Reprinted with permission from [12]).

The current view of sepsis progression is illustrated in Figure 1-1, with an initial dominant pro-inflammatory response during the early stages of sepsis followed by a reversal to an anti-inflammatory response over time [12]. It has been observed that the majority (>80%) of patient deaths occur in the later stages, presenting with hallmarks of immunosuppression [13]. It is in the later stages where severe sepsis and septic shock occur, the transition from sepsis usually occurring within the first 24 hours of hospitalisation [14]. Further more the diagnosis and treatment of sepsis within the critical “golden hours” is essential to provide maximum benefit in terms of outcome [14-16]. Studies regarding the treatment of sepsis have focussed on controlling the levels of anti-inflammatory mediators, with poor results. Of over 20 separate clinical trials of therapeutics for sepsis, only activated protein C has shown to be of clinical benefit [17, 18]. Protein C has an inhibitory effect on factors associated with blood coagulation, fibrinolysis and the immune system [19]. Reduced coagulation has clinical benefit in sepsis but in certain circumstances can lead to an increase in serious bleeding [20]. Despite the lack of success of clinical trials, aimed at improving the outcome for patients who develop sepsis, a better understanding of the clinical manifestations of the disease has been determined. Potential mechanisms that lead to immunosuppression include:

1. Shift from an inflammatory (type 1 T helper cell) response to an anti-inflammatory (type 2 T helper cell) response [9, 21]
2. Anergy [8, 22]
3. Apoptosis-induced loss of CD4 T cells, B cells and dendritic cells [23]
4. Immunosuppressive effect of apoptotic cells [11, 24].

The combination of these factors leads to immunosuppression and an enhanced risk of death from bacterial infection. One direct effect of immunosuppression is a reduction in the levels of immunoglobulins. In patients suffering from burns injuries, decreased IgA, IgD, IgG and IgM have been observed in the first week after injury [25]. Levels of IgA, IgM and IgG reach a minimum level within the first 48 hours of injury [26]. Low levels of Ig reduce the body's ability to effectively deal with bacterial infection, which is one of the primary complications resulting in death from sepsis. Levels of IgE fall initially after trauma but switch to supranormal levels weeks after the injury. This increase is believed to be caused by the onset of infection and not by problems associated with B-cell regulation [27].

Clearly the impairment of the immunological response to bacterial infection after severe injury and trauma is a key marker of the progression of sepsis, development of severe sepsis, septic shock and cause of death. Immunoglobulins, as part of the humoral response, are a major part of the immunological response required to clear infection. Studies of IgM and IgG levels from patients with septicaemia, by Pollack *et al.* [28], showed that patients with total IgG concentrations >1,000 mg/dL had improved survival compared with patients with <1,000 mg/dL. Patients with levels of IgM >150 mg/dL showed a reduced improvement compared with patients with <150 mg/dL. Clinical trials have attempted to use intravenous injections of IgG, IgM and IgA as therapeutics in sepsis, to impair the effects of immunosuppression, with mixed results [17, 29, 30].

A problem with targeting therapeutics in clinical trials for sepsis is identifying candidates with comparable clinical symptoms. To determine candidates that may benefit from intravenous injection the level of immunoglobulins within the patient's serum needs to be determined. Current methods to measure the immunoglobulin content of serum include the enzyme linked immunosorbent assay (ELISA) [31] and radial immunodiffusion [32]. The problem with these methods is

that results take a minimum of 2 hours to process by which time the advantage of early stage treatment is lost. There is a clear need for a rapid method to quantify the levels of serum immunoglobulin to determine potential candidates that may benefit from therapeutic interventions in the early stages of sepsis.

Recent advances in microfluidic lab-on-a-chip (LOC) devices for point of care (POC) diagnostics show promise as a potential means to develop a device for the rapid measurement of serum immunoglobulin levels [33-36]. POC testing can be described as bedside, near patient, remote, and decentralised laboratory testing. Essentially it is a device capable of supplying clinical diagnosis for patients without the need for laborious laboratory tests [36]. The general requirements for such devices are portability, high sensitivity and simple operation. More practical considerations include low cost, low power consumption and an ability to produce results rapidly, ideally to the extent of real-time patient monitoring. Microfluidic LOC technology has the capacity to fulfil the requirements of rapid POC diagnosis.

Microfluidic LOC technology can be used in the development of POC diagnostics for reducing the amount of sample required, decreasing the analysis time and integrating parallel analysis in a single device [37]. Microfluidic devices can be designed to integrate sample injection, sample throughput, and sample analysis. Thus the movement of sample fluid can be precisely controlled by software for simple operation, which means accurate measurements can be taken without the skill of an experienced technician.

To measure immunoglobulins obtained from human serum requires the isolation and purification from a complex mixture often consisting of cells, proteins, deoxyribonucleic acid (DNA), and other biomolecules. It has been known for decades that antibody binding proteins can be used for affinity capture and purification of antibodies [38]. Antibody binding proteins are used for the industrial scale purification of antibodies using large scale chromatography supports [39]. The potential of microfluidic affinity chromatography using antibody binding proteins has yet to be determined for the application to microfluidic POC technology.

Figure 1-2 (see overleaf) illustrates a cross section of a device conceived to achieve affinity separation of antibodies within a microfluidic channel. The separation principle is based upon the conjugation of protein patches that have

different association constants for biomarkers in solution. As the biomarkers flow through the microfluidic device they associate with the surface and are retained for different time periods depending upon the size of the device, the size of the protein motif and the association constant of the interaction [40]. The dimensions of the device are such as to keep the Reynolds number <2000 , which in theory would ensure that laminar flow occurs in the channel [41]. Using an external pump the fluid flow can be controlled to ensure the fluid travels at a velocity suitable to allow effective mass transfer, by convection, of analyte onto the protein conjugated surface [42].

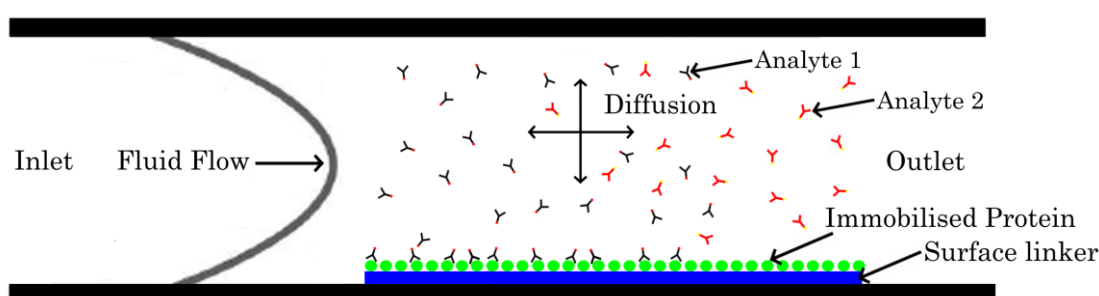


Figure 1-2 Cross section of a proposed microfluidic affinity chromatography device. The channel surface is patterned with a bifunctional linker and conjugated with proteins to the surface. As the two analytes are transported by convection and diffusion they associate with surface immobilised protein. When the analytes are eluted depends on the size of the device, the size of the protein motif and the association constant of the interaction.

For such a microfluidic affinity chromatography system to be realised, a method to pattern high densities of antibody binding protein, in micron scale motifs, is required. High densities of protein are required to maximise the availability of association sites on the surface to ensure saturation of the protein patches does not occur before separation has been achieved. Preferably the proteins need to be conjugated on the surface in such a way as to ensure each protein is accessible to Ig. The surface needs to be modified to stop the protein from denaturing upon conjugation with the surface and to prevent non specific protein adsorption. Conjugated protein must retain affinity to Igs, ideally with an association constant comparable to that found in the solution phase, and have long term stability. In order to separate Igs by affinity chromatography antibody binding proteins with different association constants for Igs are required.

To integrate the protein patches within a microfluidic channel the conjugation method must be appropriate to align patterns site specifically on the surface. To create multiple protein motifs, within a single microfluidic channel,

requires sequential or simultaneous conjugation of different proteins in adjacent patterns. An alignment system is therefore crucial to control where the motifs are patterned on the surface but then also to align a microfluidic channel on top of the patterns.

1.2 Aims and Scope of Work

The development of conjugation techniques to pattern proteins on surfaces has increased dramatically over the past decade, witnessed in the high number of reviews published on the subject [43-48]. One of the main challenges in manufacturing a viable microfluidic LOC system is manipulating a surface for compatibility with the conjugation of more than one protein, while retaining protein recognition properties and preventing non specific protein adsorption. This coupled with the requirement of features patterned on the micro/nanometre-scale poses a significant challenge. The aim of this research is to develop a conjugation technique, which can be used to covalently attach functional antibody binding proteins onto a surface in high density patches. The long term aims, beyond the scope of this thesis, is to demonstrate the potential of this technology for the controlled alignment of antibody binding proteins within a microfluidic device suitable for rapid quantification of serum antibody content.

The design of a technique to pattern proteins onto surfaces, that includes the prevention of non specific protein adsorption, the retention of protein recognition properties and the production of protein motifs at the micron and nanometre scale are the primary aims of this thesis. The design and fabrication of microfluidic channels and the quantification of antibody separation are not part of the work presented in this thesis. However, some attempts to consider the future integration of microfluidic technology have been included.

1.3 Summary of Main Achievements

A number of innovations were achieved during the course of this research, these are outlined briefly here:

A conjugation method for generating protein motifs on silicon was demonstrated. The protocol was used to conjugate protein in micron and submicron scale motifs reproducibly.

A set of conditions to give a reproducible film of dextran immobilised on glass surfaces, using the minimal amount of reagent, was determined. Compared with previous studies a 30 fold reduction in reagent was achieved. The conditions used to reproducibly generate dextran films were integrated into the development of a protein conjugation technique. Protein was conjugated onto glass surfaces using an aryl azide conjugated dextran. The method produced micron scale motifs of protein, which retained recognition for analyte.

A novel design for a protein patterning mask was developed to generate adjacent motifs of protein on aryl azide modified dextran surfaces. With the aid of a novel alignment/illumination setup, built in-house, two proteins were conjugated in adjacent motifs.

1.4 Organisation of Thesis

A three-part literature review is presented next. The association of Igs with Ig binding proteins is first examined. These include the association specificity for different domains of the Ig specific to the proteins. The second part reviews methods to conjugate dense, stable proteins on surfaces that prevent non specific adsorption. This includes substrate modification, use of surface spacers and methods of protein conjugation. The final section reviews current state-of-the-art methods to generate micron and submicron motifs of protein on surfaces.

Chapter 3 contains the materials and methods used in the thesis for the development of a site specific protein conjugation protocol.

In Chapter 4, a novel method to conjugate protein on silicon <100> surfaces is investigated. The fabrication of a photolithographic mask and the UV-initiated conjugation of a heterobifunctional linker, used to conjugate protein, to silicon are described. The evaluation and optimisation of the protein conjugation method, including characterisation of the silicon modification, are discussed.

Chapter 5 details the development of a novel approach to conjugate protein to glass surfaces using a dextran photolinker. A method is proposed detailing the modification of glass surfaces with an aryl azide conjugated dextran. Firstly optimisation of a dextran conjugation method, including characterisation of the layer generated, is discussed. Subsequent modification of the immobilised dextran, to conjugate protein, is investigated to determine the accessibility and association of surface conjugated protein with analyte. The synthesis and characterisation of an aryl azide modified dextran is detailed. A protocol to conjugate the dextran photolinker to glass is presented, including methods to characterise the immobilisation and subsequent conjugation of protein with the glass surfaces. The design and fabrication of two photolithographic masks and how they are applied to the generation of micron scale multiple protein motifs is documented.

Finally, Chapter 6 contains a summary of the achievements of this research, which is followed by suggestions for future work.

2

Biomolecule Patterning for Microfluidic Applications

2.1 Introduction

Presently, quantification of the different Igs in patient serum requires lengthy processing approaches for diagnostic purposes. Currently the method of choice, to determine serum antibody titre of patients, involves application of an enzyme linked immunosorbent assay protocol [31]. The ELISA involves time consuming procedures (>2 hours) involving conjugation of antibodies to the ELISA plate surface and washing of unbound antibody. Also not all ELISA protocols provide quantitative information on the binding kinetics of the reaction, which has been shown to be clinically relevant [49].

Advances in microfabrication technology have lead to the miniaturisation of bioanalytical and diagnostic techniques for POC devices. One of the most studied are microfluidic devices [50, 51]. Flow in microfluidic devices occurs at low Reynolds numbers (<2000) and a laminar flow regime is formed. The reduction in scale from macro to micro channels increases the surface area to volume ratio, which with the correctly designed system allows for efficient interaction of the soluble agent with the solid/liquid phase [52]. The scale of the device allows input of smaller (nL/pL/fL) volumes of sample for analysis and allows processing at the point of care, which can reduce diagnostic turnaround times [53]. Microfluidic devices have already been developed for environmental monitoring [54], drug discovery [55], genomics [56], proteomics [57], and clinical diagnosis [58, 59]. Essentially all these systems

function by the same principles involving the quantitative analysis of specific analyte within a complex solution.

One of the more challenging requirements that is now needed for developing microfluidic POC technology is the attachment of multiple proteins in micron sized motifs within a microfluidic channel. Many applications require highly dense patches of protein attached to the channel surface, which serve as the sensing region for quantitative analysis. As the scale of devices is reduced, and the number of tests multiplexed on the same chip, the demand for innovative fabrication techniques increases. The fabrication of devices containing biomolecules adds an additional complexity to processing techniques due to the instability of proteins. Proteins can become denatured in some organic solvents [60], are susceptible to temperature and pH change [61], ultra violet (UV) damage [62], and are prone to biofouling. To circumvent these limitations many groups pattern surfaces with chemical linker groups, which are compatible with processing techniques and can be subsequently used to conjugate proteins [58, 63, 64]. These linkers are often bifunctional with the ability to react with the microfluidic channel to present a surface chemistry that can react with proteins to immobilise them upon the surface.

This review considers proteins that associate specifically with antibodies, bioconjugate chemistries, as well as methods appropriate to fabricate micron sized motifs of bioconjugated proteins on surfaces. The current state-of-the-art techniques used in the fabrication of micron and nanometre scale patterns of bioconjugated proteins on surfaces are discussed and evaluated.

2.2 Association of Immunoglobulins with Antibody Binding Proteins

The principle aim of the work presented in this thesis is to develop surfaces for integration within a microfluidic affinity chromatography device suitable for the rapid quantification of Igs from patient serum. An understanding of the structural variation of Ig types and potential methods of separating these molecules is fundamental to defining a suitable strategy for creating such a device.

2.2.1 Immunoglobulin Structure

The characteristic structure of a monomeric unit of Ig is a protein consisting of two identical heavy and light chains held together by a series of disulfide bonds. The molecule is composed of a total of 12 structural domains, 4 per heavy chain and 2 per light chain. The domain situated at the N-terminal of each chain is classified as the variable region, and the remainder are termed constant regions. The constant domains of the light chain govern whether the chain is kappa (κ) or lambda (λ) type, while the heavy chain constant domains (C_H) mediate cell signalling and determine the Ig class [65]. The different amino acid sequences responsible for the heavy chain constant domains form five classes (IgG, IgA, IgM, IgD, and IgE), with a further four IgG (I-IV) and two IgA (I-II) subclasses. Igs are a group of glycoproteins and contain between 3 to 13 % carbohydrate, depending on class, which enhance structural stability. The illustrations in Figure 2-1 (a) (see overleaf) show the classic representation of the structure of the Ig molecule and potential fragments that have been produced from the original Ig molecule. The 5 different classes of Ig are shown in Figure 2-1 (see overleaf) detailing the variation in structure found in the Ig family.

All Igs are expressed at the cell surface or secreted from B-lymphocytes, where they act as receptors for foreign species termed antigens. Cell surface antibodies have an additional hydrophobic transmembrane domain which tethers the antibody to form a B-cell receptor. In serum there are significant differences in levels of the five Ig classes, as recorded in Table 2-1, with IgG making up >80 % of total serum antibody content in humans [66]. The high levels of IgG can be attributed to the long half-life of 23 days in human serum compared with other Igs (Table 2-1). When taking into account total human Ig, including serum Igs, the most abundant is IgA as high levels are found at mucosal surfaces within the lymphatic system. Secretory IgA is stabilised by association with a secretory component to protect against proteolytic cleavage. IgA and IgM also form multimers connected by a stabilising J chain, to form a tetravalent dimer and a decavalent pentamer respectively.

Characteristic	IgG	IgA	IgM	IgD	IgE
Serum level (% of total Ig)	85.0	7.0-15.0	5.0	0.3	0.02
Half-Life (days)	23.0	5.8	5.1	2.8	2.5

Table 2-1 Characteristics of Igs in human serum [66]

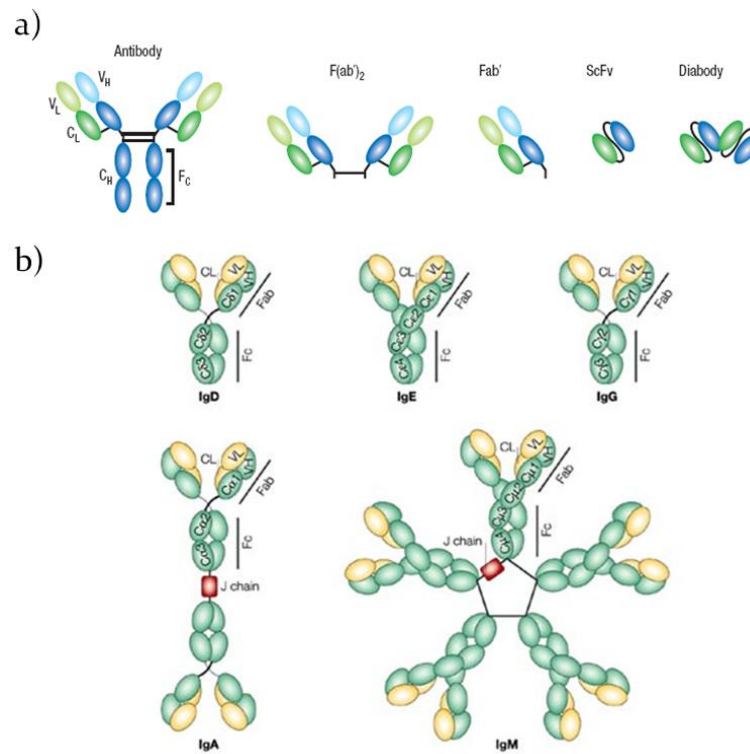


Figure 2-1 Ig variation – (a) Immunoglobulin components can be isolated as fragments, each of which have specific properties. Transgenic organisms have been developed specifically to produce defined regions of the Ig molecule. Possible fragments include F(ab)₂, Fab, ScFv, and diabodies. (b) Igs are Y-shaped heteromeric protein complexes composed of two light chains (MW = 25 kilodaltons (kDa)) and two heavy chains (MW = 55 kDa). Light chains form disulfide bridges with the N-terminus of the heavy chains to form two arms (the Fab portion), which contain the antigen-binding sites. The Fc domain has the capacity to interact with molecules such as complement or Fc receptors. Mammals have five different Ig classes (IgA, IgD, IgE, IgG and IgM), the class being dependent on the heavy chain type. Reprinted with permission from [67, 68].

Certain genera of Gram-positive bacteria carry genes which encode cell surface proteins that bind Ig of various mammalian species. Three of the most studied proteins originate from certain strains of *Staphylococcus aureus*, *Streptococcus pyogenes*, and *Peptostreptococcus magnus*, designated protein A, G, and L respectively. The Ig binding proteins, along with other cell wall proteins [69], are implicated in bacterial survival within an infected host [70]. Each protein has specific Ig binding properties that have been exploited for affinity chromatography separation of Igs for decades [38]. Work by Schudel *et al.* [71] demonstrates the potential of Ig binding proteins for quantitative binding assays within a microfluidic device.

2.2.2 Protein A

Staphylococcal protein A (SpA) is an Ig binding protein found on the bacterial cell wall surface and secreted by *Staphylococcus aureus* [72]. It is extensively used as an immunological tool for affinity chromatography in the separation of Igs due to its well characterised interaction with the Fc region [38]. The protein was first isolated in 1940, by Verwey [73], and the gene sequence was cloned into *Escherichia Coli* in 1983, by Lofdahl *et al.* [74]. The gene sequence for protein A consists of three regions: the signal sequence, which controls the secretion process [72], 5 highly homologous extracellular Ig binding domains [75] and the C-terminal X domain, believed to be responsible for tethering the protein to the bacterial cell wall [76].

The 5 extracellular domains are arranged successively in the order E, D, A, B and C, from the N-terminus of the protein [75]. Each of the 5 extracellular domains has an approximate molecular weight of 7000, while the C-terminal X domain is considerably larger with a molecular weight of 15000. The X domain consists of a repeat and a constant region, which links the multidomain protein with the bacterial cell surface. The repeat region has a series of 12 octapeptide repeats that are involved in binding to peptidoglycan on the bacterial cell wall. The constant region includes hydrophobic amino acids that are believed to facilitate cell membrane interaction [76].

2.2.2.1 The Fc Binding Interaction with Protein A

The interaction between protein A and the Fc region of Igs has been well studied and results show that binding is primarily exhibited between the C_H2-C_H3 domain interfaces. Lindmark *et al.* [77] reviewed the binding affinity of protein A with IgG, IgA, and IgM of different mammalian species. In humans, protein A binds predominantly with IgG, more notably subclasses I, II, and IV, but can also interact with IgA, IgM, and IgE. The presence of the positive charge on Arg-435 in IgG III compared with His, in other subclasses, is believed to cause a steric clash on protein A interaction.

The crystal structure of the domain B of *Staphylococcal* protein A, in complex with human Fc, was solved by Deisenhofer in 1981 with a 2.8 Å resolution [78]. Crystallography specified two antiparallel α -helices that form the dominant secondary elements of the B domain between residues Glu-128 to Leu-136 and Glu-

144 to Asp-155. Two contacts are observed in the crystal structure but, due to the low pH (4.1) of crystallisation, only the first is considered to occur at physiological pH. Formation of the complex buries 1234 \AA^2 of solvent-accessible area, between the C_{H2} and C_{H3} regions of Fc and the α -helical regions of domain B [78]. The complex is primarily composed of hydrophobic interactions, with only 4 hydrogen bonds between the Fc and domain B.

Nuclear magnetic resonance (NMR) spectroscopy provided evidence for a third α -helix, using recombinant B domain, which was unresolved by crystallography. Work by Gouda *et al.* [79] discovered a bundle of three α -helices: helix I (Gln-10 to His-19), Helix II (Glu-25 to Asp-37), and Helix III (Ser-42 to Ala-55). Helix II and III run antiparallel to each other, while the helix I is tilted at 30° compared with helix II and III. Residues involved in binding to Fc were further refined in subsequent studies to Phe-14, Tyr-15, Glu-16, Leu-18, and His-19 in Helix I, and Asn-29, Glu-33, Leu-35, and Lys-36 in Helix II [80].

2.2.2.2 The Fab Binding Interaction with Protein A

In addition to binding the Fc region of Igs, protein A has a second distinct interaction with Fab [81]. The specific site of interaction was defined in 1985, by Vidal *et al.* [82], and found to bind with the Ig V_H domain. Sasso *et al.* [83] showed that protein A binds with Fab of different classes with varying affinity, with 22 % polyclonal IgA, and 15 % IgG F(ab')₂ bound to protein A agarose. Both Sasso *et al.* [83] and Roben *et al.* [84] reported that protein A interacts specifically through variable regions of the V_{HIII} subgroup of Igs. Initial work implicated domain D and E as being responsible for the protein A/Fab binding interaction [84, 85]. Later work, by Jansson *et al.* [86], determined that in fact all individual domains of Protein A can bind Fab with similar affinity.

Structural studies of the interaction between individual protein A domains and Fab have been carried out showing a structurally separate site to the interactions made on Fc binding [87, 88]. The crystal structure showed burial of 1220 \AA^2 on complex formation between Fab of human IgM and domain D, as determined with a 1.4-\AA radius probe. The outcome was comparable to the 1234 \AA^2 observed by Deisenhofer *et al.* [78] upon binding with the Fc region, but notably the interactions are significantly different, with Fc binding largely a result of

hydrophobic interactions and Fab binding being dominated by polar interactions [78, 87]. Figure 2-2 (a) shows residues from the V_H site responsible for binding interactions with domain D. Figure 2-2 (b) shows the interactions between domain B (brown) and the V_H region residues (blue) of human IgM. The residues from domain D are found on helix I and II, and the loop between them. Crystallography coupled with NMR studies performed by Meininger *et al.* [88] describe the specificity of protein A for the V_{HIII} subgroup. Analysis concluded that seven core residues, Arg/Lys-19, Gly-65, Arg-66, Thr-68, Ser-70, Gln-81, and Asn-82 conserved in the V_{H3} subgroup encode specificity. Changes to one or more of these residues, found in other V_H subgroups, restrict interaction with the Fab binding region of protein A [87, 88].

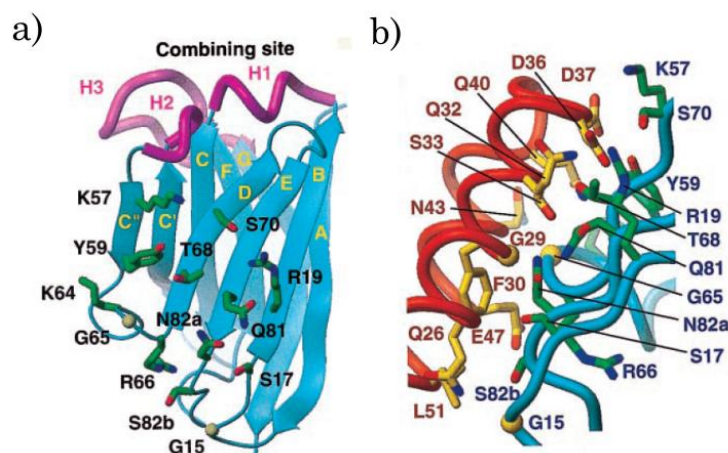


Figure 2-2 Structural representation of the complex between domain D of protein A and Fab'2A2 from human IgM. (a) Ribbon diagram of the V_H region of Fab showing the residues of interest that interact with domain D. (b) Structure diagram detailing the residues of domain D and Fab 2A2 involved in the interaction. Kabat numbering is used for the V_H residues (blue); domain D is numbered (in brown). Contact residues are identified if 20 \AA^2 or more of their surface are buried in the interface and if they make at least one van der Waals contact. Figures were reprinted with permission from [87].

2.2.3 Protein G

The bacterial cell wall Fc receptor protein G (SpG) can be found on the surface, or secreted by, C and G strains of *Streptococcus* [89]. It was first purified in 1984, by Björck and Kronvall, from a human group G *Streptococcal* strain (G148) [90]. Studies by Akerstrom *et al.* [91] indicated that the SpG has a greater avidity than SpA for Ig of different mammalian species. SpG was shown to interact with polyclonal IgG from human, cow, rabbit, goat, rat, and mouse species.

The structure of SpG consists of 3 Ig binding domains (C1, C2, and C3) separated by two linker regions (D1 and D2), with a C-terminal membrane anchor domain. The C domains consist of a sequence of 55 amino acids each separated by a 16 amino acid linker region [92]. The membrane anchor consists of a W and M domain involved in cell wall and membrane interactions respectively. The W domain sequence is highly regular and contains specific repeats within the sequence. The repeats consist of a proline rich region followed by a pentapeptide (Lys-Lys-Glu-Asp-Ala) repeated six times. The domain is extremely hydrophilic and is believed to be important in facilitating the orientation of the proteins on the cell surface. The M domain, similar to that found in protein A, consists of a sequence of 21 hydrophobic residues that interact with the cell membrane [92].

2.2.3.1 The Fc Binding Interaction with Protein G

Both X-ray crystallography [93-95] and NMR spectroscopy [96, 97] have been used to determine the structural interactions between the IgG and the SpG domains. The secondary structure of the Ig binding domain consists of one α -helix and four β -sheets. The two inner β -sheets, β_1 and β_4 , are parallel while the outer sheets, β_2 and β_3 , run anti-parallel to β_1 and β_4 respectively. The α -helix runs diagonally across the β -sheets at an approximate angle of 140° between the axis of β_2 and β_3 .

SpG has been shown to interact at the hinge region between the C_{H2} and C_{H3} domain of IgG. Work by Sauer-Eriksson *et al.* [95] determined that the protein interaction was made up of three distinct regions. The regions are formed of hydrogen bonds and salt bridges, the first interface consisting of 4 charged and 3 polar residues. Lys-28 and Gln-32, situated on the α -helix of SpG, form connections with Lys-248, Glu-280, Glu-382, Ser-426 and Gln-438 of the Fc domain. The second interface is formed by Glu-27 and Lys-31, from the α -helix of SpG, which form interactions with Ile-253 and Ser-254. The third region includes Asn-35, Val-39, Asp-40, Glu-42, and Trp-43 of SpG, which network with His-433, Asn-434 and Tyr-436 from the Fc domain of IgG.

2.2.3.2 The Fab Binding Interaction with Protein G

The complex formed between SpG and the Fab region of Ig consists of hydrogen bonds between the second β -strand of SpG and the last β -strand of the C_{H1} domain of Fab. A hydrogen bond is formed by the strong dipole-dipole interaction between

hydrogen (e.g. N-H of the peptide backbone) and an electronegative atom (e.g. C=O from the peptide backbone). The interaction involves primarily backbone residues from SpG but is also influenced by the burial of non-polar residues from Fab and SpG, which become shielded upon binding [95].

2.2.4 Protein L

Protein L is a multidomain cell-wall protein found in 10 % of the bacterial species *Peptostreptococcus magnus*. This bacterium is part of the native flora of the skin, oral cavity, gastrointestinal tract, and urogenital tract, but is also the causative agent in various infections [98]. A study of *Peptostreptococcus magnus* from patients suffering a gynaecological infection, bacterial vaginosis, showed 4 of the 7 strains isolated expressed protein L. A region of coding DNA from these strains was then used for screening a total of 23 other *Peptostreptococcus magnus* strains from clinical specimens as well as *streptococcal*, *staphylococcal*, and *Escherichia coli* DNA libraries. It was found that the protein L gene was unique to *Peptostreptococcus magnus* and was strain specific, meaning that the gene was missing entirely rather than down regulated in certain *Peptostreptococcus magnus* strains [99]. The Ig binding protein was first discovered in 1985, by Myhre and Erntell [100], and designated protein L in 1988, by Lars Björk, because of its specificity for Ig light chains [101]. Both studies showed the ability of protein L to bind Fab, F(ab')₂, light chains κ and a single λ chain, IgM, IgG, IgE and IgA. No binding was found to occur with the Fc region or the heavy chain of Igs. Importantly the ability to bind antigen remained when protein L was bound with Ig, which indicated that a binding region existed away from the antigen binding site. More recently protein L has been used for the purification of the Fab', ScFvs, and diabodies (See Figure 2-1, pg 12). These immunological molecules can be mass produced, using transgenic organisms, and are promising reagents for the development of future therapeutics [67, 102].

Protein L has been sequenced from two strains of *Peptostreptococcus*, strain 312 (PpL₃₁₂) [103] and strain 3316 (PpL₃₃₁₆) [104] PpL₃₁₂ possesses five homologous Ig-binding domains, B₁-B₅[103], whereas PpL₃₃₁₆ possesses four homologous Ig-binding domains, C₁-C₄, and four albumin-binding domains, D₁-D₄ [104]. A comparison of the Ig-binding domain homology of PpL₃₁₂ and PpL₃₃₁₆ is shown in Appendix A. Unlike protein A and G, protein L has been shown to target the light chain of Igs, more specifically only the variable light chain (V_L) [105]. It has been observed that

protein L binds predominantly to κ -light chains, more specifically I, III, and IV subgroups [105, 106]. Sequence differences between κ -chain subgroups have revealed that κ I, III, and IV have nine amino acids conserved which κ II lacks. It is believed that the presence of a serine residue at position 20 of the chain, instead of Thr within the other κ -chains may affect binding. The existence of a hydrophobic group at residue 9 and a positively charged residue at 74, are also believed to interfere with PpL binding [107]. Different species have different complement ratios of κ to λ chains, 20:1 in mice, 2:1 in humans, and 1:20 in cows [108]. Within humans the percentage of κ -chain subgroups means that 60 % are κ I, 10 % κ II, 28 % κ III, and 2 % κ IV, giving PpL a 90 % binding capacity of human κ -chains [105].

2.2.4.1 The Fab Binding Interaction with Protein L

Analysis of the binding affinity of a single Ig binding domain of protein L (PpL₃₃₁₆) with the κ -light chain V_L domain of Fab gives an affinity constant (K_a) of $0.9 \times 10^9 \text{ M}^{-1}$, while the whole κ -light chain has a greater binding affinity of $1.5 \times 10^9 \text{ M}^{-1}$ [105]. Increased binding affinity is also seen with the whole Ig molecule, with an affinity of $1.5 \times 10^{10} \text{ M}^{-1}$ for IgG, IgA, and IgM [109]. The affinity of a single Ig binding domain was found to be 100 fold lower than that of the multidomain protein, with a K_a of $1.6 \times 10^{10} \text{ M}^{-1}$ [103]. Heteronuclear single quantum correlation NMR spectroscopy data, using $\text{H}^1\text{-N}^{15}$ coupling studies, showed that residues that were perturbed on complex formation with PpL₃₃₁₆ resided in the framework region of the V_L domain [107]. The residues responsible for binding are residues 8-11, 19-23, and 72-74 of the framework region, which were already regarded as the likely target as protein L does not disturb antigen binding.

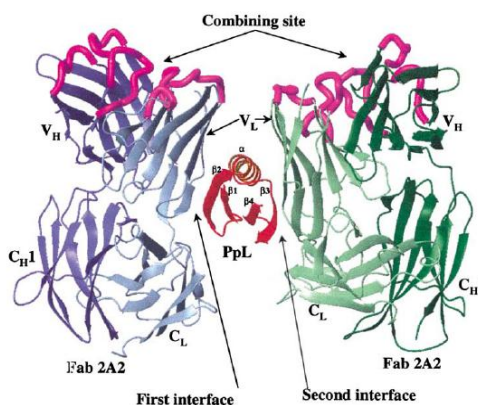


Figure 2-3 Dual interface – This figure shows a ribbon diagrammatic representation of the two binding sites of PpL₃₃₁₆ with the V_L domain. (Reprinted with permission from [110]).

NMR spectroscopy studies on PpL₃₃₁₆ have shown a secondary structure composed of two pairs of anti-parallel β -sheets that are linked by a single α -helix which lies across the β -sheets at an angle of 10 degrees [111]. Similar NMR spectroscopy studies revealed residues involved in binding that were located on the 2nd β -strand, the C-terminal of the α -helix and located on the loop between the α -helix and the 3rd β -strand. In addition to NMR studies recent X-ray crystallography data revealed that protein L has two possible binding sites for the V_L domain [110]. Figure 2-3 (see previous page) shows the sandwich effect of two light chains with protein L between; a previous study had suggested that protein L might have two binding sites, but this was largely unexpected [109]. The molecule has therefore been classified into two interfaces, site 1 and site 2. Site 1 involves the 2nd β -strand and one side of the α -helix, while site 2 involves the alternate side of α -helix and the 3rd β -strand. A full breakdown of the amino acids involved in binding sites 1 and 2 are given in appendix A and B.

2.2.4.2 The Site 1 Fab Binding Site of Protein L

On formation of the complex between Fab and site 1 a 1300 Å² of solvent-accessible area is buried with an equal number of residues being affected from each molecule; this is determined using a 1.4-Å radius probe. No backbone conformational change is observed, on complex formation, from either molecule. The interaction consists of 13 residues from the Fab molecule, there are 10 residues within the V_L framework region and the others consist of Lys-107, Glu-143 and Arg 24 from the variable light-constant light domain (V_L-C_L) connection region, the C_L region and the CDR-L1 region on strand B respectively. Interactions from the protein L domain include 12 residues in all, mainly from the second β -strand and the α -helix. The interface consists of 6 hydrogen bonds, which are detailed in Table 2-2 (see overleaf). Three are formed between main chain atoms, within the second β -strand and strand A of the Fab molecule, forming a β zipper. Analysis of mutant protein L has shown that tyrosine 53 produces a hydrogen bond with Thr-20 of the V_L region; the mutation causes a 23-fold drop in affinity [110].

V _L Region	PpL ₃₃₁₆ Domain C	Distance (Å)
Ser 9	Glu 38	2.8
Ser 9	Lys 40	3.1
Ser 10	Glu 38	2.9
Ser 10	Glu 38	3.1
Ser 12	Glu 36	2.7
Thr 20	Tyr 53	2.6

Table 2-2 Table listing the amino acid residues from the V_L domain of IgG and the C domain of PpL₃₃₁₆ that form hydrogen bonds in the site 1 interface, including the distance between interacting residues [110]

2.2.4.3 The Site 2 Fab Binding Site of Protein L

The interaction between Fab and the Site 2 causes the burial of a larger surface area (1400 Å²) than site 1, mainly through interactions with β-strands. Altogether 15 residues from the V_L region are involved in binding from the Fab molecule, 10 are common in both sites. There are 14 residues from the PpL₃₃₁₆ domain involved in the second interface from the third β-strand and the α-helix; none of these residues is common with site 1. Binding is via 6 hydrogen bonds and 2 salt bridges; although there are more interactions than in the first site, the affinity is 25-55 fold lower than that of site 1. The specific residues involved in the interface are detailed in Table 2-3.

V _L Region	PpL Domain C	Distance (Å)
Ser 7	Asp 55	2.9
Ser 10	Thr 65	3.2
Ser 12	Ala 66	2.9
Ser 12	Leu 68	2.6
Arg 18	Gly 71	3.1
Arg 24	Asp 55	2.7
Lys 107	Asp 67	2.6
Lys 107	Leu 68	2.9

Table 2-3 Table listing the amino acid residues from the V_L domain of IgG and the C domain of PpL₃₃₁₆ that form hydrogen bonds and salt bridges in the site 2 interface, including the distance between interacting residues [110]

2.2.4.4 Evaluation of the Binding Properties of Wild Type and Mutant Protein L by Stopped Flow Analysis

Fluorescence signals in biological systems can act as reporter groups to demonstrate changes to the molecular environment of the fluorescent group, which can then be related to the molecule as a whole. Stopped flow analysis allows for the

determination of the K_d of an interaction by observation of changes to fluorescence, in this case when V_L binds to protein L. By mutating residues on each interface into residues that have intrinsic fluorescence (tryptophan, tyrosine, or phenylalanine), the site-specific K_d can be determined. Both tryptophan and tyrosine have strong absorption bands at ~ 280 nm and, when excited by light at this wavelength, have characteristic emission profiles. The fluorescence of free tryptophan is centred on 350 nm and that of tyrosine around 303 nm.

Site directed mutagenesis is a technique that is used to alter single or multiple residues of a protein to determine their contribution to the properties of a protein. Mutations of PpL₃₃₁₆ have been made to introduce fluorescent reporter groups and to prevent binding with Ig at each of the two interfaces, in an attempt to determine the affinity of each site. In Graille *et al.* [112], the mutant Y64W was used to introduce a tryptophan residue into the PpL₃₃₁₆ molecule to act as a fluorescent reporter group. Two double mutants Y53F-Y64W and D55A-Y64W were made to weaken binding at the first and second sites respectively. The first mutant disrupts hydrogen bonding between Tyr-53 of PpL₃₃₁₆ and Thr-20 of the V_L domain. The second mutant disrupts both the salt bridge between Asp-55 of PpL₃₃₁₆ and Arg-24 of the V_L domain and the hydrogen bond between Asp-55 and Ser-7 (Table 2-3, see previous page). The K_d of Y53F-Y64W and D55A-Y64W were 2.8 μ M and 0.145 μ M respectively, compared with the wild type K_d of 0.13 μ M [113].

More recent work has been done to produce knockout mutations on site 1 and 2 individually, reported by fluorescent stopped flow analysis [114]. Knockout mutants, in this instance, are proteins where the genetic template that codes the protein has been altered to introduce different amino acids in either binding site 1 or 2 of the normal protein. The mutations are designed to disrupt the binding of Ig, thus preventing (or knocking out) the binding of Ig at that site. The reporter group mutants I34W and Y64W were used for site 1 and 2 fluorescence analysis respectively. The mutants I34W/Y53F/L57H and Y64W/A66W PpL₃₃₁₆ showed no changes in fluorescence, upon incubation with Ig and excitation at 295 nm, implicating a loss of binding at site 1 and 2 of these mutants respectively. A difference in fluorescence was observed at specific wavelengths as a result of Förster resonance energy transfer, a phenomenon resulting from the proximity of fluorescent groups. An observed decrease in fluorescence was caused by an alteration to the

environment of the tyrosine group Tyr⁵³, which lead to a decrease in the Förster resonance energy transfer interaction with the Trp⁶⁴ reporter group upon complex formation at site 1 but does not affect the complex formation at site 2 [114]. The observed phenomenon is the cause for the biphasic fluorescence changes that were seen in previous studies [113].

After the second binding site was determined a new model was established to interpret the complex fluorescent changes found in earlier research. The model assumes 2 sites where the K_d of each site depends on the ratios of their dissociation (k_{-1} and k_{-2}) and association (k_1 and k_2) constants (Figure 2-4). The biphasic fluorescence change observed is considered to be due to the different K_d values for each site. The wild type K_a value observed is considered to be from contributions of association rates from site 1 and site 2 (k_1 and k_2). Knockout mutants, each with a reporter group (I34W and Y64W), were used to determine K_a and K_d of each site individually. The results showed that site 1 has a K_d of 4.8 ± 0.8 nM and site 2 has a K_d of 3.4 ± 0.7 μ M. The corresponding K_a values showed site 1 had a higher K_a , of 0.25 ± 0.01 μ M⁻¹s⁻¹, than site 2 which had a lower value of 0.15 ± 0.02 μ M⁻¹s⁻¹ [114]. A full list of the 77 mutants found in the literature is displayed in Appendix B.

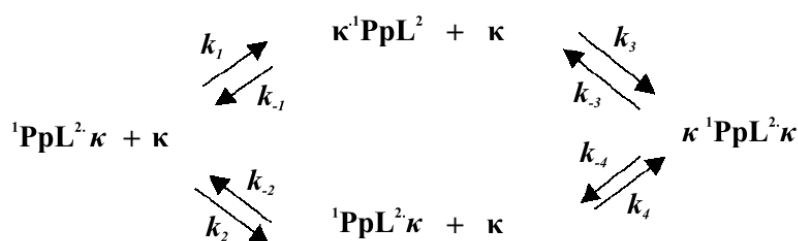


Figure 2-4 Kinetic model – This model shows the kinetics which govern κ -chain binding to PpL₃₃₁₆, complex formation is dependent on the K_d of each of the sites. Image reproduced with permission from [114].

2.3 Current Methods Applied to Conjugate Biomolecules onto Surfaces

It is crucial that micron sized motifs are bioconjugated to the surface of microfluidic devices so that high densities of immobilised protein retain specific recognition properties upon immobilisation. In addition the surfaces should be resistant to non specific protein adsorption. A number of methods have been developed previously to achieve this [44, 58, 115]. In this section potential methods to modify substrates

with protein patterns are discussed and evaluated with respect to attachment of proteins for association with Ig molecules.

2.3.1 Biomaterials Suitable for Protein Patterning

The choice of surface for the development of a microfluidic device for biological applications is of paramount importance. Two of the central material properties to consider are the ease of fabrication and surface chemistry of the substrate. Substrates that have been used in the creation of protein patterns for microfluidic devices include silicon [43], porous silicon [116], silicon nanowires [117], glass [118], quartz [119], gold [120], and polymers [45, 63, 121]. Both silicon and glass benefit from robust fabrication methodology [51]. However devices fabricated from organic polymers are becoming more common, especially as cheaper disposable technology is developed. Silicon, glass and polymer substrates have specific physical and chemical properties, which can be exploited for attachment of protein with distinct benefits and limitations.

2.3.1.1 Methods to Modify Silicon Surfaces

Unlike glass and quartz, silicon is composed of a crystal lattice structure of Si-Si bonds with only a thin oxide layer, approximately $<10 \text{ \AA}$ thick [122], on the surface. Upon removal of the oxide layer terminal hydrogen's of the crystal structure can be directly modified. Wafers of two crystal planes, $<100>$ and $<111>$ (Figure 2-5, see overleaf), are most commonly used for protein patterning. Silicon $<100>$ provides a high density of Si-H groups that can be used in reactions to modify the surface. The disadvantage of silicon as a substrate is that the oxide must be removed from the surface by etching with ammonium fluoride or hydrofluoric acid (HF) leaving hydrogen terminated surfaces. Hydroxylation reactions are most commonly used to modify hydrogen terminated surfaces, as reviewed by Buriak *et al.* [123] and Leftwich *et al.* [124].

Two relevant techniques, for protein patterning applications, which have been used to modify hydrogen terminated surfaces, were demonstrated by Linford *et al.* [125]. The techniques involved direct attachment of monolayers of alkene by photochemical [126, 127] or thermal [125] activation of the hydrogen terminated silicon surface (Figure 2-5, see overleaf). By building on these methods Yin *et al.* [128] achieved a density of 7×10^{12} DNA molecules/cm² on hydrogen terminated

silicon <100> surfaces. The density of DNA hybridised to silicon surfaces was found to be greater than that found on gold (5×10^{12} DNA molecules/cm² [129]) and glass (1×10^{12} DNA molecules/cm² [130]) substrates.

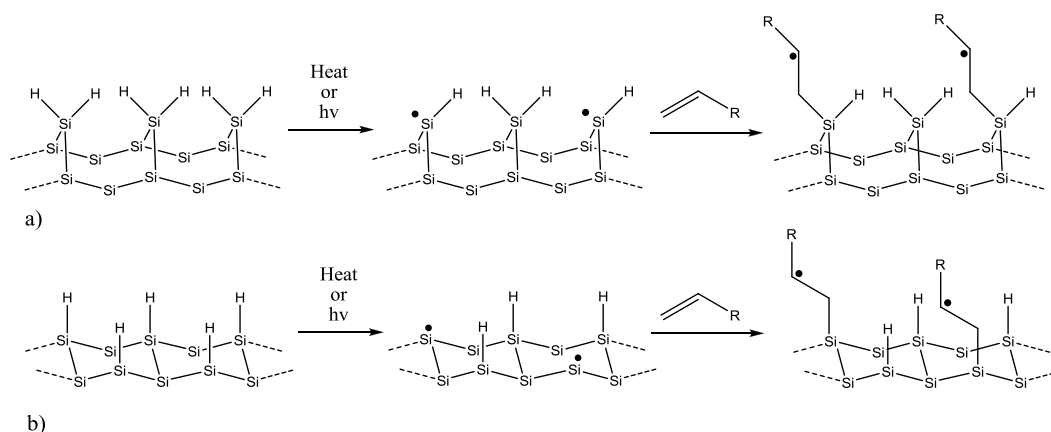


Figure 2-5 Modification of a) silicon <100> and b) silicon <111> by radical initiated alkene hydrosilylation.

Silicon is a crystalline material that is highly pure with a homogeneous surface that is extremely robust [131]. The silicon planes that have been modified, for attachment of biomolecules, are <100> planes and <111> planes, shown structurally in Figure 2-6 (see overleaf). The <111> plane has greater atomic flatness than the <100> plane but only has one dangling hydrogen bond, while the silicon <100> surface consists of Si-H, Si-H₂, and SiH₃ groups [132]. The increased availability of hydrogen bonds increases the reaction efficiency of the alkene with the surface.

In order to attach biomolecules to a silicon surface via a linker it is preferable that the alkyl chain is such that the biomolecule is oriented upwards from the surface. The structures in Figure 2-6 (see overleaf) show the orientation achieved with a bifunctional linker with 11 carbon atoms (undecene) and a bifunctional linker with 10 carbon atoms (decene). The illustration shows that the use of undecene ensures that the biomolecule (R) is orientated perpendicular to the silicon plane [133]. Undecene is therefore commonly conjugated to silicon, as described in previous studies [131-134].

The covalent attachment of linker molecules onto the surface of silicon can be achieved by (i) thermal or (ii) UV activated free radical initiated reaction [125, 126]. The temperature of thermal activation defines the length of time required for the

reaction to occur on the surface. At low temperatures (95 °C) the sample required 16-18 hours for surface conjugation. At higher reflux temperatures (165 °C) the reaction required 2-3 hours to achieve conjugation of an alkene to the hydrogen terminated silicon [135].

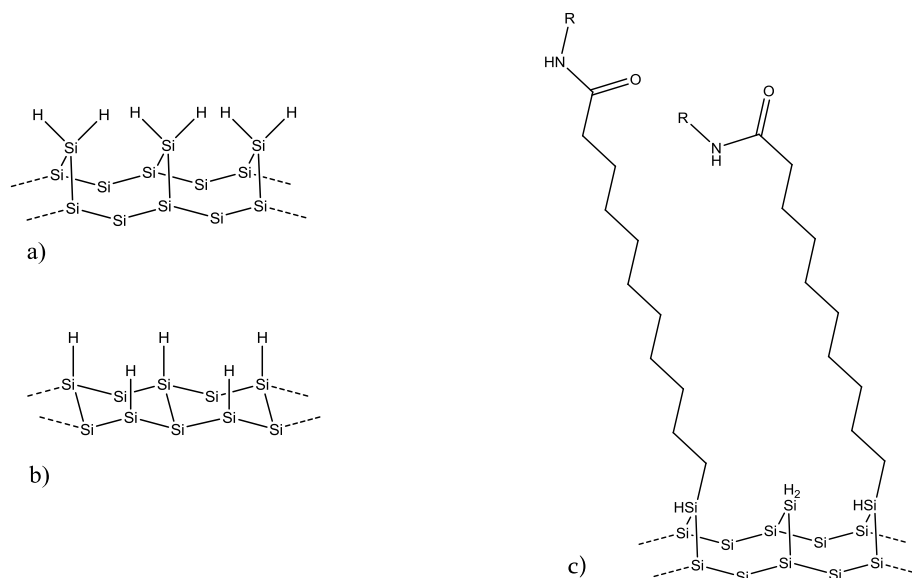


Figure 2-6 Chemical structure of silicon taken at (a) <100> plain and (b) <111> plain (adapted from [136]) (c) after the covalent attachment of biomolecules (R) on silicon <100> with an undecene (left) and decene (right) bifunctional linker.

Activation using UV and visible light has also been used to pattern hydrogen terminated silicon with alkenes. The wavelength of light used has a significant impact on the time required for the conjugation reaction to progress. Visible light was shown by Yang *et al.* [137] to be effective at producing monolayers of alkene, but required a 16 hour illumination time using 447 nm light. By using a high intensity HgXe UV lamp system and a UV power density of 150 mW/cm² Yin *et al.* [131] showed it was possible to attach alkenes successfully in 90 seconds.

Chemical groups other than alkenes can react with hydrogen terminated surfaces, which is important to understand when tailoring the surface chemistry. Initial studies involved the reaction of silicon with un-substituted alkenes, which displayed no side reactions with the surface. More recently it was observed that amino substituted alkenes are incompatible with the hydrosilylation reaction with the surface. Instead the surface can be modified with amine using a protective group, which can be released after attachment [138]. The carboxylic acid moiety of

undecanoic acid has been shown to react with hydrogen terminated silicon under reflux conditions, in mesitylene at 165 °C, but is not seen at 95 °C [139].

The density of biomolecules produced on silicon, compared with other substrates, is of particular importance when considering its application in biosensor technology. With the advent of DNA array technology the ability to produce high density arrays of oligonucleotides for DNA expression profiling has become important [140]. One of the substrates that have been used for DNA microarray methods is silicon, largely because of the low autofluorescence, inert surface, and high density patterning properties of silicon.

The density of DNA molecules that can hybridise with a complementary sequence, conjugated to silicon, was found to be 7×10^{12} molecules/cm² [128]. Hybridisation to gold and glass was observed to be lower compared with silicon, with densities of 5×10^{12} molecules/cm² [129] and 1×10^{12} molecules/cm² [130] respectively. With respect to protein conjugation to silicon surfaces, Cha *et al.* [141] modified hydrogen terminated silicon to introduce a PEG-NHS linker on the surface. A surface density of $\sim 2 \times 10^{13}$ molecules/cm² of green fluorescent protein [141] and $\sim 1 \times 10^{11}$ molecules/cm² of antibody [142, 143] has been reported. On gold, surface densities of 6.0×10^{11} [144] and recently 5.8×10^{12} molecules/cm² [145] have been reported. Glass surfaces modified with a novel protein linker gave a surface density of between 5.4 - 6.8×10^{12} molecules/cm² [146]. The values in Table 2-4 show the densities achieved on surfaces using state-of-the-art surface modification techniques. The potential for producing high densities of active biomolecules makes silicon an attractive substrate for the development of biosensor technology.

Substrate	Density (molecules/cm ²)	References
Silicon	DNA - 7×10^{12}	[128]
	Antibody - 1×10^{11}	[143]
Gold	DNA - 5×10^{12}	[129]
	Antibody - 5.8×10^{12}	[145]
Glass	DNA - 1×10^{12}	[130]
	Antibody - 6.8×10^{12}	[146]

Table 2-4 Table showing reported densities of biomolecules on silicon, glass and gold substrates.

2.3.1.2 Methods to Modify Silicon Oxide Surfaces

Silicon (with a native silicon oxide layer), glass, and quartz surfaces can all be chemically treated with silane coupling agents. These molecules chemisorb onto the surface and subsequently react with the Si-OH groups that are on the substrate surface. Standard coupling agents are organosilanes ($R-SiX_3$), where R is an organic functionality that can be modified for protein cross-linking and X is a hydrolysable group. The most common silane coupling agents are chlorosilanes or alkoxy silanes, which produce self assembled monolayers (SAMs) of alkylsiloxanes [147].

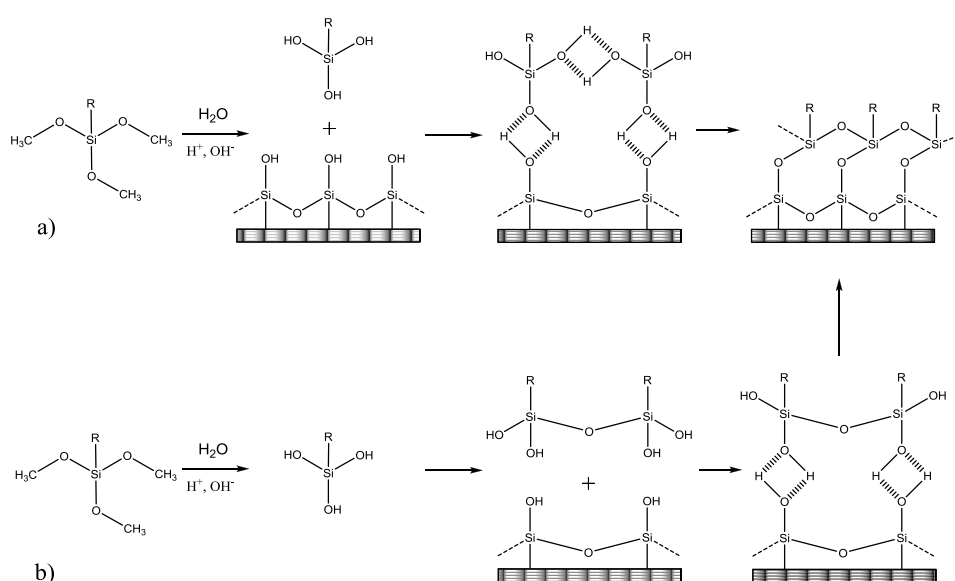


Figure 2-7 Structure representation of silanisation depicting condensation reactions between (a) surface hydroxyls prior to reaction between surface bound silanol's and (b) free silanol's prior to reaction with surface bound hydroxyl groups.

The process of silane bonding onto glass can occur via two primary mechanisms, as illustrated in Figure 2-7. The first mechanism (Figure 2-7(a)) involves the hydrolysis of the silane followed by chemisorption with surface hydroxyl groups. This is preceded by a potential condensation reaction to covalently couple the silane to the surface, or reaction between surface bound silanes to form a siloxane network. The second process (Figure 2-7 (b)) occurs in much the same manner except after the silane is hydrolysed, a solution phase polymerisation reaction occurs between free silanes. The polymer network formed can then chemisorb onto the surface and form a covalent attachment between the surface and the polymer network.

The extent of polymerisation is dependent on the water content in solution, as this determines the rate of silane hydrolysis. Wang *et al.* [148] reported monolayer growth with 1 Å root-mean-square roughness under dry growth conditions, but a long growth time of 2 days. Under wet conditions, smooth monolayers were not seen as silane aggregates were formed in solution prior to surface adsorption. The adsorption of aggregates is much faster and surfaces can be altered within hours. Work by Siberzan *et al.* [149] has shown that the monolayer formed is based upon a siloxane network with a water layer between the substrate and the network connected by a series of bridged covalent bonds [150]. The siloxane network remains extremely robust to many conditions including acid and solvent without noticeable degradation. Alkaline conditions have been shown to degrade the monolayer, due to hydrolysis of the Si-O-Si bond [151]. Applications involving the use of biomolecules generally use a pH close to physiological pH (7.4) as it is more appropriate to prevent the protein from denaturing.

Temperature also plays an important role in the production of uniform monolayers on glass surfaces. The incorporation of a baking step before or after silanisation has been shown to effect the uniformity of monolayers [152]. Heat catalyses the condensation reaction between the hydrated glass surface and the silane, as well as between the adjacent silane molecules. Use of organosilanes is not only applicable to glass surfaces but has been used for gold [153], polymer [154, 155], and metal oxide [156] surface modification. The variety of functional groups compatible with silanisation chemistry makes it an attractive mechanism for protein attachment.

2.3.1.3 Methods to Modify Polymer Surfaces

Use of polymers for microfluidic applications has progressed rapidly in the last decade, due to low material costs and the variety of chemical and physical properties that can be achieved with polymers [45, 157]. The most widely used polymer for the fabrication of microfluidic devices is poly(dimethylsiloxane) (PDMS), a synthetic polymeric organosilicon compound. Fabrication is usually based upon soft lithographic technology, developed by Whitesides [158], and provides a method to produce micro- and nano-structures.

Methods for the surface modification of PDMS are reviewed by Makamba *et al.* [159]. The two primary approaches used to modify the surface are surface oxidation [155] and radical induced grafting [159]. Oxidation can be achieved using an oxygen plasma [160], UV light [161], corona discharge [162] or chemically [155] to form a Si-OH surface. The surface can then be modified using silanisation techniques as discussed previously in §2.3.1.1. Alternatively, the polymer can be modified by the grafting of chemical groups to the surface using a free radical initiated reaction between the polymer and a suitable chemical. This mechanism of free radical polymerisation is illustrated in Figure 2-8. The energy applied to the surface results in the formation of a free radical capable of inserting within the C=C bond to form a covalent bond with the surface.

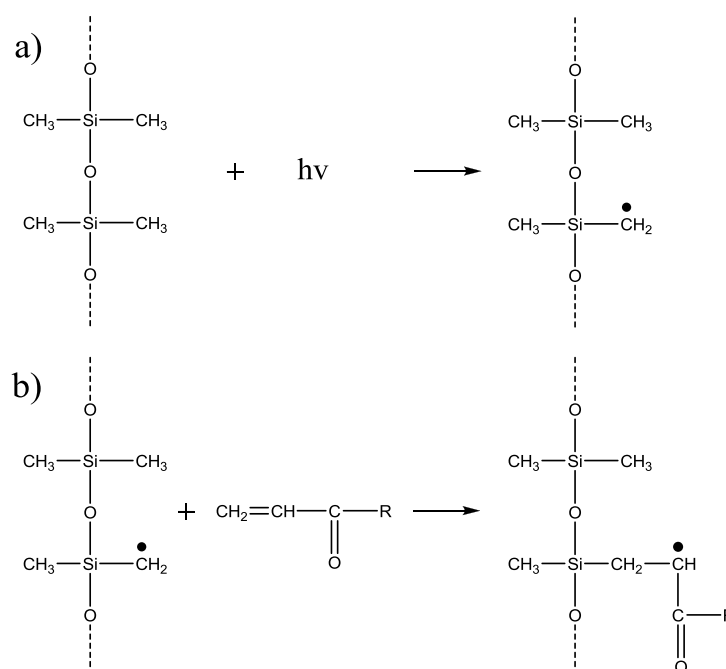


Figure 2-8 UV radical initiated graft polymerisation reaction scheme on a PDMS surface a) Formation of radicals on PDMS by UV light b) Initial step of radical initiated polymerisation (adapted from [163])

2.3.1.4 Evaluation of Substrates for Application to Protein Patterning

The research presented in this thesis focuses on the use of silicon and glass as substrates to pattern high density protein patches upon, for future integration within a microfluidic POC device. The high density of biomolecules previously patterned on silicon warrants the investigation to determine whether high densities of protein can be achieved. Glass surfaces offer a cheaper alternative to silicon.

Both glass and silicon have been used extensively in the fabrication of microfluidic devices [50, 51, 57]. Choosing a substrate ubiquitous with microfabrication techniques is beneficial, to the realisation of a microfluidic channel device, as micron scale processing methods are already developed.

2.3.2 Prevention of Non Specific Protein Adsorption

When considering what substrate is best suited for the development of protein patterns it is important to understand how proteins interact with surfaces and the physiological properties that affect the process. Properties that affect protein adsorption include charge, surface roughness, pH, ionic strength, and analyte concentration. These parameters alter the hydrophobic, electrostatic, and Van der Waals interactions between proteins and surfaces [164]. The main driving force for protein adsorption is the potential gain in entropy on interacting with a surface. Hydrophobic surfaces are most susceptible to biofouling as a result of hydrophobic domains of the protein interacting with the surface, which results in the rearrangement of domains within the protein structure leading to the protein unfolding on the surface [165].

Unlike hydrophobic interactions, which are predominantly based on the hydrophobicity of the surface, electrostatic interactions vary greatly for individual proteins. Surfaces and proteins can both have charge, which, when no external electric field is present, is largely dependent on the pH of the surrounding aqueous solution. Both surfaces and proteins have an isoelectric point (pI) defined as the pH at which a molecule or surface carries no net charge. The pI of silicon dioxide is ~ 2 which means that when the surface is in contact with a solution of pH greater than 3, hydrogen, from surface hydroxyl groups, will dissociate leaving a negatively charged surface [166].

Proteins also exhibit a net charge that is governed by the amino acid sequence of the protein and the number of ionisable residues interacting with the aqueous environment. The pIs of different amino acids, which are the structural monomer of proteins, are shown in Table 2-5 (see overleaf). At neutral pH (pH 7) Arg, Lys and His carry a net positive charge, while Asp and Glu have a net negative charge. Changes to the pH of an aqueous solution will have an effect on the net charge of a protein. Thus a negatively charged surface will adsorb proteins with a

net positive charge and repel proteins with a net negative charge [167]. The same effect is seen in polymer brushes that contain ionisable groups [168]. When ionised the structure of the brush changes as electrostatic forces modify the brush layer, as illustrated in Figure 2-9. Concurrently the ionic strength of a solution will alter the electrostatic interactions between ionisable groups, causing a reduction in the Coulomb effect at high ionic strength. The change in electrostatic forces has been used within microfluidic devices to produce an adsorption switch [169]. Suitably charged proteins adsorb onto the surface, through electrostatic interactions, while proteins without the suitable charge continue to flow through the microfluidic channel. The pH of the input solution can then be changed to alter the electrostatic properties of the protein or surface, leading to the release of a purified protein [168]. This technique is limited in solutions containing multiple proteins as different proteins can have the same charge reducing the specificity of capture. Therefore surfaces with ionisable groups are not suitable for the prevention of non specific protein adsorption of all proteins.

Amino Acid	pI	Amino Acid	pI
Alanine (Ala)	6.02	Leucine (Leu)	5.98
Arginine (Arg)	10.76	Lysine (Lys)	9.74
Asparagine (Asn)	5.41	Methionine (Met)	5.75
Aspartic Acid (Asp)	2.87	Phenylalanine (Phe)	5.48
Cysteine (Cys)	5.02	Proline (Pro)	6.10
Glutamic Acid (Glu)	3.22	Serine (Ser)	5.68
Glutamine (Gln)	5.65	Threonine (Thr)	6.53
Glycine (Gly)	5.97	Tryptophan (Trp)	5.88
Histidine (His)	7.58	Tyrosine (Tyr)	5.65
Isoleucine (Ile)	6.02	Valine (Val)	5.97

Table 2-5 Table showing the isoelectric point of different amino acids

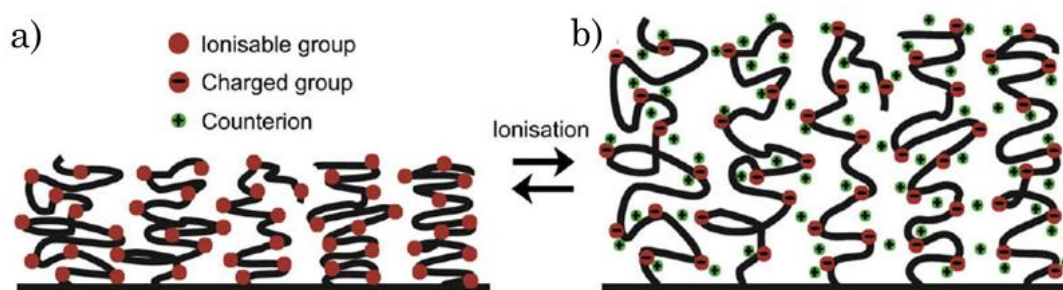


Figure 2-9 Polyelectrolyte brush coating exhibiting neutral collapsed (a) and ionised expanded state (b) (Reprinted with permission from [168])

Modification to the topography/roughness of a surface can have an effect on the non specific adsorption of protein. Work by Chen *et al.* [170] showed a 46 % increase in fibrinogen adsorption despite a surface area increase of only 8 %. This is not true for all proteins [171], Rechendorff *et al.* [172] showed a high increase in fibrinogen adsorption compared with the surface area increase, while the same surface had negligible adsorption increase with bovine serum albumin (BSA). The process is rather more dependent on the supramolecular assembly of the protein on the surface, which can change with surface roughness [173].

One of the greatest challenges when producing a surface that is resistant to proteins is finding a material that can prevent non specific adsorption of a wide variety of proteins that have different adsorption properties. Chapman *et al.* [174] listed a series of criteria for a successful surface spacer to resist biofouling. Properties included: being hydrophilic, containing H-bond acceptors, not containing H-bond donors and being electrically neutral. Both naturally occurring and synthetic polymeric compounds have been used that meet the outlined criteria. Surfaces include poly(2-hydroxyethyl methacrylate) [175], polyacrylamide [176], dextran [177], pullulan [178], and poly(ethylene glycol) (PEG) [179] have been used to prevent biofouling of surfaces exposed to biomolecule solutions.

Three adsorption mechanisms were described by Halperin *et al.* [180] regarding the interaction of proteins with polymeric surfaces. Primary adsorption can be described as the compression of a polymeric chain, by the protein, to form an interaction with the surface. Secondary adsorption is based on Van der Waals interactions between the protein and the polymeric layer. Finally, ternary adsorption is attributed to smaller proteins, which are capable of interacting within the layer [180, 181]. The illustration in Figure 2-10 (see overleaf) shows the three types of protein adsorption that can occur with polymeric brush layers designed to reduce non specific protein adsorption.

Two materials widely used to prevent non specific protein adsorption are PEG and dextran, illustrated in Figure 2-11 a and b (see overleaf) respectively, which form a hydrophilic layer when conjugated to surfaces [182-184]. PEG is particularly well characterised and has been modified to form linear SAMs [185], polymeric brushes [186] and star-shaped configurations [187], each of which have been covalently attached to surfaces. Dextran has found considerable use in the

development of surface plasmon resonance sensors [188, 189], and has been modified to form aminodextran [190] and carboxymethyl dextran (CMD) surfaces [191]. Both polymers resist proteins by shielding the surface with a well solvated layer that inhibits interactions with the underlying substrate. The effectiveness of PEG has been shown to depend on chain density and thickness [192].

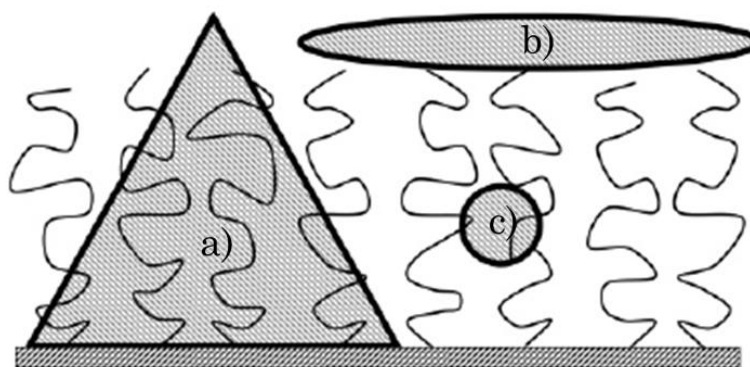


Figure 2-10 Illustration of protein adsorption at surfaces carrying PEG brushes, which may occur via three modes: (a) Primary adsorption involving an attractive contact with the surface. Here, this case is illustrated for a partially inserted protein shaped as a triangular wedge as suggested by recent models of BSA. (b) Secondary adsorption at the outer edge of the brush due to van der Waals attraction to the surface. (c) Tertiary adsorption of protein within the brush itself as a result of weak PEG-protein attraction. This is illustrated for a small globular protein of spherical shape. (Reprinted with permission from [180])

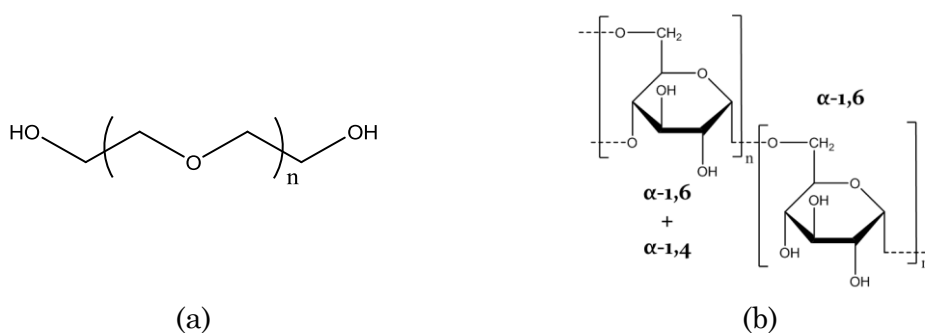


Figure 2-11 Chemical structure of the repeating polymeric units of a) PEG and b) Dextran

The work presented in this thesis involved the use of dextran as a material to prevent the non specific adsorption of protein. PEG was rejected as work has shown that PEG is prone to oxidation [193, 194]. In the case of PEG oxidation carboxyl groups are formed that can form charged surfaces, which is detrimental to the long term performance of the prevention of biofouling. Dextran has been shown to remain stable for at least 2 months within aqueous solutions [177], which is important for the long term aims of the work presented. Any surface proposed for use in the quantitative analysis of biomarkers, for diagnostic applications, needs to

be extremely stable over the long term. This is to ensure that diagnosis is accurate with no risk of false positives that could lead to a misdiagnosis.

2.3.3 Immobilising Proteins on Surfaces

The number of techniques to conjugate patterns of protein onto surfaces has increased significantly in the past decade, witnessed by the number of reviews published on current state-of-the-art techniques [44, 47, 195]. Each method has specific advantages and disadvantages and the choice is often tailored to the protein of interest. Table 2-6 shows the potential chemistries commonly available on the surface of proteins, which bioconjugation methods are customised too. These include the N-terminus and C-terminus of the protein, which are the amino and carboxyl terminations of the protein polypeptide chain respectively.

Side Groups	Amino Acids
NH ₂	Lys, N-terminus
SH	Cys
COOH	Asp, Glu, C-terminus
OH	Ser, Thr

Table 2-6 Functional groups, found in proteins, exploited to conjugate proteins to surfaces

The main considerations for attachment chemistry are specificity, orientation, and retention of protein recognition properties. The ideal method for attaching proteins includes: a single attachment site upon the protein, forming a homogeneous protein orientation, and immobilising protein with recognition properties equivalent to protein *in vivo*.

2.3.3.1 Physical Adsorption as a Method to Conjugate Proteins to Surfaces

To reiterate, proteins have the capacity to be adsorbed onto surfaces due to interactions between the protein and the surface. The large variation in possible attachment mechanisms results in a heterogeneous layer of protein on the surface. The thickness of the layer will depend on the protein and how it interacts with the surface.

Often an initial layer of protein will denature onto the surface followed by further concentration dependent protein adsorption that forms a secondary protein layer [196]. Not all proteins that adsorb to a surface will necessarily completely

denature and can retain all or partial activity. The method described by Bayiati *et al.* [197] demonstrates the adsorption of BSA-biotin and rabbit γ -globulin that retain binding recognition with streptavidin and anti rabbit IgG respectively. Physical adsorption, as a method to pattern proteins, has specific disadvantages. The fundamental problem is a failure to reproduce the protein orientation on the surface. On adsorption the protein layer has a heterogeneous orientation, which may affect the protein recognition properties and the density of protein bound to the surface. The inability to produce a surface with a reproducible protein orientation, density and recognition properties makes adsorption incompatible for the proposed application.

2.3.3.2 Covalent Attachment as a Method to Conjugate Proteins to Surfaces

The most common attachment technique for producing protein patches with defined orientation, density, and stability is covalent attachment. Covalent chemistry produces a strong covalent bond between the surface and the protein. The surface chemistries of proteins can be targeted specifically to form desired covalent bonds. Amine chemistry is commonly used for the covalent attachment of proteins to surfaces [198, 199]. One reaction used to couple protein using amine chemistry involves *N*-hydroxysuccinimide (NHS) esters that react with primary amines to form amide bonds, with efficient coupling at neutral pH (pH 7). Accessible α -amine groups present on the N-termini of proteins and ϵ -amines on Lys residues react with NHS-esters to form an amide bond [200] (Figure 2-12).

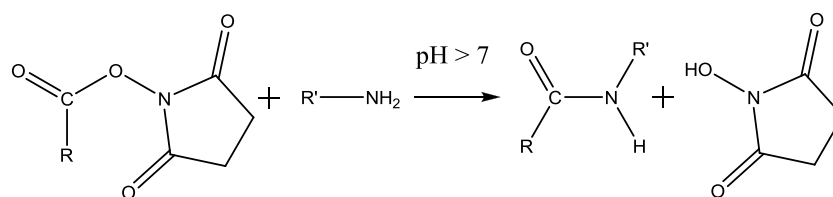


Figure 2-12 Chemical illustration of the amide bond formed by the reaction between an NHS-ester and an amino group.

Hydrolysis of the NHS-ester competes with the primary amine reaction. The hydrolysis rate increases with increasing pH and occurs more readily in dilute protein solutions. Studies performed on NHS-ester compounds indicate the half-life of hydrolysis for a NHS-ester is 12 minutes at pH 7.5 in water at 23 °C, decreasing to 1 minutes at pH 9.1 [201]. NHS-esters can be grouped into two separate classes with essentially identical reactivity towards primary amines: water-soluble and water-

insoluble. Water-soluble NHS-esters have a sulfonate ($-\text{SO}_3$) substitution. They are advantageous when the presence of organic solvents cannot be tolerated [195]. The reaction with the sulfo-NHS-esters is performed in aqueous solutions; however, it is possible to achieve greater solubility when the reagent is dissolved in organic solvents such as dimethyl sulfoxide (DMSO).

Alternatively an amine can react with aldehyde or oxirane chemistry to form a covalent bond. The aldehyde reaction, developed by MacBeath and Shreiber [202], forms a Schiff base (Figure 2-13) that can be reduced from an imine to a secondary amine by hydrogenation. The simplest oxirane, epoxide, can be used to conjugate amines and other weak nucleophiles (sulfhydryl and hydroxyl groups) in a ring-opening process [150, 203, 204]. The process requires long reaction times, especially with weak nucleophiles, but can be catalysed by using alkaline conditions. The reactions of the oxirane with amine, hydroxyl, and sulfhydryl groups create secondary amine, thioether, or ether bonds respectively.

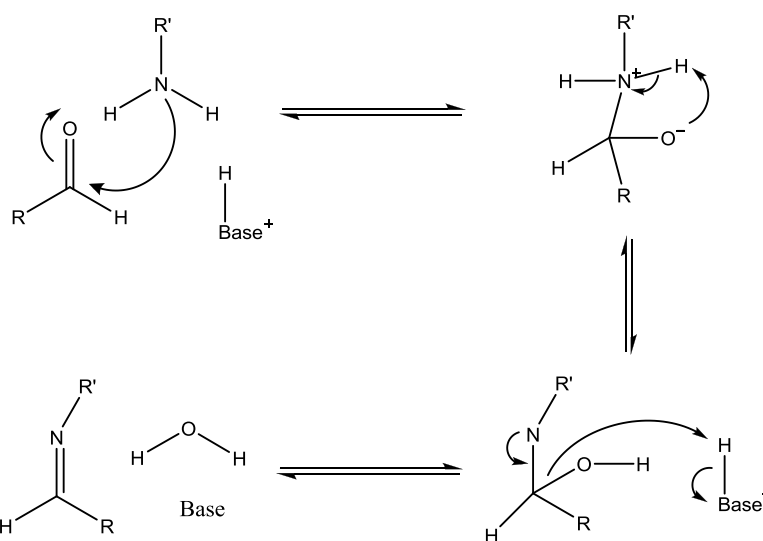


Figure 2-13 Structural illustration of the Schiff base formed by the reaction between an aldehyde and amine moiety.

Sulfhydryl groups can also react with maleimides between pH 6.5 and 7.5 to form a stable thioether linkage (Figure 2-14, see overleaf). The maleimide will also react with an amine at this pH but the reaction with sulfhydryl is favoured. The reaction with sulfhydryls is 1,000-fold faster than with amines at neutral pH, but at a pH >8.5, the reaction favours primary amines [205]. Hydrolysis of maleimides to a non-reactive maleamic acid can compete with thiol modification, especially above pH

8.0. Thiols must be excluded from reaction buffers used with maleimides because they will compete for coupling sites.

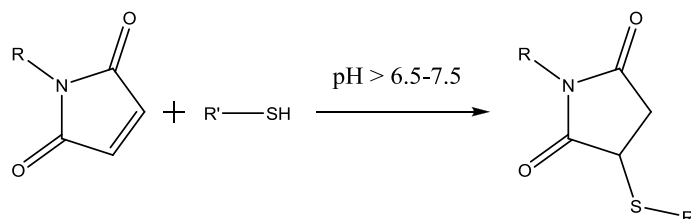


Figure 2-14 Structural illustration of the thioether bond formed by the chemical reaction between a maleimide group and thiol chemistry.

The α -haloacetyl cross-linkers contain the iodoacetyl group that react with sulfhydryl groups at physiological pH. The reaction of the iodoacetyl group with a sulfhydryl proceeds by nucleophilic substitution of iodine with a thiol producing a stable thioether linkage (Figure 2-15) [206]. Histidyl side chains and amino groups react in the deprotonated form with iodoacetyl groups above pH 5 and pH 7, respectively. Work by Wetzel *et al.* [207] describes modification of N-terminal α -amino with 90-98 % selectivity using reversible protection of cysteine residues. The main limitation of using haloacetyls is the reactivity of the compound to different nucleophiles and the potential production of iodine as a by-product. Iodine can undergo a substitution reaction with hydrogen from tyrosine, histidine and tryptophan residues [195].

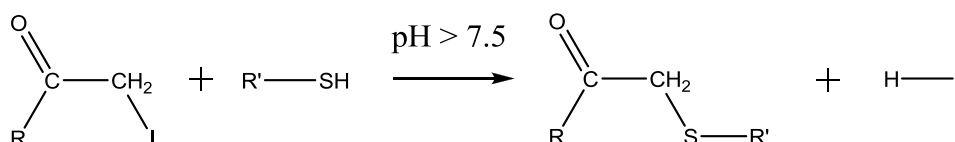


Figure 2-15 Structural illustration of the thioether bond formed by the chemical reaction between an active halogen and a thiol group.

Another potential method for the covalent conjugation of proteins involves the use of photoactivatable groups, particularly organic azides. Organic azides were first discovered by Peter Griess in 1864 and since then have become a valuable intermediate in organic synthesis. The review by Bräse *et al.* [208] documents 602 published papers on the use of organic azide chemistry, representing a huge area of research. This section will detail the reactivity of the products of azide photoactivation and how they react to conjugate protein.

Aryl azides consist of an azide moiety conjugated to an aromatic group that helps to stabilise the azide chemistry [209]. Upon photolysis the azide is converted into a reactive nitrene, which can react through different pathways with a protein. Aryl nitrenes are very reactive short-lived intermediates commonly, but not exclusively, generated by the decomposition of aryl azides. Figure 2-16 shows a chemical structure of two potential pathways of the aryl azide as described by Gritsan and Platz [210]. The aryl azide (1) on illumination forms the reactive singlet phenylnitrene ($^1\mathbf{3}$), which can undergo rearrangement to form the triplet phenylnitrene ($^3\mathbf{3}$) or benzazirine (4). The benzazirine can undergo further rearrangement to form a cyclic ketenimine (5). It is the intermediates (3-5) that can react with the protein to form a covalent link. The singlet nitrene ($^1\mathbf{3}$) can undergo an insertion reaction with C-H groups leading to hydrogen extraction or can form a triplet nitrene, which can dimerise to form the AZO compound shown in Figure 2-16. The cyclic ketenimine can react with primary and secondary amines, found on Lys residues and at the N-terminus of proteins, to form an azepine (2).

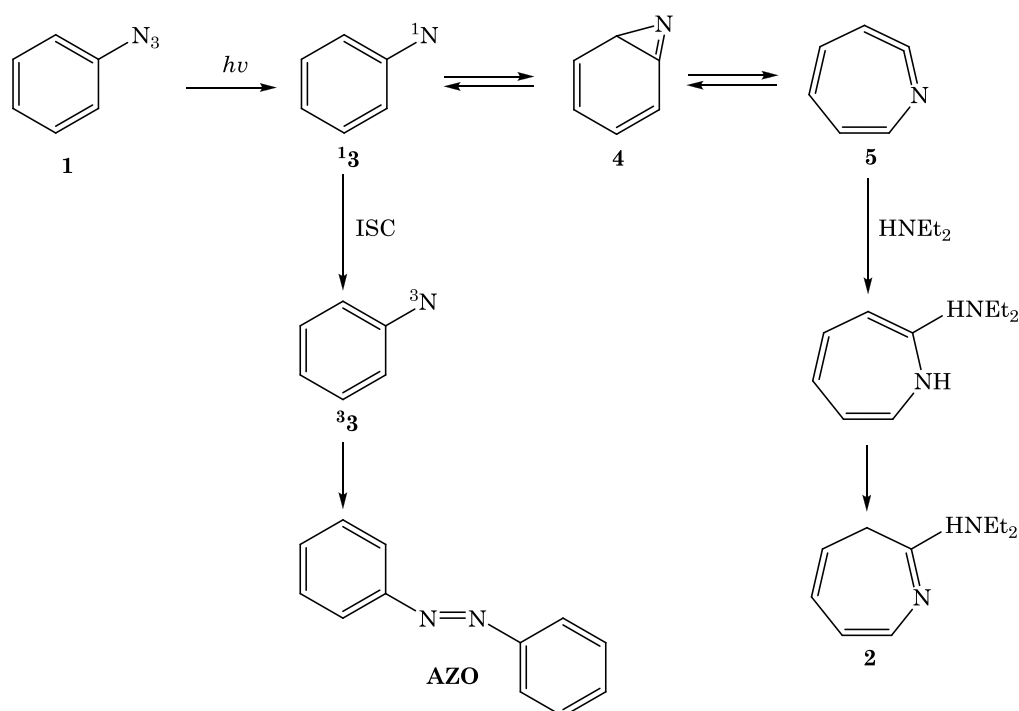


Figure 2-16 Chemical structure diagram showing the potential reaction mechanisms exhibited by phenylnitrene photochemistry (Reprinted with permission from [210]).

For use as crosslinkers four predominant aromatic groups are found in the literature: phenyl azide [211], hydroxyphenyl azide [195], nitrophenyl azide [212]

and perfluorophenyl azides [213]. They have been used in formation of organic polymers [214], protein labelling [215] and surface modification [211].

One of the ultimate challenges in the development of protein patterning technologies, suitable for microfluidic applications, is the development of a surface chemistry that is compatible with the attachment of multiple proteins. Reproducible adjacent patterns that have low levels of non specific binding are essential. Park *et al.* [46] describes the synthesis of new “photochemical surface delivery vehicles” as being ideal for the quantitative control of surface properties at the molecular level. The cyclic ketenimine formed upon photoinitiation of aryl azides offers a route to conjugate proteins via its amino groups.

Photochemical reactions can be used to covalently attach proteins to surfaces, while also allowing the site specific attachment by controlling the area of illumination. The photo-initiated method of patterning is based on surfaces presenting a chemistry that when activated by light undergoes chemical transition. This chemical transition can initiate the activation of a specific region of the surface that can be used to directly conjugate the protein. An example of this technique, described by Monsathaporn *et al.* [216], is the production of electrophilic azidoformate SAM on silicon. When subjected to UV light, in a solution of cyclohexane, the azidoformate SAM undergoes hydrogen abstraction to form carbamate terminated SAMs. Subsequently, a UV mask could be used to selectively pattern non-reactive groups leaving a back pattern of reactive azidoformate SAMs.

Dillmore *et al.* [217] studied the attachment of ligands to nitroveratryloxycarbonyl (NVOC) protected hydroquinone terminated alkanethiolates derivatised on gold substrates. An alkanethiolates mixture was used including NVOC protected hydroquinone and oligo(ethylene glycol) alkanethiols, the latter protecting the monolayer from non-specific protein adsorption. The NVOC protective group is removed by illumination at 365 nm revealing the hydroquinone group. This group is then oxidised chemically or electrochemically to form benzoquinone, without disrupting the remaining NVOC protected hydroquinone. The benzoquinone can then react with cyclopentadiene conjugate ligands via a Diels-Alder reaction. The Diels alder reaction involves a cyclopentadiene linker which is attached to the N-termini of the peptide. The glass surface is derivatised with alkanethiol SAMs containing benzoquinone groups (dienophiles). The resulting

reaction between the diene linker and the dienophile produces a covalent bond that is site-specific [218]. The problems associated with this technique involve the conjugation of the diene and peptide, as the unnatural moiety is synthetically challenging to produce. This technique requires an azido group to be formed as either a main chain or side chain group of a peptide or protein. The photo product produced on azide activation can then react with phosphinothioester immobilised surfaces to form an amide bond. This technique has already been used on the model protein Ribonuclease S' with an immobilisation time of less than a minute and a retention of 92 % protein activity. The advantage of this technique is that the methods for creation of azido proteins are already established [219].

Covalent attachment of protein is well suited to the production of stable, high density, orientated protein patterns. The amine and sulfhydryl groups, present on the surface of proteins, are of particular use for the covalent attachment of proteins as there are well defined chemical reactions specific to these groups. Limitations of amine and sulfhydryl chemistry are a requirement of aqueous environments to perform modifications. The site of conjugation between the protein and the surface is dependent on the number and distribution of side chains on the protein surface that can react to conjugate the protein. The number and distribution of conjugation sites will contribute to how reproducible a protein patches properties are on the surface, which is a fundamental requirement of the proposed research.

2.3.3.3 Affinity Immobilisation as a Method to Conjugate Proteins to Surfaces

Proteins can have, or be modified to present, chemical groups that have highly specific recognition properties with a surface bound molecule. The process involves patterning the surface with a molecule that has a high affinity for the protein of interest. The strong binding affinity between the two molecules can immobilise the protein on the surface. A well characterised affinity reaction is the biotin-avidin interaction that has one of the strongest known naturally occurring affinity interactions in biochemistry with a dissociation constant (K_d) of 10^{-15} M [220]. The interaction has been used in microarray technology as a means of producing ordered protein arrays on avidin derivatised slides (Figure 2-17, see overleaf). Using the intein fusion system [221], proteins fused by a C-terminal thioester to intein can undergo selective cleavage using a biotinylated thiol-cleaving reagent (Cys-biotin).

This forms a bond between the thiol and the Cys releasing the protein from the intein before undergoing spontaneous rearrangement. The biotinylated protein can then be attached, site-specifically, to avidin derivatised glass slides.

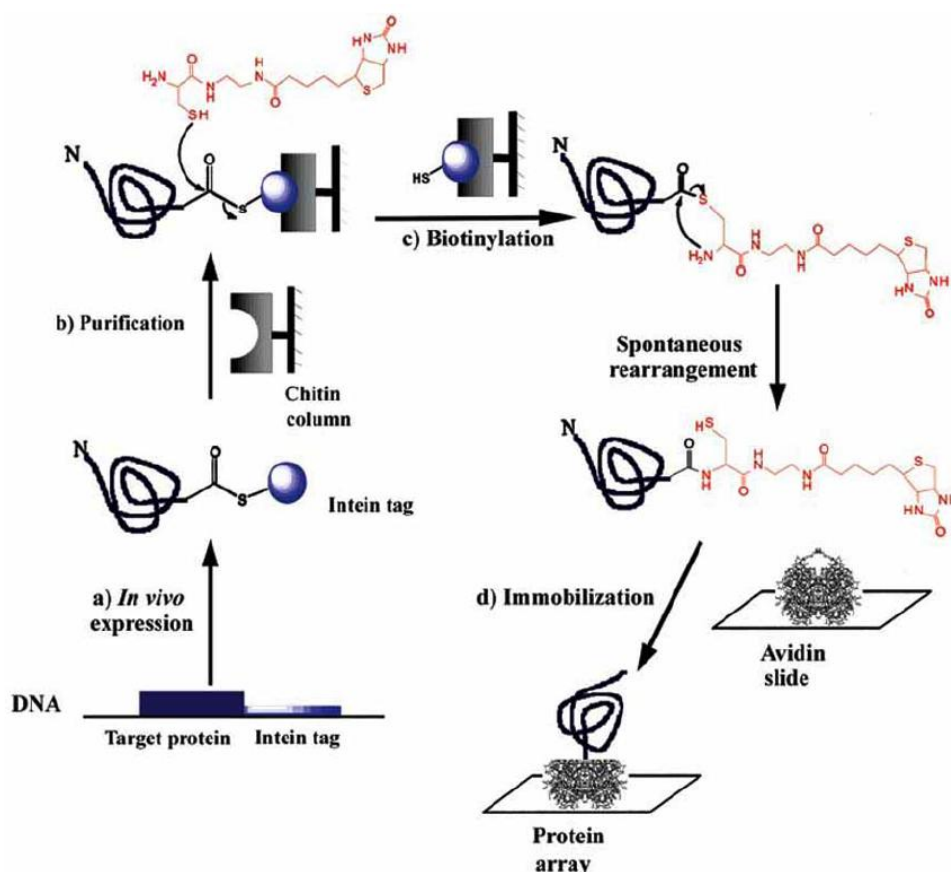


Figure 2-17 Strategy for the biotinylation of protein using the intein-fusion system for immobilisation of protein on to avidin derivatised glass slides (Reprinted with permission from [222]).

An alternative method is the production of recombinant proteins that have a polyhistidine tag (His-tag), which can be purified by affinity chromatography. The His-tag has a high affinity for nitrilotriacetic acid in the presence of Ni^{2+} . Nickel-nitrilotriacetic acid coated slides have been used to capture these recombinant proteins specifically [223]. Copper ions (Cu^{2+}) have also been used to immobilise His-tag protein by linking with a chelating iminodiacetic acid group. The work by [141] incorporates a PEG coated $\text{Si}\langle 111 \rangle$ coated slide that is terminated with iminodiacetic acid (IDA) groups. The resulting Cu^{2+} -IDA-mPEG-Si $\langle 111 \rangle$ surface was shown to specifically bind His-tag protein as well as green fluorescent protein and sulfotransferase.

Affinity based mechanisms have the advantage of being very specific to the two interacting molecules, thus reducing non specific binding. Recombinant proteins can have a single His-tag introduced onto the protein, which means the protein can be orientated on the surface. The disadvantage of using affinity based systems is the modification required to form the affinity interaction. Not all proteins remain stable when modified with a His-tag and the introduction of a biotin moiety onto a protein may alter the recognition properties of the protein.

2.3.3.4 Evaluation of Methods to Conjugate Proteins

The covalent attachment of a protein onto a surface forms a stable linkage and the number of orientations can be limited by attachment using a single chemistry found on the protein. There are a number of potential reactions that can be used to form a covalent bond with proteins. Amine groups are routinely used for attaching proteins as they are more commonly found on proteins compared with sulfhydryl groups. Therefore attachment using amine chemistry is preferred as there is no need to modify the protein structurally prior to attachment, which may have an effect on the recognition properties of the protein. Conjugation of proteins upon reaction with NHS-esters can be achieved at neutral pH, which is desirable to prevent protein denaturation from high or low pH conditions. Physical immobilisation is not suitable for the proposed application as the layer produced has a heterogeneous protein orientation which may affect the accessibility of analyte to the surface immobilised protein. Altering the protein chemically to provide attachment using affinity based immobilisation risks changing the proteins recognition properties.

2.4 Microfabrication for Protein Patterning Applications

The conjugation of protein in micron or nanometre scale patterns to surfaces requires development of extremely precise techniques for fabrication. During the conjugation reaction the protein must not be exposed to conditions that cause denaturation or photodegradation. This includes controlling pH and salt content of organic media and preventing the use of high temperatures in processing the surface. If patterns of different proteins are to be conjugated in separate motifs, then either sequential or parallel fabrication steps are necessary. For the

application described in this thesis, micron-scale pattern resolution is required. This section discusses the current state-of-the-art techniques used for protein conjugation to surfaces in micron-scale motifs.

With the advent of DNA and protein microarray technologies, significant effort has been focussed upon improvement of the bioconjugation of biomolecules on surfaces in motifs [224, 225]. Fabrication processes have been developed where dense, reproducible patterns have been achieved on a variety of different substrates with submicron and micron scale resolution. The different methods can be separated into two main categories: contact and non-contact lithography. Contact involves a physical interaction with the surface; while for non-contact no physical interaction is required.

2.4.1 Contact Lithography

In 1998 Xia and Whitesides [158] reviewed the development of a non-photolithographic technique for patterning surfaces with submicron features termed soft lithography. Soft lithography is a biocompatible technique that utilises a soft elastomeric “stamp” with micron-scale patterned relief structures [226]. Elastomeric materials are utilised as they can make conformal contact with non-planar surfaces. Fabrication of stamps often involves the creation of a master which is used to cast stamps [227]. Micro contact, microfluidic and stencil patterning are potential methods that apply soft lithography techniques to pattern biomolecules on surfaces with micron scale resolution [228, 229]. More recently nanoparticle and dip pen lithography have been used as an alternative to the classic photolithography process [230]. Nanoparticle lithography takes advantage of the self assembly properties of particles on surfaces that can be used as a mask to pattern the surface [231] or as a mask for etching the surface (including deep RIE [232]). Dip pen lithography uses an atomic force microscopy (AFM) tip as a scribe mechanism to pattern the surface [233]. Each of the contact patterning techniques is discussed in detail below.

2.4.1.1 Micro Contact Printing for Patterning Surfaces

The fabrication of stamps used in microcontact printing (μ CP) is a well documented process adapted from the silicon microprocessor fabrication techniques [234]. A silicon or glass wafer is spin coated with a thin layer of photoresist, which is a viscous material that is sensitive to UV light, and can be patterned by UV

photolithography. UV light is illuminated through a patterned mask, often composed of chrome/gold, onto the photoresist. Negative photoresist, for example Microchem SU-8 10, undergoes a crosslinking reaction upon exposure to UV light; any un-crosslinked photoresist can then be removed with a specific solvent to develop the pattern. The patterned photoresist can then be used for casting of PDMS directly [235] (Figure 2-18), or as a mask for deep reactive ion etching of silicon to form a patterned silicon template [236].

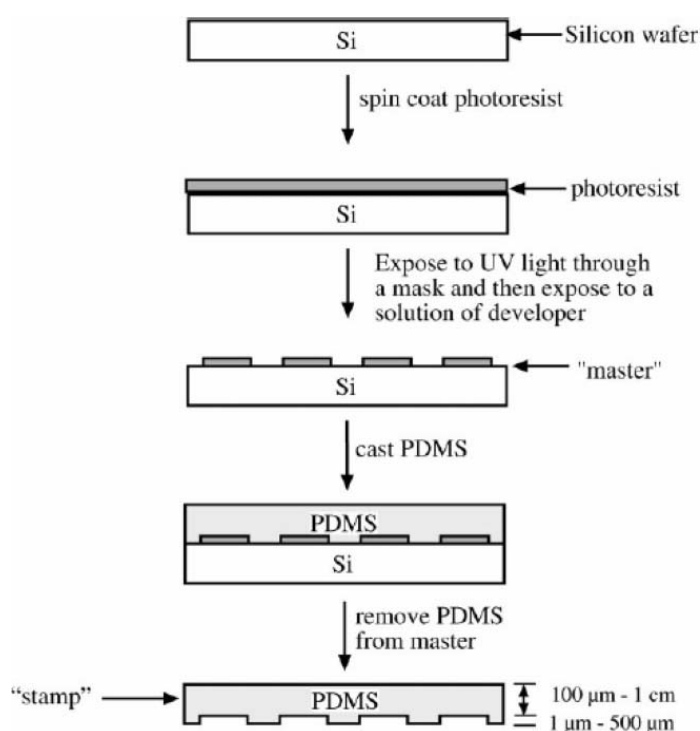


Figure 2-18 Diagram illustrating the fabrication of a PDMS stamp (Reprinted with permission from [235]).

Once the PDMS stamp is cast it is peeled from the mould and the surface "inked" with protein for surface micropatterning. The dimensions of the stamp features are crucial to ensure good patterning, and in preventing feature collapse. Potential collapse occurs in three prominent areas, lateral collapse of the stamps surface features, collapse from the stamp weight, and sagging of the stamp onto the surface (Figure 2-19). To reduce collapse the stamp is often formed as a submicron thick layer on a rigid surface.

Printing of biomolecules can be classified into two categories, direct and indirect. Direct methods entail inking with biomolecule solutions for direct

patterning on the surface [237]. Indirect patterning requires patterning SAMs to present specific surface chemistries for biomolecule conjugation [234].

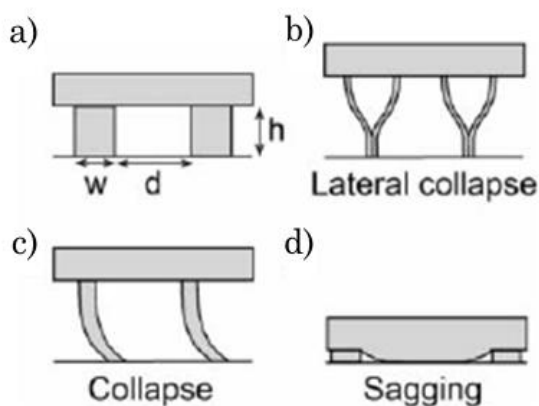


Figure 2-19 Diagram illustrating different microcontact printing failure events. (a) PDMS stamp with features of height h , width w , and gap distance d . (b) Lateral collapse occurs when adjacent structures make contact and remain adherent. (c) Collapse happens when the features buckle under the weight of the stamp. (d) Sagging occurs when the roof of the stamp collapses against the substrate (Reprinted with permission from [235]).

The scale of patterns produced by μ CP varies and is dependent on the fabrication process used to create the master. Routine patterns are developed using deep reactive ion etching of silicon and limitations are caused by the current state of the art microfabrication techniques. The paper by Pla-Roca *et al.* [238] describes patterns with dimensions of 150 nm with 400 nm periodicity, produced using poly(methyl methacrylate) (PMMA) stamps. Elastomers, like PDMS, are the most commonly used stamps due to their high elasticity and ease of fabrication.

The disadvantage of PDMS in biomolecule patterning is the hydrophobic surface, which causes poor stamp wetting properties and stamp biofouling. As dimensions reduce, elasticity also causes problems as small features have weak structural integrity under pressure. Various other polymers including hydrogels [239], PMMA, and olefin co-polymers are being investigated for use in μ CP. The elasticity, or Young's modulus, of a substance has also been found to affect stamp alignment. The paper by Pagliara *et al.* [240] demonstrates a reduction in misalignment from 4.96 ± 0.02 to 0.50 ± 0.01 μm achieved by increasing the Young's modulus from 1.8 to 2600 MPa. When producing multi-protein surfaces successive patterning requires such dimensional control to ensure that patterns are separate. Various biomolecules have been patterned using μ CP including BSA, streptavidin, antibodies, and DNA.

The use of μ CP has a number of advantages over other patterning techniques. Processing involves routine equipment found in cleanrooms and depending on feature dimensions rapid prototyping can be achieved. The array of polymers compatible with this technique allows development of surface chemistries suitable for protein patterning and biocompatibility. Using chrome mask plates can be expensive but cheaper acetate masks can be used, depending on the desired feature resolution. Ink drying, poor stamp wetting properties, stamp collapse and possible feature variation from stamp contact pressure changes are problems associated with μ CP. These problems can be alleviated by choosing the correct polymer and processing steps, but requires specific optimisation for different biomolecules. The stamp can also only be re-used so many times before biofouling of the hydrophobic PDMS surface becomes a problem.

2.4.1.2 Microfluidic Channel Patterned Surfaces

The use of microfluidics to pattern proteins for use in microfluidic channels may seem counterintuitive, but provides a number of advantages over other fabrication techniques. Microfluidic protein patterning uses micron scale channels to define regions for the introduction of biomolecules onto a substrate with high resolution. Channels are fabricated in PDMS using the same methods described for μ CP (2.4.1.1), with etched silicon or SU-8 providing a master for subsequent PDMS channel casting [241]. The channels are then aligned on surfaces and clamped together to make a conformal seal. Solution is then drawn through the channel by capillary forces between a reservoir and a flow promoting pad [242] (Figure 2-20).

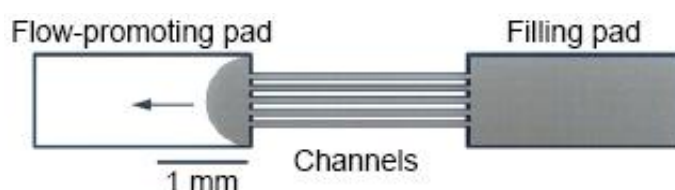


Figure 2-20 Liquid flows between the filling pad and flow-promoting pad by capillary action filling the channels and introducing biomolecules to the channel surface (Reprinted with permission from [242]).

The technique has been developed to form gradients of biomolecules on surfaces [243], which has led to its integration with μ CP to pattern biomolecule gradients with stamps [244]. Channel dimensions have been patterned at close to submicron scales [50] and then used to deposit Igs, protein A, and BSA [245]. More recently the technique has been used to create miniaturised quantitative

immunoassays [246], and in the development of enhanced patterning channels [247]. Microfluidic patterning has a number of attractive properties for the fabrication of multiple protein patches within a channel. The fabrication uses methodology identical to μ CP but instead of inking the surface the solution flows within the channels. This prevents the risk of ink drying, poor stamp wetting properties, and possible feature variation from stamp contact pressure changes. As the process works by capillary action the system does not require pumping and only small volumes of liquid (nL) are necessary to form a pattern. The main drawback of this process is the risk of channel collapse, depending on the choice of polymer and channel dimensions.

2.4.1.3 Stencil Lithography Patterned Surfaces

The process of stencil or template patterning works via a similar process to μ CP. Instead of inking a stamp and contacting it with the surface, a polymer is used to coat the whole surface and the pattern is formed as reliefs in the polymer. These reliefs are filled with biomolecule solutions to allow conjugation with an active surface. Subsequently, the stencil and surface are washed before the stencil is peeled from the surface, as the interactions between the hydrophilic surface and the polymer are weak [248]. PDMS was originally used for stencil formation [249], but more recently poly-para-xylene (ParyleneTM) has been used, due to the ease of fabrication and because it peels easily from hydrophilic substrates. The process of stencil fabrication is illustrated in Figure 2-21 (see overleaf). A thin layer of ParyleneTM (1-15 μ m) was deposited by chemical vapour deposition on the surface. The ParyleneTM was then coated with photoresist and patterned by UV photolithography to form an etch mask for ParyleneTM dry etching. After the layer was baked, O₂ plasma etching removed unmasked ParyleneTM to form the relief structures. Biomolecules were then incubated with the surface, to allow surface interaction, before washing and peeling of the ParyleneTM from the surface. Multiple protein patterning was achieved by K. Atstuta *et al.* [250] by controlling the spatial deposition by integration with microfluidic patterning as described in §2.4.1.2.

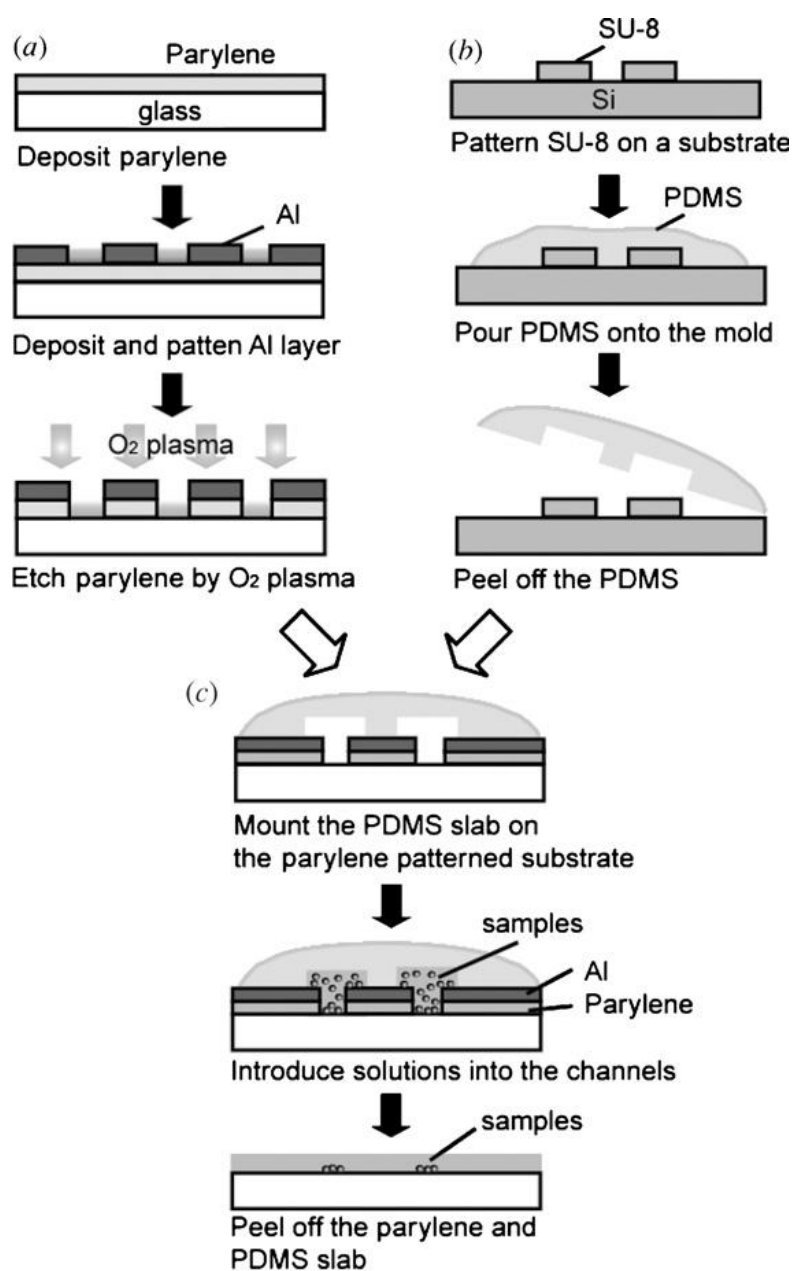


Figure 2-21 Fabrication and selective patterning process using a patterned Parylene™ sheet and a microfluidic system. (a) Parylene™ is patterned by oxygen plasma using an aluminium layer as a mask. (b) Microchannel patterns are transferred from the SU-8 mold to PDMS. (c) The PDMS sheet with microchannels is aligned and placed on the patterned Parylene™ layer for the protein patterning. After the solution is introduced and the PDMS/Parylene™ sheet removed, the samples are selectively patterned on the planar glass surface (Reprinted with permission from [250]).

Stencil patterns have been used to conjugate kinesin, microtubules, adenosine-5'-triphosphatase (ATP)ase enzymes, and BSA [251] onto substrates (i.e. silicon, glass, and cyclic-olefin-copolymer) [252]. Pattern dimensions of 2 μm have been reported and, by integration with microfluidics, multiple protein patterning can be achieved. Surface attachment of molecules, reported in the literature, relies on

adsorption but the potential for covalent chemistry is applicable. The technique has similar advantages to microfluidic protein patterning, as it uses a solution to interact with the surface.

The disadvantages are the requirement of photolithographic processing and the use of a cleanroom environment. There is also the possibility of stencil debris remaining on the surface after peeling. As the number of processing steps, to pattern multiple proteins within a microfluidic channel, increases the complexity of the fabrication protocol will also increase, which is undesirable.

2.4.1.4 Nanoparticle Lithography Patterned Surfaces

Recent developments in nanoparticle lithography have been adapted to create stamps without the requirement of UV photolithography. The process works on the principle of monolayer self assembly by nanoparticles formed during solvent evaporation [253]. There are many variations on the fabrication process but the underlying principle remains the same. A monolayer of nanoparticles is formed on the surface and then etched, often with O₂ plasma, to reduce the particle size [254]. The surface can then be used to directly produce a stamp with PDMS, or an oxide layer grown to form a master mold (Figure 2-22, see overleaf) [255]. Another process includes the addition of a thin film that is patterned to form the stamp using the nanoparticles [256].

The advantage of this technique is that it can be achieved without the requirement of photolithographic processing. The disadvantage is the control of the pattern geometry, as currently only dot arrays can be fabricated.

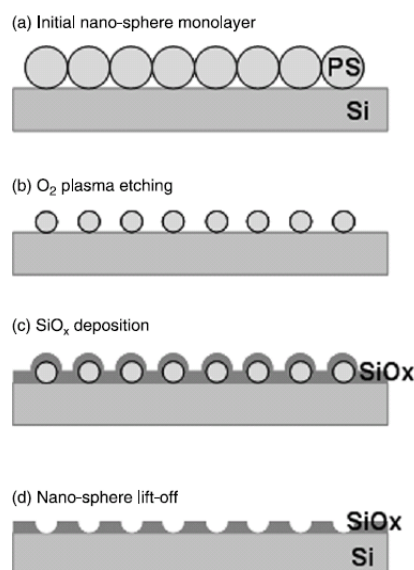


Figure 2-22 Scheme of the process for the creation of the nanotemplate: (a) nanosphere monolayer of polystyrene, is deposited on a silicon substrate; (b) plasma etching of the polystyrene beads, reduction of the size; (c) plasma enhanced chemical vapour deposition of a SiO_x layer; and (d) mechanical removal of the beads (Reprinted with permission from [255]).

2.4.1.5 Dip Pen Nanolithography Patterned Surfaces

Dip pen technology uses an AFM tip to directly pattern the surface. Two main protocols are found in the literature for surface patterning, the first involves inking the AFM tip with biomolecules, which are subsequently transferred onto the surface where the tip and surface interact. The second protocol involves scratching the surface with the AFM tip to remove SAMs, the revealed scratched pattern can then be backfilled with SAMs suitable for conjugating biomolecules [233]. Inking entails coating a tip with a desired biomolecule which can then be patterned by the nanoscale tip. This process has been developed to include the “volcano” or “nanofountain” tip, which integrates a capillary or microfluidic system into the tip fabrication process (Figure 2-23) [257].

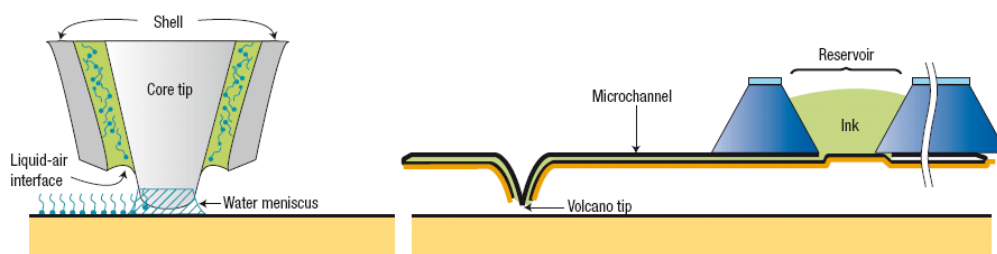


Figure 2-23 Writing mechanism of the Nano Fountain Pen. Molecular ink fed from the reservoir forms a liquid–air interface at the annular aperture of the volcano tip. Molecules are transferred by diffusion from the interface to a substrate and a water meniscus is formed by capillary condensation (Reprinted with permission from [233]).

The aim of the volcano tip is to allow continuous writing of biomolecules without the need to re-ink the tip. Alternatively, tips can be used to remove a monomolecular layer coated on the surface, which can then be back-filled with a desired SAM or biomolecule [258]. The advantage of this technique is the scale of deposition due to the nanoscale size of the tip. Problems with this technique arise from the cost of development of such systems as AFM tips and specialised volcano tips require expensive fabrication methods.

2.4.2 Non Contact Lithography

Non contact methods include photolithography and printing to form patterns on surfaces. Although contact is not directly required for these processes it is used to enhance the spatial control of the patterning, which is critical to achieve submicron resolution.

The process of optical lithography or photolithography for patterning surfaces with biomolecules stems from the adaptation of photoresist technology from the microfabrication industry. Essentially, photolithography utilises UV light to produce a surface able to conjugate biomolecules [259]. Short wavelength UV light can cause damage to proteins, and should be avoided when patterning proteins directly. Instead photolithography is used to couple or activate SAMs on the surface of substrates which can be used to conjugate a biomolecule.

More recently standard photolithography processes have been modified by the integration of scanning near-field optical microscopy (SNOM). SNOM is conventionally used to interrogate nm scale structures on surfaces [260]. The use of SNOM as a method to pattern with nm scale resolution is described in the review by Leggett [261]. Essentially the process uses an aperture to propagate light onto the surface. The propagated light is subject to diffraction but if the aperture is close enough to the surface, evanescent electric fields lead to the optical excitation at the tip. This process can be used to pattern features with sub 100 nm feature resolution [262, 263]. Protein patterns have been created on the nm scale by using this method to pattern a layer of oligo(ethylene glycol) terminated SAMs to produce aldehydes for subsequent protein immobilisation [264, 265].

Printing of proteins can be classified into two main areas, ink jet and laser printing. Inkjet involves the dispensing of protein droplets onto a surface by the

actuation of a piezoelectric crystal to eject the protein from the printer head onto the surface. Laser printing involves a forward transfer process where the protein is transferred from the surface upon vaporisation of a laser absorption layer which vaporises transferring the protein onto the substrate.

2.4.2.1 Using Photoresists for Biomolecule Patterning

The use of a photoresist for protein patterning stems from the adaption of techniques used in the microfabrication of electronic components. Positive and negative photoresists have been developed that react to UV light to form specific features on the surface. Two photoresists that react differently under UV illumination are positive and negative photoresists. When developed a positive photoresist forms relief features only in areas illuminated with UV light. Conversely a negative photoresist, when illuminated with UV light, forms crosslinks leading to the production of relief patterns in non-illuminated regions when developed (Figure 2-24). For application in protein patterning the reliefs produced reveal the surface, for modification, while protecting the rest of the surface with the remaining resist. After the photoresist is patterned, the surface can be treated to form new surface chemistry compatible with protein binding.

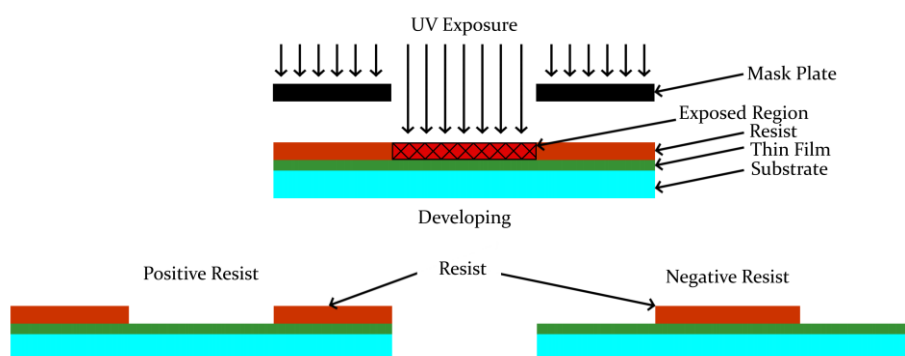


Figure 2-24 Illustration of relief structures formed after the patterning and development of a positive or negative photoresist.

Dong *et al.* [266] coated a surface with PEG and then applied a photoresist to form relief patterns. Oxygen plasma was used to etch away the PEG layer in the reliefs, which were then backfilled to eventually form a poly(acrylic acid) brush layer. BSA-FITC was then immobilised on the poly(acrylic acid) brush using EDC/NHS-mediated coupling (as described later in §3.1.1), which revealed the patterned surface by fluorescence microscopy. This EDC/NHS coupling process is compatible

with the attachment of a single protein. To apply two proteins, Lee *et al.* [267] and Jiang *et al.* [268] used a variation of the process described by Dong *et al.* [266]. Lee *et al.* [267] coated a surface with antibody, followed by a protective layer of agarose. Jiang *et al.* [268] coated a surface with either DNA or protein, followed by a protective layer of gold. The protective layers were incorporated to prevent damage to the biomolecules during surface processing. The agarose was coated with photoresist and patterned to form reliefs before using oxygen plasma to remove the agarose/antibody layer in the relief features, while the gold was patterned directly using ion beam milling. Lee *et al.* [267] then removed the photoresist and agarose and incubated the surface with a second antibody to form patterns of two different antibodies side by side. Jiang *et al.* [268] then introduced a second biomolecule before removing the gold layer. The requirement of multiple processing steps to produce more than two proteins, using this type of method, limits its application as a simple multiple protein patterning method.

To produce multiple patterns on a surface Petrou *et al.* [269] showed that some resists are compatible with biomolecule processing. The work demonstrated the integration of a polymeric film used to promote biomolecule adsorption at the surface. A commercial photoresist was coated over the polymeric film and illuminated to pattern reliefs for the subsequent adsorption of biomolecules. The surface could then be illuminated again to form a new set of reliefs and the process was repeated with a second biomolecule. The use of mild conditions for resist development and illumination prevented protein from denaturing when undergoing further surface processing.

2.4.2.2 Patterning of Surfaces Conjugated with Photoactive Caged Groups

One of the most common methods employed for the photoactivation of surfaces involves the use of caged groups. The use of caged chemistries stems from work carried out by Kaplan *et al.* [270], which describes a photoactivatable ATP analogue (ATP1). On photolysis the ATP1 generates ATP, which can then react with an ATPase enzyme. The term “caged” is used to define such protected molecules, which become de-protected on exposure to light. In the same way a caged group bound to a surface, when exposed to light, can react to form a new surface chemistry. Del Campo *et al.* [271] used a mixture of two different silanes, one with an NVO

protecting group and one with a benzoin protecting group, for patterning applications. Each group can be individually de-protected as they cleave at different wavelengths. On illumination with UV light at 411 nm the NVOC group is photochemically cleaved leaving an amine terminated surface, while illumination at 254 nm de-protects the benzoin group forming a carboxyl terminated surface. The process was used to covalently attach carboxylated poly(butyl methacrylate) particles, followed by modification in further work to pattern biomolecules [272].

Work by Christman *et al.* [225, 273] illustrated a novel method to de-protect a caged group without direct UV de-protection. Instead an acid caused surface de-protection, which was initiated using a photo-acid generator. In this case an *N-tert*-butoxycarbonyl protecting moiety bound to a methacrylate group was used to form a copolymer on a silicon surface. The terminal *N-tert*-butoxycarbonyl group was then coated with a thin film of photo-acid generator, before illumination with 365 nm light. The UV initiates the formation of an acid on the surface leading to de-protection of the *N-tert*-butoxycarbonyl group only in illuminated regions. The de-protection of the surface left an aminoxy side chain, which reacted with an *N*-terminal α -ketoamide modified streptavidin to form a covalent amide bond.

2.4.2.3 Photodegradation of Surfaces to Generate Biomolecule Patterns

Illumination with UV light can initiate a chemical degradation of surface conjugated groups to modify the surface chemistry. This process can be utilised to pattern regions of the surface for the subsequent attachment of protein. Reynolds *et al.* [262] describe the UV initiated oxidation of perfluorinated alkylthiolates, absorbed on gold surfaces, to alkylsulfonates, which are easily displaced by a fresh carboxylic acid terminated thiol. By using a photolithographic mask the oxidation and displacement can be controlled to create carboxylic acid terminated features for subsequent protein attachment. Further work, carried out by the same group, demonstrated the photochemical modification of oligo(ethylene glycol) terminated SAMs to produce aldehyde terminated surfaces [264]. The resulting aldehyde terminated surface could be used to immobilise protein directly or for further chemical modification. Work presented by Reynolds *et al.* [265] showed the aldehydes could be reacted with nitrilotriacetic acid terminated amines. The nitrilotriacetic acid terminated surface

was then used for the site specific immobilisation of a His-tag yellow fluorescent protein (Figure 2-25).

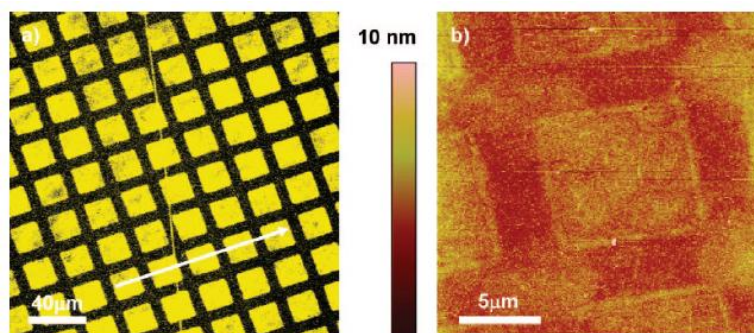


Figure 2-25 His-tagged YFP bound to photodegraded NTA-functionalised PEO-terminated films: (a) confocal microscopy image of a micrometre scale pattern of YFP formed by exposure through a mask; (b) tapping mode AFM image of the same pattern, reprinted with permission from [265].

2.4.2.4 Photoinitiated Conjugation of Biomolecule Patterns

Photoinitiated conjugation involves the modification of a surface to introduce a chemical termination capable of attaching protein upon activation. One such mechanism uses a bi-functional photochemical linker to couple a new chemical moiety to the surface. An example of such a linker is N-5-azido-2-nitrobenzoyloxysuccinimide (ANB-NOS), which upon photochemical activation introduces an NHS-ester moiety onto a surface. Kim *et al.* [274] used ANB-NOS to modify PEG hydrogels with NHS-ester groups, for the subsequent conjugation of protein. When illuminated with UV the azide is converted into a highly reactive singlet nitrene, which can react with C-H, alkyl, and nucleophiles through a variety of different reaction pathways, as described by Levya *et al.* [275]. The modification of the hydrogel was shown to occur throughout the PEG and was not just limited to the terminal hydroxyl group. The work carried out by Choi *et al.* [276] used an aryl azide to covalently couple a biotin moiety to a variety of chemically functionalised surfaces (Figure 2-26, see overleaf). Glass modified to form carboxyl, poly-L-lysine, aldehyde, aldehyde/BSA, and amine terminated surfaces was analysed to determine which chemistry improved the uniformity of biotin photo-conjugation.

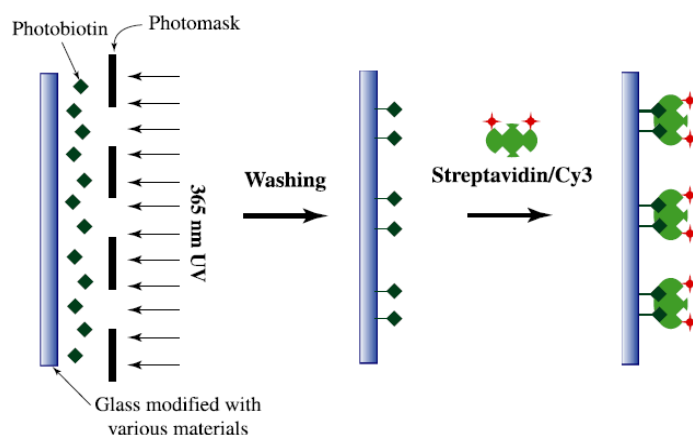


Figure 2-26 Images reproduced from [276] illustrating the conjugation of photobiotin micropatterns on a silanised glass surfaces.

Azide is not the only chemical suitable for the covalent photoinitiated conjugation of biomolecules to surfaces. Dankbar and Gauglitz [63] studied the potential of ketyl-reactive benzophenone (BP), anthriquinone, nitrene-reactive nitrophenyl azide and carbene-reactive phenyl-(trifluoromethyl)diazirine as molecular linkers on polymer surfaces [63]. The work showed that phenyl-(trifluoromethyl)diazirine had the best overall photolinking efficiency on the surfaces studied using oligonucleotides as the model biomolecule.

Photoinitiated reactions are not only suitable for altering the surface chemistry but can also be used to directly conjugate proteins. One of the earliest examples of this technique, described by Rozsnyai *et al.* [277], involved the immobilisation of antibodies onto solid supports. The process used a photo-active BP group to covalently attach the antibody onto the surface. The process was described more recently, by Toh *et al.* [278] (Figure 2-27, see overleaf), for patterning gradients of multiple proteins onto a surface. Upon illumination with 365 nm light the BP forms a transient diradical that can insert into a C-H bond of a proximal biomolecule to form a covalent bond. As the diradical is only formed upon illumination the remainder of the surface stays active for subsequent protein patterning.

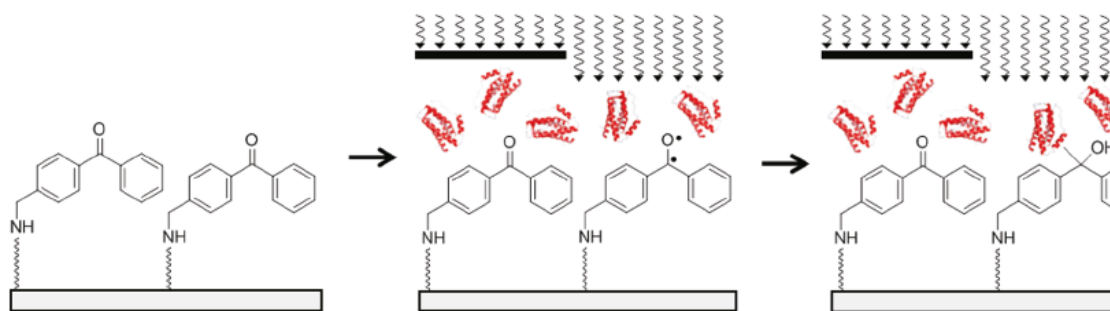


Figure 2-27 Illustration of the covalent patterning of proximal biomolecules upon BP modified surfaces by illumination with 365 nm light (Reprinted with permission from [278]).

2.4.2.5 Electron-Beam Lithography Patterned Surfaces

The current state-of-the-art technique within the microelectronics fabrication industry for producing nm scale features involves the use of electron beam (e-beam) lithography. The process involves scanning an e-beam over a surface, which in the microfabrication industry leads to the selective exposure of a resist. The process can produce features at the sub 100 nm scale without the requirement of a mask as the e-beam can be used to write directly upon the surface. E-beam lithography can also be used as a method to pattern surfaces at the nm scale for protein patterning applications [279]. 250 nm size features have been patterned for the introduction of both DNA [280] and protein [281]. Both these methods involve the removal of a SAM by e-beam lithography before back filling with 3-aminopropyltriethoxysilane (APTES), which is subsequently modified to allow the conjugation of biomolecules. A more recent protocol involves patterning multiple proteins using a set of chemically modified star PEGs. The PEGs have different chemical terminations that are used to conjugate specific proteins, which means multiple proteins can be patterned at the nm scale [282].

2.4.2.6 Printing Patterned Surfaces

The method of laser printing known as laser assisted forward transfer is a non-contact process to expel liquid onto a surface using laser power, as illustrated in Figure 2-28 (see overleaf) [283]. Generally the technique requires a precursor film which adsorbs the power from the laser and vaporises. This process causes the ejection of a biomolecule layer onto a desired substrate [284]. The physical parameters which affect the physical characteristics of the transfer are still not well understood as this is a relatively new process [285].

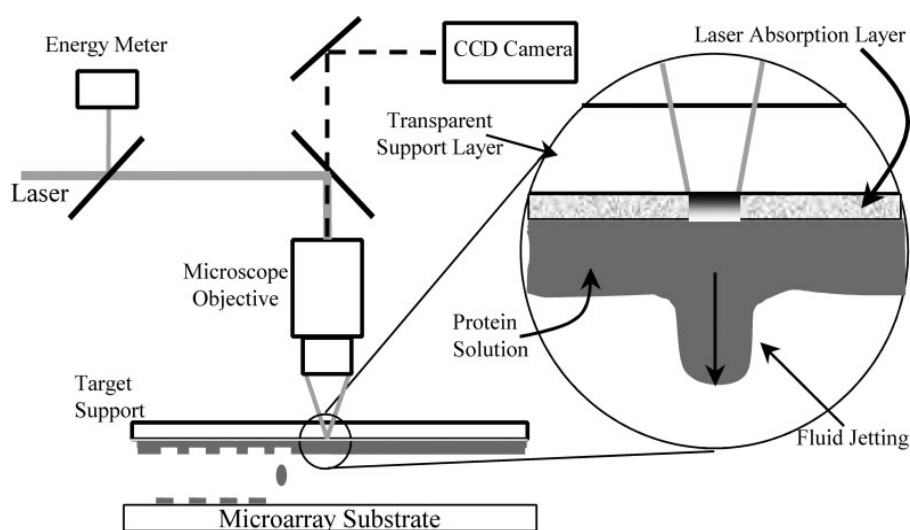


Figure 2-28 Diagram illustrating the type of apparatus used for laser printing protein microarrays. A fluid jetting mechanism enables the efficient transfer of high-resolution droplets of protein solution to microarray substrates (Reprinted with permission from [284]).

The most common form of ink-jet printer used to pattern biomolecules is drop-on-demand printing, where a specific volume of liquid is ejected by force; the types of force mechanism can be subdivided. Thermal drop on demand uses heat to vaporise a proportion of liquid, the resulting bubble expands forcing the remainder of the droplet through the dispensing nozzle. Piezoelectric drop on demand is the preferred approach for biological fluids as thermal approaches require high temperatures for droplet deposition, which is not ideal for protein samples. A piezoelectric drop on demand uses mechanical displacement, produced adjacent to the fluid filled chamber, which expels a droplet onto the substrate [286].

Both commercial [287], and in-house [288] fabricated ink-jet technologies have been used to deposit biomolecules. A fabricated device by Xu *et al.* [289] could generate spot and line diameters of 12 μm , with the capability of patterning multiple proteins simultaneously. Biomolecules patterned by ink-jet include IgG, BSA, streptavidin, and cell cultures.

2.4.3 Protein Patterning Rationale

As demonstrated in §2.4.1 and 2.4.2 there are a variety of potential methods to pattern biomolecules in micron and nm scale patterns upon appropriate surfaces. Photolithography provides a suitable method for the attachment of nm scale protein patterns and also integrates the ability to align the patterns accurately on a surface. For the development of a protein patterning mechanism that can be used to pattern

proteins within a microfluidic channel device this is a key requirement. Soft lithography techniques are limited by the requirement to re-fabricate stamps, stencils, or channels to pattern surfaces. Photolithographic masks can be fabricated from more robust materials that can last longer and be re-used more often. Use of e-beam, SNOM, and printing requires specialised equipment that increases the cost of the overall process. Photolithography can be achieved without the requirement of a cleanroom environment and UV lamps can be used that are low in cost. These advantages have led to the rationale for integrating chemistry compatible with photolithographic processing.

2.5 Summary

The use of biomaterials, prevention of biofouling, and fabrication of protein patterns for microfluidic biosensor applications were discussed. The production of microfluidic devices using silicon, glass, and polymer surfaces has excellent potential for application to medical diagnosis. The work by Fan *et al.* [290] demonstrates the potential of using microfluidic devices for diagnostic applications. The goal is to provide a robust technology for POC quantification of diagnostic biomarkers for enhanced patient care.

Among the materials considered silicon has been shown to achieve higher densities of biomolecules compared with that of glass and polymers, as an immobilisation substrate [128]. For the production of microfluidic channels PDMS show the best properties for simple fabrication and integration of sample connections. The rapid prototyping method demonstrated by Kim *et al.* [291] is particularly valuable for the development of low cost devices. Both PEG and dextran have similar effectiveness in preventing non specific protein adsorption [292]. Dextran has the advantage of better long term stability compared with PEG, which has been shown to self oxidise over time [293]. From the various methods to attach proteins onto surfaces the use of NHS-esters chemistry allow immobilisation at close to physiological pH to produce stable covalent attachment. The attachment using amine chemistry limits the potential orientations of a protein on the surface dependent on the number of Lys residues present on the protein surface. Photoattachment chemistry is particularly suitable in conjunction with the method

of photolithographic patterning. Methods of patterning biomolecules using this technique have already shown promise for producing reproducible patterns of multiple proteins. Holden *et al.* [294] reacted biotinylated fluorophores using a 488 nm laser to initiate a photobleaching free radical initiated surface functionalisation to produce patterns of biotin on the surface.

Silicon has been successfully patterned with DNA and protein using photo-attachment of NHS terminated monolayers [128, 137]. These surfaces have been well characterised and identified as potential surfaces for producing reproducible protein patterns for potential LOC applications [135, 218]. There have been limited attempts to use this technique for integration with microfluidic applications. A novel application involving the immobilisation of antibody binding proteins in micron and submicron resolution patterns on silicon is discussed in Chapter 4.

3

Materials and Methods

This chapter details the experimental protocols that were applied in the development of a site specific conjugation technique for patterning multiple proteins as outlined in Chapters 4 and 5 of this thesis. All chemicals were obtained from Aldrich Chemical Company used without further purification, unless stated otherwise. Deionised water (ELGA genetics system) was used for all the aqueous solutions. Deuterated chloroform was purchased from Apollo Scientific.

3.1 Conjugation of Proteins on Silicon Surfaces

3.1.1 Synthesis of the Bifunctional Linker Undecylenic Acid *N*-Hydroxysuccinimide Ester

The functional alkene linker undecylenic acid *N*-Hydroxysuccinimide ester (UANHS) was synthesised as described previously [131]. Molecular sieves were oven-dried over 2 days or microwave-activated. Glassware was oven-dried overnight before use for reactions requiring exclusion of moisture. A mixture of undecylenic acid (0.92 g, 5.0 mmol), 1-ethyl-3-[3-dimethylaminopropyl]carbodiimide hydrochloride (EDC) (1.4 g, 7.3 mmol) and NHS (0.85 g, 7.3 mmol) in 10 mL dichloromethane (DCM) was stirred at room temperature. The reaction was monitored by thin layer chromatography (1:9 methanol:DCM). After 1 hour the reaction was stopped and 20 mL of DCM was added. The resulting mixture was washed twice with 2 mL aqueous potassium chloride (saturated). The collected organic layer was dried over sodium sulphate, concentrated and purified by column chromatography yielding pure

product as a white solid (0.92 g, 3.3 mM, 66 %). The chemical structure in Figure 3-1 illustrates the reaction mechanism that leads to the formation of UANHS.

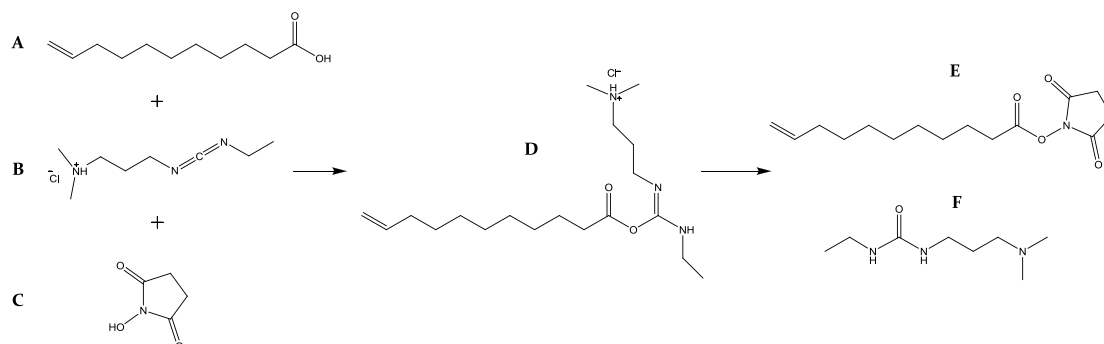


Figure 3-1 Chemical structure of the EDC/NHS coupling reaction showing the reactants (A-Undecylenic Acid, B-EDC, and C-N-Hydroxysuccinimide), the unstable *O*-acylisourea intermediate (D) and the amine reactive product UANHS (E) and the urea by-product (F).

A ^1H NMR spectrum was recorded at 400 MHz using a Bruker DPX400 spectrometer. The UANHS was dissolved in deuterated chloroform to a concentration of 25 mg/mL before being placed in an NMR tube. The chemical shifts were given in ppm, with the spectrum calibrated to the solvent peak. The J values were correct to within 0.5 Hz.

3.1.2 Photolithographic Mask Fabrication

To fabricate the chrome/gold photolithographic masks UV grade fused silica discs (Suprasil, 2 mm thick, 2.5 cm diameter, UQG Ltd, UK) were used. The discs were cleaned by sonication in acetone, isopropanol and deionised water, for 10 minutes each, to remove any grease from the surface. Next, the discs were treated in a piranha solution, which typically consist of a 3:1 mixture of 95 % weight per volume (w/v) concentrated sulphuric acid (electronic (MOS) grade, Fisher Scientific, UK): 30 % (w/v) hydrogen peroxide (general laboratory work (SLR) grade, Fisher Scientific, UK), for 30 minutes to remove any organic contaminants. The discs were then removed and washed in deionised water before baking in an oven (ED 23 Bench top Oven, Binder UK) overnight at 120 °C. Baking dehydrates the surface, promoting adhesion of evaporated metal, by the removal of surface water. Next surfaces were placed into an E-Beam evaporator (Edwards auto E500A) under vacuum at $<6 \times 10^{-6}$ mbar. The slide surfaces were coated with a 10 nm adhesion layer of chrome (99.99 % pure, C6-5016-M, Testbourne Ltd., UK) followed by a 70 nm layer of gold (99.99 %

pure, G4-5005-M, Testbourne Ltd., UK), before being removed from the evaporator and left to cool overnight, stored in a petri dish, within the cleanroom.

The positive photoresist Shipley MICROPOSIT® S1813 (Rohm and Haas Ltd., UK) was spin-coated onto the chrome/gold coated UV fused silica slides, gold surface face up, using a programmable photoresist spin coater (SCS G3P-8 Spincoat, Specialty Coating Systems (SCS) Coating Centre, UK). A typical program includes the following steps: i) spin at 500 rpm for 5 seconds to spread the photoresist; ii) ramp to 5000 rpm for 60 seconds for a uniform coating; and iii) reduce to 500 rpm for 5 seconds to settle the photoresist. The thicknesses of the S1813 photoresist, achieved using the described spin cycles, were between 1.1 μm and 1.5 μm , as measured using the KLA-Tencor P-16 stylus surface profiler.

The S1813 coated slides were prebaked for 30 minutes at 90 °C on a hotplate (EMS 1000-1, Electronic Micro System Ltd. UK). The slides were then left to cool for 30 minutes then positioned in a mask aligner (MA-6, Suss MicroTec Ltd. UK) and placed in contact with a mask plate. A schematic of the mask features is shown in Figure 3-2, consisting of a series of 10 μm lines with a 40 μm periodicity. The full pattern consisted of 120 lines each 10 μm wide and 2 mm long. The S1813 coated slides were illuminated through the mask plate with UV light (300 mJ measured with a 365 nm power meter, Suss MicroTec Ltd. UK) for 7 seconds and then removed from the aligner. The UV patterned S1813 was developed with Shipley MICROPOSIT® MF®-319 (Rohm and Haas Ltd., UK), for 75 seconds. The samples were then immersed in deionised water, to stop the developer from further etching the photoresist, before gently rinsing in deionised water.

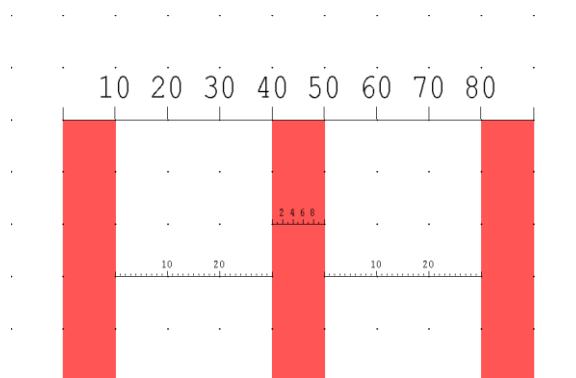


Figure 3-2 Screenshot of an L-edit software design used for mask plate manufacture. The features in pink represent transparent regions on the mask plate and consist of 10 μm wide lines with a periodicity of 40 μm .

The patterned photoresist was imaged by light microscopy (Nikon LV100D, UK) to determine whether the feature dimensions were correct. The pattern was transferred into the chrome/gold by immersion in gold etchant (1 %-10 % iodine: < 25 % potassium iodide, OM Group Ultra Pure Chemicals Ltd., UK) for 60 seconds and chrome etchant (OM Group Ultra Pure Chemicals Ltd., UK) for 10 seconds. The photoresist was cleaned from the surface by washing with acetone for 20 minutes, or until the resist was removed from the surface. The surface was then rinsed with isopropanol and deionised water before storing in a suitable container to prevent surface scratching. Surfaces were analysed by light microscopy (Nikon LV100D, UK) to ensure the feature sizes of the chrome/gold photolithographic mask and alignment features were the same proportions as the original mask plate designs.

3.1.3 Photopatterning of NHS-ester Terminated Alkene on Silicon Surfaces

A single-polished silicon wafer <100>, 1 x 1 cm, was pre-cleaned by sonicating for 20 minutes in solutions of acetone, isopropanol, and deionised water in a cleanroom environment. The samples were then immersed for 30 minutes in fuming nitric acid before washing in deionised water. The oxide was removed by etching in 5 % aqueous HF for 5 minutes, washed thoroughly with water and dried under nitrogen. Immediately after drying a 50 μ L droplet of UANHS (100 mg/mL in DCM) solution was deposited on the silicon and spin coated for 60 seconds at 2000 rpm. After spin coating the samples were transferred from the cleanroom to the laboratory, protected from UV light, for further processing.

To conjugate the alkene with the hydrogen terminated silicon, the surface was illuminated using an HgXe UV lamp (Oriel, Newport). The UV beam passed through a 254 nm bandpass filter (Thorlabs) before being reflected onto the surface through a chrome/gold photolithographic mask (the setup is shown overleaf in Figure 3-3). Prior to illumination the power density of the UV beam was recorded using a UV power meter with a 254 nm head attachment (Karl Suss), placed on the sample holder. Before illumination of a sample, the setup was configured by altering the distance between the UV source and the sample and adjusting the focus of the UV light in order to produce a 1 mW/cm² power density. The sample was then placed on the sample holder and put in contact with the chrome/gold mask before being illuminated. After illumination the wafer was washed twice with DCM for 5 minutes

and for 2 minutes with acetone. As a negative control surfaces were processed in the same way except the UANHS was not spin coated onto the surface.

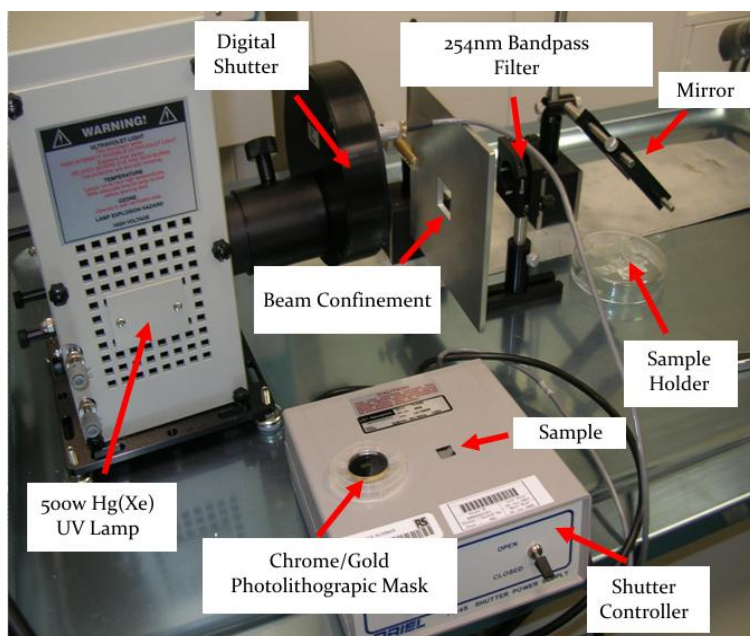


Figure 3-3 Equipment setup used for the UV illumination of silicon samples to conjugate the bifunctional linker UANHS to the H-terminated silicon surface.

3.1.4 SEM of Photopatterned Alkene Surfaces

Scanning electron microscopy (SEM) (LEO 430 SEM, Oxford Instruments) was used to image the UANHS patterned silicon surfaces, which were scanned at a low voltage without gold coating. The UANHS patterned surfaces, once evaluated by SEM, were not used for any further analysis. The negative control samples were also imaged to determine if a pattern was produced.

3.1.5 X-ray Photoelectron Spectroscopy of Photopatterned Alkene and Protein Conjugated Surfaces

Silicon samples were diced into 1 x 1 cm chips and labelled on the reverse with a diamond pen, in preparation for use with XPS. Chip surfaces were cleaned, etched with aqueous HF and spin coated with UANHS using the same methods outlined previously (§3.1.3). The whole sample was then exposed using an HgXe UV lamp (Oriel, Newport) beam (1 mW/cm² power density measured using a 254 nm UV power meter (Karl Suss)), which passed through a 254 nm bandpass filter and was reflected onto the sample surface. After illumination the samples were washed twice

with DCM for 5 minutes and for 2 minutes with acetone, before drying under nitrogen. A 10 μL droplet of NeutrAvidin (1 μM in 0.1M sodium hydrogen carbonate buffer (pH 8.4)) was deposited on the UANHS coated silicon surface and spread with a glass cover slip (18 x 18 mm, Fisher Scientific, UK). Four samples were taken at each stage of surface modification (UANHS conjugation, NeutrAvidin-UANHS conjugation), dried under nitrogen and stored at 4 $^{\circ}\text{C}$ before analysis by XPS. The XPS experiments were performed by Dr David Morgan in Cardiff, on a Kratos Axis Ultra-DLD photoelectron spectrometer using monochromatic Al K α radiation (photon energy 1486.6 eV). Survey scans were performed at a pass energy (PE) of 160 eV, whilst detailed scans were performed at PE 40 eV. All data were analysed using CasaXPS(tm) software (Version 2.3.15). All data were calibrated to the C(1s) signal, which was assigned a value of 285 eV, which is a reference value assigned to aliphatic carbons present in the organic materials studied.

3.1.6 Conjugation of Protein to Photopatterned Alkene Surfaces

Wild type single domain protein L (strain PpL₃₃₁₆) was purified by Dr. Steve Harrison, as described by Bottomley *et al.* [295], and freeze dried. Fluorescently labelled IgG was prepared using the protocol provided with the fluorescein labelling kit (Roche, Cat. No. 11 386 093 001). The protein patterning protocol was based on work described by Yin *et al.* [128] for the successful conjugation of DNA to silicon surfaces. During the research 7 different proteins were conjugated to the silicon surface for analysis: streptavidin, PpL₃₃₁₆, multidomain protein L (strain 312), multidomain protein A, NeutrAvidin and biotinylated protein A. All proteins, except single domain protein L, were commercially available from Aldrich chemical company. Protein samples were dissolved in a 0.1 M sodium carbonate solution (pH 8.4) to a concentration of between 1 and 10 μM for conjugation experiments. An aliquot of 8 μL of the protein solution was deposited on the UANHS patterned silicon wafer and covered with a cover slip (1.8 x 1.8 cm). The wafer was incubated for 20 hours at room temperature in a humid chamber. After incubation, the wafer was washed with deionised water for 1 hour.

Surfaces were analysed to determine if the addition of a 1 hour incubation in a 1 % solution of BSA, in deionised water, prior to characterisation reduced non specific adsorption upon characterisation. Surfaces were stored in deionised water

at 4 °C prior to characterisation. Surfaces conjugated with PpL₃₃₁₆, multidomain protein L and multidomain protein A were revealed by incubation with a fluorescein-labelled murine IgG (500 nM) for 30 minutes in dark conditions. Surfaces conjugated with streptavidin and NeutrAvidin were revealed by incubation with biotin-FITC (1 µM) for 30 minutes in dark conditions. Unbound fluorescent probes were removed from the surfaces by washing in deionised water for 1 hour. As a positive control a 5 µL droplet of NHS-FITC (1 µM) was deposited on protein L conjugated surfaces and spread with a cover slip (18 x 18 mm). After 1 hour the surface was washed in deionised water. All surfaces were visualised using a Zeiss Axio Observer inverted microscope, coupled with epifluorescence illumination and fitted with filter sets. For imaging, wafers were placed face down over a microscope slide towards an EC Plan-Neofluar 10x, LD A-Plan 20x or an LD Plan-Neofluar 63x objective lens.

To optimise the reproducibility of the conjugation reaction between the UANHS modified silicon and protein a series of experiments were carried out to determine if the conditions described by Yin *et al* could be improved on [128, 131]. Three different incubation buffers were used as a replacement for the 0.1 M sodium carbonate solution. 0.1 M sodium phosphate, potassium phosphate and potassium carbonate solutions, all at pH 8.4, were analysed. The power density of the UV light and the illumination time used to photopattern the UANHS was also analysed. Power densities of 1, 3, and 5 mW/cm² were tested using a 5 minute illumination time. To analyse the effect of changing the illumination time a 1 mW/cm² power density was used to pattern surfaces using 1, 3, 5, 10 and 15 minute illumination times.

3.1.7 Submicron Photopatterning of Alkene on Silicon and Subsequent Protein Conjugation

To pattern surfaces with submicron features a continuous wave UV laser beam, wavelength 266 nm, was provided by a frequency-quadrupled Nd:YAG laser (Thomson, DIVA II) as an illumination source. The beam was expanded, spatially filtered and collimated before being focused. The focused spot had a radius of approximately 1 mm and a laser fluence of 0.6 mJ/cm². To pattern the silicon the collimated beam was illuminated through a phase mask (700 nm period, Ibsen Photonics) placed in contact with a UANHS coated silicon sample (1 x 1cm). The surface was illuminated for 30 seconds before being washed twice with DCM for 5 minutes and for 2 minutes with acetone. After washing, surfaces were either

analysed directly under the SEM or incubated with Streptavidin-FITC (1 μ M in 0.1 M sodium carbonate buffer) for 20 hours. After incubation surfaces were washed for 1 hour in deionised water and dried under nitrogen before imaging with a Zeiss Axio Observer inverted microscope using a Plan-Apochromat 100x objective lens.

3.2 Conjugation of Proteins on Glass Surfaces

3.2.1 Surface Cleaning and Silanisation of Glass Surfaces

Surfaces were cleaned and silanised as described by Elender *et al.* [203]. Glass slides (76 x 26 mm, Fisher Scientific, UK) were sonicated in acetone, followed by isopropanol and deionised water, for 30 minutes in each solution to remove any grease from the surface. The slides were then washed in deionised water and dried under nitrogen. Next slides were immersed for 30 minutes in a 1:1:5 ratio of 35 % (w/v) aqueous solution of hydrogen peroxide (L14000, Alfa Aesar, UK): 50 % (w/v) ammonium hydroxide: deionised water respectively. This process removes organic contaminants from the surface and leaves a more hydrophilic surface. Finally the glass slides were rinsed with copious amounts of deionised water and stored separately in sealed containers, in deionised water at room temperature, before use.

Cleaned glass slides were removed from the deionised water and baked in an oven at 75 °C for 1 hour. The pre-baked glass was placed in a desiccator, under nitrogen flow, for 5 minutes. Glass slides were then immersed in two different concentrations, 0.1 % volume per volume (v/v) and 1 % (v/v), of GOPS, in anhydrous toluene, for 5 minutes, 1 hour, or 24 hours under nitrogen. The illustration in Figure 3-4 (see overleaf) shows the siloxane bond formed from the reaction between the silane and the hydroxyl groups present on the glass surface. After silanisation the glass was washed twice for 10 minutes in toluene, followed by a 10 minute wash with ethanol. Finally the slides were dried under nitrogen and baked in an oven for 1 hour at 75 °C and left at room temperature for 12 hours. The 12 hour period allows time for the slow crosslinking reaction that occurs between the hydrophilic surface and the GOPS. Slides were placed in sealed containers at room temperature until required.

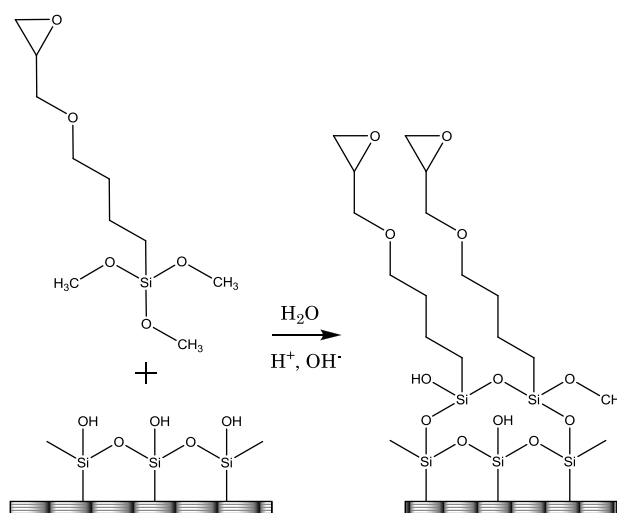


Figure 3-4 Illustration of the silanisation reaction between the glass surface and GAPS used to form an epoxy terminated surface.

3.2.2 Conjugation of Dextran to an Epoxy Functionalised Glass Surface

Solutions of dextran-FITC with concentrations of 1-300 μM were dissolved in deionised water, at room temperature. GAPS modified slides were spotted with 10 μL of each dextran solution for 12 hours, at room temperature, to determine the lowest dextran concentration required for a reproducible dextran surface coating. Slides prepared using the same method had a 10 μL droplet deposited on the surface and spread with a glass coverslip (18 x 18 mm, Fisher Scientific, UK), to determine the reproducibility over a larger area. During the 12 hour incubation period all slides were placed in a humid chamber consisting of a petri dish containing moist tissue and sealed with Parafilm® (Fisher Scientific, UK), to ensure the solutions did not dry out. After 12 hours the surfaces were removed and washed in deionised water for 1 hour before images were captured with an epifluorescence microscope (Axio Observer, Carl Zeiss, UK). The illustration in Figure 3-5 (see overleaf) shows the ether bond formed from the reaction between the oxirane ring of the epoxide and the hydroxyl group of the dextran.

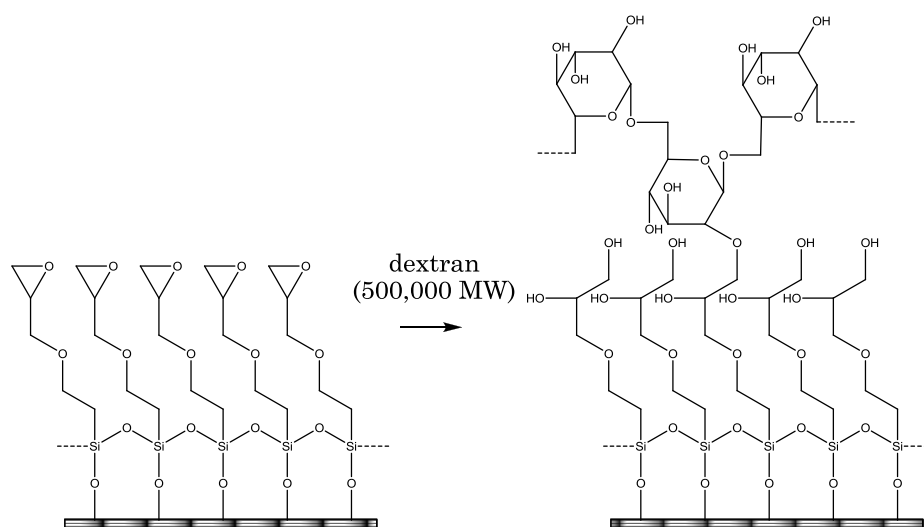


Figure 3-5 Illustration of the oxirane ring opening reaction between the epoxide terminated glass surface and dextran (500,000 MW).

To give a clear picture of how to functionalise glass with a monolayer of silane, the silanisation conditions were tested to see if the conjugation of dextran changed under different silanisation conditions. The typical parameters discussed in the literature [148, 171, 203] for altering the formation of monolayers of silane primarily involve the concentration of silane solution used in the process and the period of time the silane is incubated with the glass. Glass surfaces prepared with concentrations of 0.1 % and 1 % silane were studied, with the time of incubation for each concentration analysed at 5 minutes, 1 hour and 24 hours. The surfaces were spotted with 10 μL droplets of 5, 15 and 20 μM dextran-FITC to determine which conditions generated a reproducible dextran layer.

3.2.3 Water Contact Angle Measurements

Surfaces at different stages of processing were studied to determine the water contact angle on the surface. Static contact angle measurements were performed using a drop shape analysis system (DSA100, Krüss) using 1 μL droplets deposited onto the surface. The surface was maintained at 25 $^{\circ}\text{C}$ in humid conditions by sealing the surface in a glass chamber with a water reservoir. Measurements were taken by analysing sessile drops using the sessile drop fitting software (Krüss), with a total of five measurements averaged over each sample.

3.2.4 Protein Conjugation to Carboxymethyl Dextran Surfaces

GOPS coated slides were immersed in a 30 % (w/v) dextran solution for 12 hours and then washed with deionised water for 1 hour. Next dextran coated slides were immersed in a solution of 1 M bromoacetic acid and 2 M sodium hydroxide, at room temperature, for 16 hours to form CMD. Slides were rinsed with plenty of deionised water before the carboxyl groups were activated, to produce an active ester (O-acylisourea)-leaving group, using a 3:1 solution of EDC:NHS in ethanol for 4 hours [296]. The chemical modifications of the dextran surface, to introduce an NHS-ester moiety, are represented structurally in Figure 3-6 (see overleaf).

Streptavidin-FITC (10 μ M) and protein L (10 μ M), dissolved in 0.1 M sodium carbonate buffer (pH 8.4), were made up for incubation with the dextran-NHS-ester surface. Protein solutions were spotted or spread, with a glass coverslip (18 x 18 mm, Fisher, UK), over the dextran-NHS-ester surface and incubated for 2 hours before washing for 1 hour in deionised water. The protein L surface was then blocked, by washing with a 1 % (w/v) BSA solution for 1 hour, before incubation for 30 minutes with IgG-FITC (500 nM). The strep-FITC and protein L/IgG-FITC surfaces were analysed by fluorescence microscopy (Axio Observer, Carl Zeiss, UK) to determine biofouling and protein immobilisation properties of the surface.

Two methods were used to introduce the NHS-ester moiety to the surface by immersing the glass in EDC/NHS solution and by applying a droplet and spreading the solution with a coverslip. The coverslip controlled where the solution interacted, while reducing the quantity of EDC/NHS required. Multi-domain protein L was used for surface conjugation with the NHS-ester modified surface. On surfaces that were immersed in EDC/NHS solution the protein L was spotted onto the surface, before blocking and IgG-FITC incubation. On surfaces where the solution was restricted to the coverslip area the whole surface was incubated with protein L, prior to blocking and IgG-FITC incubation. The whole surface was incubated with IgG-FITC to directly infer the non-specific protein adsorption properties of the dextran.

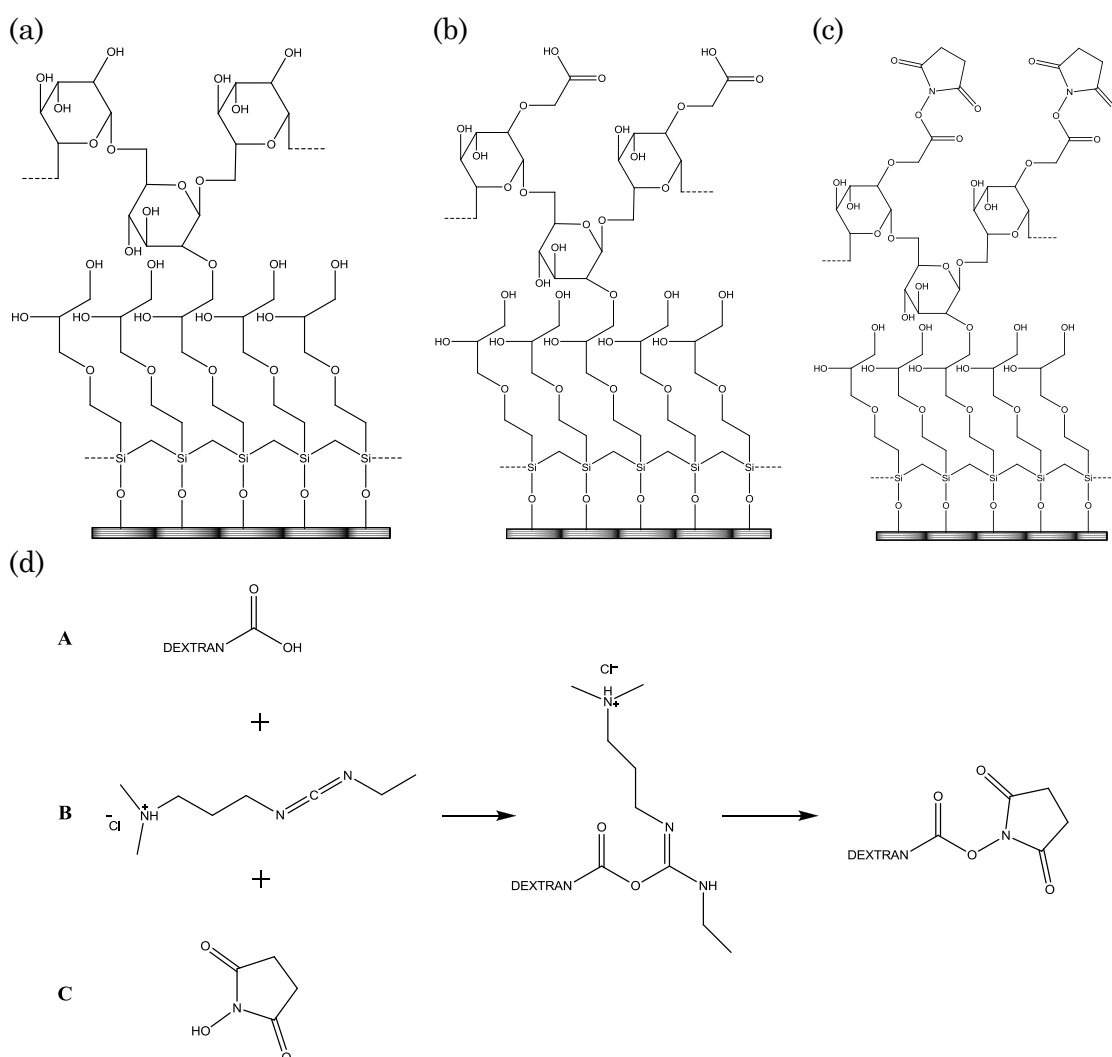


Figure 3-6 Chemical structure of surface modifications depict (a) dextran immobilised on the silanised surface, (b) the introduction of a carboxyl group by the reaction of the dextran surface with bromoacetic acid. The chemical process illustrated in (d) is the EDC mediated coupling of NHS to the carboxyl terminated dextran resulting in the formation of an NHS-ester terminated dextran shown in (c).

3.2.5 Aryl Azide Conjugated Dextran Synthesis

The method described by Bhat et al. [211] was used to conjugate an aryl azide photolinker with dextran. In brief the dextran (1 g, (500,000 MW)), illustrated in Figure 3-7 (a) (see overleaf), was dissolved in 50 mL of dry DMSO in a 100 mL round-bottomed flask, and protected from light. 4-azidobenzoic acid (0.5 g, 6.13×10^{-3} mol), illustrated in Figure 3-7 (b) (see overleaf), and 4-dimethylaminopyridine (DMAP) (0.0375 g, 6.13×10^{-4} mol) were added to this solution with stirring, before the solution was cooled to 0°C . DCC (0.625 g, 6.05×10^{-3} mol) was added to the solution and stirring was continued for 5 hours. An illustration of the conjugation

reaction between 4-azidobenzoic acid and dextran to form an ester bond is shown in Figure 3-8. After filtering off the precipitated dicyclohexyl urea, the azidated dextran was precipitated from solution by adding excess methanol.

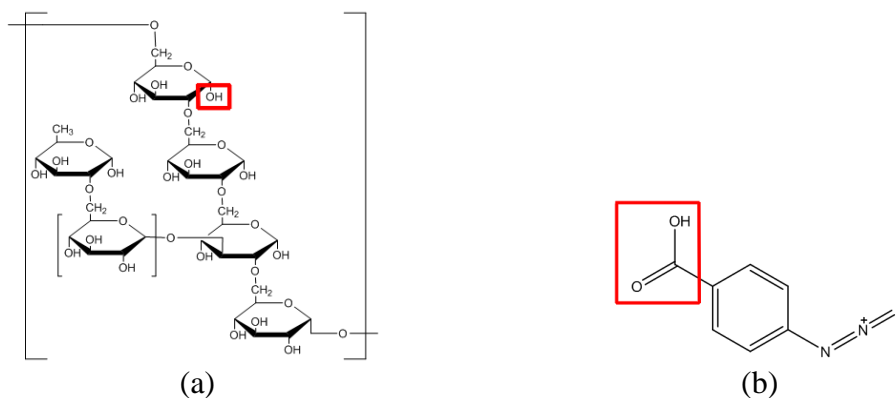


Figure 3-7 Chemical structure diagrams of the two reactants used to synthesise an aryl azide conjugated dextran, (a) dextran and (b) 4-azidobenzoic acid. The chemical groups highlighted react to form an ester bond, as illustrated in Figure 3-8.

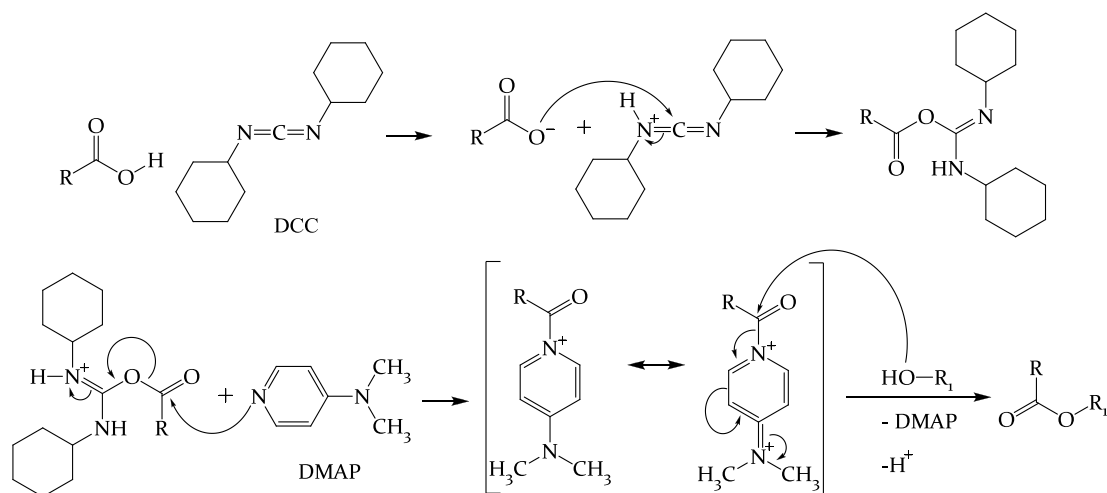


Figure 3-8 Illustration of the Steglich esterification reaction used to form an ester bond between the carboxylic acid moiety of R (4-azidobenzoic acid) and the hydroxyl group of R_1 (dextran). The DCC is a coupling agent and DMAP is a catalyst.

The precipitate was filtered, washed several times with methanol to remove any free 4-azidobenzoic acid, vacuum dried and stored at 4 °C [211]. Aryl azide conjugation was confirmed by attenuated total reflectance fourier transform infrared spectroscopy (ATR-FTIR), elemental analysis and UV absorption spectroscopy.

3.2.6 Attenuated Total Reflectance Fourier Transform Infrared Spectroscopy

A Nicolet FTIR Spectrometer (Nicolet instrument Co.) equipped with a diamond ATR accessory was employed for ATR-FTIR experiments. Powder samples of 4-azidobenzoic acid, dextran and AACD were sampled, using the same pressure for all measurements. Each spectrum comprises 32 co-added scans measured at a spectral resolution of 4 cm^{-1} in the $400\text{--}3600\text{ cm}^{-1}$ range. Spectral data were acquired with Omnic E.S.P. software version 5.2 (Nicolet instrument Co.). Baseline and ATR corrections were used for processing the spectra before quantitative analysis.

3.2.7 Elemental Analysis

Elemental analysis was used to determine the azide content of the AACD. A CE440 elemental analyser was used to determine the carbon, hydrogen, and nitrogen content, referred to as a CHN analysis, of the AACD product. The analyser is used to combust the material in pure oxygen, at a heat of $1800\text{ }^{\circ}\text{C}$, to vaporise the compound. The gaseous products of combustion are carried using helium as it is a relatively inert element compared with the material components and has a very high co-efficient of thermal conductivity. The products are passed over catalytic reagents designed to ensure complete oxidation and removal of potential contaminants. Any oxidised nitrogen is reduced and excess oxygen removed before the gases are homogenised at precise volume, pressure, and temperature. Finally a sample volume of the products is passed through three pairs of thermal conductivity meters, used to measure the product constituents. The first pair measures the thermal conductivity before and after an absorption trap, used to remove water, which is representative of the hydrogen content. The second pair is between a carbon dioxide trap, which measures the carbon content of the product. The remaining constituent is the nitrogen content mixed with the helium carrier, this is measured using a thermal conductivity meter referenced with a helium sample under the same conditions.

A 4 mg sample of AACD powder, protected from light, was sent to Warwick Analytical Service (UK) to obtain a carbon, hydrogen, nitrogen (CHN) elemental analysis of the AACD compound. The company used a CE440 elemental analyser to run the AACD sample in duplicate, to improve the accuracy of the result.

3.2.8 UV-Vis Spectrophotometry

To measure the UV absorption spectra of compounds and materials a UV-Vis spectrophotometer (Cary 50 UV-Vis spectrophotometer, Varian, UK) was used. A cuvette (Hellma) was filled with 100 μL of deionised water and placed in a UV-Vis spectrophotometer and used as a baseline signal, measured between 250-400 nm. Solutions of 1-12 μM AACD were prepared in deionised water. A 100 μL sample of each concentration of AACD was pipetted into a cuvette and the absorption measured between 250-400 nm using the spectrophotometer. The same protocol was used to measure concentrations of dextran, dissolved in deionised water. The 4-azidobenzoic acid did not dissolve in water so was made up in methanol. The baseline signal for 4-azidobenzoic acid was measured between 250-400 nm with methanol.

To measure the UV absorption spectra of the UV fused silica, used to fabricate photolithographic masks, and the bandpass and longpass filters that were used in the illumination setup (see §3.2.14) the measurement protocol using the UV-Vis spectrophotometer was modified. Firstly a baseline signal was measured between 200-500 nm with no cuvette in the machine. Then in place of the cuvette the UV fused silica or filter were placed in the cuvette holder where the light beam would travel through them, allowing the absorption properties of the glass and filters to be measured. The absorption of the UV fused silica and filters was measured separately between 200-500 nm using the UV-Vis spectrophotometer.

3.2.9 Conjugation of Aryl Azide Conjugated Dextran to Silanised Glass Surfaces

Although aryl azide is stable under standard laboratory conditions all AACD samples were protected from light, when being prepared, to prevent potential photoinitiation reactions. A 1 % (w/v) solution of AACD, in 2:1 solution of deionised water:DMSO, was made up and mixed for 1 hour to ensure it was fully dissolved. GOPS slides were prepared using the optimised protocol described previously (§3.2.2) and immersed in 1 % (w/v) AACD solution for 12 hours, at room temperature, before being washed in deionised water for 1 hour.

3.2.10 X-ray Photoelectron Spectroscopy of Aryl Azide Conjugated Dextran Surfaces

Glass slides were diced into 1 x 1 cm chips and labelled on the reverse with a diamond pen, in preparation for use with XPS. Chip surfaces were prepared using the same methods outlined previously (§3.1.5). A 10 μ L droplet of NeutrAvidin (1 μ M) was deposited on the AACD surfaces and spread with a glass cover slip (18 x 18 mm, Fisher Scientific, UK). A 500W UV lamp (Oriel-Newport, UK), was used to illuminate the sample, through a 280 nm long-pass filter (Schott glass, 280 GY 25, Comar, UK), which had a power density of 1 mW/cm² (Measured by a 365 nm UV power meter, Carl Suss, UK). The whole 1 x 1 cm surface was illuminated for 10 seconds before washing for 1 hour in deionised water. Four samples were taken at each stage of surface modification (silanisation, AACD conjugation, and protein-dextran conjugation), dried under nitrogen and stored at 4 °C before analysis by XPS. The XPS experiments were performed by Dr. David Morgan in Cardiff using the same parameters defined in §3.1.5.

3.2.11 Mask Fabrication for Multiple Alignment Patterning

UV grade fused silica (Spectrosil 2000®, 5 x 5 cm, 1 mm thick, UQG Ltd, UK) was used in the fabrication of chrome/gold photolithographic masks. Glass slides (5 x 5 cm, 1 mm thick, Fischer Scientific, UK) were used for patterning surface alignment marks. All surfaces were prepared and deposited with chrome/gold using the same protocol described in §3.1.2. To fabricate photolithographic masks the positive photoresist Shipley MICROPOSIT® S1813 (Rohm and Haas Ltd., UK) was spin-coated onto the chrome/gold coated UV fused silica surfaces and processed using the same protocols described in §3.1.2, using mask plate 1 and 2 (see Appendix C 1.2 and C 1.3 respectively).

To fabricate alignment features the negative photoresist Microchem SU-8 10 (Chestech Ltd., UK) was spin-coated onto the chrome/gold coated fused silica glass surfaces, gold surface face up, using a programmable photoresist spin coater (SCS G3P-8 Spincoat, Specialty Coating Systems (SCS) Coating Centre, UK). A typical program includes the following steps: i) spin at 500 rpm for 5 seconds to spread the photoresist; ii) ramp to 3000 rpm for 30 seconds for a uniform coating; and iii) reduce

to 500 rpm for 5 seconds to settle the photoresist. The thicknesses of the SU-8 10 photoresist, achieved using the described spin cycles, were between 9.9 μm and 10.2 μm , as measured using the KLA-Tencor P-16 stylus surface profiler.

The SU-8 10 coated samples were prebaked for 2 minutes at 65°C on a hotplate (EMS 1000-1, Electronic Micro System Ltd. UK) and then the temperature was ramped slowly (10°C/minute) to 95°C and held for 5 minutes. The SU-8 10 coated samples were left to cool for 30 minutes then positioned in a mask aligner (MA-6, Suss MicroTec Ltd. UK) and placed in contact with Mask 1 (see Appendix C.1), Photronics Inc, UK). The SU-8 10 samples were illuminated through the mask plate with UV light (300mJ measured with a 365 nm power meter, Suss MicroTec Ltd. UK) for 25 seconds and then removed from the aligner. The UV patterned SU-8 10 was then post baked for 1 minute at 65 °C on a hotplate and then the temperature was ramped slowly (10 °C per minute) to 95 °C and held for 2 minutes. Next the surface was allowed to cool for 10 minutes before being developed with Microchem SU-8 Developer (Chestech Ltd., UK), for 90 seconds. The samples were then rinsed with isopropanol, to stop the developer from further etching the photoresist, before drying under nitrogen.

The patterned photoresist, both S1813 and SU-810, were imaged by light microscopy (Nikon LV100D, UK) to determine whether the feature dimensions were correct. The pattern was transferred into the chrome/gold by immersion in gold etchant (1 %-10 % iodine: < 25 % potassium iodide, OM Group Ultra Pure Chemicals Ltd., UK) for 60 seconds and chrome etchant (OM Group Ultra Pure Chemicals Ltd., UK) for 10 seconds. The photoresist was cleaned from the surface by washing with acetone for 20 minutes, or until the resist was removed from the surface. The surface was then rinsed with isopropanol and deionised water before storing in a suitable container to prevent surface scratching. Surfaces were analysed by light microscopy (Nikon LV100D, UK) to ensure the feature sizes of the chrome/gold photolithographic mask and alignment features were the same proportions as the original mask plate designs.

Two masks plates were designed and used for the fabrication of alignment features and two photolithographic patterning masks. The two mask plates, Mask 1 (Appendix C.1) and Mask 2 (Appendix C.2), were designed to pattern aligned

features of proteins on a single substrate. Different sections of the masks were required to make the alignment marks and photolithographic masks separately.

3.2.12 Single Protein Patterning on Aryl Azide Conjugated Dextran Surfaces

Three proteins were used for the study of conjugation to AACD surfaces by UV initiated photo-attachment, streptavidin-FITC, IgG-FITC, and protein L. Stock solutions of streptavidin-FITC (1 μM), protein L (10 μM) and IgG-FITC (2.8 μM) were made. AACD surface were prepared as described in §3.2.9 and a 10 μL droplet of protein was pipetted on an AACD chip and spread by a photolithographic mask, gold face down. The surface was then illuminated with a 500W Hg(Xe) UV lamp (Oriol-Newport, UK), through a 280 nm long-pass filter (Schott glass, 280 GY 25, Comar, UK), for between 1 and 40 seconds at a power density of 1 mW/cm^2 , measured using a UV power meter (365 nm head, Karl Suss). Chips made using streptavidin-FITC (1 μM) and IgG-FITC (2.8 μM) were washed in deionised water for 1 hour before imaging by fluorescence microscopy (Axiovert Observer, Carl Zeiss) using an EC Plan-Neofluar 10x objective. The protein L (10 μM) chips were washed in deionised water for 1 hour, followed by a wash in 1 % (w/v) BSA wash for 1 hour to block the surface. The protein L surface was then rinsed in deionised water and dried under nitrogen. IgG-FITC (2.8 μM) was further diluted to give an aliquot of 500 nM IgG-FITC. Protein L chips had a 5 μL droplet of 500 nM deposited on the surface and spread with a glass coverslip (22 x 50 mm, Fisher Scientific, UK). The surfaces were incubated for 30 minutes with IgG-FITC (500 nM) before washing for 1 hour in deionised water. Finally the surfaces were dried under nitrogen and imaged by fluorescence microscopy (Axiovert Observer, Carl Zeiss) using an EC Plan-Neofluar 10x objective.

3.2.13 Purification and Characterisation of IgG Fragments Prior to Conjugation with a Fluorescent Probe

The purification, labelling and characterisation of IgG fragment described in this section, was performed by Dr. Lucy Braddick.

Papain from Papaya Latex (10 μL , 10 mg/mL suspension) was mixed with 90 μL of freshly prepared activation buffer (1 mM ethylenediaminetetraacetic acid

(EDTA), 10 mM L-cysteine, 50 mM sodium phosphate buffer pH 7.0) and incubated for 10 minutes at 37 °C. The L-cysteine was removed from the reaction mix by centrifugal ultrafiltration (10 kDa molecular weight cut off) and the L-cysteine free activated papain was reconstituted into 100 µL of digestion buffer (1 mM EDTA, 50 mM sodium phosphate buffer, pH 6.3). The digestion was initiated by the addition of activated papain to the antibody solution (1 mg/mL polyclonal mouse IgG) to give a papain/antibody ratio of 5 % (v/v). The solution was incubated at 37 °C for 2 hours. The reaction was stopped by addition of iodacetamide (30 mM final concentration) and the digest was analysed by SDS-PAGE. A Waters Biosuite Q AXC 7.5 x 75 mm column was equilibrated at 1 mL/minute with 20 mM TRIS Cl, pH 8.0. Elution of the antibody fragments was by a linear gradient 0-500 mM NaCl in 20 mM TRIS Cl. The eluted fragments were dialysed extensively against deionised water (10 kDa molecular weight cut off), freeze dried and reconstituted in 100 µL PBS.

Eluted fragments were labelled with Cy5.5 (GE Healthcare). Briefly Cy5.5 NHS-ester (5.4 µL, 1 mg/mL in DMSO) was added to 50 µL of purified sample and incubated on a shaker at room temp for 2 hours. The labelled fragments were then dialysed (3.5 kDa molecular weight cut off) against 0.15 M sodium chloride for 4 hours at room temperature then overnight at 4 °C. The solution was then changed to a 0.01 % sodium azide in 0.1 M PBS and dialysed for 4 hours at room temperature then overnight at 4 °C.

F(ab')₂ fragment (Pierce) was labelled with rhodamine, all buffers and reagents were degassed in a vacuum prior to use. A 10 fold molar excess of dithiothreitol (28.5 mM in PBS) was added to F(ab')₂ (42.78 µM, 0.01 M sodium phosphate, 0.25 M sodium chloride, pH 7.6) and incubated at 37 °C for 2 hours. The mixture was dialysed (3.5 kDa molecular weight cut off) extensively against PBS. Labelling was carried out under nitrogen and in the dark. 20 fold molar excess of freshly prepared tetramethylrhodamine-5-maleimide (10 mM in DMSO) was added to the reaction mix and incubated at room temperature for 2 hours. The reaction was stopped by adding excess mercaptoethanol. The labelled F(ab')₂ was then dialysed (3.5 kDa molecular weight cut off) against PBS extensively. The successful purification and labelling of Fc and F(ab')₂ was confirmed by dot blot against protein A and L.

3.2.14 Multiple Protein Patterning on Aryl Azide Conjugated Dextran Surfaces

Two protein combinations were used for patterning of multiple proteins on surface a control pattern, using IgG-FITC and NeutrAvidin, and an application pattern, using protein L and protein A. Stock solutions of IgG-FITC (500 nM) and protein L (10 μ M) were used, made up as described in §3.2.12. Stock solutions of NeutrAvidin (1 μ M), protein A (10 μ M) and biotin-4-fluorescein (1 μ M) were made up in 0.1 M phosphate buffer saline (PBS, pH 7.4). Glass surfaces with patterned alignment marks, fabricated as described previously (§3.2.1 and 5.6) were conjugated with AACD using the same method as surfaces in §3.2.9. To pattern multiple proteins an alignment system was used, which was built in-house with help from Dr. Nic Perney. The surfaces were attached to a sample holder platform (Figure 3-9 (a)) with double sided tape (Fisher Scientific, UK) to prevent the sample from moving, while allowing simple removal after processing. The sample was aligned, using the mask holder platform (Figure 3-9 (b)), close to the surface but without full contact.

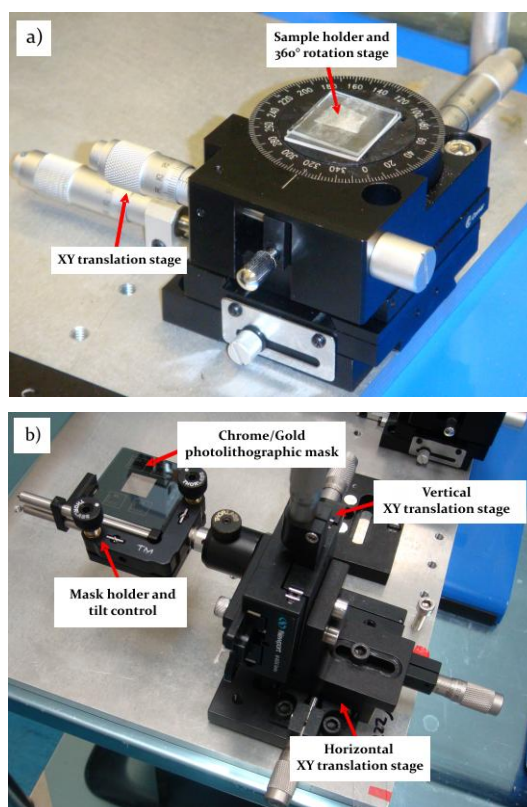


Figure 3-9 Images of alignment setup containing a) XY translation stages and 360° sample rotation stage (Newport), and b) chrome/gold mask XY and Z translation stages (Newport) and a tilt control (Thorlabs).

The alignment system shown in Figure 3-10 was then brought together and fine alignment achieved. Once alignment was complete the mask was removed from the surface and a 20 μL droplet of protein was deposited between the mask and sample. The mask was then brought back close to the sample surface and re-imaged, to ensure correct alignment, before placing the mask in full contact.

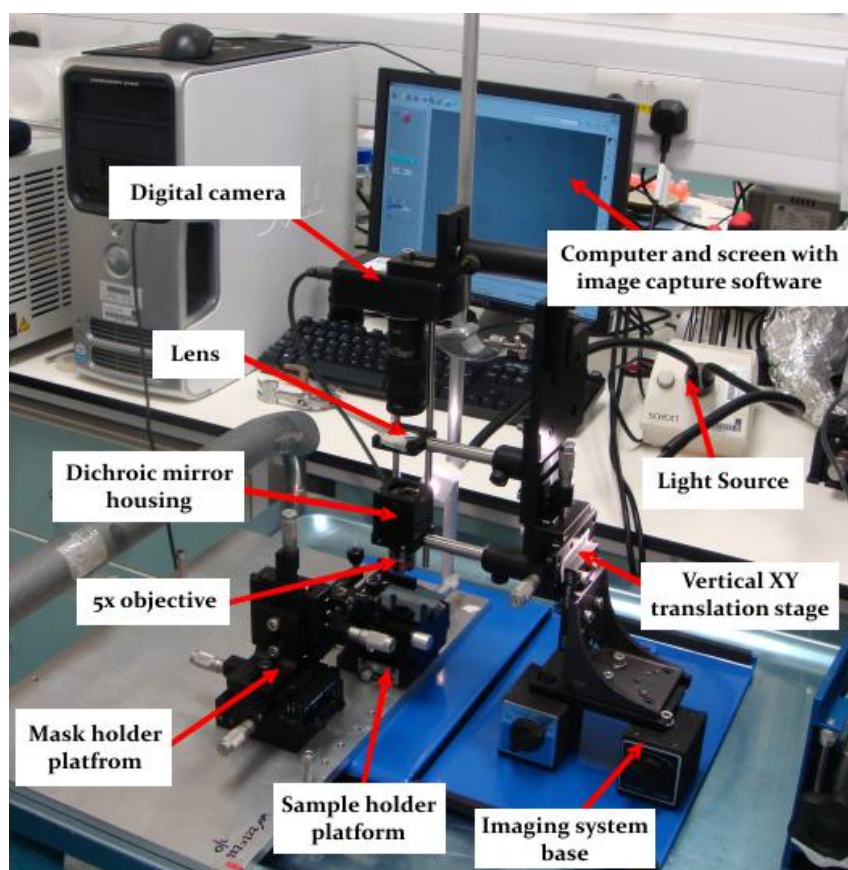


Figure 3-10 Image of complete alignment setup with alignment mark and mask image capture system (Gene Snap software), CCD camera (LW135M, Framos), lens (Comar, UK), 5x objective (Carl Zeiss, UK), dichroic mirror (Comar, UK), and white light source (Thorlabs, UK) shown over the sample holder/mask platform system used for surface alignment.

The image capture system was then removed and replaced by the UV illumination setup shown in Figure 3-11 (see overleaf). A 500W Hg(Xe) UV lamp (Oriel-Newport, UK) was used for illumination, through a 280 nm long-pass filter (Schott glass, 280 GY 25, Comar, UK), for 10 seconds at a power density of 1 mW/cm^2 , measured using a UV power meter (365 nm head, Karl Suss). The aligned mask/sample was first blocked from the UV beam, using aluminium foil and the electronic shutter (Oriel-Newport, UK) opened. The beam trajectory was aligned to fall upon the mask/sample through the 280 nm longpass filter. The shutter was then closed and the aluminium foil removed from blocking the mask/sample. The shutter

was then opened, allowing UV to illuminate the mask/sample, for 10 seconds before being closed. The mask was then carefully retracted from the surface and the sample peeled from the rotation platform. Next surfaces were rinsed with deionised water to remove any un-conjugated protein then dried under nitrogen. The sample was then returned to the rotation platform and the process repeated using the next set of alignment marks and a second protein solution.

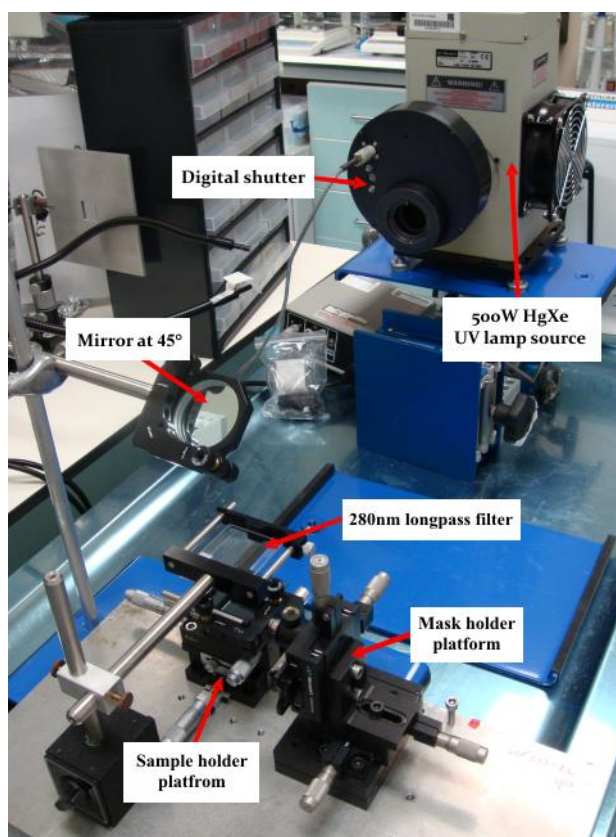


Figure 3-11 Image of the illumination setup. The 500W Hg(Xe) UV lamp (Oriel-Newport, UK) has a digital shutter (Oriel-Newport, UK), which when opened illuminates the 45° mirror (Comar, UK), which reflects light through the 280 nm longpass filter (Comar, UK) onto the aligned mask/sample below.

After illumination samples were washed in deionised water for 1 hour followed by a 1 % (w/v) BSA wash for 1 hour. Samples conjugated with IgG-FITC first then NeutrAvidin had a 10 μ L droplet of biotin-4-fluorescein (1 μ M) deposited on the surface and spread with a glass coverslip (22 x 50 mm, Fisher Scientific, UK). Surfaces were incubated for 40 minutes before washing in deionised water for 1 hour and imaging by fluorescence microscopy (Axio Observer, Carl Zeiss, UK). The surfaces conjugated with protein A and protein L had a 10 μ L droplet of IgG-FITC (500 nM) deposited on the surface and spread with a glass coverslip (22 x 50 mm,

Fisher Scientific, UK) for single binding studies. For specific binding studies a 10 μ L droplet of rhodamine labelled F(ab')₂ (2.2 μ M) was used instead of IgG-FITC (500 nM). Surfaces were incubated for 40 minutes before washing in deionised water for 1 hour and imaging by fluorescence microscopy. Filter set 15 and filter set 9 (Carl Zeiss, UK) were used to analyse the rhodamine and FITC surfaces, by fluorescence microscopy, respectively.

3.2.15 Protein Surface Concentration Analysis

AACD surfaces were prepared using the same protocol as described previously (§3.2.9). A 5 μ L droplet of protein L (10 μ M) was deposited on the surface and spread with an 18 x 18 mm glass coverslip. The whole surface was illuminated using the same 500 W Hg(Xe) UV lamp (Oriel-Newport, UK), through a 280 nm long-pass filter (Schott glass, 280 GY 25, Comar, UK), for 10 seconds at a power density of 1 mW/cm², measured using a UV power meter (365 nm head, Karl Suss). The surfaces were then washed in deionised water for 1 hour, followed by a wash in 1 % (w/v) BSA wash for 1 hour to block the surface. The protein L surface was then rinsed in deionised water and dried under nitrogen. A 10 μ L droplet of IgG-FITC (500 nM) was deposited on the protein L patch and spread over the whole surface using a 22 x 50 mm glass coverslip and incubated for 40 minutes. Finally, the surface was washed in deionised water for 1 hour and dried under nitrogen before stripping.

To strip the surface a 10 mL solution of sodium hydroxide (0.1 M, pH 12) was used. The IgG-FITC/protein L chip was placed in a petri dish (5 cm diameter) and 1 mL of the sodium hydroxide solution deposited over the patterned surface. The surface was placed on a shaker at 30 rpm for 30 minutes before the solution was removed. The solution was neutralised with 6 μ L of 5 M hydrochloric acid before aliquoting into 500 μ L vials for freeze drying. The samples were frozen in liquid nitrogen and then placed under vacuum in a freeze drier (Perkin Elmer, UK) and left overnight. The samples were re-suspended in 200 μ L of PBS buffer (0.1M, pH 7.4) and the fluorescence of the solution analysed using a fluorimeter (Perkin Elmer, UK). The solutions were excited at a wavelength of 494 nm and the emission scanned between 500 and 560 nm.

To determine the concentration of IgG-FITC stripped from the surface a standard curve of fluorescence intensity against concentration was produced. Serial

dilutions of IgG- FITC were made to produce concentrations of between 50 and 500 nM. A 200 μ L sample of each concentration was treated with 1 mL of 0.1 M sodium hydroxide (pH 12) for 30 minutes before neutralising with 6 μ L of 5 M hydrochloric acid. The samples were freeze dried under the same conditions and re-suspended in 200 μ L of PBS (0.1 M, pH 7.4). Each concentration was analysed by fluorimetry using an excitation wavelength of 494 nm and the emission scanned between 500 and 600 nm.

4

Bioconjugation of Micron and Submicron Protein Motifs on Silicon Surfaces

4.1 Introduction

Many challenges still remain with respect to selective bioconjugation of proteins to surfaces in defined micron sized patterns. The creation of highly dense, reproducible patterns of protein conjugated on a surface, where the protein retains specific recognition for analyte is key [50]. Further criteria include: defining patterns with submicron scale resolution and producing a homogeneous orientation upon the surface. To achieve the criteria set it is advantageous to ensure biomolecular recognition molecules are covalently linked by a method that later allows integration of a microfluidic channel.

As discussed in Chapter 2, the conjugation of DNA to silicon surfaces was achieved in far higher densities than for any other substrate [128] and thus the investigation of protein conjugation on silicon is warranted. Silicon is a robust atomically flat substrate with a low intrinsic autofluorescence [297] that has been utilized in the fabrication of microfluidic devices [50]. Described here is a UV initiated conjugation reaction to covalently attach a heterobifunctional cross-linker onto a hydrogen terminated silicon <100> surface. Previous work has revealed that the cross-linker undecylenic acid *N*-hydroxysuccinimide (UANHS) is capable of producing highly dense patterns of DNA with excellent reproducibility on silicon [128].

4.2 The Fabrication of Photolithographic Masks for Silicon Patterning

In order to produce highly dense patterns of protein a photolithographic mask was required. The mask defines where the UV light illuminates the surface, which directs the conjugation of the bifunctional linker. The mask can also be used to align the protein patches for integration with a microfluidic channel. The protocol used to fabricate chrome/gold photolithographic masks is described in §3.1.2.

Transmission images of the chrome/gold patterned masks produced after fabrication are shown in Figure 4-1. The image shows white lines, which are transparent regions, where the chrome/gold has been etched to form the pattern. The scale of the features correlates to within $<1 \mu\text{m}$ of the original mask design. Results taken from the whole surface recorded 120 lines of $10 \mu\text{m} \times 2 \text{mm}$ dimensions as defined from the original mask pattern.

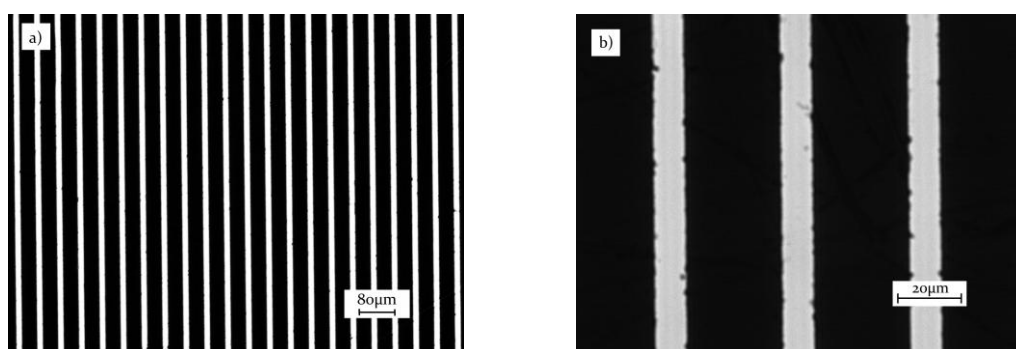
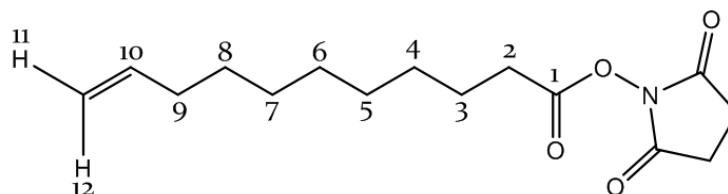


Figure 4-1 Transmission image of $10 \mu\text{m}$ features of the Chrome/Gold Photolithography mask captured at (a) EC Plan-Neofluar 10x objective and (b) a LD A-Plan 63x objective.

4.3 Photopatterning of Alkene Patterns on Silicon

4.3.1 Synthesis of Undecylenic Acid *N*-Hydroxysuccinimide ester

The protocol used to synthesise and characterise UANHS, by NMR, is described in §3.1.1. The NMR assignment, in Figure 4-2, was consistent with that for UANHS described by Yin *et al.* [131].



^1H NMR (400MHz, CDCl_3) δ 5.81 (1H, ddt, $J = 17.1, 10.0, 6.5\text{Hz}$, H^{10}), 4.98 (1H, ddd, $J = 17.1, 3.5, 1.5\text{Hz}$, H^{12}), 4.92 (1H, ddt, $J = 10.0, 2.0, 1.5\text{Hz}$, H^{11}), 2.59 (2H, t, $J = 7.5\text{ Hz}$, H^2), 2.03 (2H, qt, $J = 7.01, 1.5\text{Hz}$, H^9), 1.74 (2H, qn, $J = 7.47$, H^3) 1.46-1.34 (4H, m, $\text{H}^{4,8}$), 1.36-1.27 (6H, m, $\text{H}^{5,6,7}$);

Figure 4-2 NMR spectra assignment of undecylenic acid *N*-hydroxysuccinimide (UANHS)

4.3.2 Scanning Electron Microscopy of Photopatterned Silicon

Surfaces were Photopatterned with UANHS and analysed using SEM, as described in §3.1.4. The images in Figure 4-3 (see overleaf) show 10 μm lines, of UANHS, patterned on the silicon surface. The number of lines and periodicity of the features are consistent with the features defined on the chrome/gold mask. The contrast change seen in the image is due to a change in the secondary electron profile, on conjugation of the UANHS. No pattern was observed on control samples, which were not coated with UANHS, indicating the pattern is a result of the conjugation of UANHS on the silicon surface.

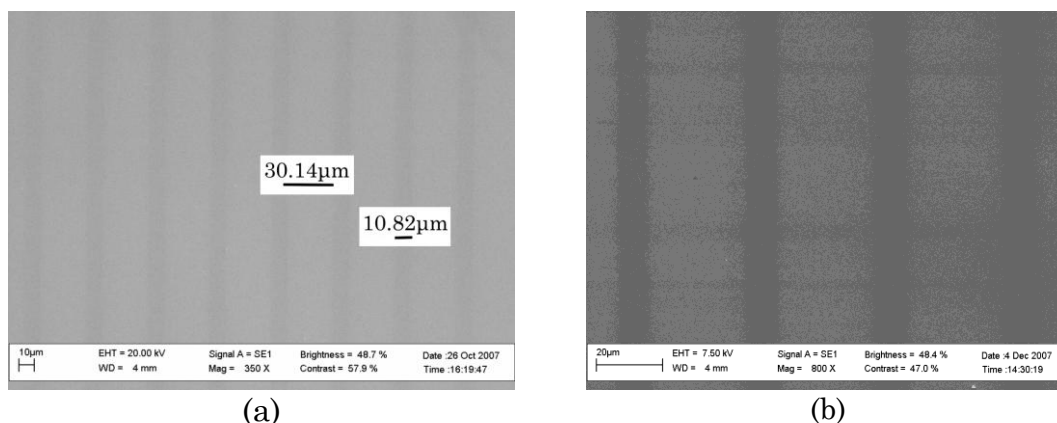


Figure 4-3 SEM image of UANHS derivatised surfaces with 10 μm features. Captured at (a) 350x magnification and (b) 800x magnification.

4.3.3 X-ray Photoelectron Spectroscopy of Photopatterned Silicon

The first application of X-ray photoelectron spectroscopy (XPS), or electron spectroscopy for chemical analysis, was demonstrated in 1967 by Siegbahn and co-workers [298]. The research described the irradiation of a sample with X-rays causing the emission of photoelectrons, which were detected to produce an energy spectrum. The principle is governed by the photoelectron effect described by Einstein in 1905. The process can be represented by the equation:

$$KE = h\nu - BE$$

where the kinetic energy of the emitted photoelectron (KE) is equal to Planck's constant, h (6.62×10^{-34} J s), multiplied by the frequency of radiation, ν (Hz), minus the binding energy (BE) of the electron. All elements, except hydrogen, have core electrons whose binding energy levels are characteristic of the specific element. Each element will therefore produce a characteristic set of peaks in the photoelectron spectrum [299]. The peak intensity can be used to quantify the concentration of the element within the sampled region. Quantification of chemical changes to the element, from oxidation or bond formation, can be determined from chemical shifts in the peaks. The local chemical environment has an effect on the binding energy, which can be used to characterise bonding. The XPS protocol is limited to probing chemistry within the first 5-10 nm of the surface, dependent on the X-ray source used. The reason for this is that, once emitted, the photoelectron can only penetrate a certain distance before undergoing scattering. This distance is dependent on the initial kinetic energy of the photoelectron and the nature of the solid [300].

Surfaces were prepared as described in §3.1.5 for analysis by XPS. The full XPS spectra for UANHS and NeutrAvidin functionalised silicon can be seen in Appendix D (1.1 and 1.2). The main peaks are given below and assigned to specific surface chemistry.

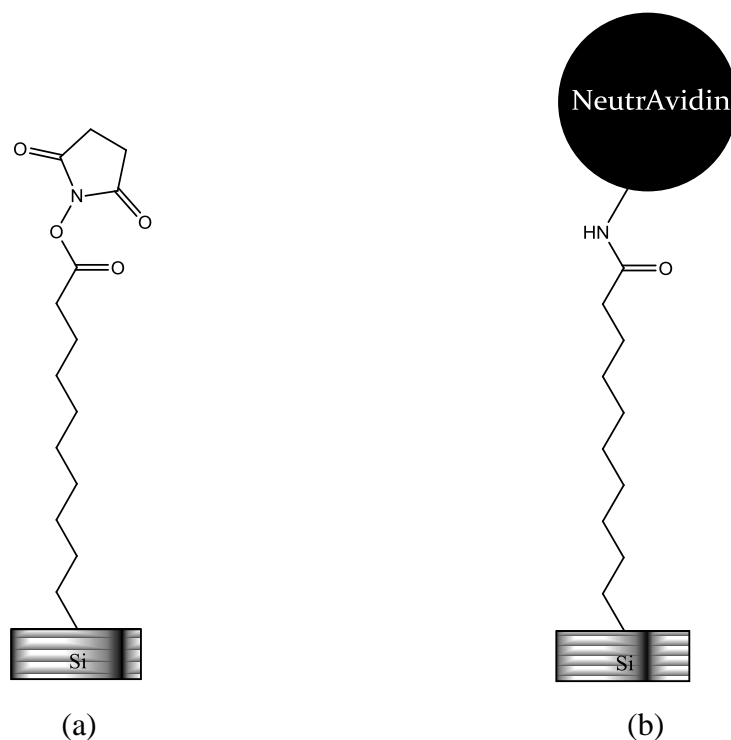
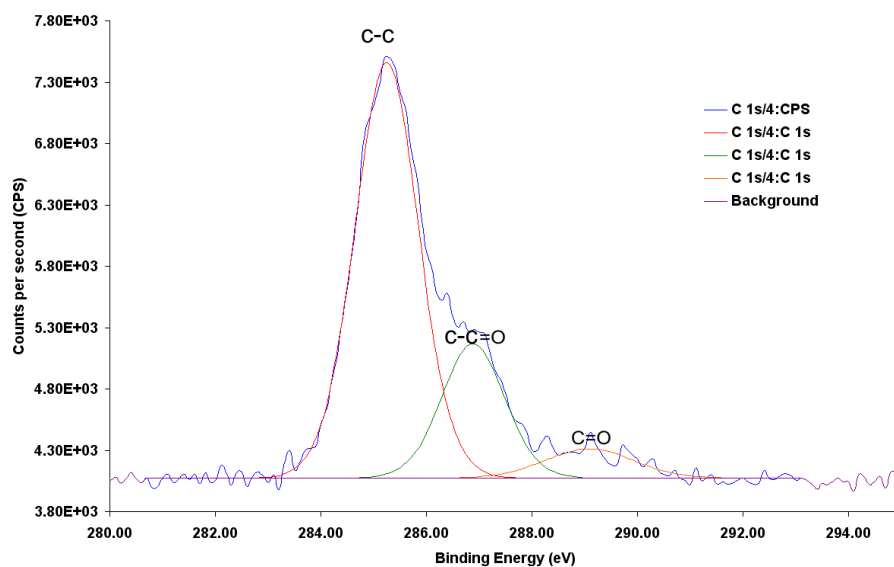


Figure 4-4 Illustration of the two surface modifications involved in conjugating protein with silicon including: (a) Conjugation of UANHS with silicon and (b) Immobilisation of NeutrAvidin on the UANHS conjugated surface.

The peaks shown in Figure 4-5 (see overleaf) were measured from silicon surfaces conjugated with UANHS, as illustrated in Figure 4-4 (a). The three carbon peaks of Figure 4-5 (see overleaf) (a) (285.2, 286.89 and 289.09 eV) can be attributed to the aliphatic carbon chain, the α -carbons adjacent to the carbonyl carbon atoms and the carbonyl carbon atoms respectively [137]. The single peak at 400.6 eV, shown in Figure 4-5 (see overleaf) (b), is from the nitrogen of the *N*-Hydroxysuccinimidyl-ester on the silicon.

a) Carbon



b) Nitrogen

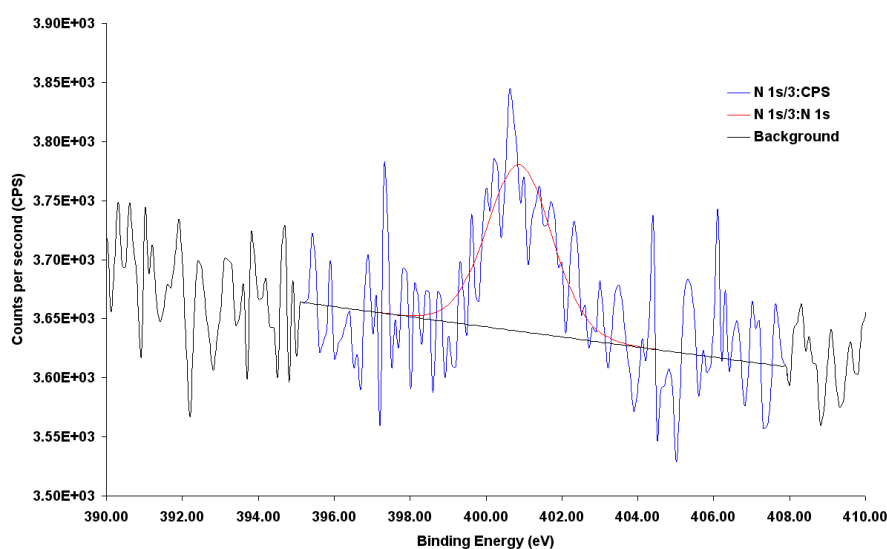
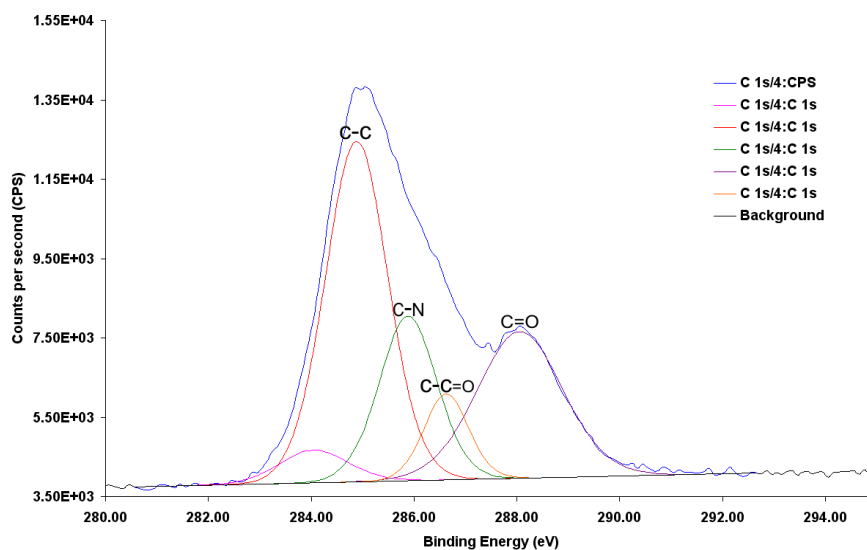


Figure 4-5 Peak fitting of data from XPS experiments (see §3.1.5) carried out on UANHS conjugated surfaces showing a) peaks assigned to carbon bonds and b) peaks assigned to nitrogen bonding

The peaks shown in Figure 4-6 (see overleaf) were measured from UANHS modified silicon surfaces conjugated with NeutrAvidin, as illustrated in Figure 4-4 (b) (see page 89). The introduction of a peak at 288.06 eV is characteristic of the amide bond present in peptide linkages of NeutrAvidin and formed by the conjugation of the protein onto the UANHS surface [301, 302]. The observation of two nitrogen peaks at 400 eV and 401 eV, compared with one at 400 eV for UANHS

surfaces, shows the clearest evidence for the immobilisation of NeutrAvidin on the surface [302].

a) Carbon



b) Nitrogen

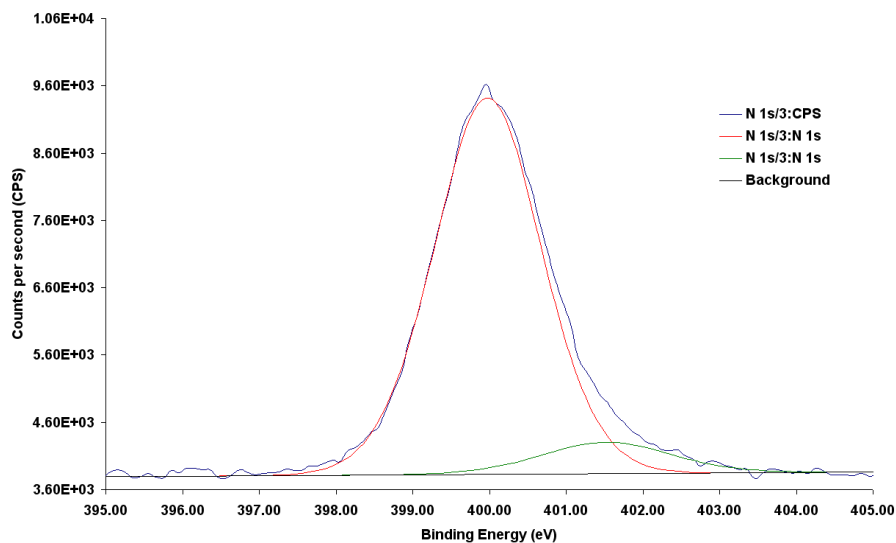


Figure 4-6 Peak fitting of data from XPS experiments (see §3.1.5) of NeutrAvidin conjugated silicon surfaces showing a) peaks assigned to carbon bonds and b) peaks assigned to nitrogen bonding.

The XPS data presented here shows that the silicon surface has been successfully modified with UANHS, which was then used for the subsequent conjugation of NeutrAvidin, as illustrated in Figure 4-4 (a) and (b) (see page 89).

4.4 Immobilisation of Proteins on Alkene Patterned Silicon

4.4.1 Conjugation of Streptavidin

First attempts at patterning the silicon surface with protein used streptavidin-FITC as a model protein. Streptavidin is commonly used for attachment to surfaces as it is a potential intermediate to allow further conjugation based upon the affinity reaction with biotin [273]. First trials used streptavidin-FITC to determine directly if protein could be conjugated to a UANHS patterned silicon surface. The structures in Figure 4-7 shows the stages involved in conjugating the streptavidin-FITC to the surface.

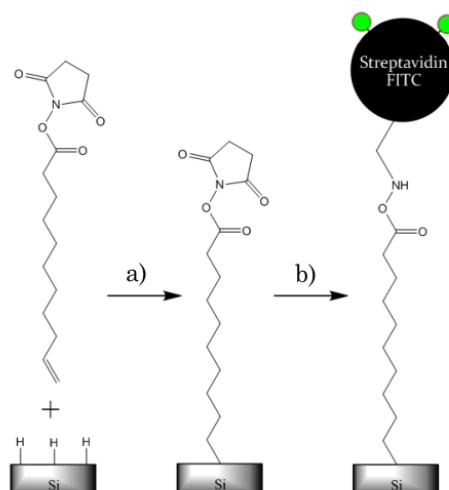


Figure 4-7 Chemical structures of the surface modifications used to produce the images in Figure 4-8 (see overleaf) including: (a) Conjugation of UANHS to silicon and (b) Conjugation of streptavidin-FITC.

Fluorescence images of the streptavidin-FITC (10 μM) immobilised surface can be seen in Figure 4-8 (see overleaf). The attachment protocol is effective at conjugating a reproducible pattern of streptavidin-FITC to the UANHS patterned surface. The next stage of conjugation analysis was to determine if once bound to the surface the protein retained recognition properties.

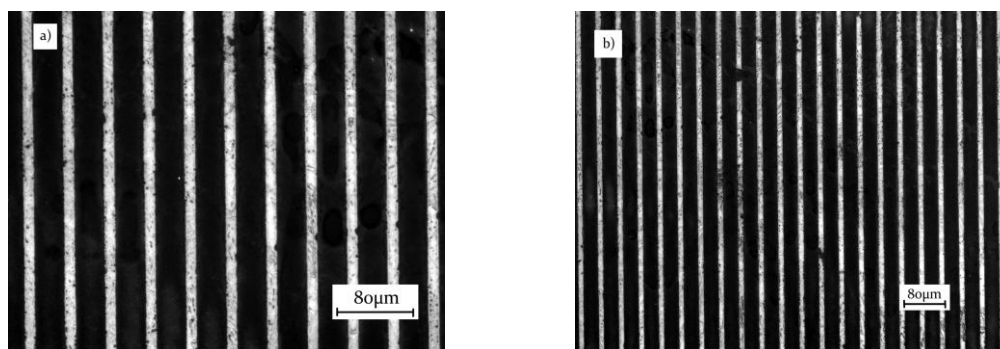


Figure 4-8 Epifluorescence images of streptavidin-FITC ($10\ \mu\text{M}$) captured using (a) an LD A-Plan 20x objective, 5 second image capture and (b) an EC Plan-Neofluar 10x objective, 3 second image capture.

To analyse whether the protein remained binding specificity upon patterning the surface was conjugated with streptavidin ($10\ \mu\text{M}$), and visualised by incubation with biotin-FITC ($1\ \mu\text{M}$). The surface processing, illustrated in Figure 4-9, involved conjugation of streptavidin with the UANHS patterned surface before incubating with fluorescently labelled biotin. To reduce non specific biomolecule adsorption the protocol included a 1 % (w/v) BSA wash, as described in §4.4.

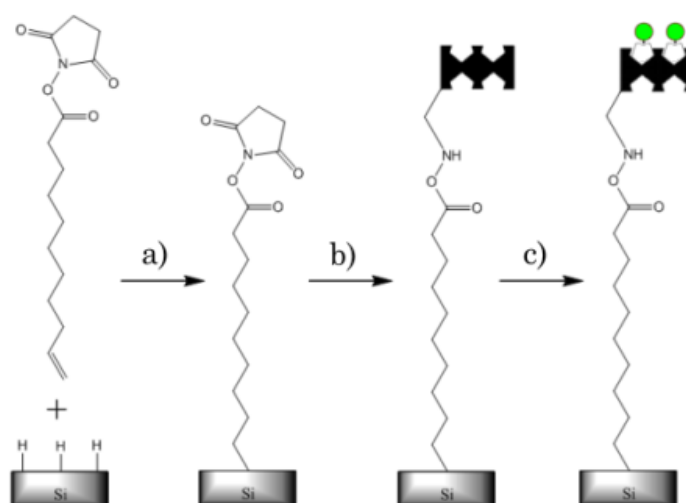


Figure 4-9 Chemical structures of the surface modifications used to produce the images in Figure 4-10 (see overleaf) including: (a) Conjugation of UANHS to silicon, (b) Immobilisation of streptavidin and (c) Incubation of the streptavidin immobilised surface with biotin-FITC.

The images in Figure 4-10 (see overleaf) show the fluorescent pattern revealed upon incubation of the streptavidin surface with fluorescently labelled biotin. The images show the retention of recognition between the immobilised streptavidin and the fluorescently labelled biotin. The retention of recognition

properties by the immobilised biomolecule is paramount for the development of functional protein patches aligned within a microfluidic channel.

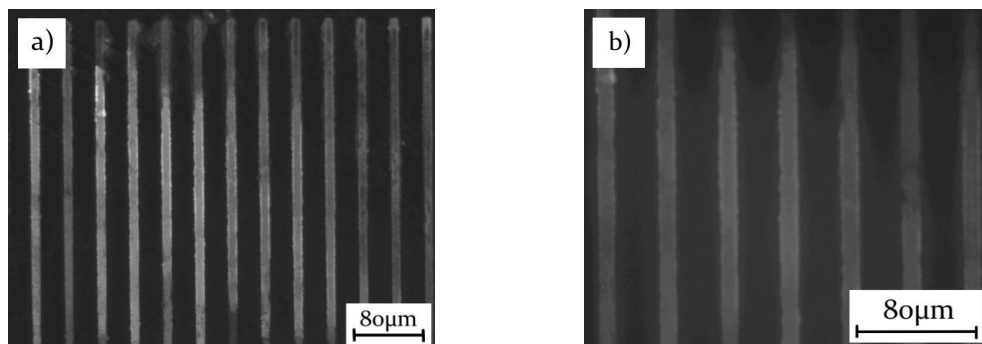


Figure 4-10 Epifluorescence image of biotin-FITC ($1 \mu\text{M}$) bound to streptavidin ($10 \mu\text{M}$) derivatised surfaces captured with (a) an EC Plan-Neofluar 10x objective, 3 second image capture and (b) an LD A-Plan 20x objective, 5 image capture.

4.4.2 Conjugation of Single Domain Protein L

Having attached streptavidin to the surface successfully and shown that the binding properties for biotin were retained, the single binding domain PpL₃₃₁₆ was similarly attached to the surface. The difference between single domain protein L and multidomain protein L are discussed in §2.2.4.1. The steps taken to immobilise PpL₃₃₁₆ on the surface are shown in the chemical structures in Figure 4-11 (see overleaf). The surface was incubated with PpL₃₃₁₆ ($10 \mu\text{M}$) and subsequently incubated with fluorescently labelled polyclonal mouse IgG (500 nM) to reveal the protein patterned surface.

Samples were analysed, using the protocol described in §3.1.6 with and without a 1 % BSA wash to determine how effective the step was at preventing surface fouling when using fluorescently labelled IgG. Silicon itself has low auto-fluorescence which makes it a good substrate for fluorescent imaging.

A key problem in the site specific immobilisation of protein is biofouling by biomolecules during incubation. When these biofouling molecules are fluorescent they mask specific interactions taking place on the surface compared with the non specific interactions. To prevent such fouling BSA, which is anticipated to adsorb on the surface, is used to provide a barrier that will reduce the association of fluorescent biomolecules of interest with the surface thus preventing non specific adsorption.

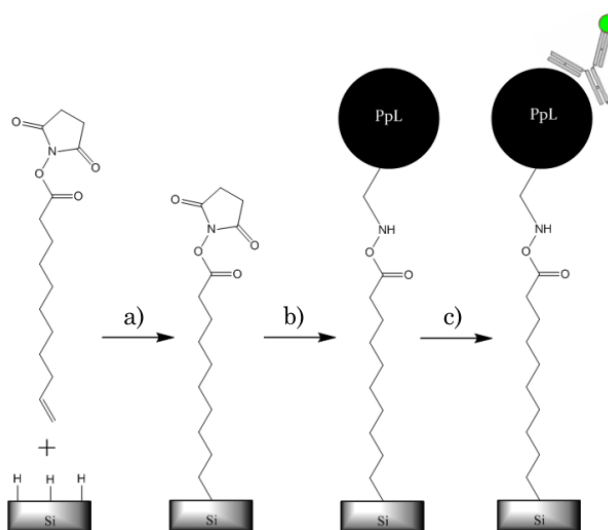


Figure 4-11 Chemical structures of the surface modifications used to reveal the immobilisation of PpL₃₃₁₆ on silicon, including: (a) Conjugation of UANHS to silicon, (b) Immobilisation of PpL₃₃₁₆ and (c) Incubation of the PpL₃₃₁₆ immobilised surface with IgG-FITC.

Figure 4-12 (a) shows a PpL₃₃₁₆ (10 μ M) patterned surface incubated with fluorescently labelled polyclonal mouse IgG (500 nM) without blocking with 1 % BSA. High levels of non specific binding can be observed over the surface, which mask any specific interactions. Conversely Figure 4-12 (b) shows a surface made using the same protocol with the addition of a 1 % BSA wash for 1 hour. The blocking step clearly reduces the non-specific binding of fluorescent IgG with the surface. The contrast between the pattern and the background is greatly increased and specific surface interactions can be observed.

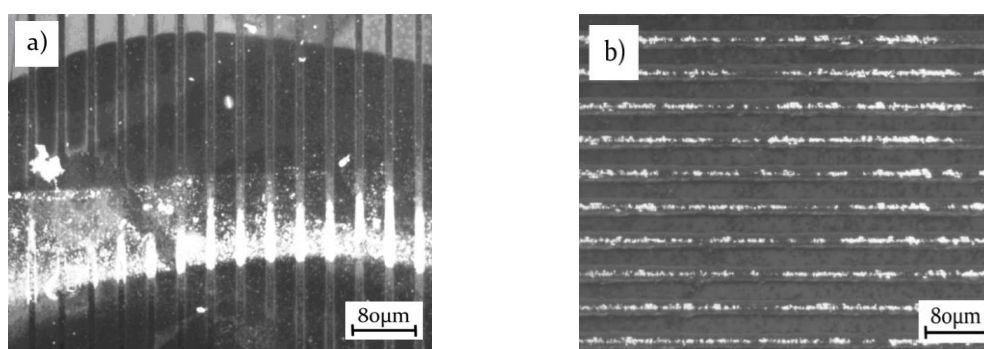


Figure 4-12 Epifluorescence image of IgG-FITC (500 nM) bound to PpL₃₃₁₆ (10 μ M) derivatised surfaces incubated after (a) no BSA pre-wash and (b) a 1 % BSA pre-wash. Both images were captured using an EC Plan-Neofluar 10x objective with a 4 second image capture.

Analysis of different buffer conditions showed no significant change in the reproducibility of PpL₃₃₁₆ patterning. Experiments therefore used the original buffer solution, 0.1 M sodium carbonate, which gave the best results. The buffer was kept

at pH 8.4 to ensure amine groups present on the PpL₃₃₁₆ remained in a deprotonated form allowing non-charged amine groups to interact with the ester group on the UANHS patterned surface. A high pH increases the rate of hydrolysis of the NHS-ester groups [201]; however the conditions used here showed no significant prevention of protein conjugation, thus negating the need to reduce the pH of the buffer.

To improve reproducibility, the effect of changing the UV power density and exposure time on PpL₃₃₁₆ conjugation was analysed. The protocol described in §3.1.6 was used with changes to the power density investigated. Surfaces processed with recorded power densities of 1, 3 and 5 mW/cm² were analysed. Samples that were exposed to power densities >1 mW/cm² showed over exposed regions, which did not conjugate proteins. The protocol described in §3.1.6 was then used with changes to the time of exposure. Samples were illuminated at 1 mW/cm² for 1, 3, 5, 10 and 15 minute illumination times. All samples prepared with an illumination time below 5 minutes showed no protein conjugation and above 5 minutes showed overexposure. 5 minutes was therefore used as the threshold time for conjugation to occur using the setup defined. Examples of PpL₃₃₁₆ surfaces incubated with IgG-FITC that have been over and underexposed can be seen in Figure 4-13 (a) and (b) respectively (see overleaf). Finally the protocol described in §3.1.6 was used to investigate the effect of using different protein buffer conditions on conjugation. Results showed samples prepared using 0.1 M sodium carbonate buffer produced more reproducible results compared with samples prepared using the other buffers analysed.

The work described led to the determination of a set of conditions that gives reproducible coverage of PpL₃₃₁₆ patterns on the surface of silicon. The optimised parameters are:

1. Use of a 254 nm bandpass filter
2. A recorded surface power density of 1 mW/cm²
3. An illumination time of 5 minutes.
4. A PpL₃₃₁₆ concentration of 10 µM dissolved in a 0.1 M sodium carbonate buffer (pH 8.4).
5. Incubation with 1 % BSA solution for 1 hour before fluorescent probe incubation.

The samples displayed in Figure 4-14 show a characteristic surface produced with the optimised parameters, with a surface coverage of ~80 %. The variations in intensity over the lines may be a sign of reduced coverage as a result of different accessibility of the PpL₃₃₁₆ with IgG-FITC.

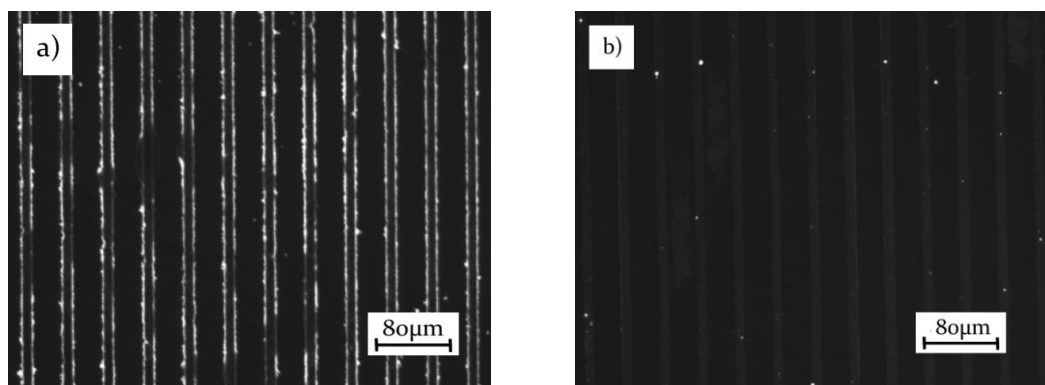


Figure 4-13 Images of IgG-FITC (500 nM) bound to PpL₃₃₁₆ (10 μ M) derivatised surfaces that have been (a) over and (b) under exposed. Images were captured with an EC Plan-Neofluar 10x objective, 5 second image capture.

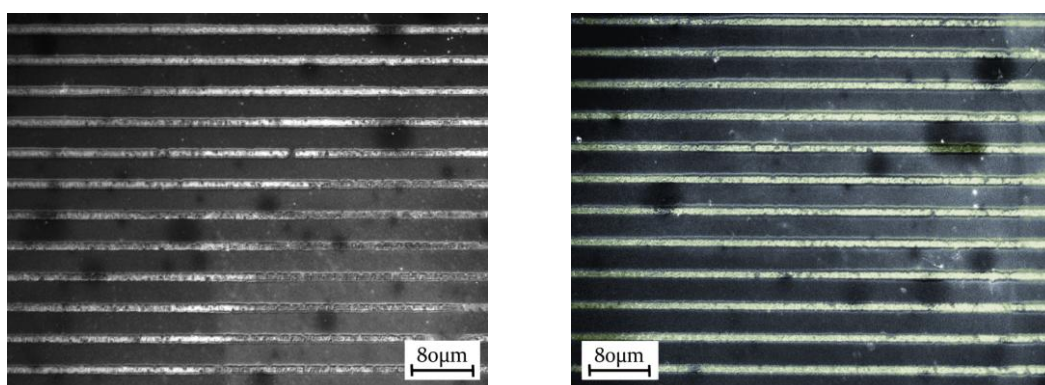


Figure 4-14 Images of IgG-FITC (500 nM) bound to PpL₃₃₁₆ (10 μ M) derivatised surfaces captured with an EC Plan-Neofluar 10x objective, 5 second image capture.

4.4.3 Conjugation of Multidomain Protein L

Experiments involving multidomain protein L, carried out using the protocol described in §3.1.6, did not react as well using the optimised conditions determined for PpL₃₃₁₆. The images in Figure 4-15 show results obtained with the multidomain protein L (10 μ M) on incubation with IgG-FITC (500 nM). The first striking feature is the increased intensity within the patterned lines compared with patterns of PpL₃₃₁₆. This is not unexpected as multidomain protein L has 5 possible Ig binding domains (see §2.2.4.1), compared with one Ig binding domain in the case of PpL₃₃₁₆, which may increase the number of IgG molecules able to bind. The other noticeable feature is that the conjugation is not reproduced over the whole surface, as only

patches of functional protein are observed on the surface. The steps taken to immobilise multidomain protein L on the surface are shown in the chemical structures in Figure 4-16.

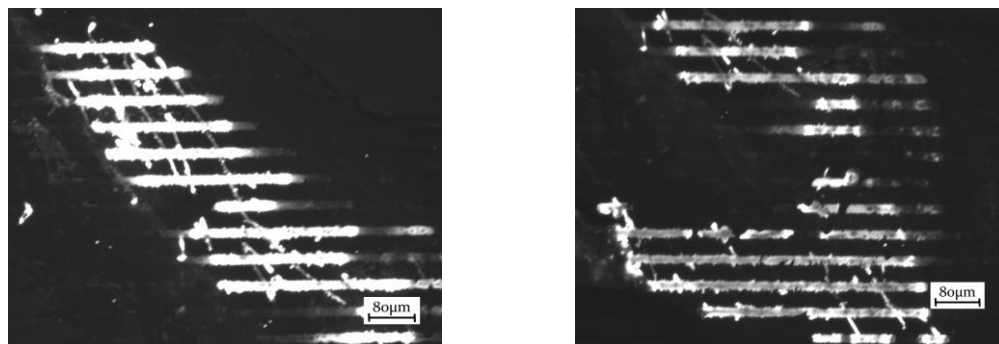


Figure 4-15 Images of IgG-FITC (500 nM) bound to protein L (10 μ M) derivatised surfaces captured with an EC Plan-Neofluar 10x objective with a 1 second image capture.

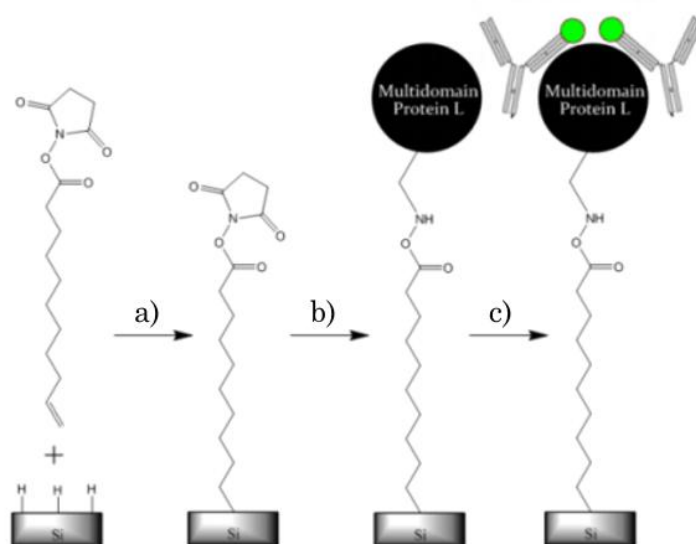


Figure 4-16 Chemical structures of the surface modifications used to produce the images in Figure 4-15 including: (a) Conjugation of UANHS to silicon, (b) Immobilisation of multidomain protein L and (c) Incubation of the protein L immobilised surface with IgG-FITC.

4.4.4 Conjugation of NeutrAvidin

Further work to improve the reproducibility of the pattern did not provide improved results. To determine why the protocol was not working a previously successful model system (NeutrAvidin) was analysed. This was to determine if the result was protein specific or a problem with the batch of silicon or alkene being used.

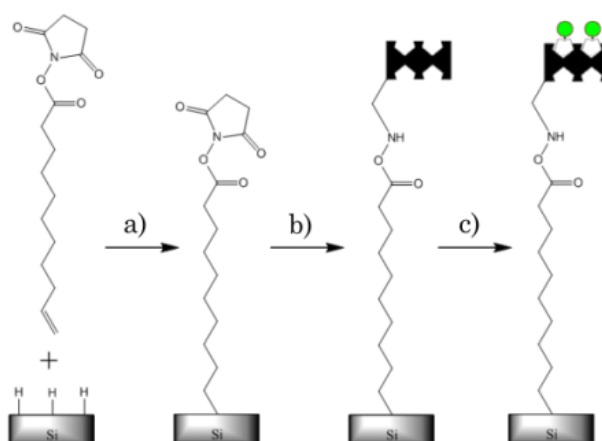


Figure 4-17 Chemical structures of the surface modifications used to produce the images in Figure 4-18 including: (a) Conjugation of UANHS to silicon, (b) Immobilisation of NeutrAvidin and (c) Incubation of the NeutrAvidin immobilised surface with biotin-FITC.

To circumvent the conjugation problems associated with direct conjugation of multidomain protein L the protocol described in §3.1.6 was used to conjugate NeutrAvidin ($1\ \mu\text{M}$) to the surface. By conjugating the surface with avidin, which had been shown to conjugate previously (§4.4.1), the biotin/avidin reaction could be used to conjugate a biotin modified protein. The steps taken to immobilise NeutrAvidin on the surface are shown in the chemical structures in Figure 4-17 (see previous page). NeutrAvidin was chosen as this protein is neutrally charged compared with streptavidin, which may reduce electrostatic adsorption. First it was confirmed whether NeutrAvidin was capable of forming reproducible protein patches, with retained protein viability. Figure 4-18 shows a NeutrAvidin ($10\ \mu\text{M}$) surface incubated with biotin-FITC ($1\ \mu\text{M}$), the surface shows a reproducible intensity over the surface. The contrast between the motif and the surface demonstrates the prevention of biofouling on the silicon surface.

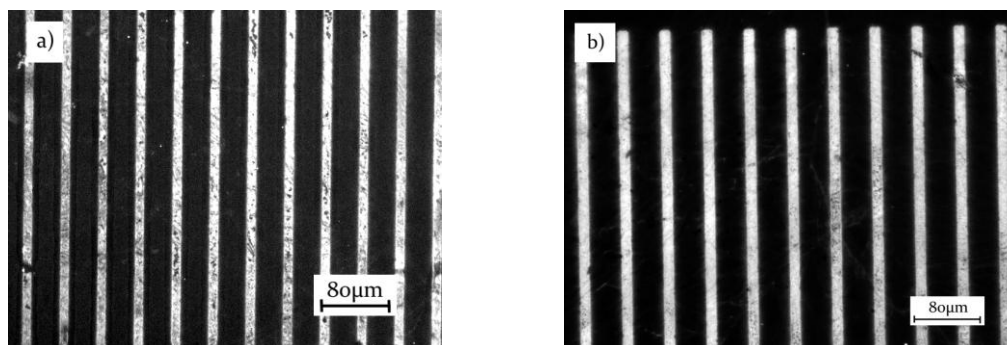


Figure 4-18 Epifluorescence images of biotin-FITC ($1\ \mu\text{M}$) bound to a NeutrAvidin ($10\ \mu\text{M}$) conjugated surface captured at LD A-Plan 20x objective with (a) a 5 second image capture and (b) a 4 second image capture.

4.4.5 Conjugation of Biotinylated Protein A

NeutrAvidin ($10\ \mu\text{M}$) was conjugated to surfaces using the protocol described in §3.1.6. The NeutrAvidin was then used as a surface anchor for subsequent attachment of a biotinylated protein A ($1\ \mu\text{M}$). The surface was then incubated with fluorescent murine IgG ($500\ \text{nM}$) to analyse if the protein A remained viable on the surface. The images in Figure 4-19 clearly shows the addition of the NeutrAvidin prior to protein A-biotin conjugation allows the protein A to remain viable when conjugated to the silicon surface. The steps taken to immobilise biotinylated protein A on the surface are shown in the chemical structures in Figure 4-20.

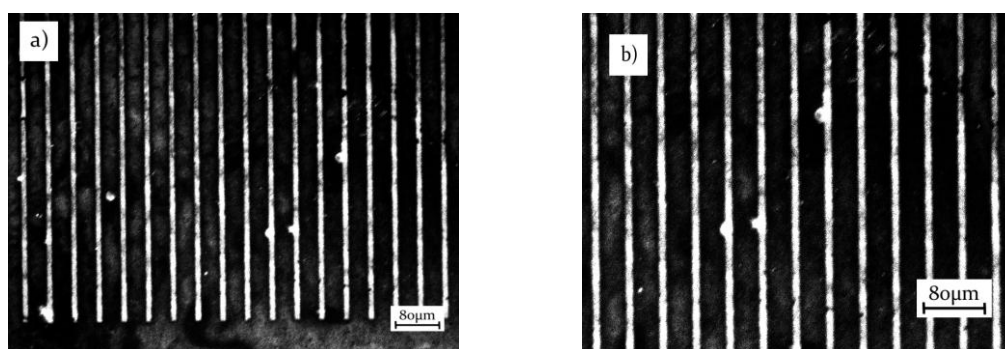


Figure 4-19 Epifluorescence images of IgG-FITC ($500\ \text{nM}$) bound to a protein-A biotin ($1\ \mu\text{M}$), which is associated to a NeutrAvidin ($10\ \mu\text{M}$) immobilised surface taken using a) an EC Plan-Neofluar 10x objective, 3 second image capture and b) an LD A-Plan 20x objective, 5 second image capture.

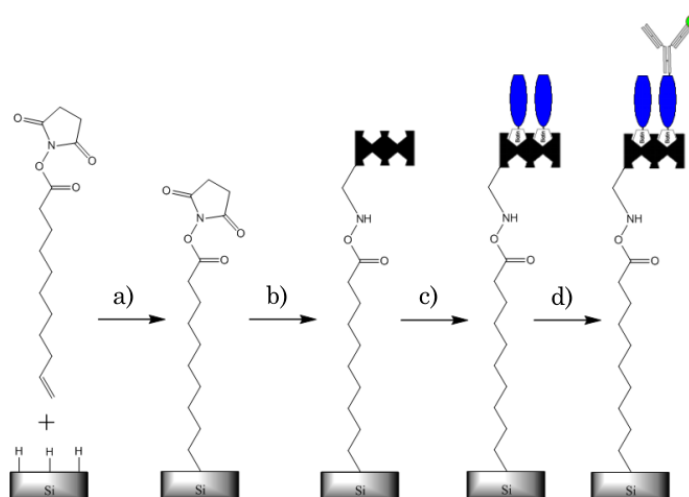


Figure 4-20 Chemical structures of the surface modifications used to produce the images in Figure 4-19 including: (a) Conjugation of UANHS to silicon, (b) Immobilisation of NeutrAvidin, (c) Incubation of the NeutrAvidin surface with biotin-protein A and (d) Incubation of the protein A terminated surface with IgG-FITC.

4.5 Submicron Patterning of Protein

The chrome/gold masks fabricated using the protocol described in §4.2 are not suitable for submicron patterning. To pattern protein motifs at the submicron scale a phase mask was used. The illustration in Figure 4-21 shows the formation of an interference pattern produced by the phase mask. The features fabricated in the phase mask cause the beam to diffract generating two outgoing beams. This creates an interference pattern dependent on the period of the phase mask used.

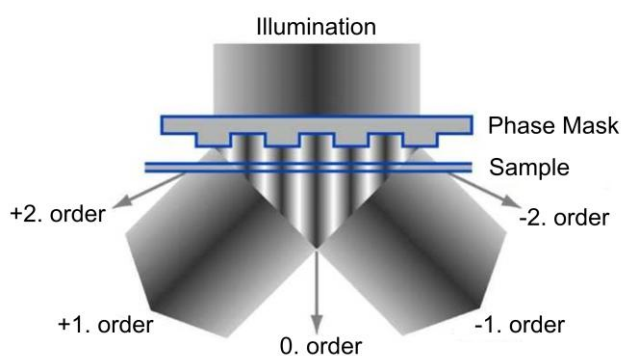


Figure 4-21 The phase mask uses a +1/-1 order principle, where light is diffracted equally into the plus first and minus first orders. Self-interference between these two orders creates an interference pattern with half the pitch of the Phase mask pitch (Reprinted with permission from Ibsen Photonics).

Figure 4-22 (see overleaf) shows an SEM image of a submicron patterned UANHS surface with 140 nm wide features. Surfaces incubated with fluorescently labelled streptavidin showed concurrent patterns with the same dimensions as observed under SEM (Figure 4-23) (see overleaf). The results demonstrate that submicron patterns of protein on silicon are achievable, which represents a significant achievement.

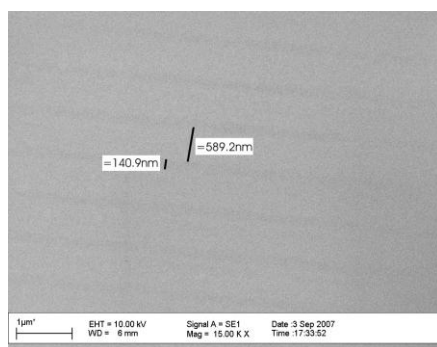


Figure 4-22 SEM image of UANHS derivatised surfaces with 140 nm features (magnification x15,000)

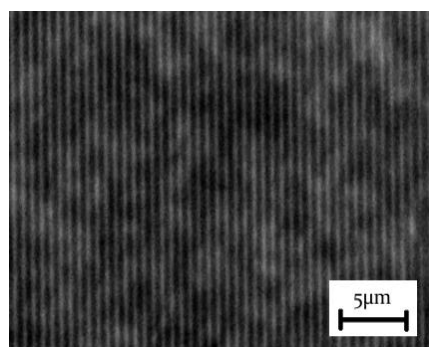


Figure 4-23 Epifluorescence image of streptavidin-FITC (1 μM) conjugated surfaces. Imaged using a Plan-Apochromat 100x oil immersion objective, 11.2 millisecond image capture.

4.6 Summary

High densities of DNA conjugated with silicon surfaces had been achieved previously [128]. In fact, based upon a literature review, silicon was found to have the highest density of DNA conjugated with the surface compared with other substrates [130, 145]. Silicon therefore warranted investigation to determine if high density patterns of protein were achievable. Protein conjugation techniques were based upon the work of Huabing Yin [128, 131], which describes the covalent attachment of DNA oligonucleotides to the surface of silicon <100>. The protocol was modified to attach proteins onto silicon including: streptavidin, NeutrAvidin, single domain protein L and multi domain protein L. The effect of buffer, UV power density, and illumination time on the reproducibility of patterning was investigated. Prevention of non-specific binding was examined resulting in the integration of a blocking step using 1 % BSA to reduce biofouling.

The linker, UANHS, used to conjugate protein on the silicon was successfully characterised by NMR and chemically modified surfaces were analysed by XPS. The NMR data was comparable with results published by Yin *et al.* [128], which used UANHS to conjugate DNA with silicon. The XPS data was also compared with published results, demonstrating that UANHS was successfully conjugated with the silicon surface [137]. The XPS data also confirmed that the UANHS remained functional, allowing the subsequent immobilisation of NeutrAvidin [302]. This study, similar to research undertaken with DNA [128], demonstrated that submicron

scale motifs of protein were achievable. Feature sizes as small as 140 nm were possible using the silicon patterning technique described in this thesis. Patterns of streptavidin, NeutrAvidin and single domain protein L were reproducible. The successful conjugation of submicron scale protein motifs on surfaces that prevent non specific adsorption, shown here, is vital to the development of microfluidic technologies.

5

Bioconjugation of Multiple Micron Sized Protein Patterns on Glass Surfaces

5.1 Introduction

The results presented in Chapter 4 demonstrate that photolithography can be used as a method to fabricate bioconjugated micron and submicron patterns of protein on silicon. It was found that the surface was prone to biofouling and non specific adhesion. To build upon the work described in Chapter 4, a protein attachment technique was devised that is based upon conjugation via a surface 'spacer' to the protein. The method integrated photoinitiated conjugation of protein with biofouling prevention and minimised the requirement of a cleanroom environment for surface processing. To date no patterning method has incorporated (i) an anti-fouling dextran layer, (ii) silane chemistry and (iii) a photolithographic method together to create protein patterns on a surface. The material of choice for this work was glass, a low cost transparent substrate, but the process would be expected to be useful for bioconjugation of protein to any silicon oxide surface.

The work presented in this chapter focuses on the development of a novel method to attach multiple proteins to a surface using a dextran modified with a photocrosslinker. The method allows for the sequential conjugation of different protein motifs to the surface. Full characterisation of surfaces and intermediates are described.

5.2 Protein Patterning on Glass Surfaces

Glass surfaces have received a lot of attention in the development of protein microarray technology, as it is a compatible surface with current DNA microarray hardware and software tools [64]. The process of silanisation, as described in §2.3.1, has been used previously as a method to modify surfaces for conjugation with proteins [303]. Typically the surface is cleaned and oxidised, using chemical [304] or plasma oxidation [305], increasing the proportion of hydroxide groups on the surface. This leaves a hydrophilic surface available to undergo a condensation reaction with free silanols to covalently couple the silane to the surface. The important group, in terms of protein patterning, is the variable R-group which is presented on the surface once silanisation has taken place.

5.2.1 Evaluation of Methods used to Silanise Glass

Glass surfaces described in this chapter were modified with a silane linker, 3-glycidoxypropyltrimethoxysilane (GOPS), to present a monolayer on the surface terminated with epoxide groups. A more common method involves the use of APTES for surface functionalisation, because of the reactivity of the amino terminated surface. Work by Yu *et al.* [306] demonstrates the use of APTES to attach dextran to PDMS surfaces, for the subsequent patterning of antibodies, within a microfluidic device. Silanes have also been directly conjugated or modified to produce aldehyde [307], poly(lysine) [308], NHS-ester [309], carboxyl [310] and maleimide [311] functional groups on surfaces. As well as being used to modify glass with chemistries that can conjugate biomolecules, silanes can also be terminated with chemicals designed to passivate a surface. The work by Jo and Park [312] demonstrated the conjugation of a silane with a polyethylene glycol, directly coupled to the silane, capable of preventing non-specific protein adsorption.

Aspects of the silanisation process have been studied in an attempt to produce a reproducible dextran layer on the surface. Different solvents have been used for the liquid phase deposition of silanes including ethanol [313], isopropanol [203], acetone [314], and toluene [150], amongst others [315]. The work by McGovern *et al.* [315] found that the use of toluene gave uniform, high density, films.

This was attributed to the ability of toluene to extract water from the substrate, required to hydrolyse the silane, which produces free silanols that are able to couple with the surface. The amount of silane used also affects the silanisation process significantly, as the higher the concentration of silane, the more water is required for silane hydrolysis to occur.

In this chapter the effect of silane concentration and silanisation time are studied to determine which conditions are best suited to increase the reproducibility of a dextran-FITC layer on the glass surface. The solvent conditions, pre and post bake temperatures and the use of a nitrogen atmosphere for silanisation are integrated into the method based on previously published work [203, 315]. The wide range of potential surfaces and possible biologically active chemistries compatible with silane chemistry, make it suitable for a universal attachment methodology.

5.2.2 Conjugating Protein to Dextran Surfaces

As outlined in §2.3.2 dextran is a naturally occurring carbohydrate composed of a chain of glucose units. The chain is formed of a main chain of α -1,6-glycosidic linkages [316], between glucose monomers, that generate a hydrophilic polymer. Dextran has been used widely in the development of surface plasmon resonance based biosensors [317, 318]. Commercially available Biacore chips (Biacore AB, Uppsala, Sweden) use carboxymethyl dextran (CMD) surfaces with different chain lengths, suitable to different applications. The CM-5 surface, considered the most versatile chip, is formed of a 500,000 MW CMD coupled to a gold surface (www.biacore.com). An illustration of a CMD coupled to a gold surface is shown in Figure 5-1 (see overleaf). The paper by Löfås *et al.* [319] describes methods for the chemical modification of CMD surfaces, used to couple biomolecules, for application in surface plasmon resonance systems. The methods described do not use a photochemical reaction to attach biomolecules to the surface and are therefore incompatible with protein patterning using photolithographic techniques.

To produce a surface capable of conjugating proteins using photolithography a method of attaching a photocrosslinker to the dextran, prior to immobilising the modified dextran on the surface, was required. The work by Elender *et al.* [203] described a simple methodology to covalently couple dextran to glass surfaces using GOPS. The oxirane ring undergoes a ring-opening reaction with hydroxyl groups

[320], present on the dextran, which can be used to form a covalent bond between the dextran and the surface. The resulting dextran surface has been used to attach biomolecules by conversion of the dextran to CMD, which can be modified to present NHS-ester moieties [296, 321]. This process uses a carbodiimide (*N,N'*-dicyclohexylcarbodiimide (DCC) [322], *N,N'*-diisopropylcarbodiimide [321] and EDC [296]) that reacts with carboxyl groups to form an unstable intermediate, which can react with *N*-hydroxysuccinimide to form an NHS-ester [195]. The NHS-ester moiety is capable of covalently binding proteins by reacting with amines on the protein surface to form an amide bond.

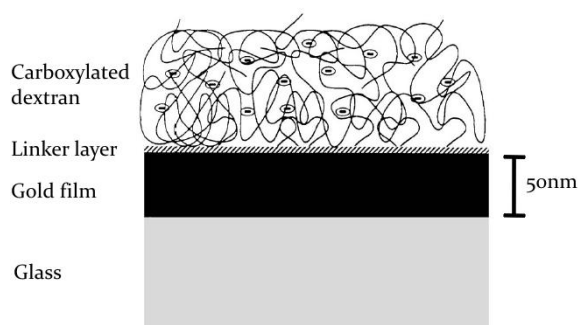


Figure 5-1 Illustration of a gold surface modified with CMD, reprinted with permission from [323].

The methods outlined in §2.3.3.2 show the range of techniques that have been applied to conjugate biomolecules by photoinitiation. The technique applicable to the aims of this thesis needs to be effective at attaching multiple proteins covalently to a surface. Patterning with photoresist is compatible with the production of multiple protein motifs, by using specific solvent and environmental conditions [269]. However, the method described by Petrou *et al.* [269] is not suitable for the aims of this thesis because the protein is adsorbed on the surface and not covalently attached. As discussed in §2.3.3.1 protein adsorption is potentially reversible and produces a heterogeneous protein orientation, which may change the proteins' recognition properties. Ideally, protein patterns require covalent attachment such that the protein remains stable and retains recognition properties. The use of caged photochemistry is limited by the reactivity of the chemistry towards proteins once de-protected. With any sequential patterning technique, a method to alter the surface after de-protection (e.g. EDC/NHS modification) would impact the chemistry of any proteins already bound with the surface. This is also true of any photoattachment technique used to conjugate a protein reactive chemistry with the

surface. For example the NHS-ester group of ANB-NOS can react with protein conjugated surfaces prior to UV initiated immobilisation.

Both photodegradation of the surface and surface conjugated photolinkers are suitable to the formation of multiple protein patterns. Aldehyde groups, formed by photodegradation, can react with a protein to form a Schiff base, which can be reduced to a stable amide bond. As the photolinker is immobilised on the surface it cannot interact with protein immobilised prior to activation. Surface coupled photolinkers have the same benefits of site specific activation without the potential for unwanted cross reactions. When considering a method suitable to covalently couple active patterns of multiple proteins, sequentially, a surface coupled photochemistry is desirable. Surface bound photolinkers can conjugate proteins upon photoinitiation and are suitable for integration with photolithography [324]. A protocol is envisaged whereby a dextran, modified with an aryl azide photolinker, can be immobilised on a surface for the subsequent conjugation of multiple protein motifs. A proposed method to conjugate proteins using an aryl azide conjugated dextran (AACD) is illustrated in Figure 5-2.

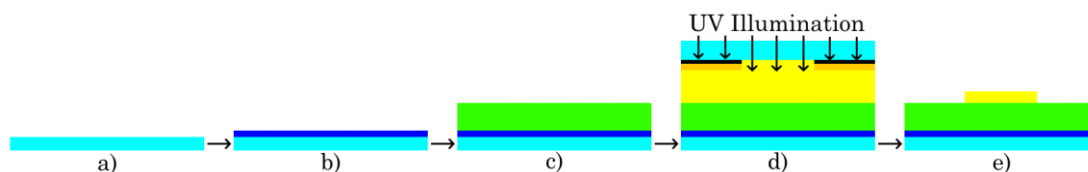


Figure 5-2 Illustration of the process envisaged to conjugate protein motifs on glass surfaces. Bare glass (a) is silanised with GOPS (b), which when incubated with AACD conjugates the dextran photolinker with the surface (c). Upon illumination with UV light a photoinitiated reaction forms a covalent attachment with protein in solution (d). Using a photolithographic mask the site of illumination can be controlled to produce protein motifs (e).

5.3 Optimisation of Conditions to Immobilise Dextran on Glass

The first stage in the development of the proposed protocol was to optimise the silanisation of glass for the conjugation of dextran to the surface. In the paper by Elender *et al.* [203] a 30 % w/v, or 300 μ M, solution of dextran is used for attachment to the silanised surface. This is a high concentration of reagent. It was important therefore to determine if such an excess was required for surface modification, or if

the reagent use could be reduced, with no discernable effects on the reproducibility of the resulting layer.

The images shown in Table 5-1 depict results obtained using three concentrations of dextran-FITC attached to glass surfaces silanised with 1 % GOPS for between 5 minutes and 24 hours. The black regions of the image show the background signal from the bare glass substrate, while the grey and white regions show the dextran-FITC immobilised surface. Results show that the dextran-FITC on the surface silanised for 5 minutes has a lower intensity compared with the samples silanised for 1 and 24 hours. After 1 hour there is a small increase in intensity compared with surfaces silanised for 24 hours.

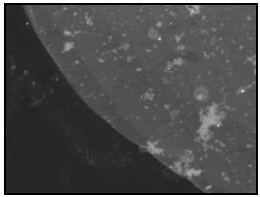
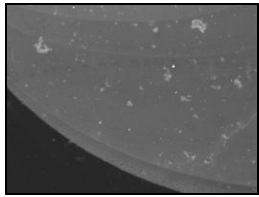
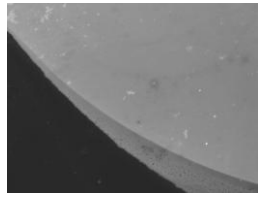
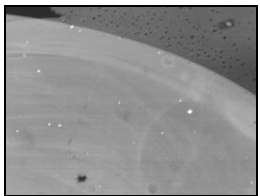

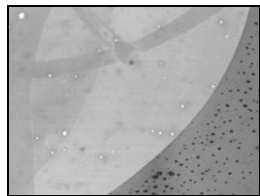

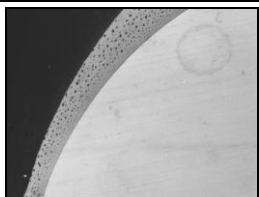

	Dextran-FITC concentration (μM)		
	5	15	20
1 % GOPS 5 minute silanisation			
1 % GOPS 1 hour silanisation			
1 % GOPS 24 hours silanisation			

Table 5-1 Table depicting the fluorescent edge of spots of dextran-FITC (5-20 μM) incubated with silanised glass surfaces. Glass surfaces were prepared with a 1 % GOPS solution incubated with the glass for between 5 minutes and 24 hours. All images were captured using an EC Plan-Neofluar 10x objective with a 2 second image capture (Axio Observer, Carl Zeiss, UK) for comparison.

The images shown in Table 5-2 (see overleaf) illustrate results obtained using three concentrations of dextran-FITC attached to glass surfaces silanised with 0.1 %, GOPS. When comparing these images with results found using 1 % GOPS there is a marked improvement in the overall reproducibility of the dextran-FITC surfaces produced. Therefore the use of 0.1 % GOPS compared with 1 % GOPS increases the

intensity of dextran-FITC conjugated with glass surfaces. Unlike the results shown in Table 5-1 the surfaces silanised for 1 hour and 24 hours in Table 5-2 show no significant difference in fluorescence intensity. To determine the minimum dextran-FITC concentration required, five images of each surface were captured under the same conditions (10x magnification, 2 second image capture) and processed to determine the minimum concentration that gave a reproducible intensity of dextran-FITC. A set of 3 repeats of each surface concentration, prepared identically, were analysed. The use of repeats improved the accuracy of the result and ensured the process was reproducible. By preparing the samples in bulk using the same reagents it was possible to negate a potential influence from processing abnormalities. The surfaces were therefore prepared in parallel and each image was captured using the same parameters for comparison. Each image was processed, using Matlab, to give the mean greyscale value, and the average of the three values taken. The average values were plotted on a graph showing the average grey scale intensity versus dextran-FITC concentration, including the degree of error (Figure 5-3, see overleaf).

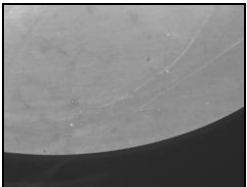
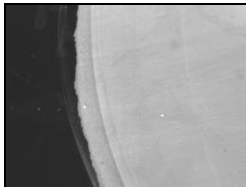
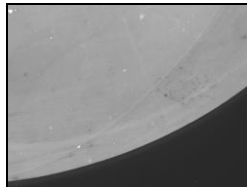

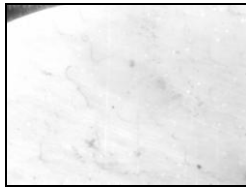
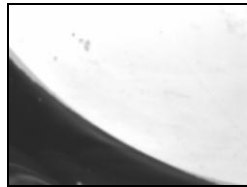
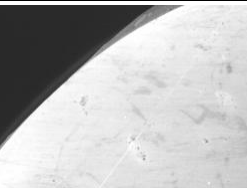
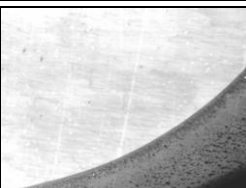
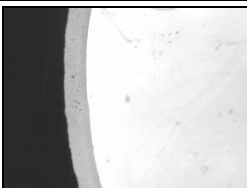
	Dextran-FITC concentration (μM)		
	5	15	20
5 minute silanisation			
1 hour silanisation			
24 hours silanisation			

Table 5-2 Table depicting the fluorescent edge of spots of dextran-FITC (5-20 μM) incubated with silanised glass surfaces. Glass surfaces were prepared with a 0.1 % GOPS solution incubated with the glass for between 5 minutes and 24 hours. All images were captured using an EC Plan-Neofluar 10x objective with a 2 second image capture (Axio Observer, Carl Zeiss, UK) for comparison.

The graph shows the greyscale intensity increases rapidly between 1 and 20 μM , after which the intensity plateaus out. For this set of processing conditions 20

μM can be defined as the minimum concentration above which there is no significant intensity increase. This concentration equates to a 30-fold reduction in dextran required to give an appropriate surface, compared with previously published work [203, 325].

The results presented in this section were evaluated to establish the best set of conditions for the fabrication of a reproducible layer of dextran on glass surfaces. A protocol involving the silanisation of glass for 1 hour in 0.1 % GOPS prior to incubation with 20 μM dextran produced the most reproducible layer.

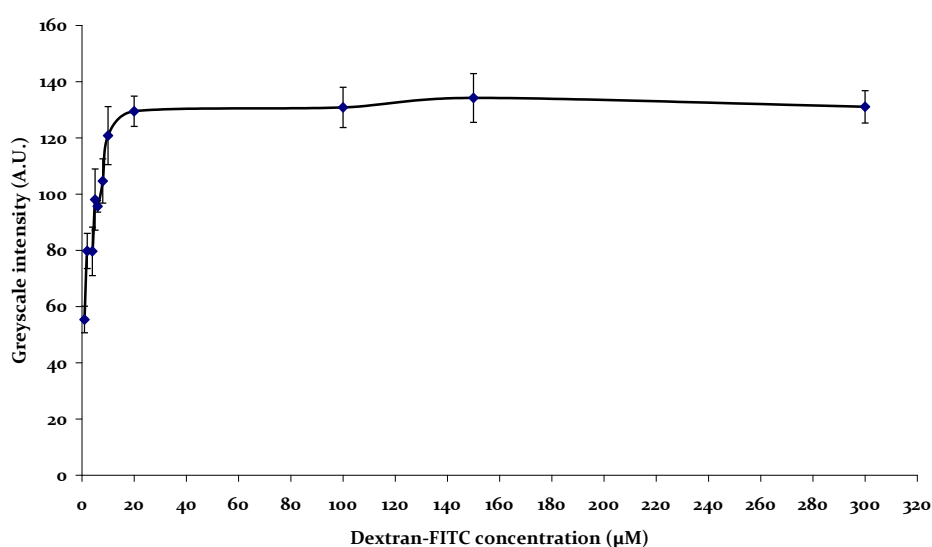


Figure 5-3 Graph showing the average greyscale of surfaces incubated with different concentrations of dextran-FITC, captured by epifluorescence microscopy (Axio Observer, Carl Zeiss, UK). Each image was taken using an EC Plan-Neofluar 10x objective and captured with an exposure time of 2 seconds. The average grey scales of 3 images were taken and the standard deviation between the averages calculated.

5.3.1 Water Contact Angle Measurements of Glass Surfaces Immobilised with Dextran

Water contact angle measurements were taken using the method described in §3.2.3. The contact angle measurements, shown in Table 5-3 (see overleaf), demonstrate the transition from a hydrophilic surface when clean to a more hydrophobic surface upon silanisation with GOPS. The contact angle recorded is in agreement with previously published data on GOPS silanised surfaces [43, 326]. The reduction in contact angle, on immobilisation of dextran, demonstrates the hydrophilic properties of the long chain polysaccharide.

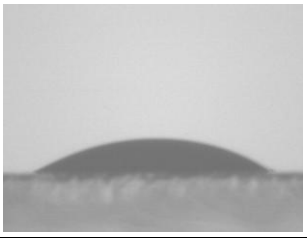
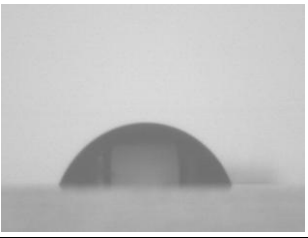
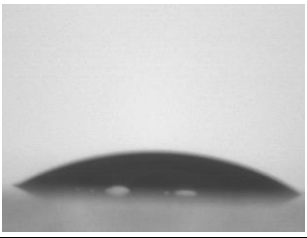
	Glass oxidised in 1:1:5 H ₂ O ₂ :NH ₄ OH :H ₂ O	Glass silanised with 0.1 % GOPS for 1 hour	GOPS silanised glass incubated with 20 μM dextran for 12 hours
Contact angle surface image			
Contact angle	<20°	61°±5°	<20°

Table 5-3 Table of contact angle measurements taken at different stages of surface processing. All images were taken of a 1 μL droplet on the surface, in a humid chamber, using the same contact angle measurement equipment (Krüss DSA100). Drops were fitted using the sessile drop fitting software (Krüss) and an average contact angle was determined from 5 images.

5.4 Synthesis and Characterisation of an Aryl Azide Conjugated Dextran

To create motifs of protein on glass surfaces immobilised with dextran, using photolithography, the dextran on the surface needed to be modified with a photolinker. To synthesise a photoreactive dextran a photoinitiator, 4-azidobenzoic acid, was conjugated with the dextran to produce an AACD. The section describes the synthesis and characterisation of the aryl azide conjugated dextran photolinker.

5.4.1 Characterisation of the Reactants and Product of Aryl Azide Conjugated Dextran Synthesis by Attenuated Total Reflection Fourier Transform Infrared Spectroscopy

ATR-FTIR measurements were taken using the method described in §3.2.6. ATR-FTIR is a technique for analysing the infrared (IR) absorption spectrum of a solid or liquid. The instrument works by passing an IR beam at an angle of incidence greater than the critical angle into a high refractive index crystal. The beam reflects within the crystal a number of times before exiting onto a spectrometer. The internal reflectance creates an evanescent wave on the surface of the crystal which projects a few microns beyond the crystal surface. For successful analysis of solids and liquids a surface contact to the crystal is crucial, due to the minimal penetration

of the evanescent wave. Liquids are easy to coat the crystal while solids are used as fine powders to allow them to be compacted into a solid disc at the crystal surface. When in contact with wavelengths of the IR spectrum, energy can be absorbed causing an attenuation of the evanescent wave. The attenuation to the IR beam is transferred through the crystal to the IR spectrometer which is visualised as an IR spectrum. ATR-FTIR was used to study the IR absorption produced by the reactants and product of the AACD synthesis. The aim was to quantify the successful conjugation of the 4-azidobenzoic acid to the dextran.

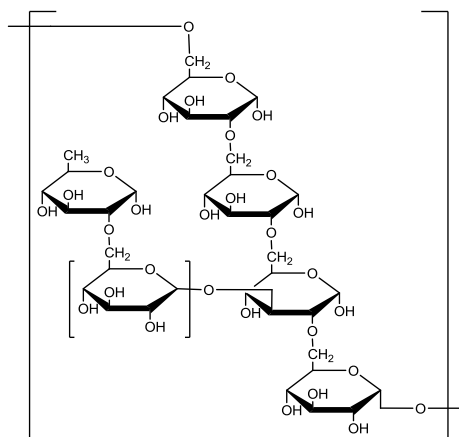


Figure 5-4 ChemDraw image of the glucose units that make up dextran, and the bonds present in the polymeric structure.

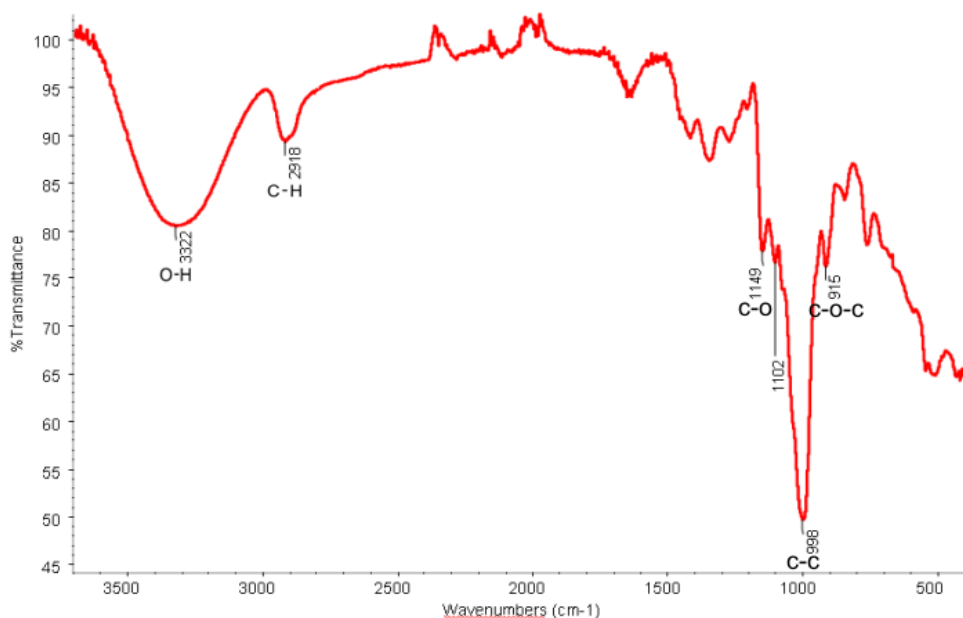


Figure 5-5 FTIR spectrum showing the main IR absorption peaks of dextran (500 kDa). The prominent bands are the O-H stretch at 3200 cm⁻¹ and the valent C-O and C-C vibrations at 1149 and 998 cm⁻¹.

Dextran (500 kDa) (Figure 5-4, see previous page) is a long chain carbohydrate that consists of α -1,6 glycosidic linkages between glucose molecules, and branching from α -1,4 linkages.

The FTIR spectrum (Figure 5-5) shows characteristic peaks of dextran. The broad band in the region of 3332 cm^{-1} is due to the hydroxyl stretching vibration of the polysaccharide. The band in the region of 2918 cm^{-1} is caused by a C–H stretch vibration [327, 328]. The absorption peak at 915 cm^{-1} indicates the existence of α -glycosidic bond. The main characteristic bands found in the spectra of dextran at 1149, 1102 and 998 cm^{-1} are due to valent vibrations of C–O and C–C bonds and deformational vibrations of the CCH, COH and HCO bonds. The band at 1149 cm^{-1} is assigned to an exocyclic C–O stretch characteristic of the glycosidic bridge. The peak at 1102 cm^{-1} is due to the vibration of the C–O bond at the C-4 position of glucose. The presence of a peak at 998 cm^{-1} is due to the great chain flexibility present in dextran around the α -1,6 glycosidic bonds as shown previously by Shingel *et al.* [329].

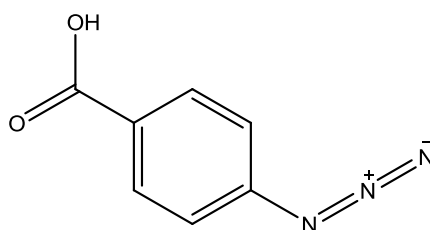


Figure 5-6 ChemDraw image of 4-azidobenzoic acid, showing the carboxylic acid and azide moieties attached to a benzyl ring.

4-azidobenzoic acid (Figure 5-6) is a para di-substituted benzene with aryl azide and carboxylic acid moiety.

The FTIR spectrum (Figure 5-7) shows characteristic peaks of 4-azidobenzoic acid. The band in the region of 2102 cm^{-1} is the characteristic absorption peak of the azide group [211]. The absorption peaks at 1674, and 1280 cm^{-1} indicate the C=O and C–O stretch of the aromatic carboxylic acid respectively. The peaks distributed between 1600 cm^{-1} and 1424 cm^{-1} are the main absorption bands associated with the C=C and C–C vibrations distributed within the aromatic benzene structure. The absorption at 856 cm^{-1} and 764 cm^{-1} is typical of the C–H stretch and deformation respectively.

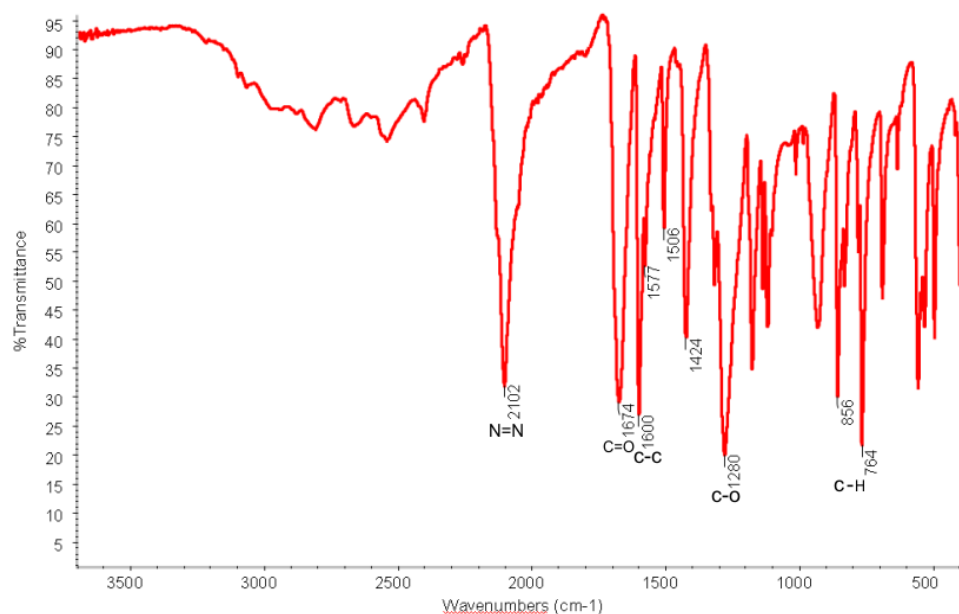


Figure 5-7 FTIR spectrum showing the main IR absorption peaks of 4-azidobenzoic acid). The peak of interest is the azide peak at 2102 cm^{-1} .

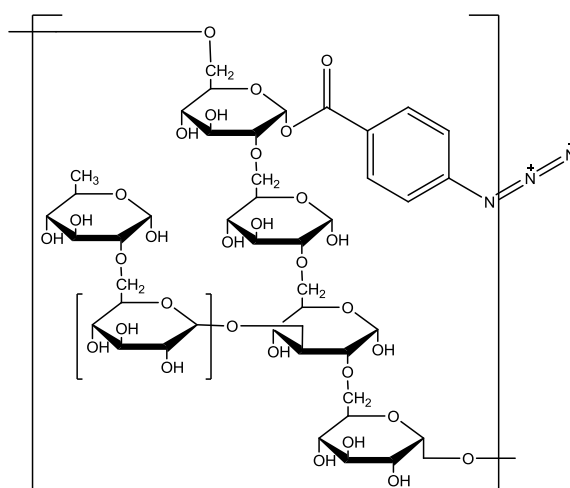


Figure 5-8 ChemDraw image of the aryl azide conjugated dextran showing the modification of the glucose units to conjugate the aryl azide moiety.

AACD (Figure 5-8) is a long chain carbohydrate that consists of α -1,6 glycosidic linkages between glucose molecules, and branching from α -1,4 linkages. Some hydroxyl groups on the glucose are reacted to form ester linkages to an aryl azide.

Like the dextran a band in the region of 3321 cm^{-1} , due to the hydroxyl stretching vibration of the polysaccharide, and a band at 2930 cm^{-1} , due to C–H stretching vibration, are observed in the FTIR spectrum of AACD (Figure 5-9, see overleaf) [327, 328]. The presence of the peak at 915 cm^{-1} indicates the retention of

the α -glycosidic bond. The main characteristic bands at 1151, 1105 and 1000 cm^{-1} are due to the valent vibrations of C–O and C–C bonds and deformational vibrations of the CCH, COH and HCO bonds as mentioned previously for dextran. The peaks at 2127 cm^{-1} , 1603 cm^{-1} , and 1277 cm^{-1} are indicative of the introduction of the aryl azide onto the dextran. The characteristic peak of azide can be seen at 2127 cm^{-1} , along with the C=C peak at 1603 cm^{-1} . The presence of the peak at 1714 cm^{-1} and the increase in intensity of the peak at 1005 cm^{-1} represent the presence of the ester group formed by the conjugation reaction.

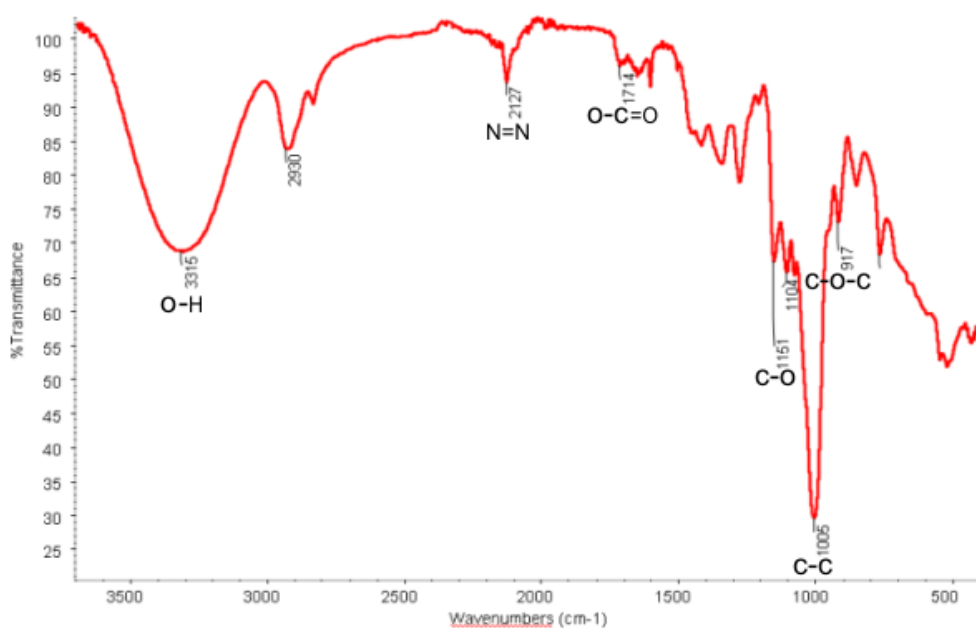


Figure 5-9 FTIR spectrum showing the main IR absorption peaks of aryl azide conjugated dextran. The O-H stretch at 3200 cm^{-1} and the valent C-O and C-C vibrations at 1149 and 998 cm^{-1} from the dextran and the N=N and ester group are introduced at 2127 cm^{-1} and 1714 cm^{-1} respectively from the conjugated aryl azide.

5.4.2 Characterisation of Aryl Azide Conjugated Dextran by Elemental Analysis

Elemental analysis was carried out using the method described in §3.2.7. The results of the elemental analysis gave a constituent percentage of C 39.45 %, H 6.67 % and N 1.11 % for AACD. These percentages were used to calculate the mass percentage contribution from the azide, aryl azide and the dextran. To calculate these values a number of assumptions were made:

1. All the nitrogen measured was from the azide moiety.

2. The remaining 52.77 % mass was from contributions from oxygen in the AACD.
3. The formula $C_7H_4N_3O_2$ was used to define the aryl azide moiety.
4. The remaining mass present after taking into account the mass contribution of the aryl azide moiety was from the dextran.
5. All the dextran contributions were from dextran with a molecular weight of 500,000.

Using this set of criteria the mass of each constituent of the AACD was calculated, shown in Table 5-4.

Element	Mass percentages from elemental analysis (%)	Mass (g)	Molecular weight (MW)	Moles of each element (mol)
Carbon	39.45	0.000789	12.01	6.570E-05
Hydrogen	6.67	0.000133	1.008	1.323E-04
Nitrogen	1.11	0.000022	14.01	1.585E-06
Oxygen	52.77	0.001055	16.01	6.592E-05

Table 5-4 Table showing the mass contributions of the four elements within the synthesised AACD compound.

Assuming that all the nitrogen is from the azide moiety the moles of azide is calculated as 5.28E-07. The moles of azide can be used to determine the mass contribution of the aryl azide moiety upon conjugation using the formula $C_7H_4N_3O_2$. The mass and moles values for each of the elemental components of the aryl azide moiety are shown in Table 5-5.

Element	Molecular weight of aryl azide components	Mass of aryl azide components (g)	Moles of aryl azide components (mol)
Carbon (7)	84.07	4.441E-05	3.697E-06
Hydrogen (4)	4.032	2.130E-06	2.113E-06
Nitrogen (3)	42.03	2.220E-05	1.585E-06
Oxygen (2)	32.02	1.691E-05	1.056E-06

Table 5-5 Table containing the mass and mol contributions of the 4 elements that make up the aryl azide moiety conjugated to the dextran.

After removing the mass contributions from the aryl azide moiety the mass contributions of the dextran can be determined, shown in Table 5-6 (see overleaf).

Element	Mass from dextran contribution (g)	Moles from dextran contribution (mol)
Carbon	7.446E-04	6.200E-05
Hydrogen	1.313E-04	1.302E-04
Oxygen	1.038E-03	6.486E-05

Table 5-6 Table containing the remaining mass and mol contributions, after removing contributions from the conjugated aryl azide, which are attributed to the elements found in the dextran.

The total mass from the dextran can be assumed to be the collective mass of the remaining components, which is calculated as 1.914E-03 g. Using a molecular weight of 500,000 for the dextran the moles of dextran is calculated as 3.829E-09 moles. The total weight contributions from the azide, aryl azide, and dextran are displayed in Table 5-7.

Substance	Mass contribution (mg)
Initial compound	2.000
Azide (N ₃)	0.022
Aryl azide (C ₇ H ₄ N ₃ O ₂)	0.086
Dextran	1.914

Table 5-7 Mass of AACD compound constituents calculated using elemental analysis data.

The weight percentage (wt %) contribution of the aryl azide moiety conjugated to the dextran can therefore be calculated as 4.3 %.

5.4.3 Characterisation of the Reactants and Product of Aryl Azide Conjugated Dextran Synthesis by Absorption Spectroscopy

Absorption spectra were obtained using the methods described in §3.2.8. The spectra in Figure 5-10 (see overleaf) show the UV absorption of 4-azidobenzoic acid, dextran, and AACD solution. The spectra show the presence of a peak maximum at 277 nm, for AACD, and 275 nm for 4-azidobenzoic acid. The peak maximum of the conjugated aryl azide group is red shifted compared with that of 4-azidobenzoic acid, which correlates to previous work presented by Zhu *et al.* [330, 331]. The red shift may be due to the electron delocalisation of the aryl azide group caused by the ester bond formation [332].

The work by Bhat *et al.* [211], Zhu *et al.* [330] and Ito *et al.* [332] described the derivation of the extent of aryl azide modification by UV absorption spectroscopy.

The assumption was made that the absorption coefficient of the 4-azidobenzoic acid group at 275 nm was the same as the aryl azide group at 277 nm [332]. This assumption meant a standard curve of 4-azidobenzoic acid absorption could be used to determine the amount of aryl azide conjugated. This method was not used in this research as the observed shift of the peak maximum from 270 nm, for 4-azidobenzoic acid, to 275 nm, for AACD, may demonstrate a change in the absorption properties. The data acquired using elemental analysis was therefore used to estimate the extent of dextran modification.

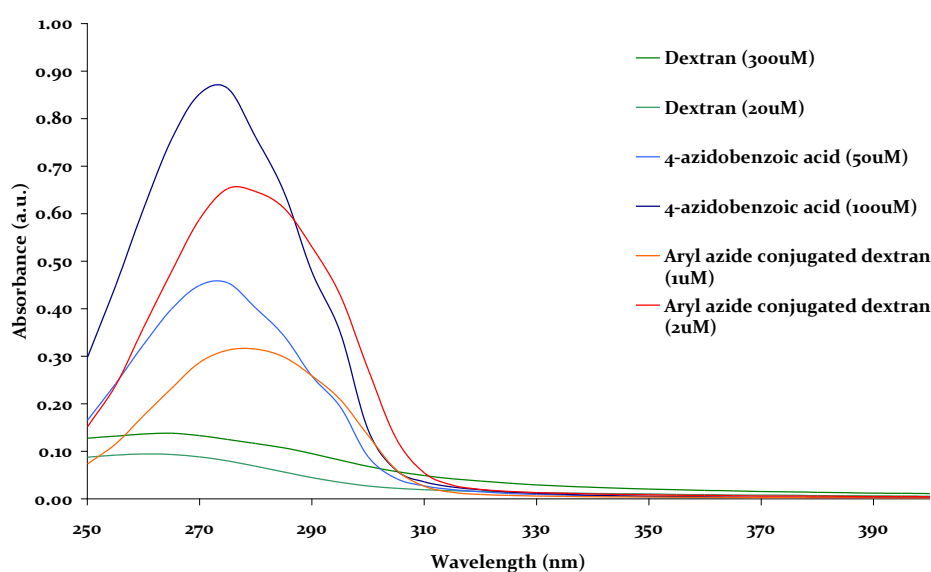


Figure 5-10 UV absorption spectra of dextran and AACD solution in water and 4-azidobenzoic acid solution in methanol (a.u. denotes arbitrary units).

5.5 Characterisation of Aryl Azide Conjugated Dextran Immobilised on Glass

Having successfully characterised the conjugation of an aryl azide with dextran, surfaces were prepared to immobilise AACD on glass.

5.5.1 Water Contact Angle Measurements

Water contact angle measurements were taken using the method described in §3.2.3. The contact angle measurement, shown in Table 5-8 (see overleaf), shows the

transition from a relatively hydrophilic surface compared with the GOPS surface measured in §5.3.1. The reduction in contact angle, on immobilisation of the AACD, demonstrates the retention of the hydrophilic properties of the long chain polysaccharide. The contact angle was higher compared with unmodified dextran surfaces prepared in §5.3.1. This is likely to be caused by the replacement of a number of hydroxyl groups on the dextran with the aryl azide moiety. The aryl azide termination is known to have a more hydrophobic character compared with that of the hydroxyl group [333].

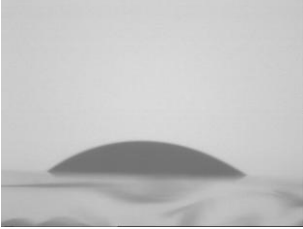
GOPS silanised glass incubated with 20 µM AACD for 12 hours	
Contact angle surface image	
Contact angle	32°±3°

Table 5-8 Table of contact angle measurements of an AACD layer immobilised on a glass surface. All images were taken of a 1 µL droplet on the surface, in a humid chamber, using the same contact angle measurer (Krüss DSA100). Drops were fitted using the sessile drop fitting software (Krüss) and an average contact angle was determined from 5 images.

5.5.2 X-Ray Photoelectron Spectroscopy

XPS experiments were carried out using the method described in §3.2.10. XPS was used, in this instance, to probe changes to surface chemistry on the glass substrate at each stage of processing. Samples of GOPS silanised glass, AACD immobilised glass, and NeutrAvidin conjugated glass slides were analysed. The modification to the glass surfaces can all be resolved within the field of detection of XPS. The full spectrum measured at each stage can be found in Appendix D 1.3-1.5; the main peaks are discussed below.

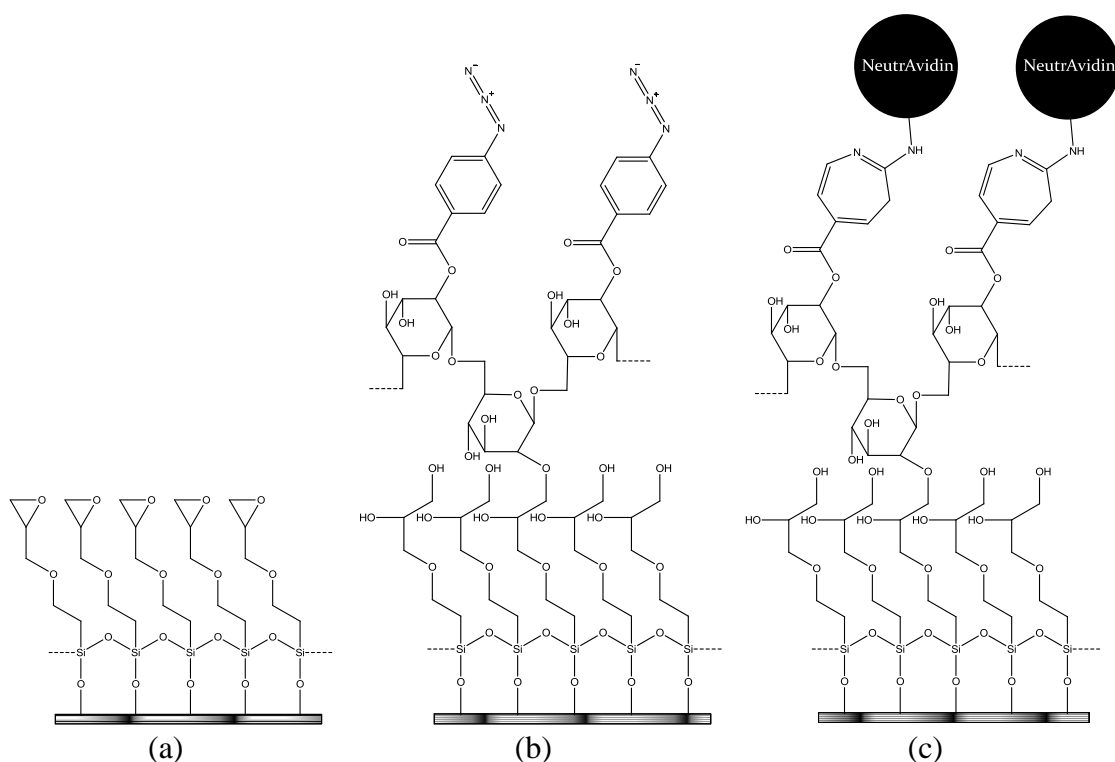


Figure 5-11 Illustration of the three surface modifications involved in conjugating protein with glass surfaces including: (a) Silanisation with GOPS, (b) Immobilisation of AACD, and (c) Photoinitiated conjugation of NeutrAvidin.

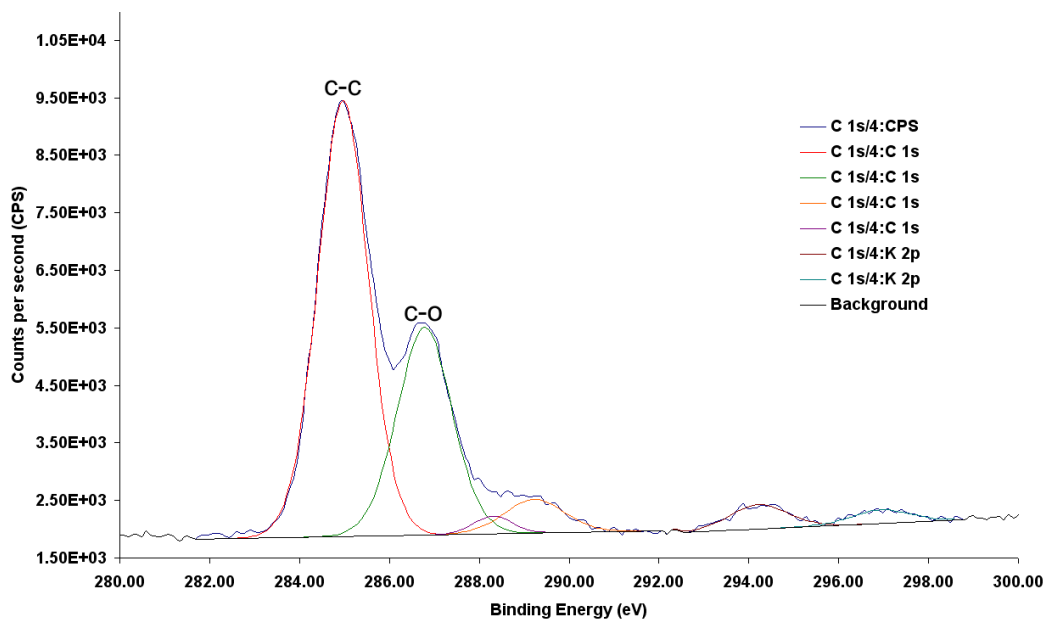
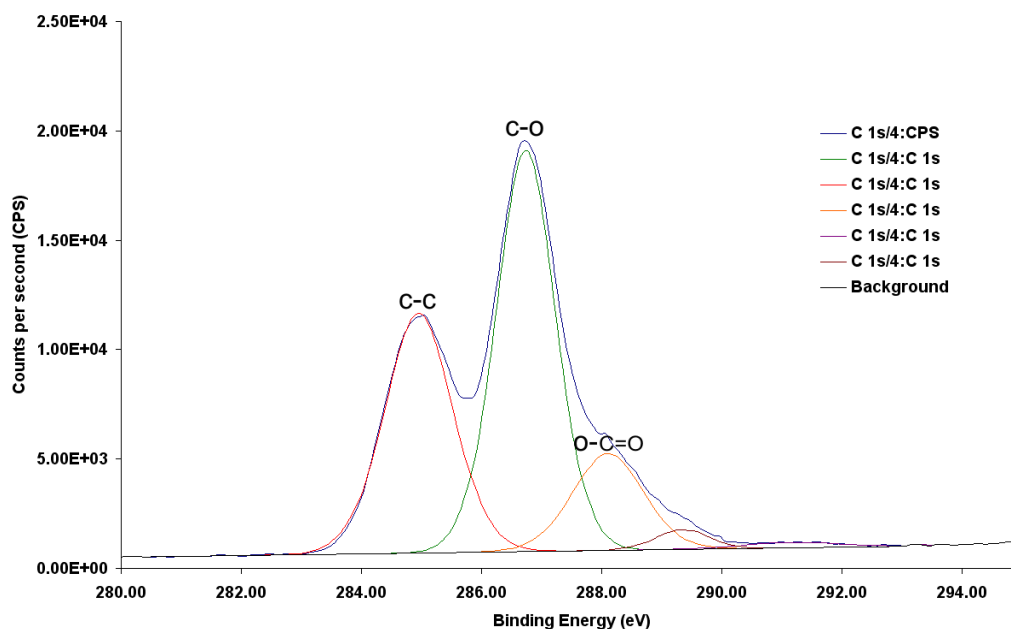


Figure 5-12 Peak fitting of data from XPS experiments (see §3.2.10) of NeutrAvidin conjugated silicon surfaces showing peaks assigned to carbon bonds.

The peaks here were measured from surfaces silanised with GOPS, as illustrated in Figure 5-11 (a). The peak at 286.5 eV was likely to be representative of the C-O ether bond in GOPS [334]. Measurement of a peak at 285 eV is that of the aliphatic

carbon groups of the silane. The peak at 287 eV is from the ether bond of the epoxide moiety on the surface [335].

a) Carbon



b) Nitrogen

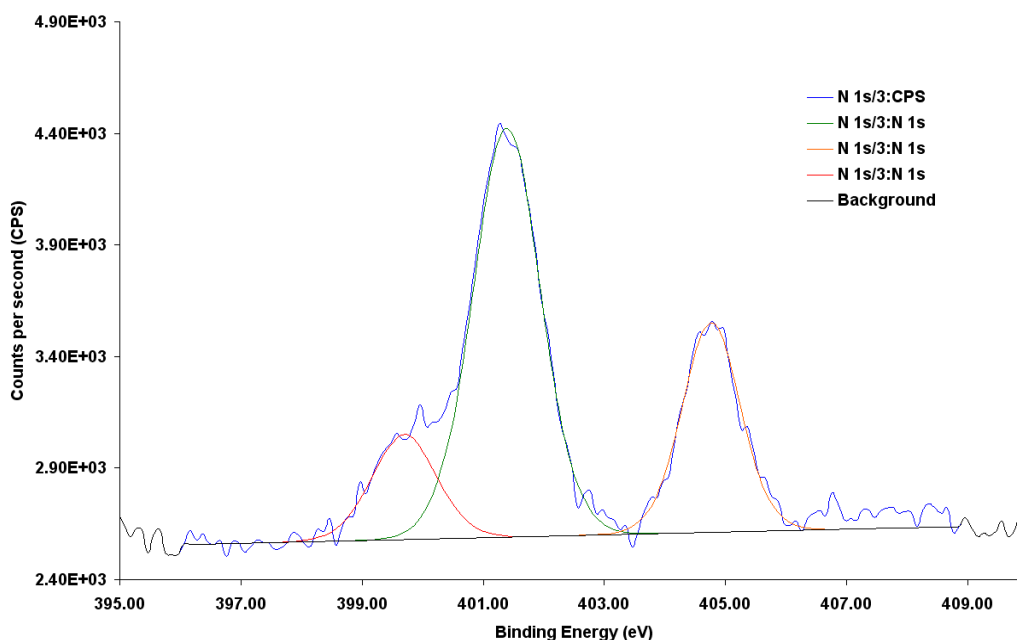
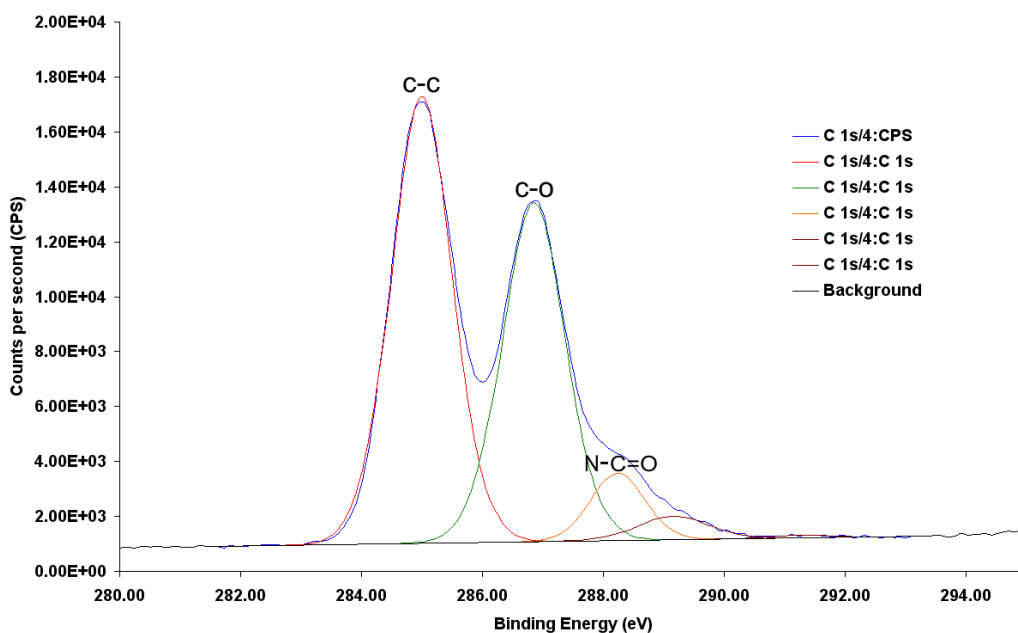


Figure 5-13 Peak fitting of data from XPS experiments (see §3.2.10) of GOPS modified glass surfaces showing a) peaks assigned to carbon bonds and b) peaks assigned to nitrogen bonding.

The peaks here were measured from surfaces immobilised with AACD, as illustrated in Figure 5-11 (b) (see pg 121). The increase in the C-O peak at 286 eV,

compared with the GOPS XPS, was representative of the increase of ether bonds found in the dextran [302]. It is likely that the peak at 288 eV represents the C=O of the ester linkage of the AACD. The introduction of nitrogen peaks at 400.5 eV and 404.1 eV shows the presence of the azide group, the smaller peak at 404.1 eV corresponding to the middle nitrogen atom of the azide group [336].

a) Carbon



b) Nitrogen

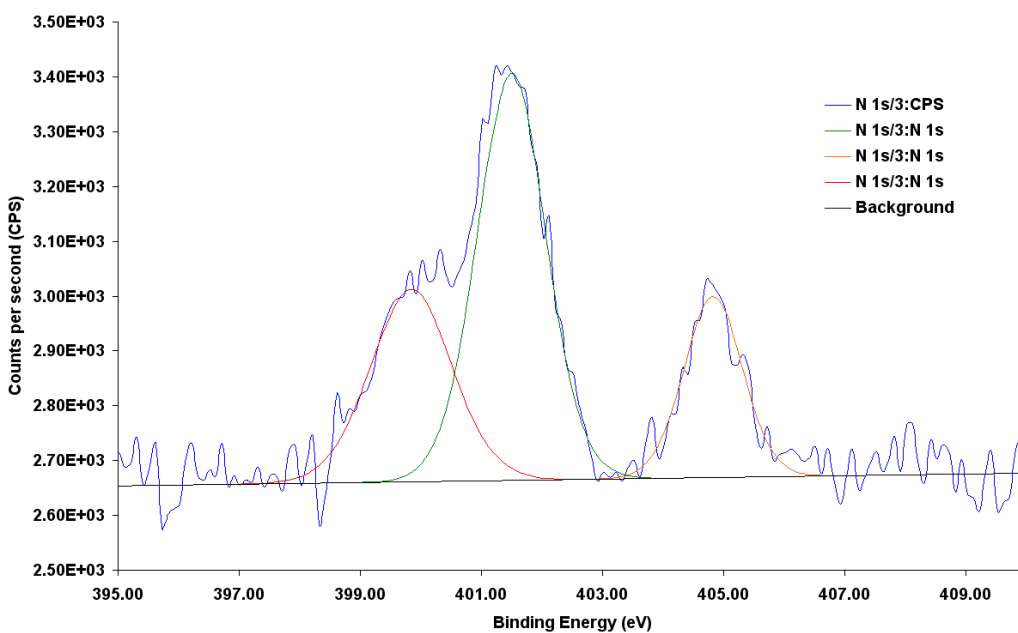


Figure 5-14 Peak fitting of data from XPS experiments (see §3.2.10) of NeutrAvidin conjugated glass surfaces showing a) peaks assigned to carbon bonds and b) peaks assigned to nitrogen bonding.

The peaks here were measured from surfaces conjugated with NeutrAvidin, as illustrated in Figure 5-11 (c) (see pg 121). The peak at 288-288.5 eV is characteristic of an amide bond [301, 302], the increase in the peak at 400eV compared with the AACD XPS is likely to be a result of NeutrAvidin conjugated to the surface [302].

The XPS data presented here demonstrate the successful modification of glass with GOPS, as illustrated in Figure 5-11 (a) (see pg 121). The GOPS surface could then be used to immobilise aryl azide conjugated dextran on the glass. Importantly the azide moiety is retained after the AACD is immobilised on the glass. This moiety is crucial for the subsequent photoinitiated conjugation of protein with the glass. Thus NeutrAvidin was successfully conjugated with AACD immobilised glass surface, as illustrated in Figure 5-11 (c) (see pg 121).

5.6 Masks and Alignment Mark Fabrication for Aligned Protein Patterning

To site specifically align protein motifs on the AACD surface a method to control the photoinitiated reaction between the AACD and the protein is required. Photolithographic masks and alignment features were fabricated for integration within an alignment setup used in patterning multiple protein motifs.

5.6.1 Alignment Features

Alignment features were present on the photolithographic mask and the surface functionalised with the AACD spacer. Two different types of photoresist, positive Shipley MICROPOSIT® S1813 and negative Microchem SU8-10, were used to pattern the alignment features. The process by which these photoresists function is discussed in § 2.4.2.1 and illustrated previously in Figure 2-24 (page 52).

The alignment features and masks were fabricated using the method described in §3.2.11. The features shown in Figure 5-15 (a) and (d) (see overleaf) represent the designs created in L-edit, used to fabricate the mask plate. The purple features shown in Figure 5-15 a) and d) (see overleaf) are areas on the mask plate designed to be covered with a layer of chrome, to block UV light, while the white

areas are transparent. Thus when the features are processed with Shipley S1813, as in Figure 5-15 b), the purple area contains photoresist and the white area forms relief structures when developed. Conversely when features are processed with Microchem SU8 10, as in Figure 5-15 d), the purple areas form reliefs and the white area is covered with photoresist. On etching of the chrome/gold in the patterned reliefs the transparent fused silica substrate is revealed. The transmission images in Figure 5-15 (c) and (f) show the dark chrome/gold features and the transparent fused silica after the resist is removed. The dimensions of the alignment features were found to be accurate to within $\pm 0.4 \mu\text{m}$ of the original mask plate designs.

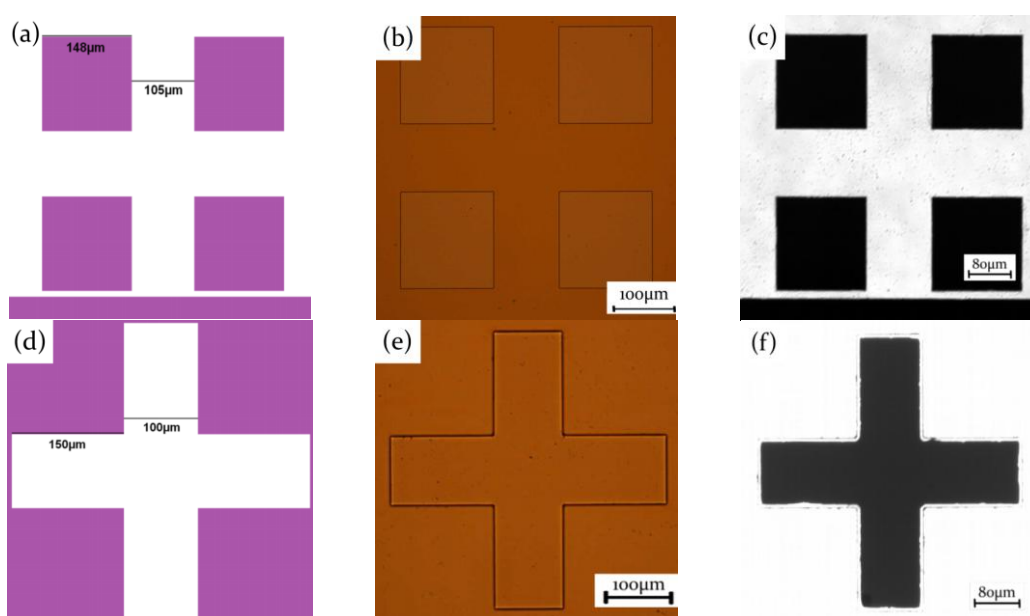


Figure 5-15 Alignment features formed using a design created using L-edit ((a) and (d)), where purple is representative of chrome and white of transparent UV fused silica. The bright field images, captured using an EC Plan-Neofluar 10x objective, in (b) and (c) are surfaces patterned using the feature design in (a) using S1813. While (e) and (f) are patterned using the feature design in (d) using SU8-10. The two photoresists form an inverse pattern compared with one another, due to the different properties of the resists and were processed using the protocol described in §3.2.11.

5.6.2 Photolithographic Mask 1

The first mask design for multiple protein patterning (Mask 1) was based on a 90° rotation mask to pattern two proteins on the same surface. The design shown in Figure 5-16 illustrates the method by which the mask can produce two patterns using the two sets of alignment features. The surface alignment features can be used to align the first set of marks followed by realignment to the same surface features for the second illumination. The mask is designed such that on rotation the UV windows illuminate new parts of the surface after realignment.

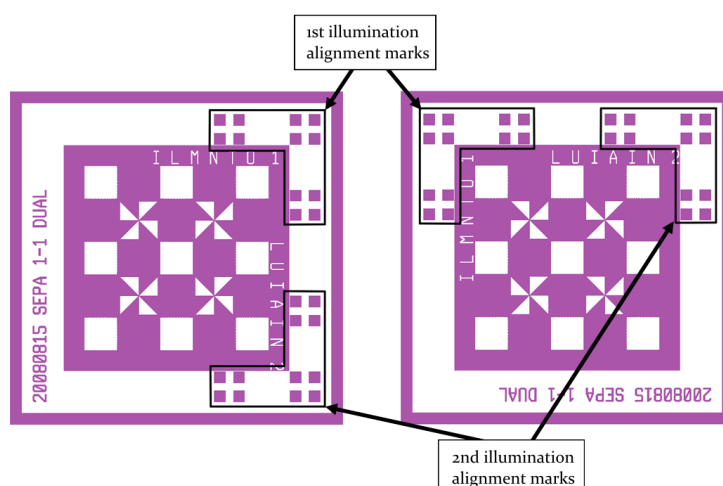


Figure 5-16 Images of the Mask 1 design produced in L-edit. The left image shows the orientation of the mask for the first protein illumination. The mask is then rotated 90° anti-clockwise, to the orientation shown in the right image, for the second illumination.

The schematic in Figure 5-16 shows a low magnification image of the mask consisting of two primary features, the checkerboard and windmill pattern. The actual checkerboard and windmill designs are shown in greater detail in Figure 5-17 (a) and (d) (see overleaf) respectively. In these images the first illumination patterns the areas in white and the second illumination patterns the areas in purple. The process of resist development needed to be optimised to achieve good resolution structures. The result of the optimisation process can be seen in Figure 5-17 (b) and (e) (see overleaf), where the features are well defined on the surface. When etched the pattern is transferred into the chrome/gold below to produce the photolithographic mask patterns. The transmission images in Figure 5-17 (c) and (f) (see overleaf) show the successful transfer of the pattern.

The main problem encountered when processing the photoresist was an inhomogeneous development rate over the features. It was observed that any agitation of the sample was detrimental to the production of uniform features. The surfaces were therefore placed in developer for different time periods before analysis of feature dimensions, by light microscopy. The images of patterned photoresist in Figure 5-18 (see overleaf) are of surfaces placed in developer for (a) 60 seconds, (b) 75 seconds and (c) 90 seconds. The images show that after 60 seconds the pattern is underdeveloped and at 90 seconds the features are overdeveloped. A time of 75 seconds was found to be an ideal development time to produce correct feature dimensions.

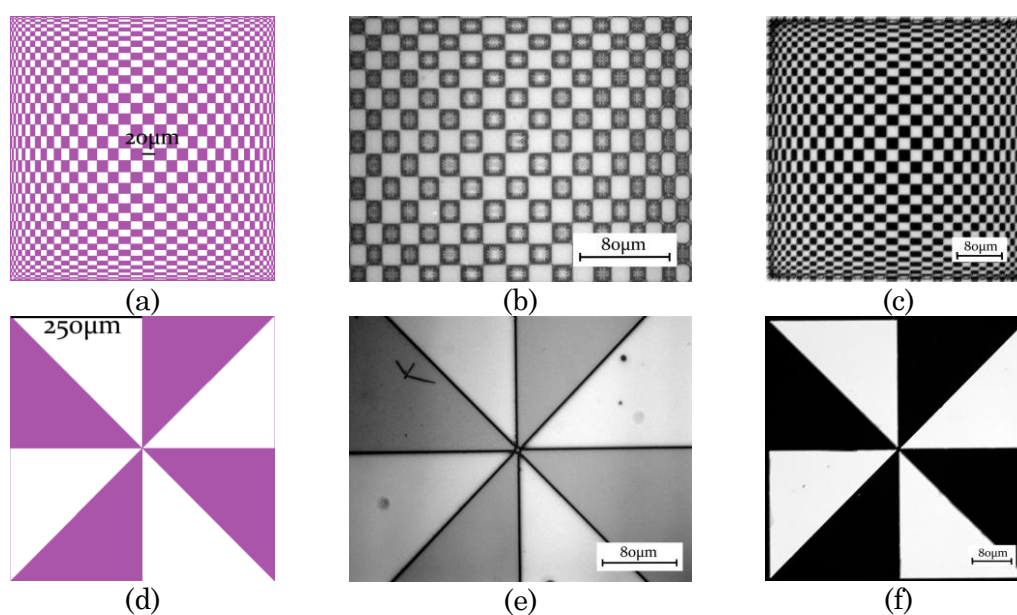


Figure 5-17 Mask features formed using a design created in L-edit ((a) and (d)), where purple is representative of chrome and white of transparent UV fused silica. The bright field images, captured using an EC Plan-Neofluar 10x objective, in (b) and (e), are features patterned in S1813. The transmission images taken with the same 10x objective, in (c) and (f) are the features transferred into chrome/gold after etching. Images b, c, e and f were taken during the process described in §3.2.11.

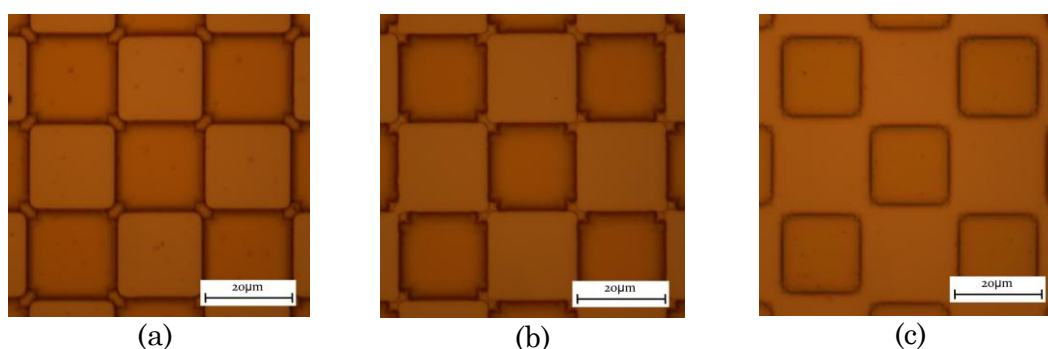


Figure 5-18 Bright field images, taken using an EC Plan-Neofluar 10x objective, of S1813 photoresist patterned on chrome/gold surfaces developed for (a) 60 s, (b) 75 s and (c) 90 s.

The transfer of the pattern into the chrome/gold was also analysed to determine suitable etching times. Initial studies used a thickness of 20 nm chrome and 120 nm gold, for surface deposition, which caused undercutting when etched. To prevent undercutting the thickness of the chrome was reduced to 10 nm and the gold to 70 nm. The thinner metal layers limited undercutting and transferred the feature dimensions accurately onto the mask, while retaining the capacity to block UV light.

5.6.3 Photolithographic Mask 2

After working with mask 1 it became apparent that the alignment resolution, using the setup described later in §5.8.2, would not be suitable for achieving aligned patterns reproducibly using this mask. Having identified this, Mask 2 was devised with an improved alignment tolerance to demonstrate that proteins could be patterned in aligned motifs. The mask was produced with four sets of features including:

1. Mask alignment features (Figure 5-19 (a))
2. Pattern size resolution features (Figure 5-19 (b and c))
3. Horizontal pattern alignment tolerance features (Figure 5-20 (a) (see overleaf))
4. Vertical pattern alignment tolerance features (Figure 5-20 (b) (see overleaf))

The mask alignment features were the same as those used for the checkerboard pattern, except illumination of the second protein was after a 1 mm translation and not a 90° rotation. The size of the pattern achievable using the AACD was tested using a set of square windows with diameters ranging from 4-100 μm .

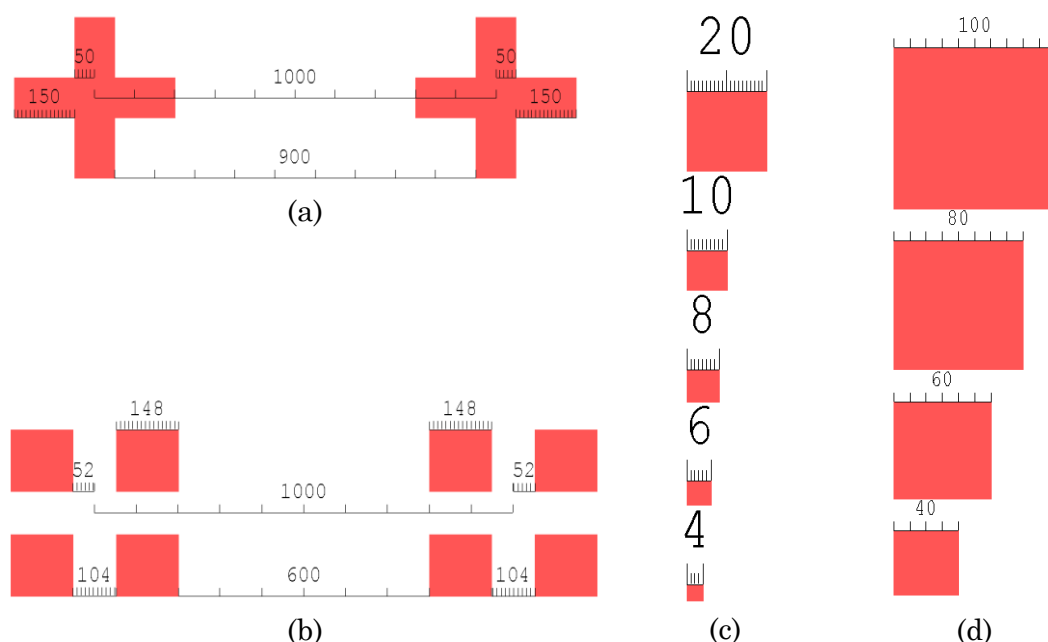


Figure 5-19 Design of mask and alignment features produced using L-edit. The features are representative of (a) the surface alignment features and (b) the mask alignment features. The features in (b) and (c) are square windows ranging in size from 4-100 μm .

The vertical and horizontal alignment tolerance features are designed to allow features to be patterned next to each other with a $\pm 10 \mu\text{m}$ tolerance. The aim of this design was to guarantee that one patch of protein would be aligned directly next to another using a system with a potential alignment error of $\pm 8 \mu\text{m}$. With this design a simple, low cost, setup capable of patterning two proteins on the same surface next to each other could be achieved. The features have one set of parallel squares which pattern the first protein on the surface, seen on the right half of Figure 5-20 (a) and (b). The scale bars on these figures show where the features would be after a transverse movement of 1 mm.

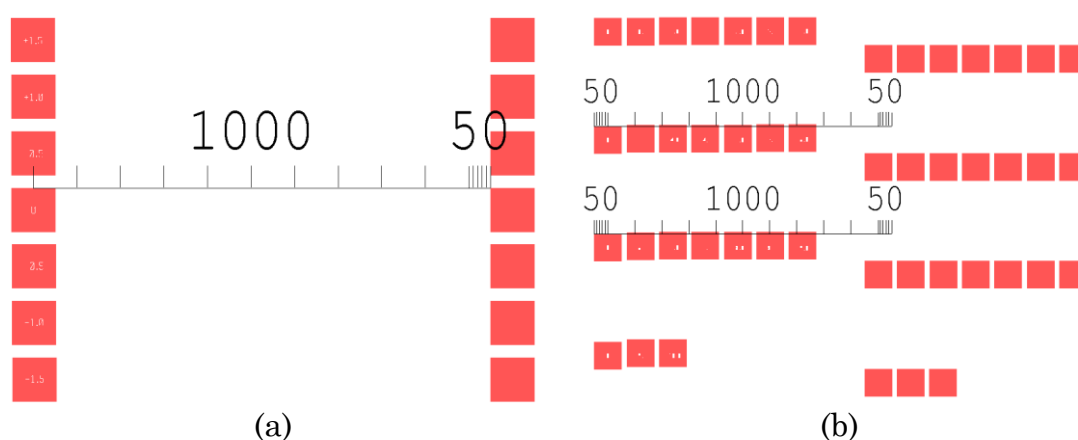


Figure 5-20 Design of mask and alignment features designed using L-edit. The features enhance the horizontal (a) and vertical (b) alignment tolerance of the mask. The squares without numbers in are parallel to one-another. The squares with numbers have a deviation from a central square of $\pm 10 \mu\text{m}$.

The tolerance of the features is formed from minor deviations from a central square. The image in Figure 5-21 (see overleaf) shows a magnified version of the three squares in the bottom left corner of Figure 5-20 (b). When the mask is traversed 1 mm the zero square should be exactly above a square from the first protein patterning. The other squares including -9.5 and -10.0 deviate from the zero square vertically by the number value (i.e. the -10.0 is $10 \mu\text{m}$ below the zero square). The feature has squares $\pm 10 \mu\text{m}$ above and below the plain of the zero square. Thus if the alignment is vertically shifted by $+10 \mu\text{m}$ the $-10 \mu\text{m}$ square will be exactly above the first protein square. The same is true of the horizontal alignment except using the horizontal plain as a deviation point.

Using the optimised parameters determined during the fabrication of mask 1 the features of mask 2 were patterned using S1813 onto chrome/gold surfaces and

transferred by wet etching of the metal under layer. Analysis of the photoresist (Figure 5-22 (a and b)) and etched (Figure 5-22 (c and d)) surfaces, by light microscopy, showed excellent feature resolution comparable to that of the mask plate designs.



Figure 5-21 Design of vertical alignment tolerance features that, in these features, are -9.5 and 10 μm below the plain of the ideal alignment pattern (zero).

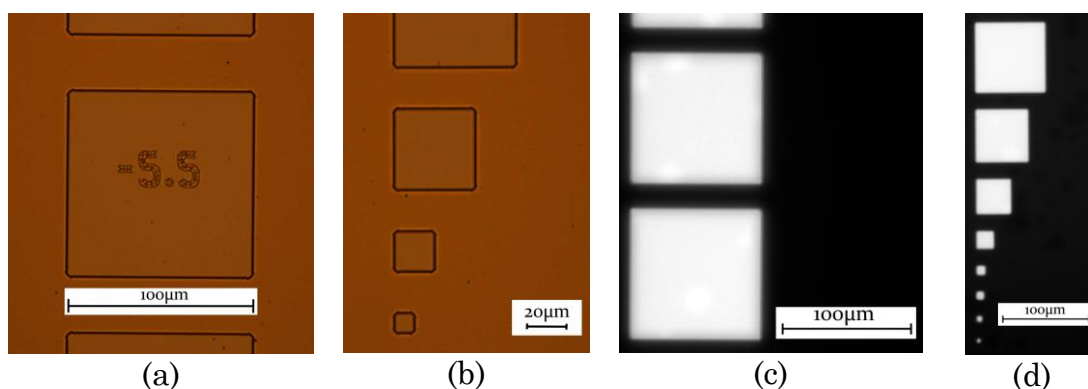


Figure 5-22 Bright field images of S1813 patterned chrome/gold surfaces (a and b) and features etched into the chrome/gold layer (c and d). The images were taken during the fabrication process described in §3.2.11.

5.7 Protein Attachment to Dextran Surfaces

With a set of parameters suitable for the attachment of dextran to glass surfaces, with good reproducibility, it was possible to continue the process of changing the dextran chemistry to allow protein attachment.

5.7.1 Conjugation of Protein Carboxymethyl Dextran surfaces

The aims of the experiments presented here were firstly, to analyse whether a protein could be conjugated to dextran and not become denatured on the surface, and

secondly, to assess non-specific binding by dextran. The method used to conjugate protein on carboxymethyl dextran surfaces is described in §3.2.4.

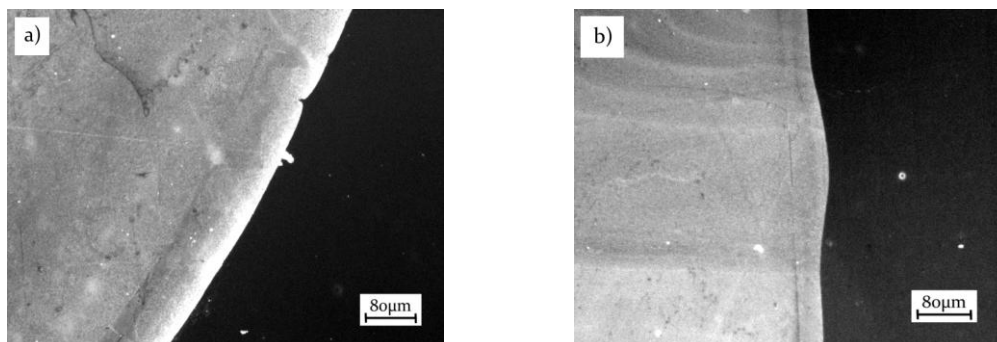


Figure 5-23 Epifluorescence images of IgG-FITC (500 nM) associated on a protein L (10 μ M)-dextran surface. Image (a) shows IgG-FITC is restricted to the spot of protein L on the surface. Image (b) shows protein L is restricted to the area where the EDC/NHS solution was incubated. Both images show immobilisation and excellent contrast between the protein and dextran surface (EC Plan-Neofluar 10x objective, 2 second image capture).

The images shown in Figure 5-23 show IgG-FITC (500 nM) bound to protein L (10 μ M) immobilised onto the surface of dextran. The light regions are a result of the fluorescent signal from IgG-FITC and the dark regions show the background fluorescent signal from the glass. The spot of protein L in Figure 5-23 (a) illustrates the ability of the dextran surface to prevent non-specific adsorption of IgG-FITC. The IgG-FITC was incubated with the whole surface but associates specifically to the protein L spot and not to the bare dextran. The edge shown in Figure 5-23 (b) (see previous page) demonstrates the requirement of the NHS-ester moiety for protein L immobilisation. The protein L, having been incubated with the whole surface, is only immobilised on the NHS-ester modified region. These images indicate the successful modification of the surface with EDC/NHS and the subsequent immobilisation of an active form of protein L.

5.8 Patterning Proteins on Aryl Azide Conjugated Dextran Surfaces

To pattern protein upon the AACD immobilised surface illumination with UV light was required, to initiate the conjugation reaction between the AACD and the protein. With the peak absorption of the AACD determined it was established whether the HgXe UV lamp system (Oriel, Newport) was compatible with illumination. The inset in Figure 5-24 shows the manufacturer guidelines on power density achievable using

three different lamp sources. The 500 W Hg(Xe) shows a high irradiation above 270 nm suitable for our application.

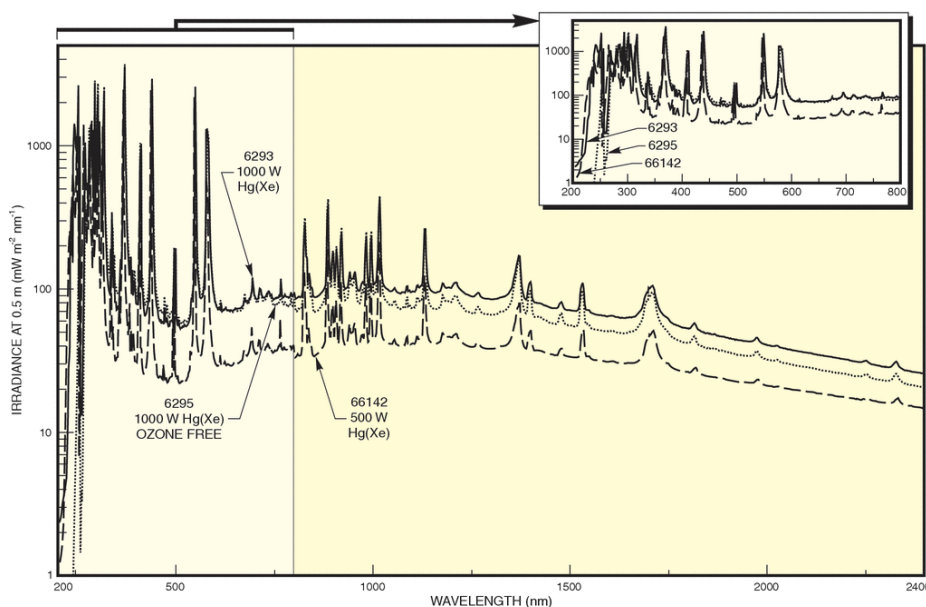


Figure 5-24 Power output spectra from the 500W Hg(Xe) UV lamp system supplier (Oriol, Newport).

To reduce the potential for protein damage, associated with using UV light to couple proteins onto the dextran surface, an effort to filter unwanted wavelengths of light was studied. Three filters were analysed to see which were compatible with the photo-activation protocol. The filters included a 280 and 315 nm longpass filter and a 320 nm bandpass filter. The absorption spectra of the different filters and the UV fused silica used for the photolithographic mask fabrication was determined using the method described in §3.2.8. The spectra in Figure 5-25 show that the 320 nm bandpass filter restricts less low wavelength light than the 280 and 315 nm longpass filters. The UV fused silica shows no significant absorption in the wavelength range of activation, so will have no filtering effect on the UV light.

The absorption measurements in §5.4.3 (Figure 5-10, pg 119) recorded an absorption between 250-300 nm for AACD. The absorption of protein L (28 μM) in deionised water (Figure 5-26, see overleaf) was measured, using the method described in §3.2.8, to determine the protein absorption maximum. The absorption spectra of the filters were compared with the protein L (Figure 5-26, see overleaf) and AACD (Figure 5-10, pg 119) absorption data. The absorption data demonstrated

that the 280 nm longpass filter did not filter all the wavelengths absorbed by AACD but did filter wavelengths absorbed by protein L (Figure 5-26). The 280 nm longpass filter could therefore be used to filter wavelengths absorbed by the protein.

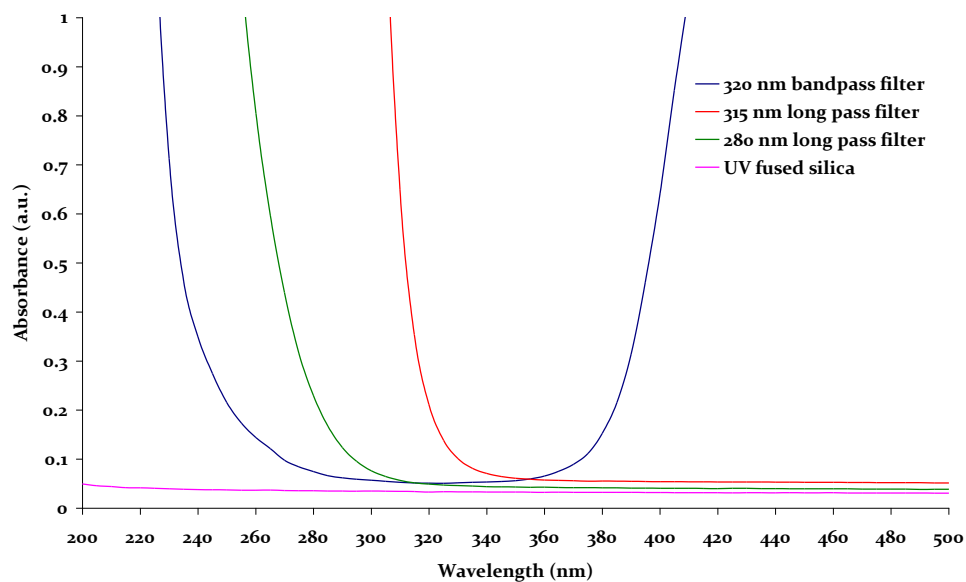


Figure 5-25 Absorption spectra of UV fused silica used in the fabrication of the photolithographic mask and three filters that absorb different wavelengths of UV light. The absorption spectra were taken using the protocol described in §3.2.8.

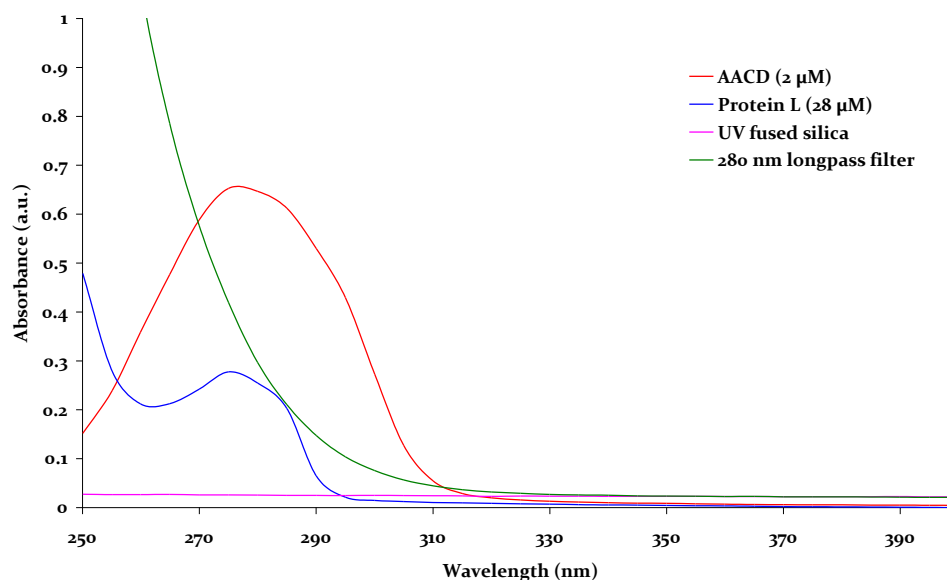


Figure 5-26 Absorption spectra of aryl azide conjugated dextran (AACD), protein L (28 μM), UV fused silica and a 280 nm longpass filter measured between 250-400 nm. The absorption spectra were taken using the protocol described in §3.2.8.

5.8.1 Photochemical Coupling of Single Proteins

Conjugation of single proteins by photoactivation was achieved using the method described in §3.2.12. When UV light illuminates the AACD the azide is converted into a reactive cyclic ketenimine, which can react to covalently attach the protein. The amount of protein attached is therefore, to some extent, concentration dependent. As the concentration increases the probability of a protein molecule being in proximity of the cyclic ketenimine to form a covalent bond increases. To determine the minimum concentration required to conjugate the maximum amount of protein to the surface a range of streptavidin concentrations was studied, measuring the resultant fluorescence intensity of the pattern compared with the concentration.

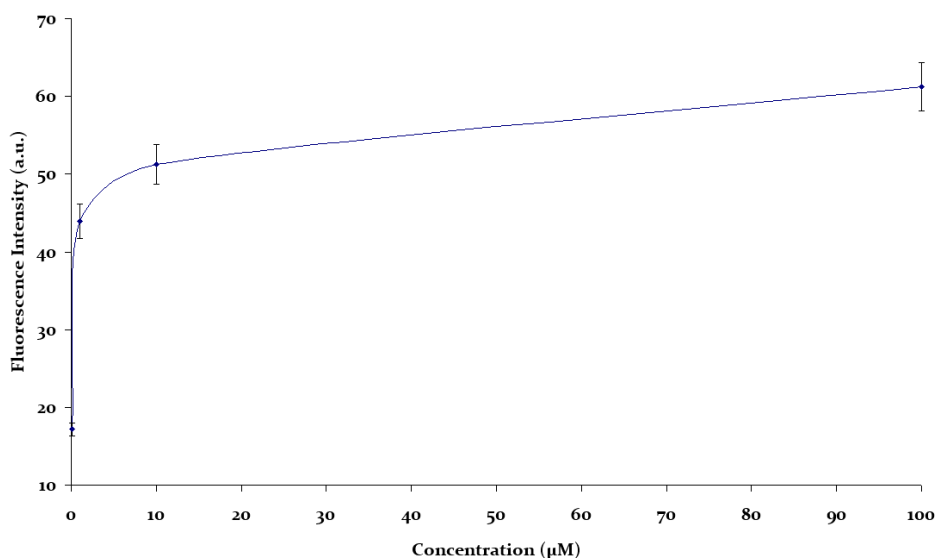


Figure 5-27 Graph of average fluorescence intensity of features patterned using the methods described in §3.2.12 against changes to the protein concentration used in the patterning process. All the images analysed were captured with an EC Plan-Neofluar 10x objective with a 2 second image capture time.

By assuming that an increase in fluorescence intensity, on incubation with biotin-FITC, was as a result of an increased conjugation of streptavidin, a suitable concentration for reproducible patterning was determined. The graph in Figure 5-27 shows the average fluorescence intensity of different streptavidin concentrations conjugated to the surface after incubation with a solution of biotin-FITC (1 µM). As the protein concentration increases the average intensity of the pattern also increases. Above a concentration of 10 µM there is no marked improvement on the intensity of the pattern. It is important to note that this is a qualitative analysis of

the surface as the increased intensity may not be attributed to an increased surface density of protein. The concentration range is also specific to streptavidin and may not be suitable to other proteins. Despite this the evidence of increased intensity found from higher concentrations of protein fits with the theoretical principle of conjugation and has been previously described [278]. Solutions $>1 \mu\text{M}$ were used for following experiments to reduce the possible limitations that concentration may have on proximal conjugation.

The time required to produce reproducible patterns of protein L on the surface of the AACD was also tested. The formation of the reactive cyclic ketenimine, on aryl azide photo-activation, is known to occur on a femtosecond timescale [337]. To reduce the potential for the formation of singlet oxygen species [62], on UV illumination, the minimum illumination time was determined. Surfaces were prepared as described in §3.2.9 and streptavidin ($10 \mu\text{M}$) was conjugated to the surface using the protocol described in §3.2.12. The only modification made to the protocol was the time of illumination used for each surface.

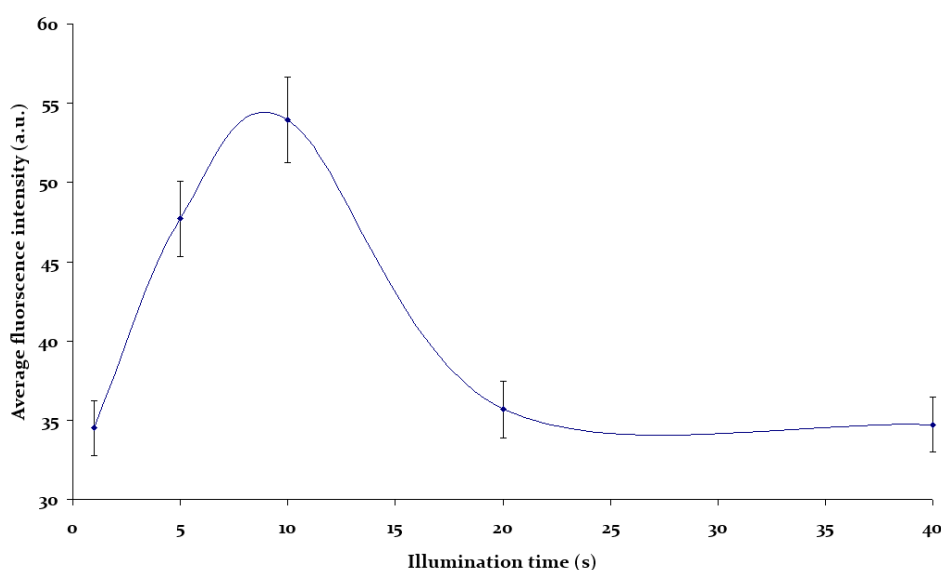


Figure 5-28 Graph of average fluorescence intensity of streptavidin/biotin-FITC motifs patterned using the methods described in §3.2.12 against changes to the illumination time of the patterning process. All the images used to determine the intensity were captured with an EC Plan-Neofluar 10x objective with a 2 second image capture time.

The graph in Figure 5-28 show the average fluorescence intensity of surfaces illuminated using a range of times to immobilise streptavidin on the surface. The images show that a 10 seconds illumination forms motifs with the maximum intensity. Any illumination time >10 seconds does not increase the fluorescence

intensity on incubation with biotin-FITC (1 μM). A time of 10 seconds was therefore used for following experiments to reduce the potential impact of the UV light on the protein. This is a 6-fold lower illumination time compared with other photoinitiated conjugation methods previously reported [278].

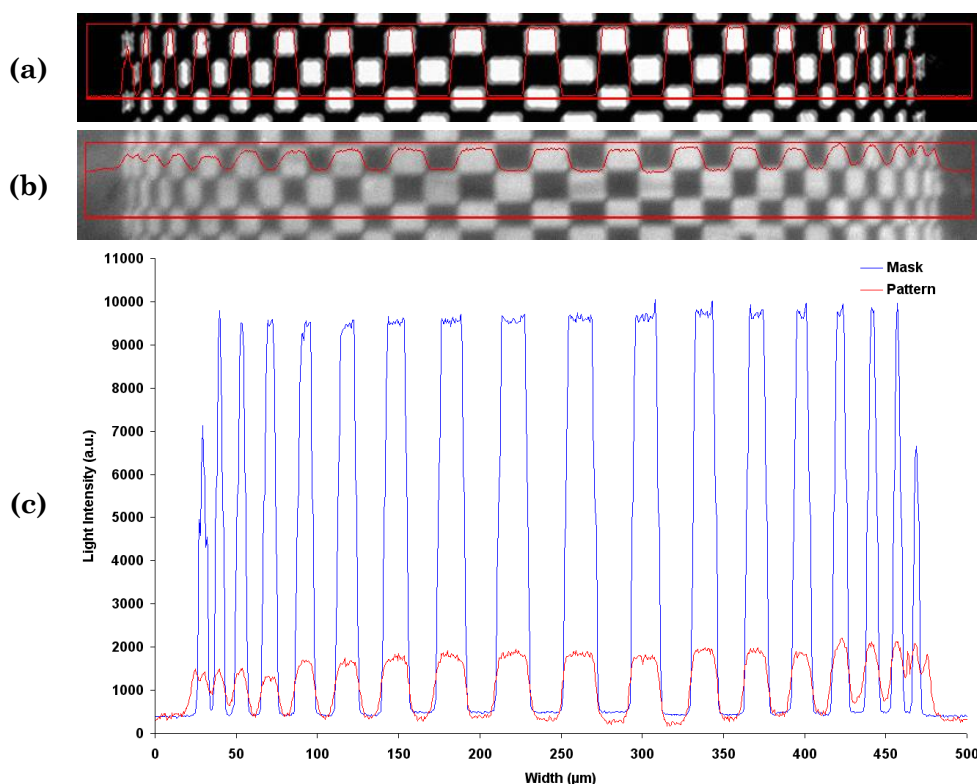


Figure 5-29 Images (a) and (b) show line profiles taken from an image of the mask (a) and the subsequent protein pattern produced using the mask (b). The graph (c) shows the combined line profiles from the two images. The full width half maximum of each feature was compared to determine the resolution of the patterns. Images (a) and (b) were taken using an EC Plan-Neofluar 10x objective using bright field and 3 second image capture respectively.

To analyse the resolution of patterns produced compared with the fabricated mask used to transfer the protein pattern, line profiles of the patterned features were analysed. Figure 5-29 (a) shows the line profile from the mask used to transfer the pattern, while Figure 5-29 (b) shows the line profile of the fluorescent protein patterned on the surface. The full width half maximum of each profile was used to determine the difference between the mask and the transferred pattern. Figure 5-29 (c) show the line profile of the mask (blue) and fluorescent protein (red) together. Results showed the features transferred were $2.2 \mu\text{m} \pm 0.54 \mu\text{m}$ larger than the original mask features.

5.8.2 Motifs Produced by Aligning Multiple Proteins on Glass Surfaces

To pattern multiple proteins onto the AACD surface Mask 2 was used in the protocol described in §3.2.14 to increase the alignment tolerance. The design of the mask was developed to produce two or more proteins side by side using a simple in-house built alignment system. The potential error of the alignment mark features is $\pm 8 \mu\text{m}$ when accurate alignment is used, due to the gap between the surface alignment features and the mask alignment features (Figure 5-30 (a)). To counter this potential error and allow two proteins to be patterned side by side, Mask 2 was designed and fabricated to allow a $\pm 10 \mu\text{m}$ tolerance in both the horizontal and vertical axis. Figure 5-30 (b) shows an exaggerated design of the patterned features used to increase the tolerance of the patterning process.

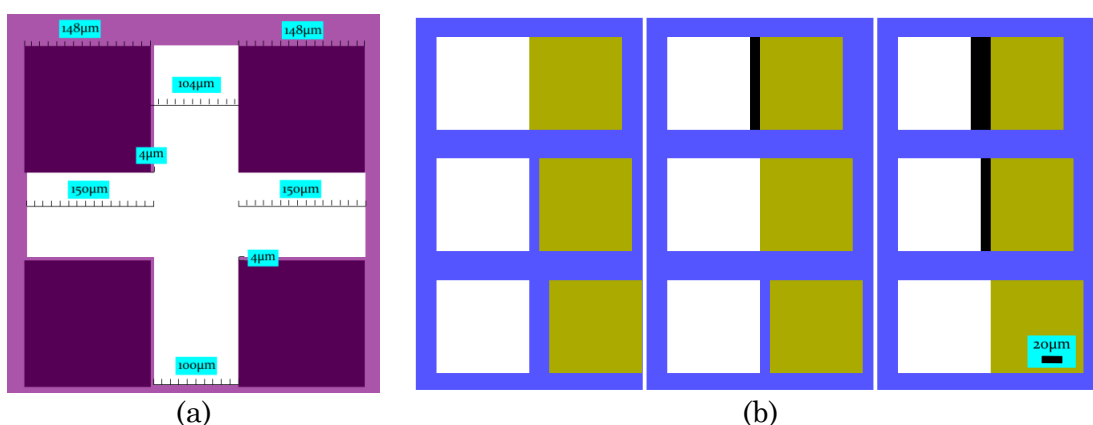


Figure 5-30 Illustration showing (a) Overlapping image of the surface (cross) and mask (squares) alignment features with a $5 \mu\text{m}$ gap, which could cause a potential $\pm 10 \mu\text{m}$ translation error. Overlapping features in (b) represents the Mask 2 features designed to counter translation error. The patterns represents a $-10 \mu\text{m}$ error pattern (left), a $0 \mu\text{m}$ error pattern (centre) and a $+10 \mu\text{m}$ error pattern (right). The green squares represent the first protein illuminated and the white the second protein.

The smallest feature size on both of the masks fabricated (mask 1 and 2) was $4 \mu\text{m}$. Analysis of the protein pattern dimensions, which were produced upon transfer of the mask pattern to form the protein pattern, showed that protein patterns were only limited by the minimum feature dimensions of the photolithographic mask (Figure 5-31). The difference between the size of protein pattern features and mask features was found to be $< 1 \mu\text{m}$.

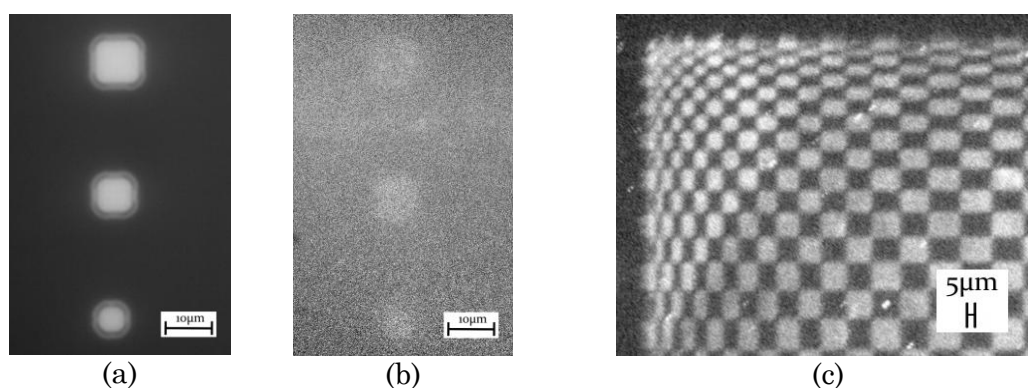


Figure 5-31 Image (a) shows a bright field transmission image of the smallest features found on Mask 2 (4 x 4 µm). The epifluorescence images in (b and c) show patterns of IgG-FITC (500 nM) bound to protein L (10 µM) immobilised surfaces captured using (b) an LD Plan-Neofluar 63x objective and (c) an LD A-Plan 20x objective, with (b) a 6 second and (c) a 2 second image capture. The images show features as small as 4 x 4 µm can be successfully transferred onto the surface.

The patterns in Figure 5-32 (see overleaf) show two proteins patterned using Mask 2. The patterns achieved in Figure 5-32 (a) and (b) (see overleaf) show the alignment potential of the system to achieve patterns of protein side by side with micron scale accuracy. The potential problem with the system can be seen in Figure 5-32 (c) and (d) (see overleaf), caused by angle inaccuracies. When the illumination is such that the patches are aligned parallel the patterning process occurs as in Figure 5-32 (a) and (b), but if there is even a small angle variation the effect is significant to the patterning process as seen in Figure 5-32 (c) and (d) (see overleaf). In this case the patterns close to the alignment features (Figure 5-32 (c) see overleaf) show limited effect but as the patterns move away from the alignment feature the angle effect is more prominent (Figure 5-32 (d) see overleaf). Despite the potential alignment problems the patterns achieved are reproducible. Patterns close to the alignment features exhibited patterning with <math><20\ \mu\text{m}</math> accuracy, while patterns further from the alignment features could be patterned with <math><100\ \mu\text{m}</math> resolution.

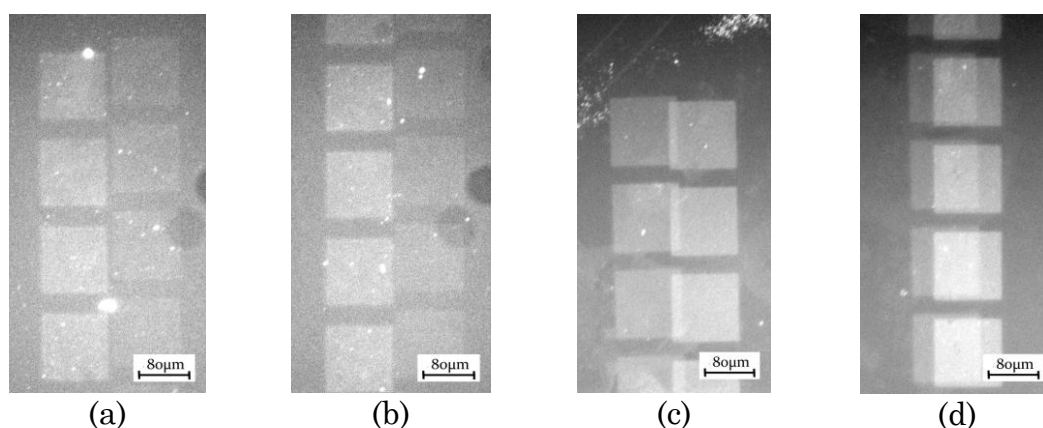


Figure 5-32 Epifluorescence images of IgG-FITC (500 nM) bound to protein A (14 μ M) and protein L (10 μ M) patches immobilised on aryl azide dextran surfaces. Images (a) and (b) show a column of protein L patches on the left and a column of protein A patches on the right. Concurrently images (c) and (d) show a column of protein A patches on the left and protein L on the right. All images were captured using an EC Plan-Neofluar 10x objective, with a 3 second image capture.

The patterns produced in Figure 5-32 also show fluorescence intensity variations based on the protein patterned. The fluorescence images in Figure 5-32 (a) and (b) are patterned first with protein A and then with protein L. The fluorescence images in Figure 5-32 (c) and (d) are the opposite way around, with protein L patterned first and protein A second. When IgG-FITC binds to these two patches a higher intensity signal is found on the protein L patches compared with that on the protein A patches. This observation does not necessarily mean the proteins are active on the surface but could be a result of non specific protein adsorption to denatured protein present on the surface.

To demonstrate that the proteins remained active on the surface and that the observed binding was not simply non specific protein adsorption, a rhodamine labelled F(ab')₂ fragment of IgG was used to probe the surface. An illustration of the conjugation procedure is shown in Figure 5-33 (see overleaf), involving the aligned conjugation of protein L and protein A on the AACD surface. The F(ab')₂ fragment has a strong binding affinity with protein L but not with protein A, as illustrated in Figure 5-33 (c) (see overleaf).

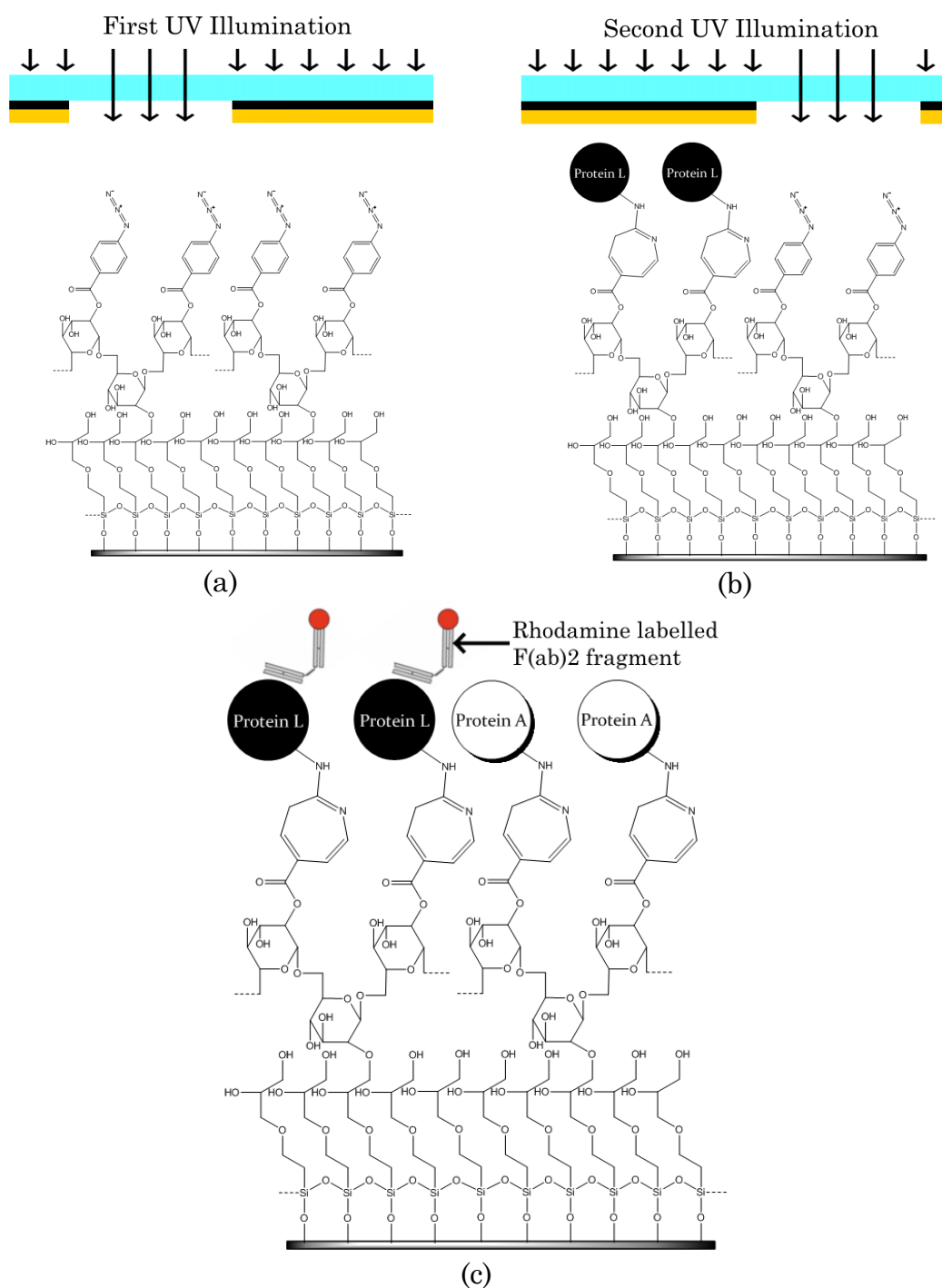


Figure 5-33 Illustration of the protocol used to show the site specific conjugation of proteins that retain specific recognition properties. The first illumination (a) activates the AACD forming the reactive cyclic ketenimine, which reacts with amine groups present on protein L. The second illumination (b) activates the remaining aryl azide groups leading to protein A conjugation. When the protein patterned surface is incubated with rhodamine labelled F(ab)2 (c) binding should be observed with protein L only.

The fluorescence images in Figure 5-34 (a) and (b) (see overleaf) show a rhodamine labelled F(ab)2 (2.2 μ M) bound to a protein L patterned feature. More

importantly the fluorescence images in Figure 5-34 (c) and (d) show the background fluorescence of the protein A and L patches in the same respective area. The images show that the rhodamine labelled F(ab')₂ fragment binds only with the protein L patch and not with the protein A patch. Figure 5-34 (b) even shows a reduction in non specific adsorption due to the presence of the protein A on the patch.

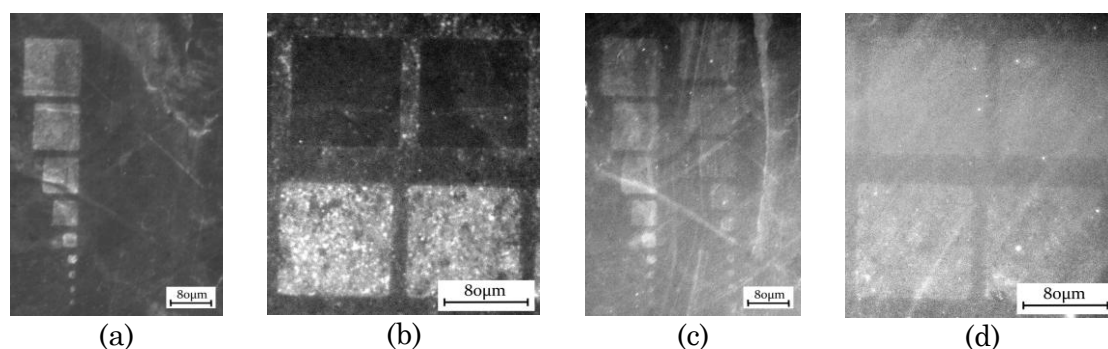


Figure 5-34 Epifluorescence images of protein modified glass surfaces. Images (a)/(b) and (c)/(d) were taken with Carl Zeiss filter set 15 and 9 respectively. Images (a)/(b) show a tetramethylrhodamine labelled F(ab')₂ (excitation wavelength 552 nm, emission wavelength 578 nm, 2.2 µM) associated with surface conjugated protein. Images (c)/(d) show background fluorescence images taken with filter set 9. The fluorescence images were captured in the same location using the different filter sets where images (a)/(c) and (b)/(d) correspond to each other. In (a) and (b) the protein A patterns show no fluorescence, but the protein L shows strong fluorescence. Both the protein L and A patches can be visualised when imaging with filter set 9, as observed in (c) and (d). Images (a)/(c) and (b)/(d) were captured with an EC Plan-Neofluar 10x objective and an LD A-Plan 20x objective respectively. Images (a)/(c) and (b)/(d) were captured with a 4 and 2 second image capture respectively.

5.9 Study of Protein L Surface Density Conjugated to Glass Surfaces

Preliminary work was carried out in an effort to determine the surface density of protein L immobilised on the aryl azide conjugate dextran surface using the protocol described in §3.2.15. To effectively analyse the concentration the method involved stripping of surface bound IgG-FITC from the surface for quantification. The stripping buffer was composed of a high pH wash, which is routinely used to completely strip antibodies from surfaces. The buffer was used to wash the surface before neutralising the solution and freeze drying the stripped antibody.

A standard curve of IgG-FITC concentration was determined by treating different concentrations of IgG-FITC under the same conditions used for stripping, to ensure consistency. The spectra in Figure 5-35 (see overleaf) show the fluorescence

intensity of different IgG-FITC concentrations after processing in the stripping buffer. By taking the area under the curve, between 510 nm and 540 nm, a standard curve see (Figure 5-36, see overleaf) was generated and used to determine the concentration of solutions stripped from the surface.

Two samples were stripped and analysed giving an average concentration, calculated from the standard curve (Figure 5-36, see overleaf), of 3.11 ± 1.30 nM. By calculating the area of the patterned surface and the number of molecules released from the surface the number of molecules/cm² was determined. Results showed the 18 x 18 mm coverslip produced a pattern with an area of 3.24 cm². A 3.11 nM concentration equated to 3.74×10^{14} molecules associated on the patterned motif. Thus a surface density of 1.16×10^{11} molecules/cm² was confirmed.

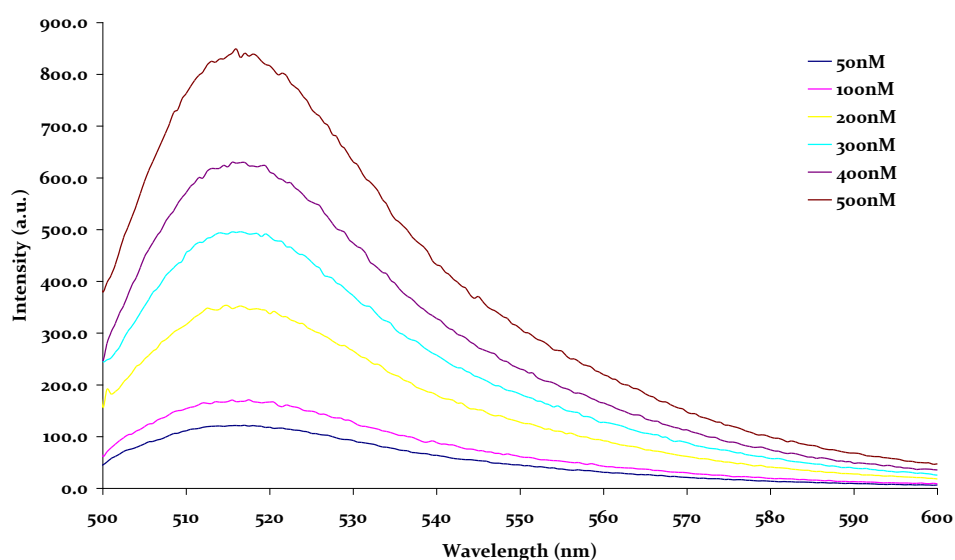


Figure 5-35 Normalised fluorescent intensity emission spectra of a range of IgG-FITC concentrations, using an excitation wavelength of 494 nm. The characteristic emission of IgG-FITC can be seen at 517 nm. The experimental protocol used to determine the absorption is detailed in §3.2.15.

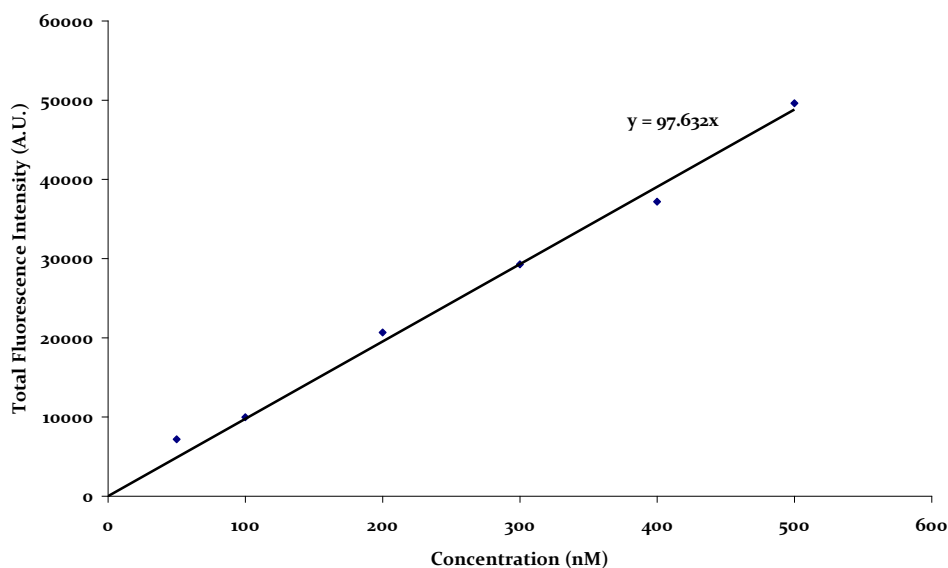


Figure 5-36 Standard curve of IgG-FITC concentration against total fluorescence intensity using the area under the curve between 510 and 550 nm. The experimental protocol used to determine the absorption is detailed in §3.2.15.

Further samples are required to more accurately determine the surface concentration, but from preliminary analysis a high density of protein L has been achieved. By assuming a ratio of 1:1 IgG-FITC:protein L the surface density is one order of magnitude lower than previously reported concentrations of antibodies on gold [338, 339], glass [146] and hydrogel [340] surfaces and equivalent to recent work on silicon [143]. The density on the surface is one order of magnitude below the maximum density of a monolayer of IgG, theoretically calculated as 4.06×10^{12} molecules/cm² by Lee *et al.* [146]. Dense patterns of multiple proteins, aligned in motifs on the same surface, can therefore be achieved using the protocol.

5.10 Summary

The research presented in this chapter documented the generation of multiple protein motifs conjugated to AACD modified glass surfaces. Dextran was used to form a passive layer between the surface and protein to prevent the protein denaturing upon conjugation with the surface. Dextran was preferred, compared with other surface spacers [259, 312], as it is known to prevent non specific adsorption of protein and has long term stability [177, 189]. An aryl azide photolinker was conjugated with the dextran, which forms a reactive cyclic

ketenimine upon photoactivation. The advantage of producing the cyclic ketenimine group, compared with other photolinkers [46], is that it reacts specifically with amino groups [210]. By conjugating proteins via amino groups, present on the protein surface, the orientation of the protein can be controlled.

The modification of a glass surface to introduce an AACD was based on work published by Elender *et al.* [203] and Bhat *et al.* [211]. The integrated method involved the silanisation of glass with GOPS to produce an epoxide terminated surface. When the silanised surface is incubated with the AACD a ring opening reaction between the oxirane ring of the epoxide and the hydroxyl groups of the AACD formed a covalent bond with the surface. Previous research involved the use of a high concentration, 30 % w/v, of dextran to modify the glass surface [203]. The concentration of silane solution, time of silanisation and concentration of dextran used to modify glass surfaces was investigated. Results demonstrated that a 1 % solution was as effective as a 30 % solution in producing a reproducible layer of dextran-FITC, equating to a 30-fold reduction in concentration compared with previous research [203, 325]. By reducing the concentration of reagent, used to modify the glass surface, a single AACD preparation was used to prepare all the samples presented in this thesis. To confirm the successful modification of the glass XPS was used to characterise chemical changes to the surface. Results demonstrated the successful modification of the surface with AACD and the subsequent conjugation of protein [302, 335, 336].

Photolithographic masks were designed and fabricated to facilitate the alignment of multiple protein motifs on the AACD surface. The patterns were accurate to <1 μm , compared with the size of the original mask features, and could be patterned in an area as small as 4 x 4 μm . An in-house built alignment setup was used to pattern adjacent motifs. Adjacent patterns could be aligned reproducibly with a 10-100 μm tolerance. The photolithographic mask can be re-used and the in-house alignment system provides an inexpensive and practical approach for patterning aligned motifs of proteins on surfaces. Preliminary analysis of the surface density of protein L recorded a density of 1.16×10^{11} molecules/cm², which is within one order of magnitude of current state-of-the-art patterning techniques [143, 146, 338]. Protein L and A remained active once conjugated to the surface, with

F(ab')₂ only interacting with protein L on the surface, thus showing binding remained specific .

6

Conclusions and Suggestions for Future Work

6.1 Thesis Summary and Conclusion

The ability to quantify the level of Ig from patient serum, rapidly, is critical to ensure improved diagnosis and patient management in the early stages of sepsis. Microfluidic LOC technologies have shown potential in the development of POC technologies for the rapid quantification of biomolecules in solution [53]. Thus the aim of this thesis work was to design and produce a protocol to generate protein motifs on a surface that could be integrated with the fabrication of a microfluidic device. In particular, the protocol is designed to pattern multiple antibody binding proteins aligned specifically upon a surface. The surface was designed to be integrated within a microfluidic affinity chromatography device to be used for the rapid separation and quantification of antibodies in serum.

Ideally, for affinity separation, the density of available proteins on a surface needs to be high to maximise the availability of association sites on the surface to ensure saturation of the protein patches does not occur before separation has been achieved. A protein should remain stable, when conjugated with the surface, preferably with a single orientation to ensure each protein is accessible to analyte. Non specific adsorption of protein must be avoided and conjugated proteins need to retain recognition for target analytes, ideally with an association constant comparable with that found in solution phase. To integrate protein motifs within a microfluidic channel device the conjugation method must incorporate the specific alignment of motifs on the surface. To pattern multiple proteins a sequential or

parallel conjugation method that can generate adjacent protein motifs is required. An alignment system is therefore central in controlling where the motifs are patterned on the surface but also for the subsequent alignment of the microfluidic channel on top of the patterns.

To separate a mixture of Igs in a microfluidic device a proposed system involving affinity separation of Ig classes was devised. The premise of the work is that as a mixture of Igs flow over a surface conjugated protein, which has affinity for Ig in solution, the Ig will associate with the protein causing a 'slow down' of the Ig. The time of interaction with the surface is specific to the association rate of the Ig with the surface immobilised receptor. It is believed that flowing Ig over surfaces conjugated with multiple proteins that have different association rates with Ig classes will result in Ig classes eluting at different times. The research described in this thesis concentrated on the association properties of IgG with surface bound proteins, as IgG is the most abundant Ig found in human serum [66]. Antibody binding proteins were considered the best candidates for affinity separation of Ig molecules as they show specific binding with Ig and a number of mutants have been studied with different association rates with Ig [113, 114, 341].

The initial investigation into the patterning of antibody binding protein with surfaces focussed on the conjugation of proteins with silicon. High densities of DNA conjugated with silicon surfaces had been achieved previously [128]. In fact, based upon a literature review, silicon was found to have the highest density of DNA conjugated with the surface compared with other substrates [130, 145]. Silicon therefore warranted investigation to determine if high density patterns of protein were achievable. Protein conjugation techniques were based upon the work of Huabing Yin [128, 131], which describes the covalent attachment of DNA oligonucleotides to the surface of silicon <100>. The protocol was modified to attach proteins onto silicon including: streptavidin, NeutrAvidin, single domain protein L and multi domain protein L. This study, similar to research undertaken with DNA [128], demonstrated submicron scale motifs of protein were achievable. Feature sizes as small as 140 nm were possible using the silicon patterning technique described in this thesis. Patterns of streptavidin, NeutrAvidin and single domain protein L were reproducible. The linker, UANHS, used to conjugate protein on the silicon was successfully characterised by NMR and chemically modified surfaces

were analysed by XPS. The NMR data was comparable with results published by Yin *et al.* [128], which used UANHS to conjugate DNA with silicon. The XPS data was also compared with published results, demonstrating that UANHS was successfully conjugated with the silicon surface [137]. The XPS data also confirmed that the UANHS remained functional, allowing the subsequent immobilisation of NeutrAvidin [302].

The silicon surface was prone to biofouling from IgG-FITC, which could be reduced by blocking the surface with BSA. However patterns produced with multidomain protein L could not be reproducibly achieved on silicon. To pattern a multidomain antibody binding protein on silicon a NeutrAvidin layer was first conjugated to the silicon surface. A biotinylated multidomain protein A was then immobilised on the NeutrAvidin via the association of biotin with NeutrAvidin. The resulting protein A immobilised surface retained binding recognition with IgG-FITC. This successfully eliminated the problem of reproducibility, while retaining the ability to pattern micron scale features with low levels of non specific protein adsorption. To produce motifs of multidomain antibody binding proteins, without the use of biotinylated protein, an alternative method of conjugation was investigated.

After further review of existing patterning methods, including the use of hydrophilic surface spacers and the modification of surfaces with photolinkers, a new protocol whereby a surface was modified with a dextran conjugated with a photolinker was proposed. Dextran was used to form a passive layer between the surface and protein to prevent the protein denaturing upon conjugation with the surface. Dextran was preferred, compared with other surface spacers [259, 312], as it is known to prevent non specific adsorption of protein and has long term stability [177, 189]. An aryl azide photolinker was conjugated with the dextran, which forms a reactive cyclic ketenimine upon photoactivation. The advantage of producing the cyclic ketenimine group, compared with other photolinkers [46], is that it reacts specifically with amino groups [210]. By conjugating proteins via amino groups, present on the protein surface, the orientation of the protein can be controlled.

The modification of a glass surface to introduce an AACD was based on work published by Elender *et al.* [203] and Bhat *et al.* [211]. The integrated method involved the silanisation of glass with GOPS to produce an epoxide terminated

surface. When the silanised surface is incubated with the AACD a ring opening reaction between the oxirane ring of the epoxide and the hydroxyl groups of the AACD formed a covalent bond with the surface. Previous research involved the use of a high concentration, 30 % w/v, of dextran to modify the glass surface [203]. The protocol was optimised in an effort to reduce the concentration of dextran required to produce a reproducible dextran layer on the surface. A fluorescently labelled dextran, dextran-FITC, was analysed to determine the minimum concentration required to achieve a uniform dextran layer. Results demonstrated that a 1 % solution was as effective as a 30 % solution in producing a uniform layer of dextran-FITC, equating to a 30-fold reduction in concentration compared with previous research [203, 325]. By reducing the concentration of reagent, used to modify the glass surface, a single AACD preparation was used to prepare all the samples presented in this thesis. To confirm the successful modification of the glass XPS was used to characterise chemical changes to the surface. Results demonstrated the successful modification of the surface with AACD and the subsequent conjugation of protein [302, 335, 336].

Photolithographic masks were designed and fabricated to facilitate the alignment of multiple protein motifs on the AACD surface. The patterns were accurate to $<1 \mu\text{m}$, compared with the size of the original mask features, and could be patterned in an area as small as $4 \times 4 \mu\text{m}$. An in house built alignment setup was used to pattern adjacent motifs. Adjacent patterns could be aligned reproducibly with a 10-100 μm tolerance. The photolithographic mask can be re-used and the in-house alignment system provides an inexpensive and practical approach for patterning aligned motifs of proteins on surfaces. Preliminary analysis of the surface density of protein L recorded a density of 1.16×10^{11} molecules/cm², which is within one order of magnitude of current state-of-the-art patterning techniques [143, 146, 338].

In summary, it has been demonstrated that both silicon and glass surfaces can be modified to site-specifically conjugate proteins with the surface. On silicon motifs of 140 nm are achievable, while on glass 4 μm scale patterns were achieved. The proteins retained binding recognition when conjugated with the surfaces and non specific protein adsorption was prevented. By incorporating a photoactive surface, photolithography and alignment features, site-specific patterning of multiple

proteins was realised. Preliminary results suggest high density protein motifs, patterned adjacent to one another, were achieved using an AACD modified surface.

6.2 Future Work

Although the aryl azide has been successfully used to conjugate protein onto the dextran surface, other photochemistry may be better suited. The photo-attachment of protein described in Chapter 5 required the use of <315 nm wavelength light for coupling. Proteins predominantly adsorb light at a wavelength of 280 nm; it is therefore preferable to choose an activation wavelength above this. The review by Park *et al.* [46] discusses potential photochemistry and its use for surface modification. Molecules including BP, PTD, and a perfluorinated form of aryl azide can be activated at wavelengths >300 nm. Carboxylic acid derivatives of these photolinkers are available, which could be used instead of 4-azidobenzoic acid, to synthesise a photo-active dextran linker. This would abolish the potential risk of protein or surface degradation from short wavelength UV light. The main limitation of using these photolinkers is that they do not specifically target amino residues on the protein, unlike the cyclic ketenimine produced upon aryl azide activation. There is a need for novel photolinkers capable of reacting with amine chemistry specifically when activated under long wavelength UV light.

The protein patterns produced in Chapter 5 showed that proteins can be site specifically patterned and aligned with micron scale resolution. Limitations to the technique were found from rotational inaccuracies, which can be easily reduced by modifications to the alignment system. The image in Figure 6-1 (a) (see overleaf) shows the alignment concerns associated with using the current setup. Even a small change in the rotation can lead to significant changes further from the alignment features. The solution is to integrate two sets of alignment marks above and below the features to improve the reproduction of alignment, as shown in Figure 6-1 (b) (see overleaf). In general the alignment system can be improved by increasing the resolution of the camera, having two distant points of alignment and reducing the scale of the alignment features.

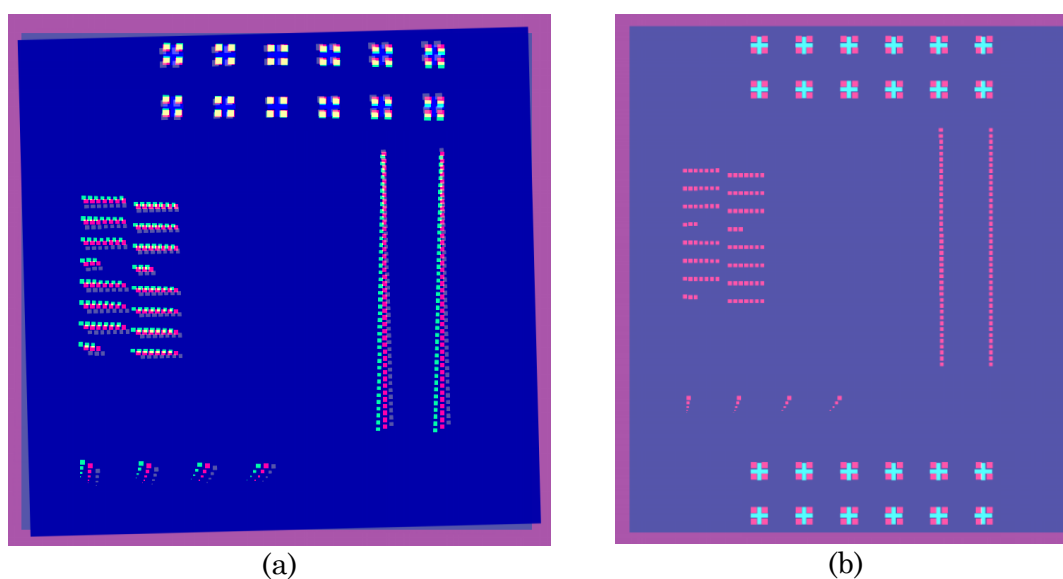


Figure 6-1 Illustration of (a) alignment inaccuracies and (b) a potential mechanism to solve the problem.

6.2.1 Microfluidic device fabrication

With the implementation of alignment improvements and improved photochemistry a set of masks could be fabricated to integrate protein patterns within a microfluidic channel. The photolithographic mask shown in appendix C.2 shows a series of channels and masks designed for this purpose. The same features used to align the protein patches can be used for microfluidic channel alignment. This change should enable reproducible alignment of multiple proteins patterned within a single microfluidic channel, leading to the eventual realisation of a quantitative antibody separation device. A simple proof of principle experiment involves the same rationale as the experiment illustrated in Figure 6-2 (see overleaf). Protein L binds specifically to Igs that have a κ light chain as part of its structure. Using fluorescently labelled antibodies with κ light chain and another with λ light chain microfluidic affinity chromatography can be demonstrated. By allowing a mixture of κ and λ chain to flow over a protein L immobilised surface separation should occur leading to the elution of λ chain first followed by κ chain.

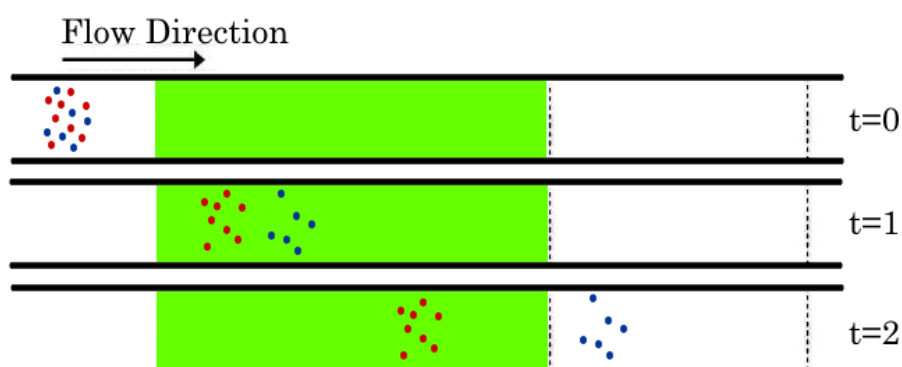


Figure 6-2 Top view of an affinity separation device taken at three time intervals. The surface receptors (green) have an affinity for the red molecules and no affinity for the blue molecules. As the molecules flow through the channel the red molecules are separated from the blue molecules as they spend an increased amount of time associating and dissociating with the surface.

Modelling work completed by Friedrich *et al.* [342] defined a set of conditions for the effective mass transfer of analyte within a microfluidic device. Further to this work a set of parameters was determined for a potential microfluidic channel device for the separation of antibodies using affinity chromatography within the channel. The estimated density of protein L found in this thesis, 1.16×10^{11} molecules/cm², and the binding affinity of protein L for IgG found in the literature (see Appendix B) were used to determine a potential separation time. The analysis time achieved, using the model, was as low as 30 minutes, which would equate to a 4-fold reduction in diagnostic time. To improve the accuracy of the model a series of experiments are required to refine the input parameters. Firstly, a greater number of samples need to be analysed to quantify the surface density of protein L on the surface. Secondly, the affinity of the surface bound protein L for immunoglobulin needs to be quantified.

Appendix A

Protein L Sequence Alignment

The illustration in Figure A-1 demonstrates the sequence alignment between strain 312 and 3316. The numbering systems given in different publications are also shown.

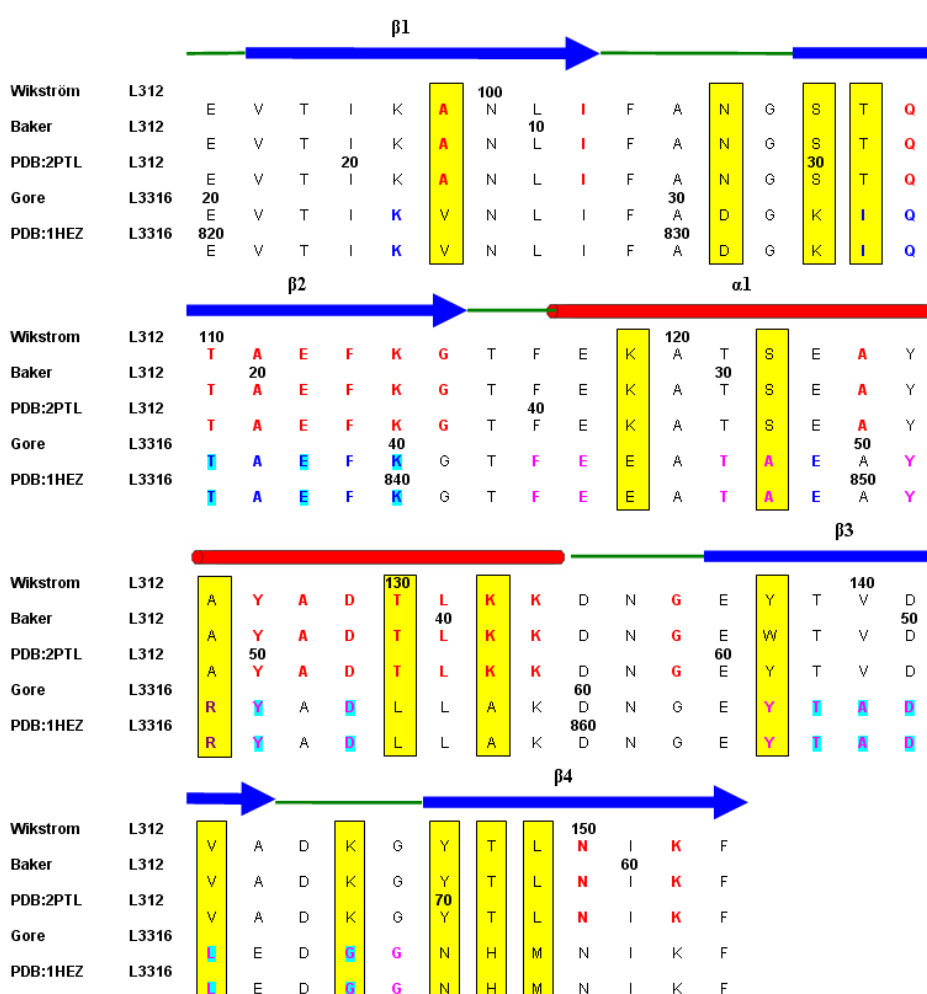


Figure A-1 Sequence alignment of single domains from *Peptostreptococcus magnus* strains 312 and 3316. The yellow highlighted residues display sequence variations between strains. Residues emboldened in red are those shown by NMR studies to have major chemical shifts on complex formation [107]. Residues emboldened in blue and pink have been shown by X-ray crystallographic studies [112] to be key residues involved in complex formation at the site 1 and site 2 binding sites respectively. The Arginine (R) of strain 3316, emboldened in purple, is believed to be involved in interactions at both binding sites. The residues highlighted in blue are those implicated by X-ray crystallography to form hydrogen bonds with the antibody VL domain. The numbering systems used are found in Wikstrom [111], Baker [341], Gore [295], and the protein databank (PDB) files 2PTL and 1HEZ (www.pdb.org).

Appendix B

Protein L Mutants

The images below are structural illustrations of the single domain of protein L from strain 312, created in Swiss Prot PDB viewer with the protein L PDB file 2PTL (www.pdb.org). Different amino acids have been highlighted to show potential conjugation sites (Figure B-1) and the conjugation sites in relation to the active site amino acids of the protein (Figure B-2)

- Red amino acids – Lys residues, which are potential surface attachment sites
- Yellow amino acids – Amino Acids that have been shown by NMR spectroscopy to have a major chemical shift upon V_L chain binding
- Blue amino acids – Amino Acids that do not show a major chemical shift by NMR spectroscopy upon V_L chain binding

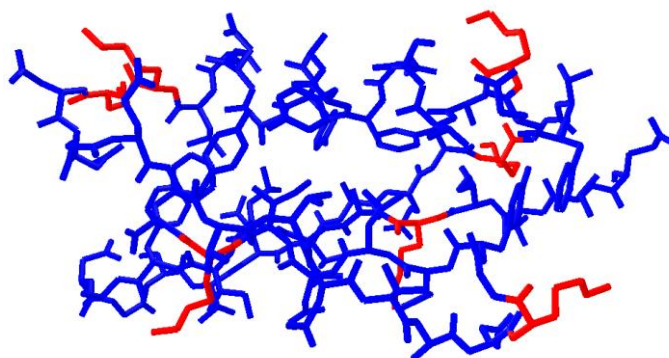


Figure B-1 Lys residues present in Strain 312 of protein L. Image of protein L created using SwissProt PDB viewer (PDB:2PTL), the red residues indicate Lys residues. These residues display amines which can be used for the covalent immobilization to a surface.

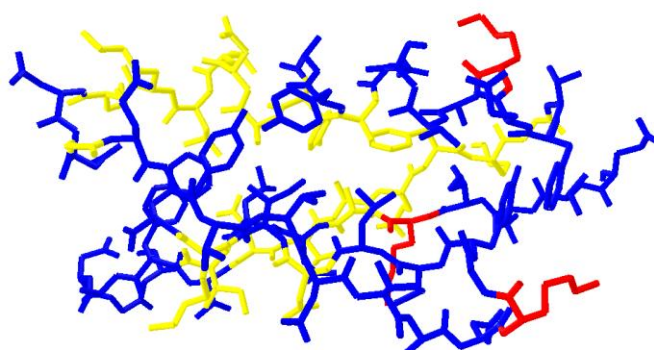


Figure B-2 Binding site residues and Lys present in Strain 312 of protein L. Image of protein L created using SwissProt PDB viewer (PDB:2PTL) The red residues indicate Lys residues not involved in antibody V_L domain binding. Yellow residues are those involved in antibody V_L domain binding.

The two tables shown below and overleaf (Tables B-1 and B-2 (see overleaf)) contain the dissociation rates of a series of protein L mutants produced by the Baker group [341]. The dissociation rates, associated with the two binding site model, of each mutant is given. The mutants are displayed in amino acid residue order.

Mutant	Fast phase apparent dissociation rate (second ⁻¹)	Slow phase apparent dissociation rate (second ⁻¹)	Mutant	Fast phase apparent dissociation rate (second ⁻¹)	Slow phase apparent dissociation rate (second ⁻¹)
E17A	0.079 ±0.011	0.0063 ±0.00046	A34R	0.11 ±0.021	0.026 ±0.0036
V18A	0.10 ±0.012	0.0073 ±0.0012	A34C	0.075 ±0.020	0.0051 ±0.0014
T19A	0.94 ±0.13	0.0069 ±0.00041	E35A	0.079 ±0.0080	0.0070 ±0.0012
I20A	0.0997 ±0.0088	0.0071 ±0.00069	F36A	0.11 ±0.023	0.0094 ±0.00070
I20V	0.098 ±0.0094	0.0069 ±0.00016	F36L	0.097 ±0.0086	0.0070 ±0.00057
K21A	0.099 ±0.011	0.0064 ±0.00015	F36W	0.097 ±0.025	0.0055 ±0.00023
A22G	0.080 ±0.0037	0.0062 ±0.00020	K37A	0.091 ±0.0072	0.0073 ±0.0012
N23A	0.11 ±0.0062	0.0077 ±0.00048	G38A	0.10 ±0.0044	0.0075 ±0.00074
L24A	0.096 ±0.0067	0.0097 ±0.00096	T39A	0.079 ±0.0033	0.0068 ±0.00032
I25A	0.090 ±0.013	0.0066 ±0.0012	F40G	0.13 ±0.0002	0.0099 ±0.00045
F26A	0.080 ±0.0042	0.0069 ±0.00056	F40L	0.12 ±0.014	0.0094 ±0.00095
F26L	0.086 ±0.010	0.0069 ±0.00075	E41A	0.085 ±0.0026	0.0072 ±0.00015
A27P	0.082 ±0.0069	0.0076 ±0.00052	K42G	0.097 ±0.0098	0.0074 ±0.00085
N28A	0.083 ±0.0004	0.0065 ±0.00029	A43G	0.087 ±0.011	0.0070 ±0.00047
G29A	0.081 ±0.014	0.0071 ±0.00080	T44A	0.034 ±0.0012	0.0072 ±0.00077
S30A	0.088 ±0.013	0.0068 ±0.00069	S45A	0.11 ±0.016	0.0082 ±0.00111
T31A	0.089 ±0.011	0.0068 ±0.0013	S45G	0.083 ±0.012	0.0074 ±0.00063
Q32A	0.10 ±0.013	0.010 ±0.0012	E46G	0.081 ±0.00064	0.0065 ±0.00106
T33A	0.090 ±0.0044	0.0070 ±0.00029	E46I	0.0099 ±0.022	0.0080 ±0.00193

Table B-1 Mutants produced by the Bakers group taken from [341]. The residue assignments are base on PDB file 2PTL and the apparent dissociation rates were measured by surface plasmon resonance.

Mutant	Fast phase apparent dissociation rate (second ⁻¹)	Slow phase apparent dissociation rate (second ⁻¹)	Mutant	Fast phase apparent dissociation rate (second ⁻¹)	Slow phase apparent dissociation rate (second ⁻¹)
A34V	0.098 ±0.011	0.0096 ±0.00019	A47G	0.13 ±0.011	0.0088 ±0.00053
A34G	0.088 ±0.0050	0.0071 ±0.00051	A47V	0.079 ±0.0009	0.0082 ±0.00003
Y48A	0.13 ±0.013	0.0098 ±0.0015	D64A	0.080 ±0.0060	0.0062 ±0.00075
Y48H	0.091 ±0.0068	0.0082 ±0.00004	V65A	0.12 ±0.013	0.0091 ±0.00035
A49G	0.10 ±0.016	0.0083 ±0.0013	V65C	0.047 ±0.0046	0.0055 ±0.0014
Y50A	0.12 ±0.0025	0.020 ±0.00177	A66G	0.089 ±0.0032	0.0074 ±0.00053
Y50F	0.096 ±0.0095	0.0074 ±0.00122	D67A	0.090 ±0.0002	0.0057 ±0.00002
A51G	0.078 ±0.0020	0.0060 ±0.00037	K68A	0.091 ±0.0018	0.0073 ±0.00031
D52A	0.077 ±0.0038	0.0066 ±0.00011	G69A	0.053 ±0.0099	0.0057 ±0.00009
D52G	0.11 ±0.0054	0.0086 ±0.00107	Y70A	0.075 ±0.013	0.0069 ±0.00068
T53G	0.081 ±0.0054	0.0065 ±0.00033	Y70L	0.074 ±0.0085	0.0068 ±0.00001
L54A	0.080 ±0.0014	0.0081 ±0.00040	T71A	0.12 ±0.0033	0.0090 ±0.00009
K55A	0.066 ±0.0020	0.0059 ±0.00032	L72A	0.092 ±0.0088	0.0075 ±0.00118
K56A	0.078 ±0.0038	0.0056 ±0.00003	N73A	0.098 ±0.0022	0.0077 ±0.00020
N58A	0.075 ±0.0071	0.0059 ±0.00067	I74A	0.081 ±0.0051	0.0074 ±0.00095
G59A	0.072 ±0.0003	0.0066 ±0.00001	I74V	0.095 ±0.0048	0.0082 ±0.00070
E60A	0.10 ±0.0006	0.0078 ±0.00002	K75A	0.095 ±0.0027	0.0076 ±0.00099
W61Y	0.10 ±0.0039	0.0077 ±0.00071	F76V	0.11 ±0.011	0.0082 ±0.00011
T62A	0.081 ±0.0005	0.0067 ±0.00007	F76L	0.089 ±0.0086	0.0064 ±0.00055
V63A	0.085 ±0.0075	0.0065 ±0.00023			

Table B-2 Mutants produced by the Bakers group taken from [341]. The residue assignments are base on PDB file 2PTL and the apparent dissociation rates were measured by surface plasmon resonance.

The images below are structural illustrations of the single domain of protein L from strain 3316, created in Swiss Prot PDB viewer with the protein L PDB file 1HEZ (www.pdb.org). Different amino acids have been highlighted to show potential conjugation sights (Figure B-3) and the conjugation sights in relation to the active site amino acids of the protein (Figure B-4)

Red amino acids –	Lys residues, which are potential surface attachment sites
Yellow amino acids –	Amino Acids that have been shown by X-Ray crystallography to make up Site 1 of the V _L binding domain of protein L
Pink amino acids –	Amino Acids that have been shown by X-Ray crystallography to make up Site 2 of the V _L binding domain of protein L
Blue amino acids –	Amino Acids that do not show a major chemical shift by NMR spectroscopy upon V _L chain binding
Purple amino acid –	Arginine 52, believed to be involved in both Site 1 and 2 of the V _L binding domain of protein L

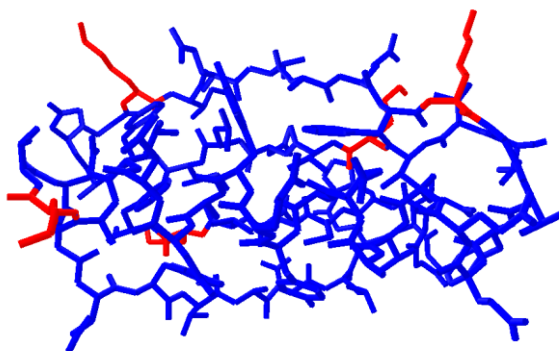


Figure B-3 Lys residues present in protein L from strain 3316. Image of protein L created using SwissProt PDB viewer (PDB:2PTL), the red residues indicate Lys residues. These residues display amines which can be used for the covalent immobilization to a surface.

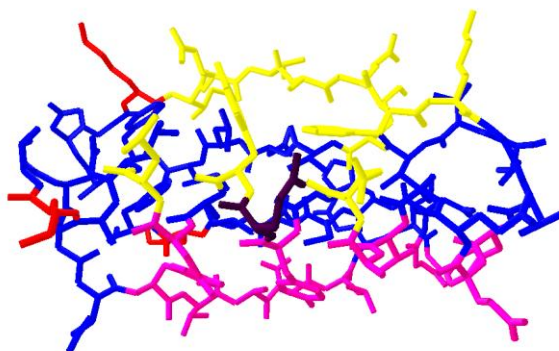


Figure B-4 Binding site residues and Lys residues present in protein L strain 3316. The image of protein L was created using SwissProt PDB viewer (PDB:1HEZ) The red residues indicate Lys residues not involved in the antibody V_L domain binding. Yellow residues are those that make up Site 1 of the V_L binding domain. Pink residues are those that make up Site 2 of the V_L binding domain. The purple amino acid is Arg-52, believed to be involved in both site 1 and 2 of the V_L binding domain.

The two tables (Tables B-3 and B-4 (see overleaf)) shown below and overleaf contain the dissociation rates of a series of protein L mutants produced by the Gore group [113, 114, 343, 344]. The dissociation rates, associated with the two binding site model, of each mutant is given. The mutants are displayed in amino acid residue order.

Mutant	K_d site 1	K_d site 2
I34W	I34W 0.075 μM I34WY53F 4.54 μM I34WA66W 0.048 μM I34WD55EY64WT65ED67TL68Q 0.059 μM	I34W Not Determined I34WY53F Not Determined I34WA66W No Detectable Binding I34WD55EY64WT65ED67TL68Q No Detectable Binding
R52A	R52AY64W 0.174 μM	R52AY64W 1.038 μM
Y53F	Y53FL57H No Detectable Binding Y64WY53F Not Determined Y64WY53FL57H No Detectable Binding I34WY53F 4.54 μM Y53FD55NL57HY64W No Detectable Binding	Y53FL57H 4.58 μM ±0.83 μM Y64WY53F 2.83 μM Y64WY53FL57H 3.4 μM I34WY53F Not Determined Y53FD55NL57HY64W 0.967 μM
D55N	D55NY64W 0.017 μM D55NY64WD67N 0.65 μM Y53FD55NL57HY64W No Detectable Binding	D55NY64W 1.79 μM D55NY64WD67N 1.038 μM Y53FD55NL57HY64W 0.967 μM
D55E	D55EY64WT65ED67TL68Q 0.075 μM I34WD55EY64WT65ED67TL68Q 0.059 μM	D55EY64WT65ED67TL68Q No Detectable Binding I34WD55EY64WT65ED67TL68Q No Detectable Binding
L57H	Y53FL57H No Detectable Binding Y64WY53FL57H No Detectable Binding Y53FD55NL57HY64W No Detectable Binding	Y53FL57H 4.58 μM ±0.83 μM Y64WY53FL57H 3.4 μM Y53FD55NL57HY64W 0.967 μM

Table B-3 Table showing the dissociation constants of IgG with different protein L mutants [113, 114, 343, 344].

Mutant	K _a site 1	K _a site 2
Y64W	Y64W 0.0375 μM Y64WY53F Not Determined Y64WY53FL57H No Detectable Binding D55NY64W 0.017 μM D55NY64WD67N 0.65 μM D67NY64W 0.029 μM R52AY64W 0.174 μM Y53FD55NL57HY64W No Detectable Binding D55EY64WT65ED67TL68Q 0.075 μM I34WD55EY64WT65ED67TL68Q 0.059 μM	Y64W 3.8 μM Y64WY53F 2.83 μM Y64WY53FL57H 3.4 μM D55NY64W 1.79 μM D55NY64WD67N 1.038 μM D67NY64W 7.66 μM R52AY64W 1.038 μM Y53FD55NL57HY64W 0.967 μM D55EY64WT65ED67TL68Q No Detectable Binding I34WD55EY64WT65ED67TL68Q No Detectable Binding
T65E	D55EY64WT65ED67TL68Q 0.075 μM I34WD55EY64WT65ED67TL68Q 0.059 μM	D55EY64WT65ED67TL68Q No Detectable Binding I34WD55EY64WT65ED67TL68Q No Detectable Binding
A66W	A66W 37.5nM ±7.3 nM I34WA66W 0.048 μM	A66W No Detectable Binding I34WA66W No Detectable Binding
D67N	D55NY64WD67N 0.65 μM D67NY64W 0.029 μM	D55NY64WD67N 1.038 μM D67NY64W 7.66 μM
D67T	D55EY64WT65ED67TL68Q 0.075 μM I34WD55EY64WT65ED67TL68Q 0.059 μM	D55EY64WT65ED67TL68Q No Detectable Binding I34WD55EY64WT65ED67TL68Q No Detectable Binding
L68Q	D55EY64WT65ED67TL68Q 0.075 μM I34WD55EY64WT65ED67TL68Q 0.059 μM	D55EY64WT65ED67TL68Q No Detectable Binding I34WD55EY64WT65ED67TL68Q No Detectable Binding

Table B-4 Table showing the dissociation constants of IgG with different protein L mutants [113, 114, 343, 344].

Appendix C

Photolithographic Mask Layouts

This section provides schematics of the original mask plate designs used for the fabrication of alignment and photolithographic mask features.

C.1 Photolithographic Mask 1

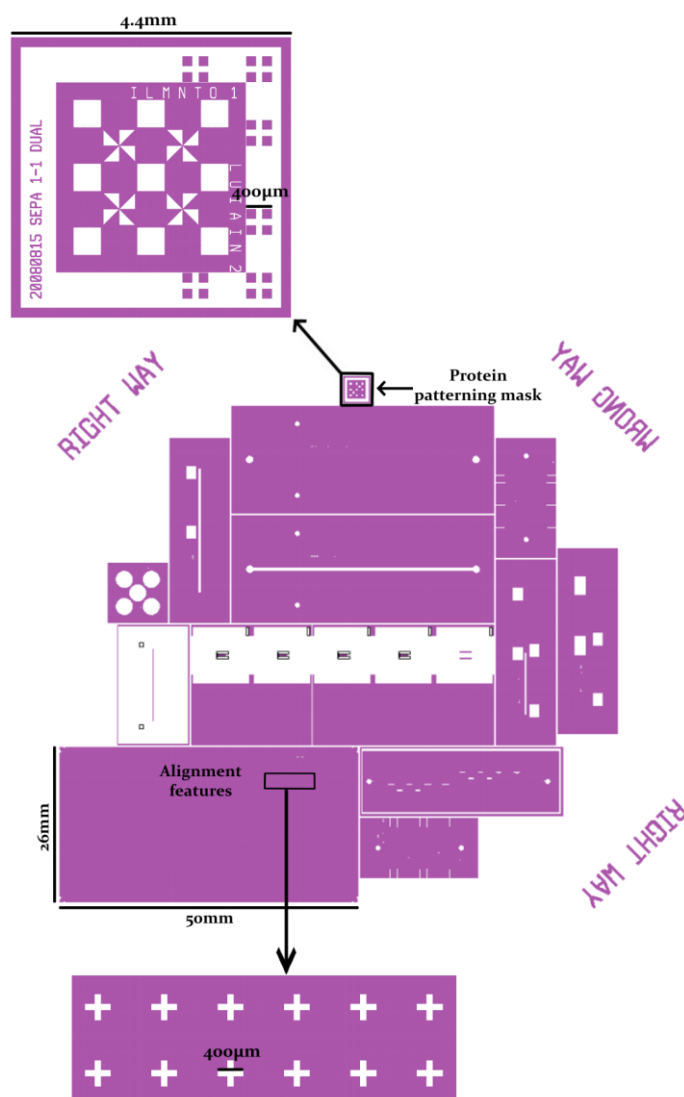


Figure C-1 Layout of mask 1, taken from L-edit, illustrating the features of interest (alignment features and protein patterning mask) designed for preparation of surfaces used in the investigation of surface patterning.

C.2 Photolithographic Mask 2

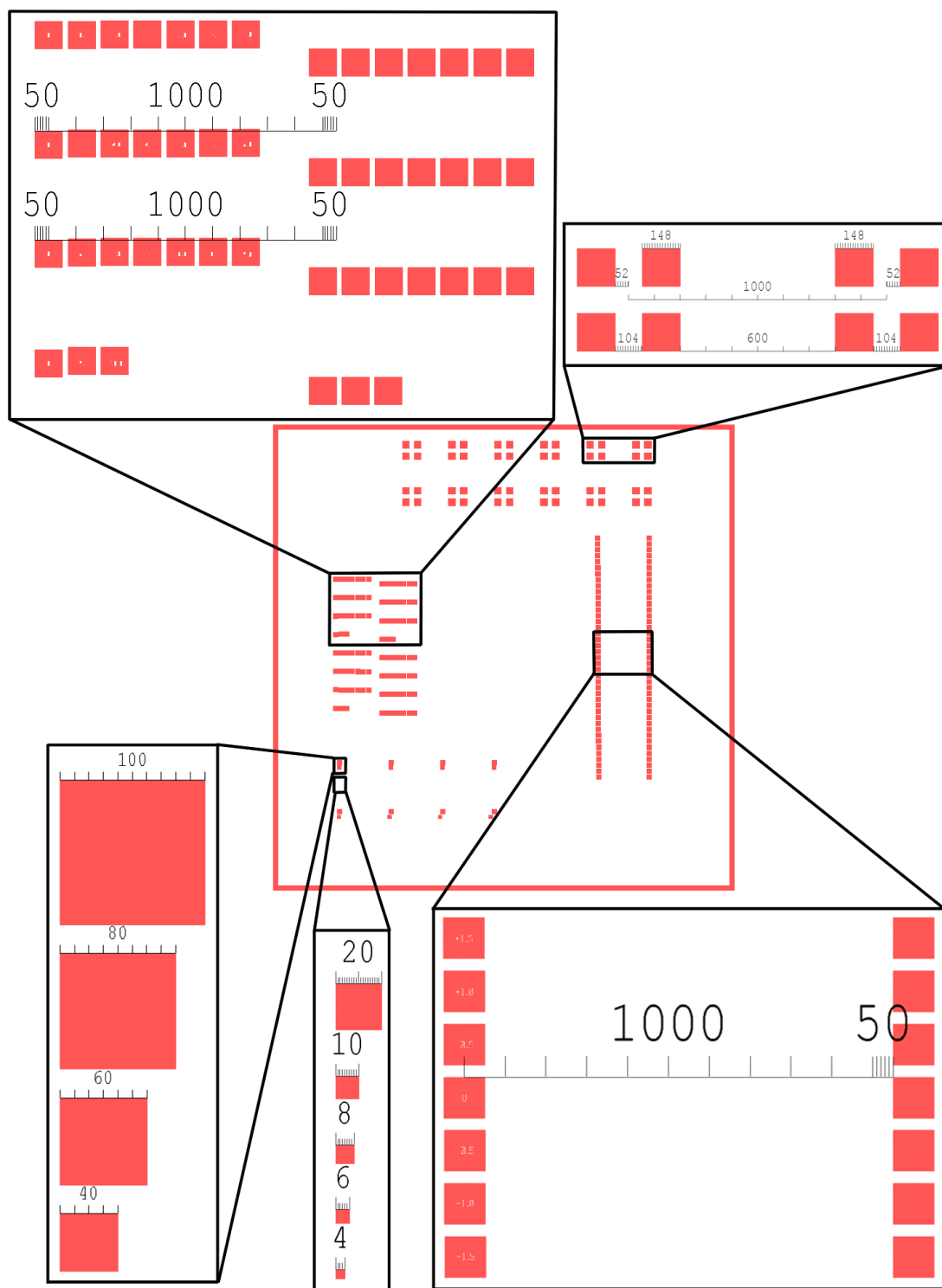


Figure C-2 Layout of mask 2, taken from L-edit, illustrating the features of interest designed for the preparation of surfaces used in the investigation of multiple protein patterning.

Appendix D

X-Ray Photoelectron Spectra

D.1 X-Ray Photoelectron Spectra of Modified Silicon Surfaces

D.1.1 Undecylenic Acid N-hydroxysuccinimide ester Modified Silicon

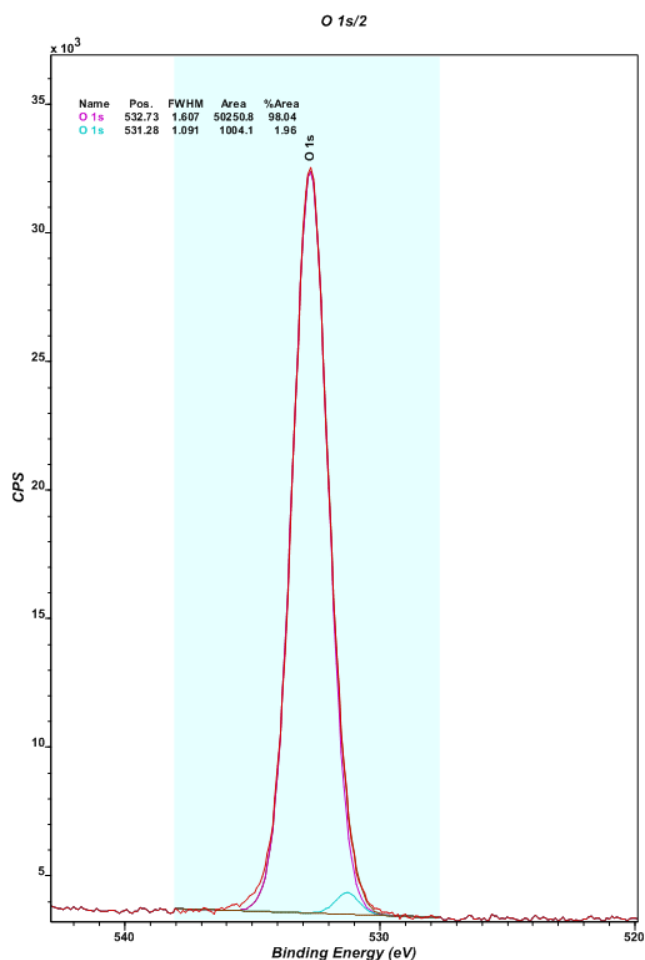


Figure D-1 Expanded X-ray photoelectron spectra peaks from likely oxygen moieties on UANHS modified silicon surfaces. Surfaces were prepared and analysed using the methods described in §3.1.5.

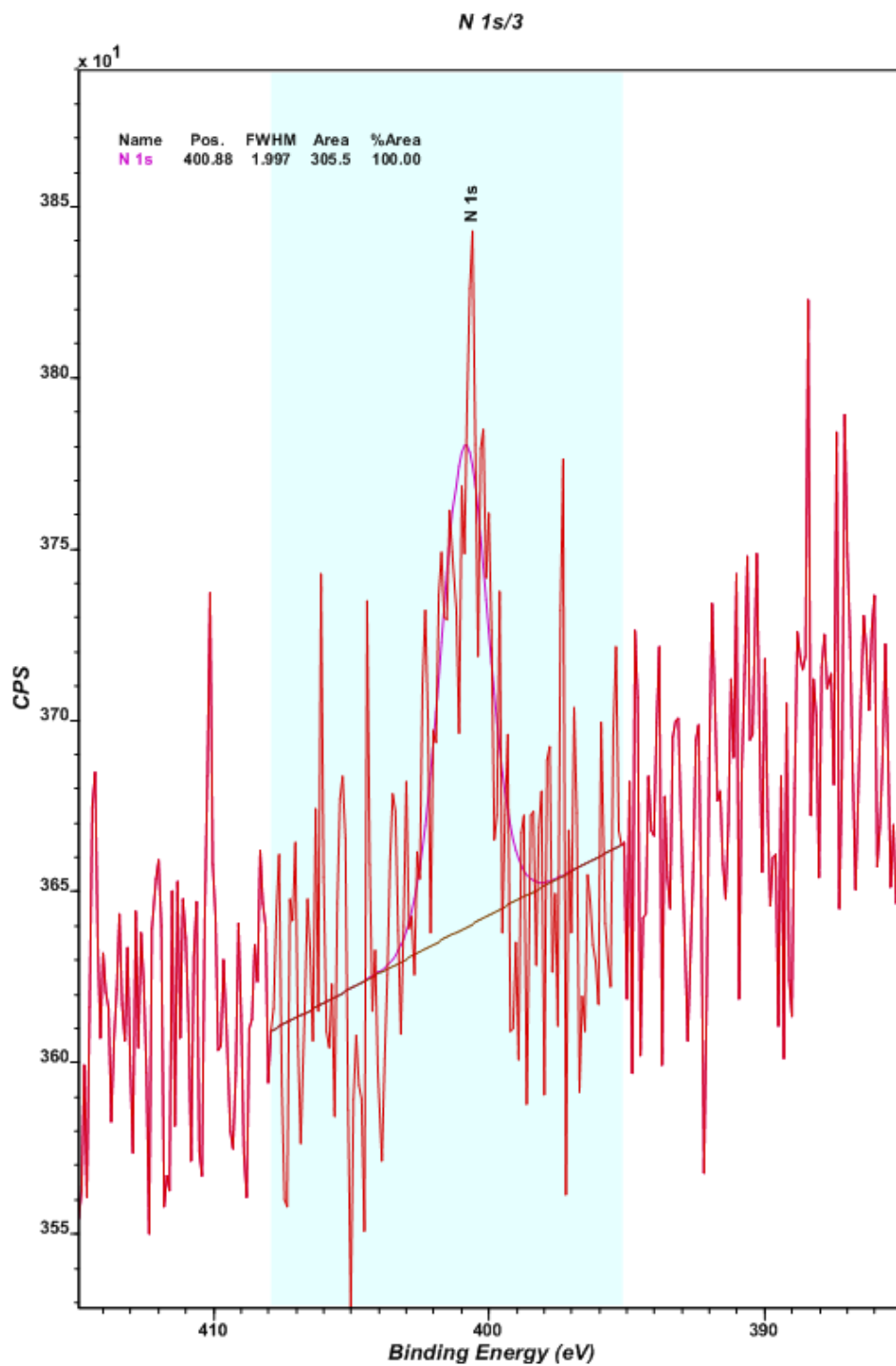


Figure D-2 Expanded X-ray photoelectron spectra peaks from likely nitrogen moieties on UANHS modified silicon surfaces. Surfaces were prepared and analysed using the methods described in §3.1.5.

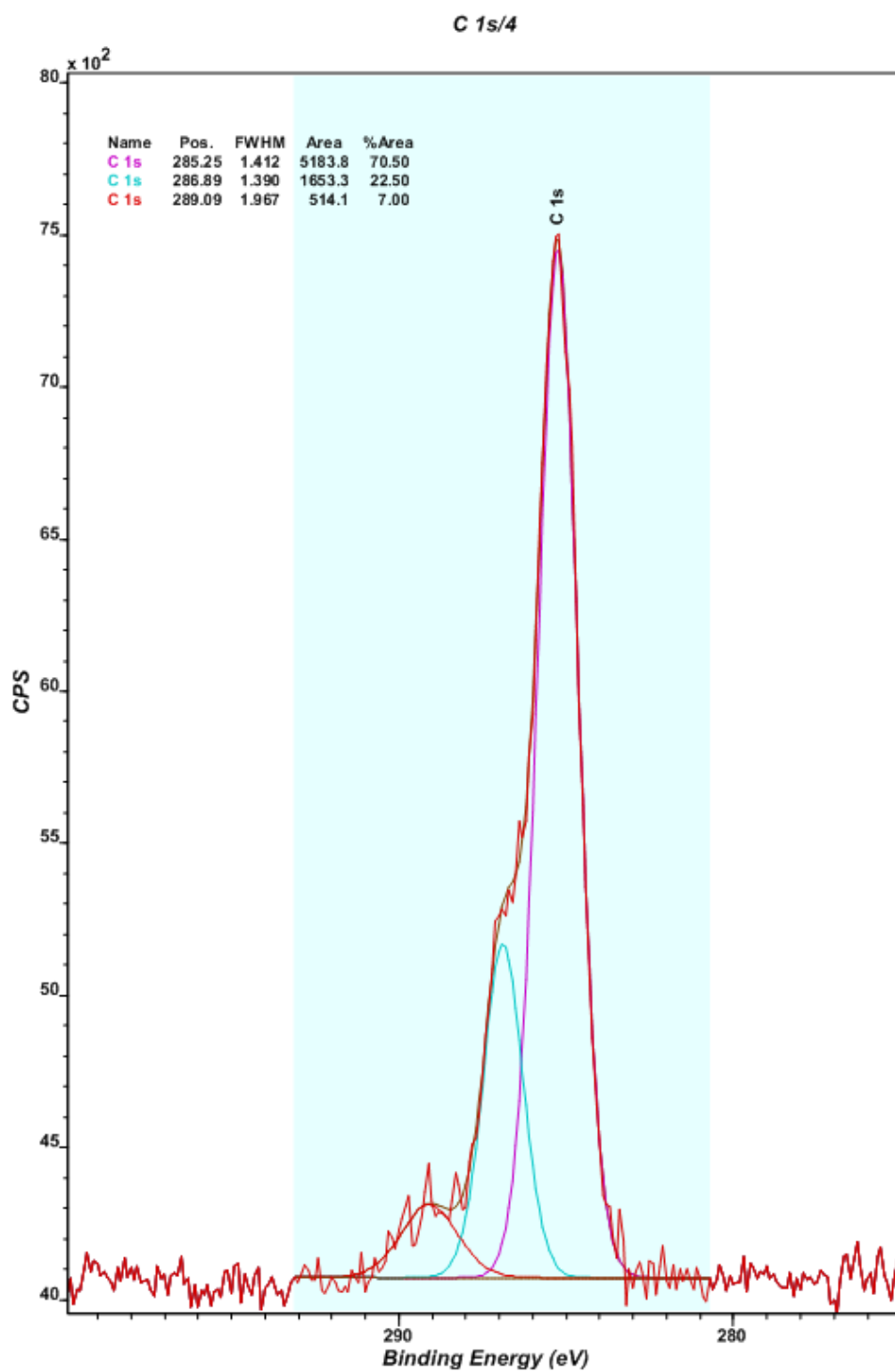


Figure D-3 Expanded X-ray photoelectron spectra peaks from likely carbon moieties on UANHS modified silicon surfaces. Surfaces were prepared and analysed using the methods described in §3.1.5.

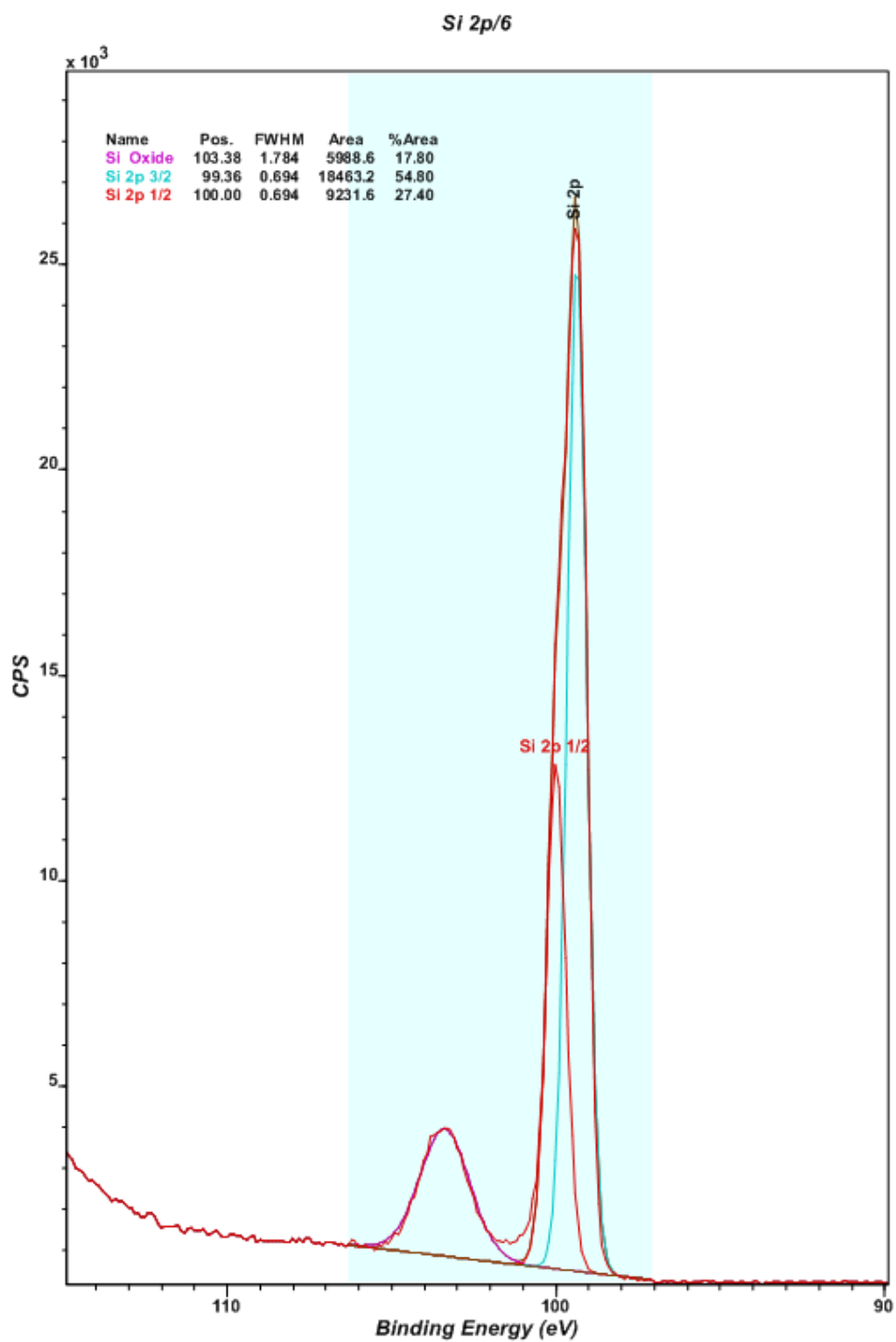


Figure D-4 Expanded X-ray photoelectron spectra peaks from likely silicon moieties on UANHS modified silicon surfaces. Surfaces were prepared and analysed using the methods described in §3.1.5.

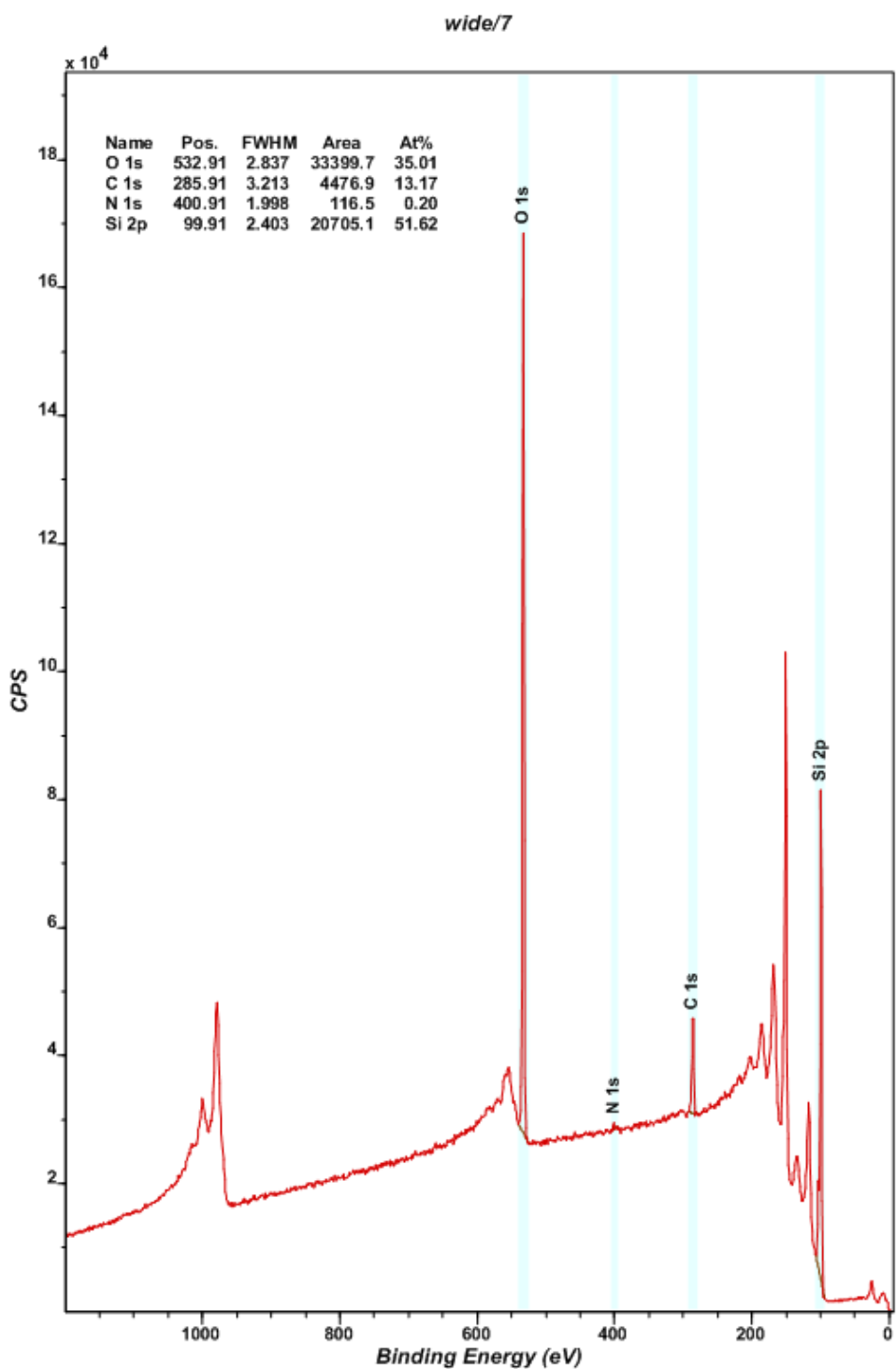


Figure D-5 Complete X-ray photoelectron spectra peaks from likely chemical moieties on UANHS modified silicon surfaces. Surfaces were prepared and analysed using the methods described in §3.1.5.

D.1.2 NeutrAvidin Modified Silicon

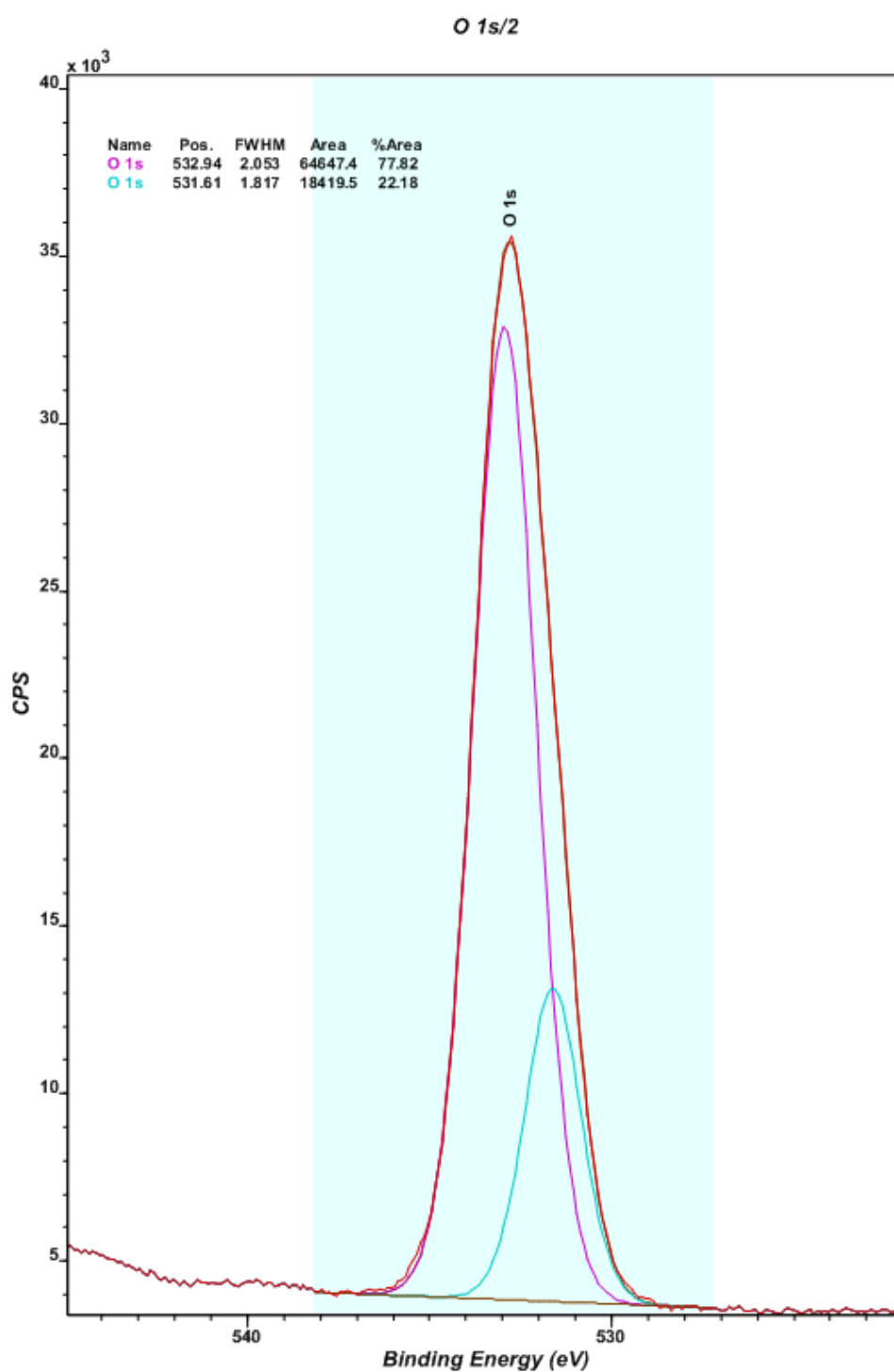


Figure D-6 Expanded X-ray photoelectron spectra peaks from likely oxygen moieties on NeutrAvidin conjugated silicon surfaces. Surfaces were prepared and analysed using the methods described in §3.1.5.

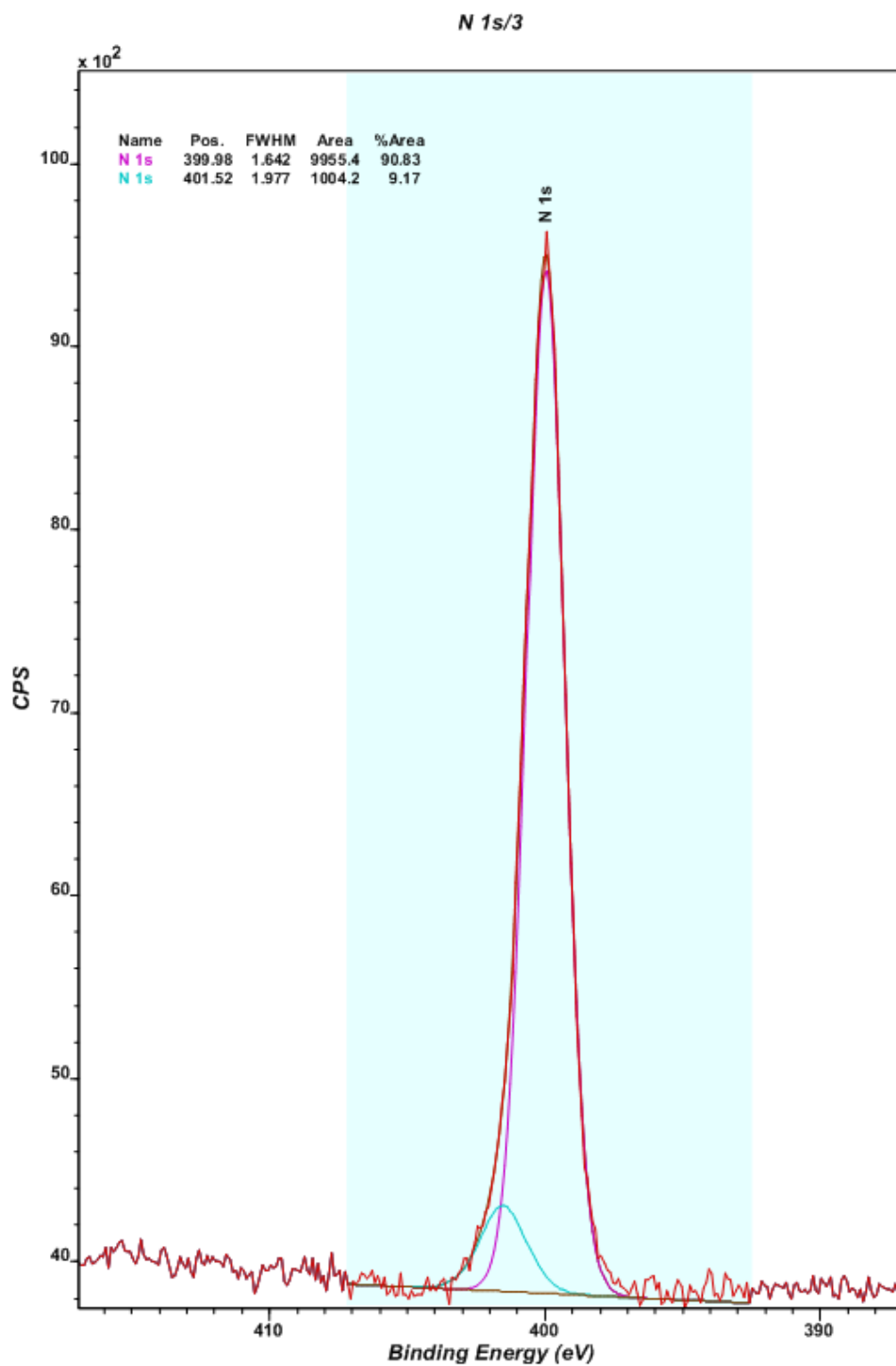


Figure D-7 Expanded X-ray photoelectron spectra peaks from likely nitrogen moieties on NeutrAvidin conjugated silicon surfaces. Surfaces were prepared and analysed using the methods described in §3.1.5.

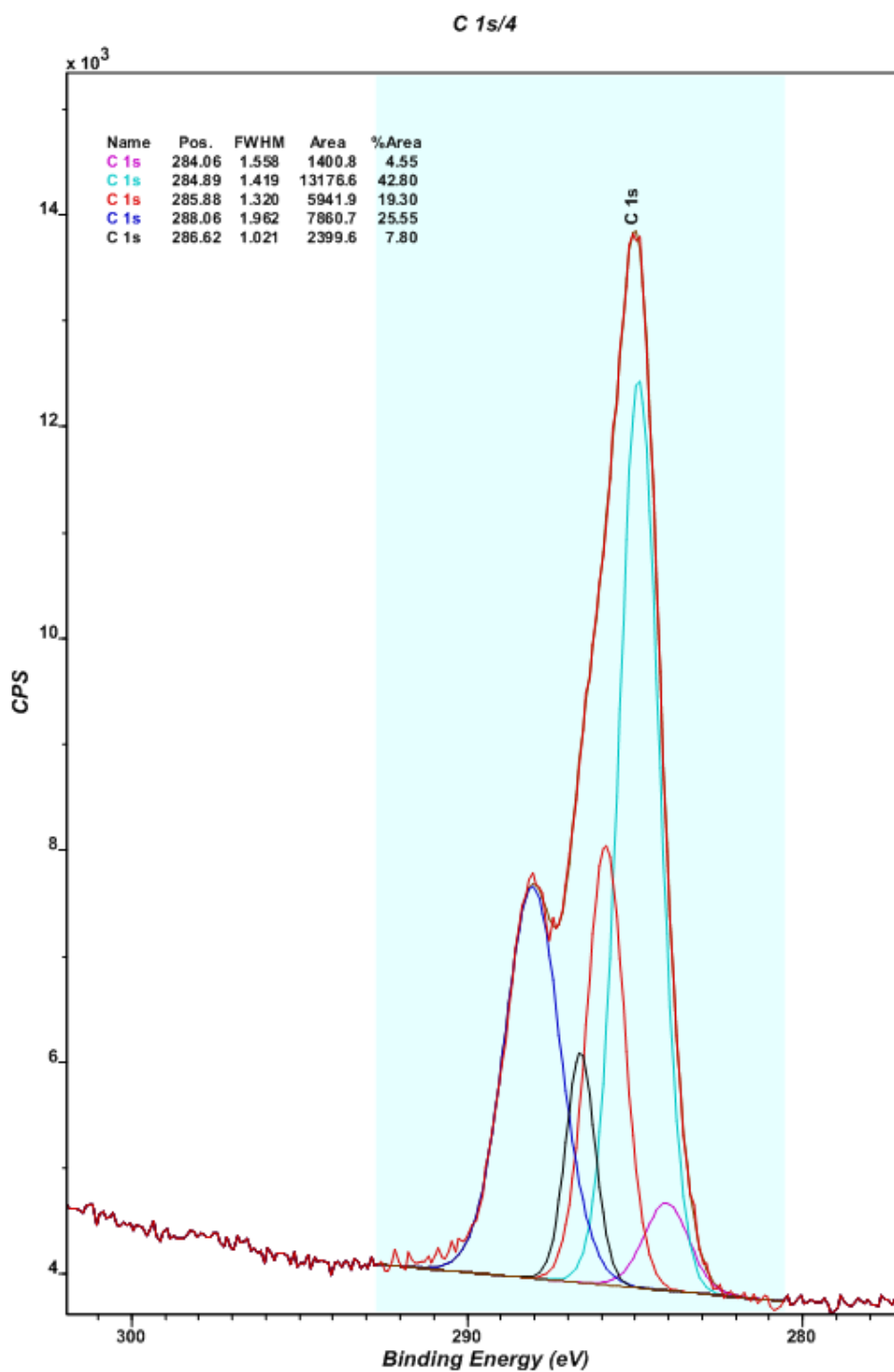


Figure D-8 Expanded X-ray photoelectron spectra peaks from likely carbon moieties on NeutrAvidin conjugated silicon surfaces. Surfaces were prepared and analysed using the methods described in §3.1.5.

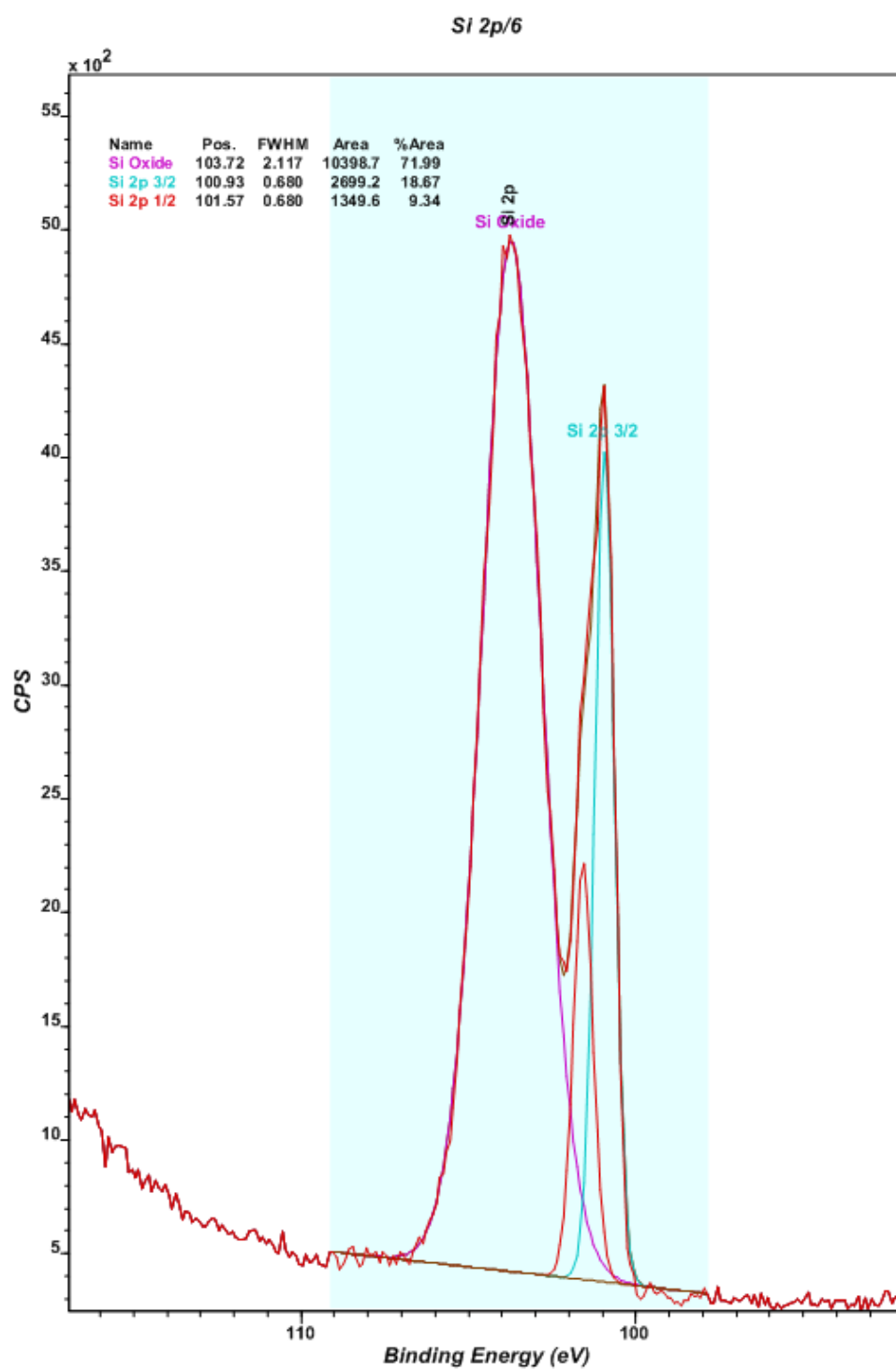


Figure D-9 Expanded X-ray photoelectron spectra peaks from likely silicon moieties on NeutrAvidin conjugated silicon surfaces. Surfaces were prepared and analysed using the methods described in §3.1.5.

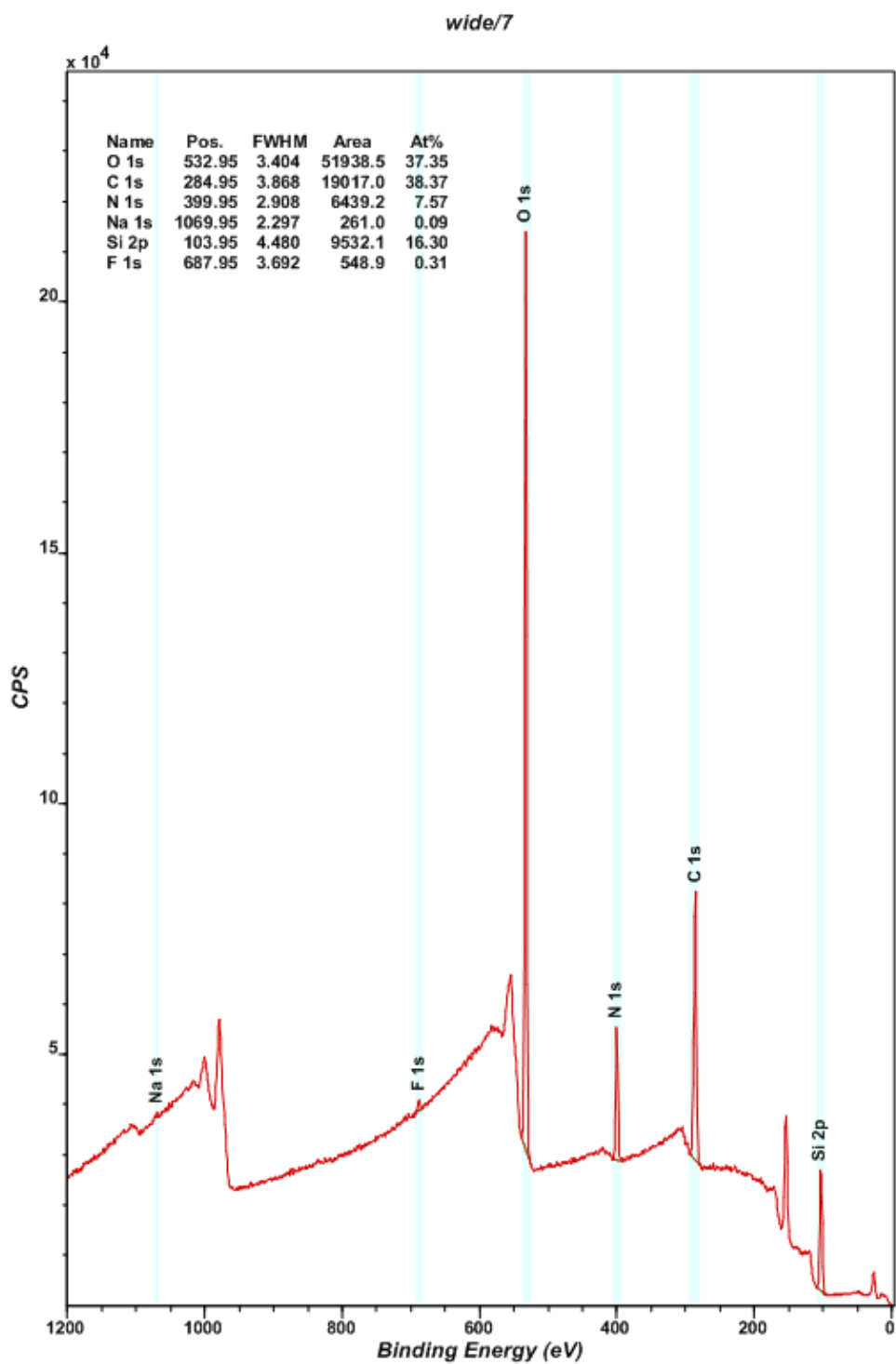


Figure D-10 Complete X-ray photoelectron spectra peaks from likely chemical moieties on NeutrAvidin conjugated silicon surfaces. Surfaces were prepared and analysed using the methods described in §3.1.5.

D.2 X-Ray Photoelectron Spectra of Modified Glass Surfaces

D.2.1 3-Glycidoxypropyltrimethoxysilane Modified Glass

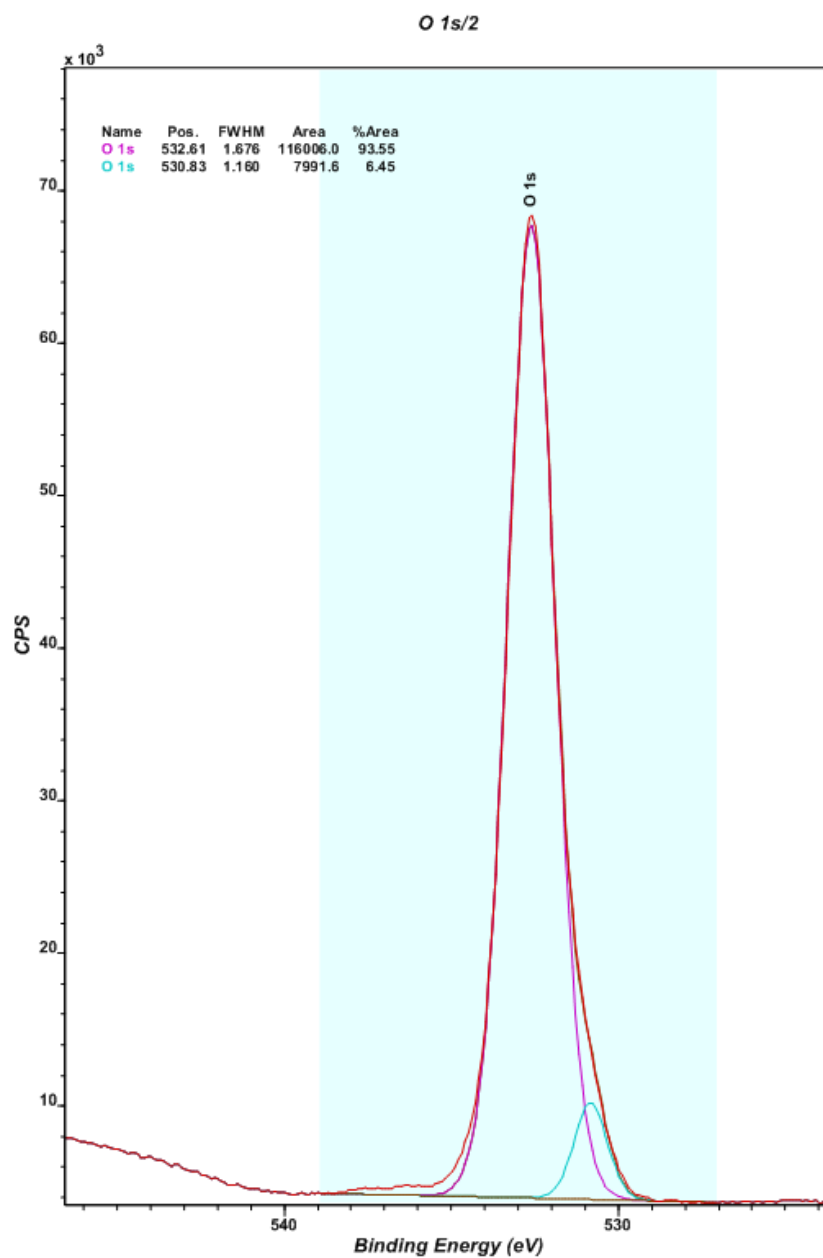


Figure D-11 Expanded X-ray photoelectron spectra peaks from likely oxygen moieties on GOPS modified glass surfaces. Surfaces were prepared and analysed using the methods described in §3.2.10.

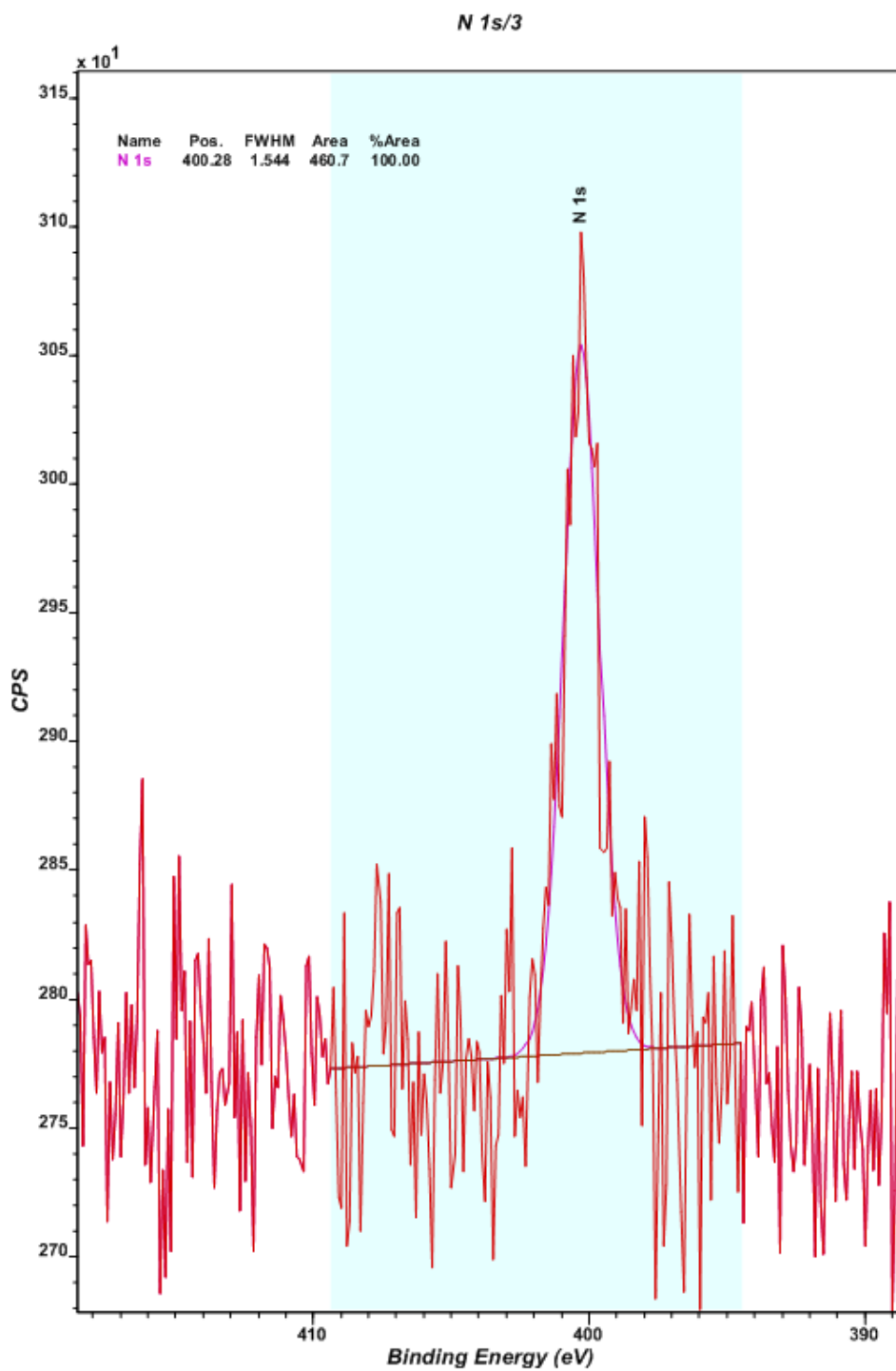


Figure D-12 Expanded X-ray photoelectron spectra peaks from likely nitrogen moieties on GOPS modified glass surfaces. Surfaces were prepared and analysed using the methods described in §3.2.10.

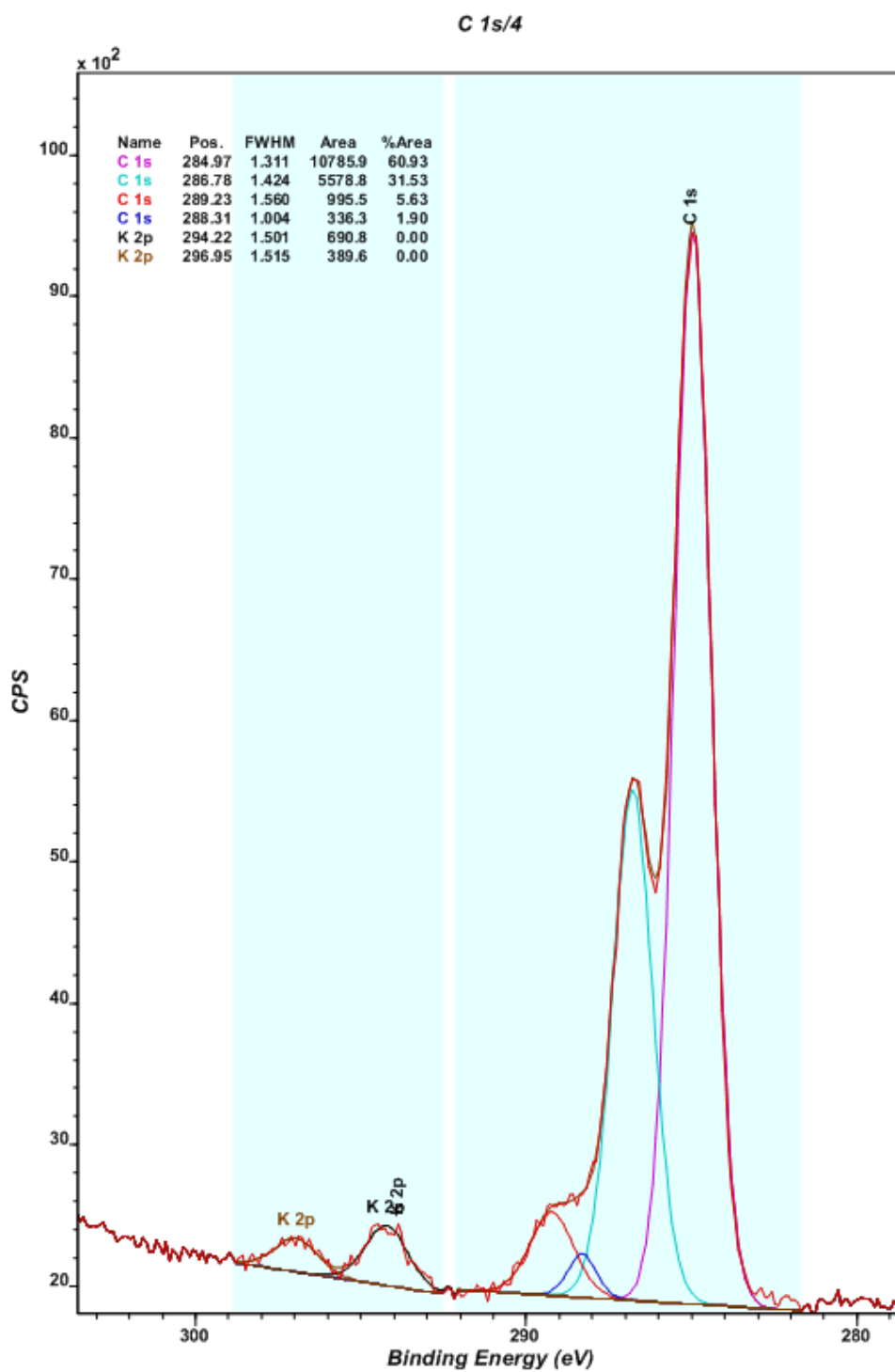


Figure D-13 Expanded X-ray photoelectron spectra peaks from likely carbon moieties on GOPS modified glass surfaces. Surfaces were prepared and analysed using the methods described in §3.2.10.

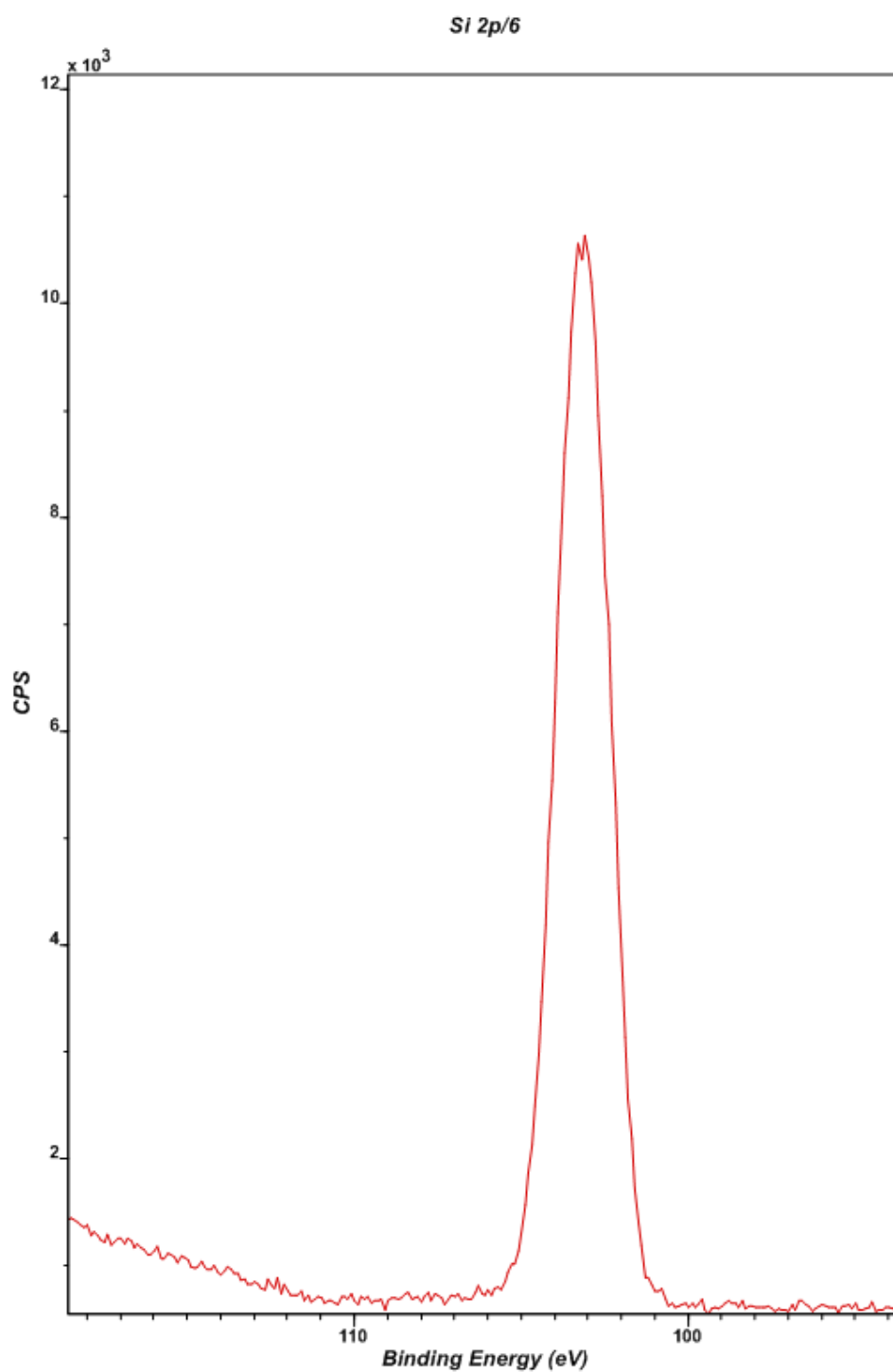


Figure D-14 Expanded X-ray photoelectron spectra peaks from likely silicon moieties on GOPS modified glass surfaces. Surfaces were prepared and analysed using the methods described in §3.2.10.

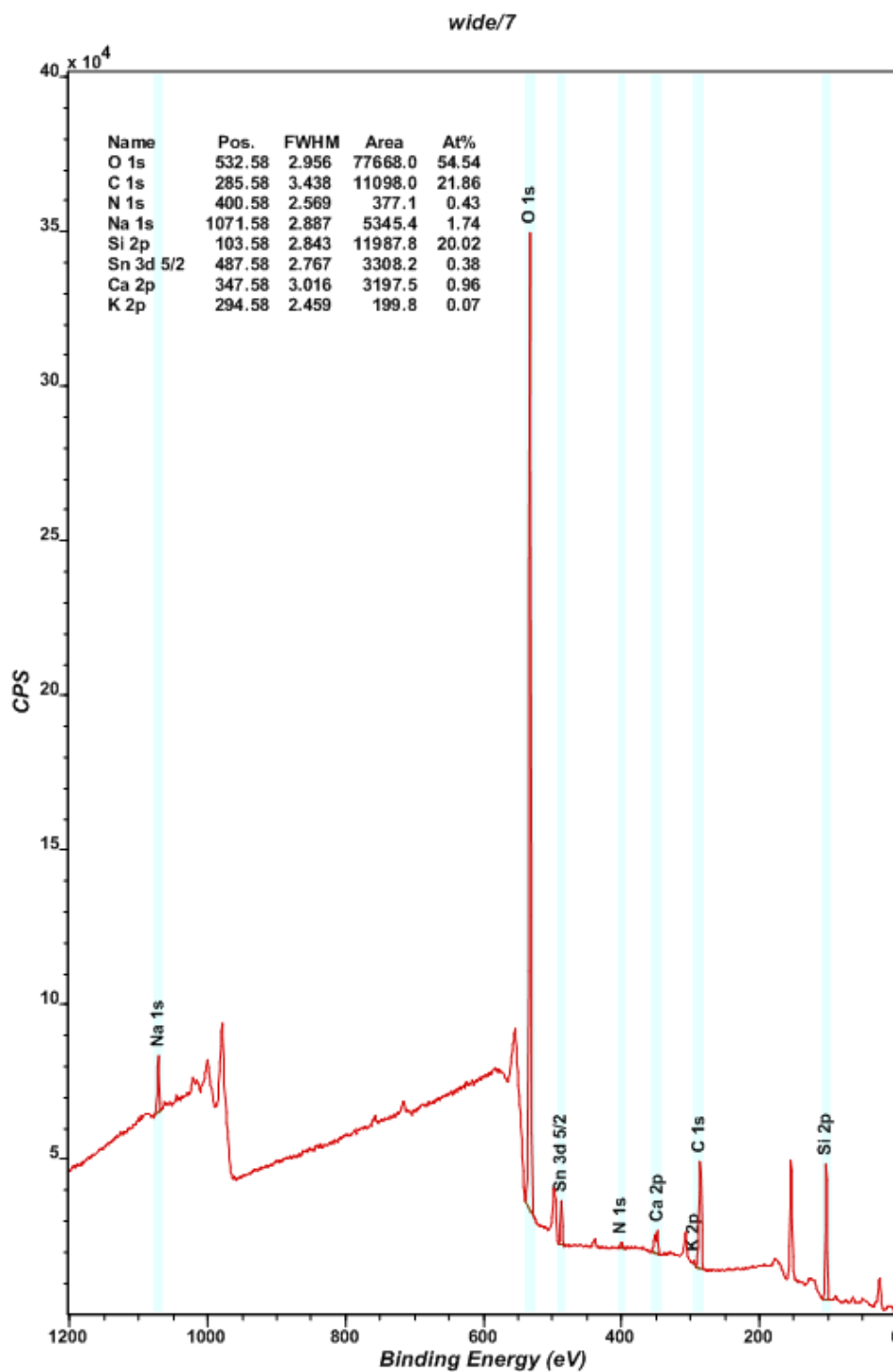


Figure D-15 Complete X-ray photoelectron spectra peaks from likely chemical moieties on GOPS modified glass surfaces. Surfaces were prepared and analysed using the methods described in §3.2.10.

D.2.2 Aryl Azide Conjugated Dextran Modified Glass

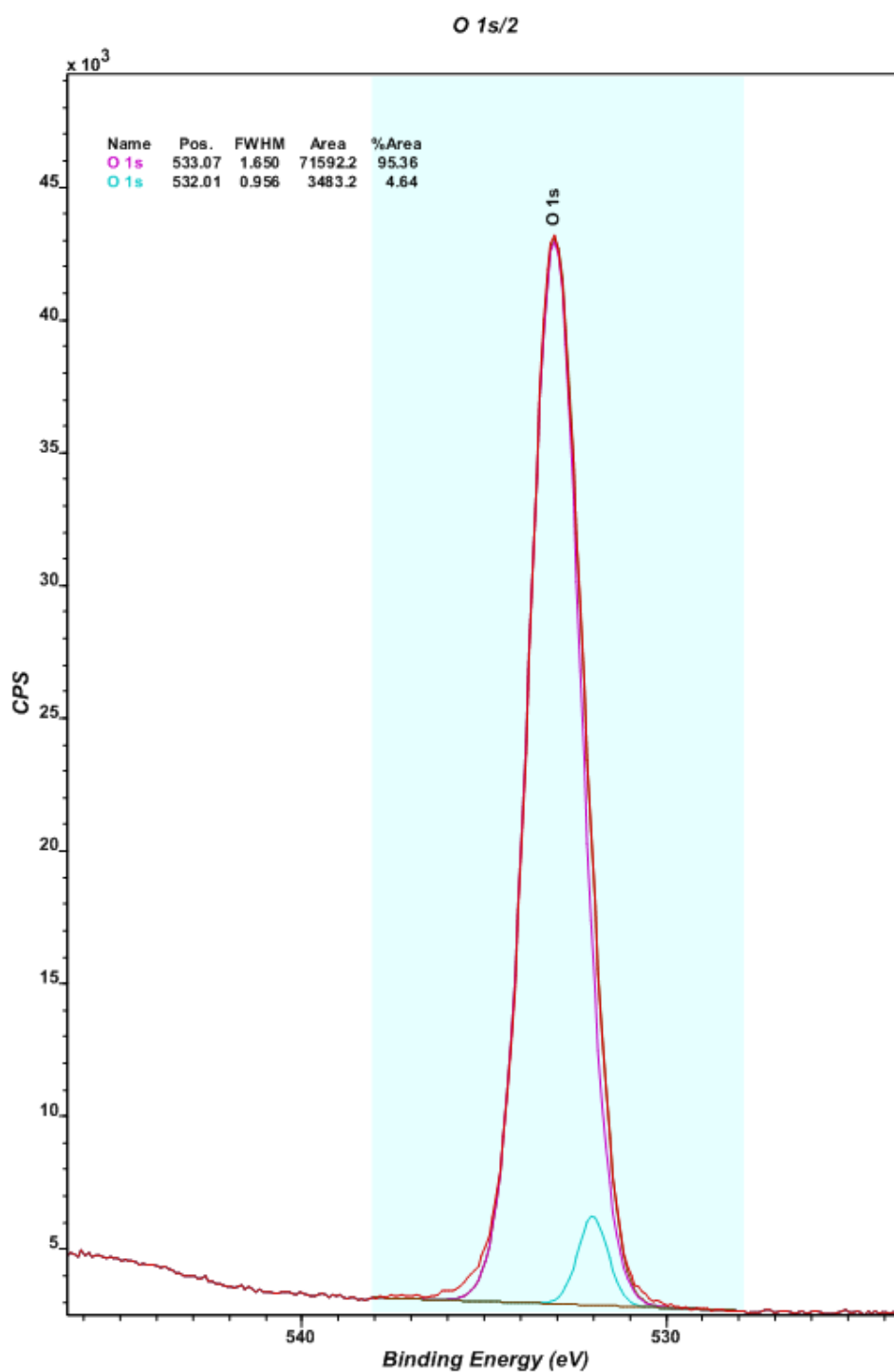


Figure D-16 Expanded X-ray photoelectron spectra peaks from likely oxygen moieties on aryl azide conjugated dextran modified glass surfaces. Surfaces were prepared and analysed using the methods described in §3.2.10.

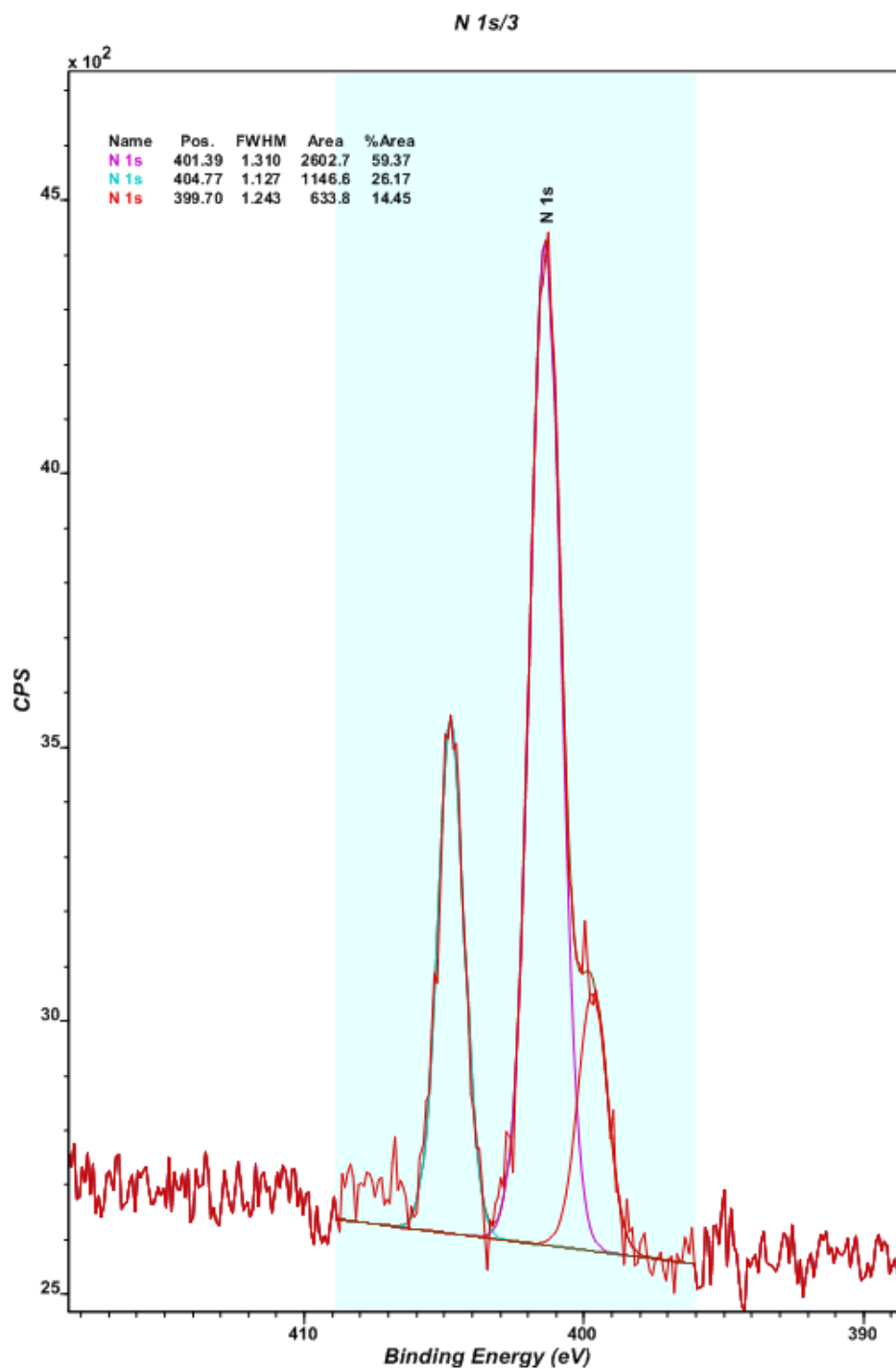


Figure D-17 Expanded X-ray photoelectron spectra peaks from likely nitrogen moieties on aryl azide conjugated dextran modified glass surfaces. Surfaces were prepared and analysed using the methods described in §3.2.10.

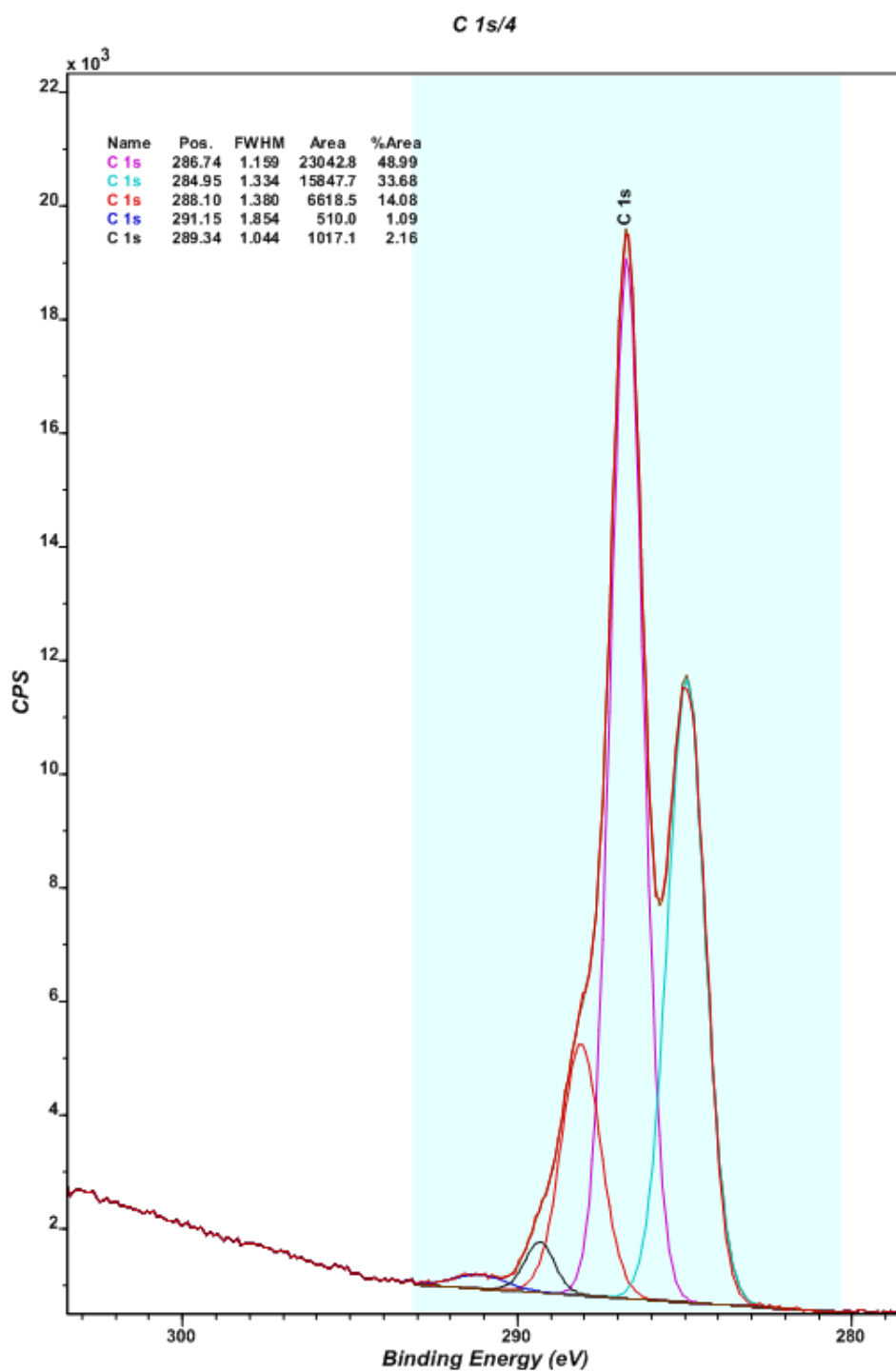


Figure D-18 Expanded X-ray photoelectron spectra peaks from likely carbon moieties on aryl azide conjugated dextran modified glass surfaces. Surfaces were prepared and analysed using the methods described in §3.2.10.

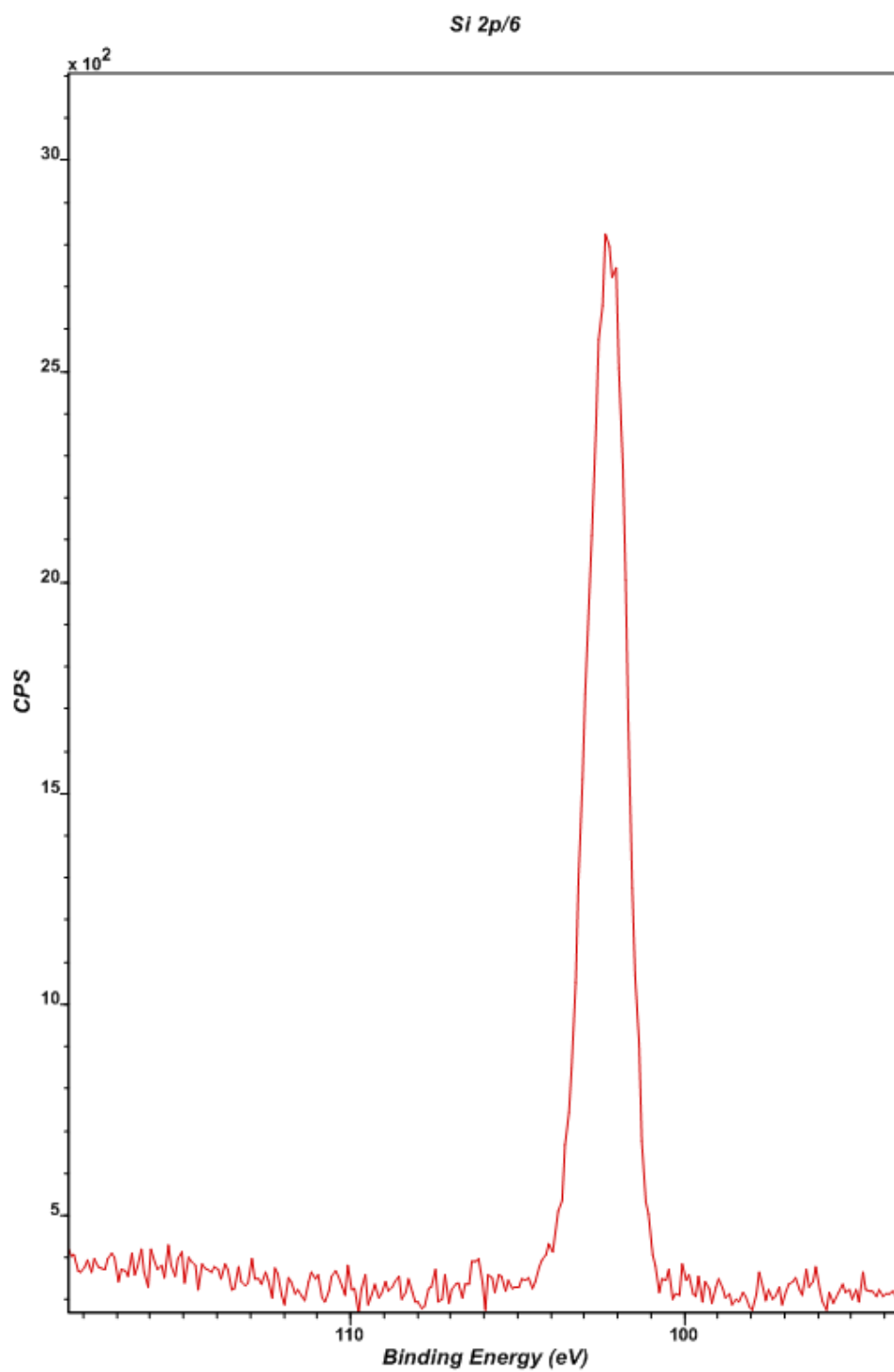


Figure D-19 Expanded X-ray photoelectron spectra peaks from likely silicon moieties on aryl azide conjugated dextran modified glass surfaces. Surfaces were prepared and analysed using the methods described in §3.2.10.

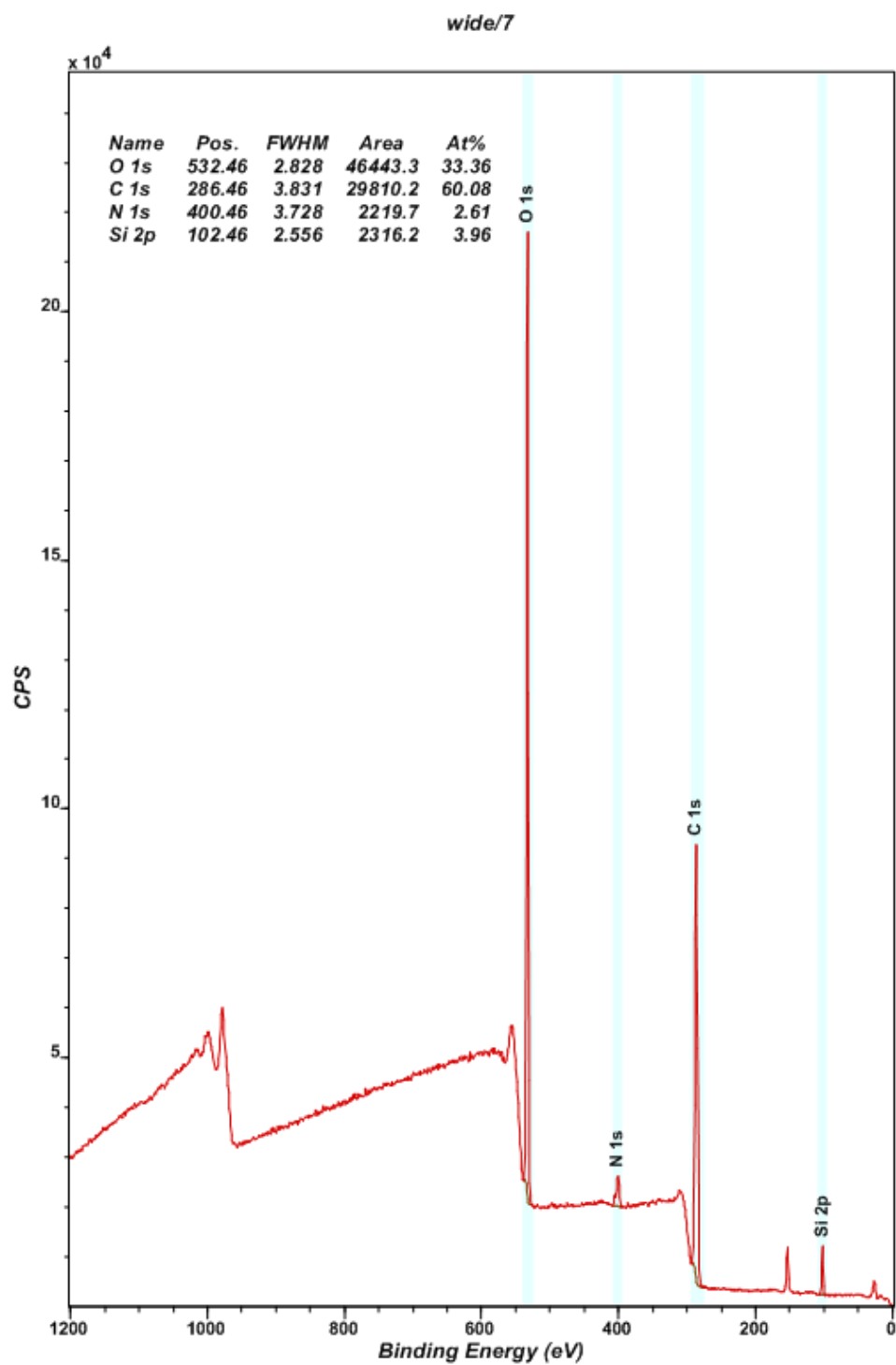


Figure D-20 Complete X-ray photoelectron spectra peaks from likely chemical moieties on aryl azide conjugated dextran modified glass surfaces. Surfaces were prepared and analysed using the methods described in §3.2.10.

D.2.3 NeutrAvidin Modified Glass

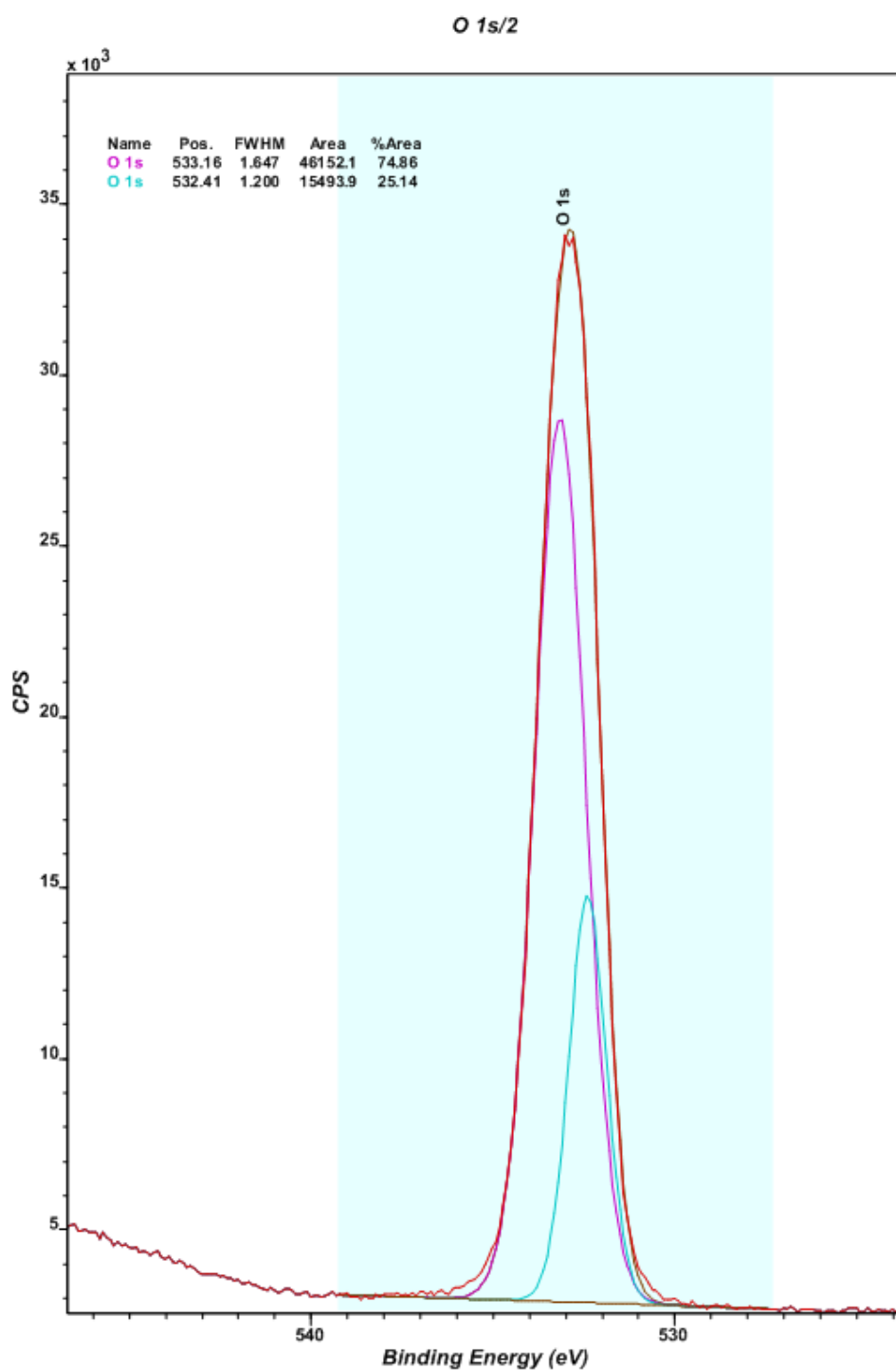


Figure D-21 Expanded X-ray photoelectron spectra peaks from likely oxygen moieties on NeutrAvidin conjugated glass surfaces. Surfaces were prepared and analysed using the methods described in §3.2.10.

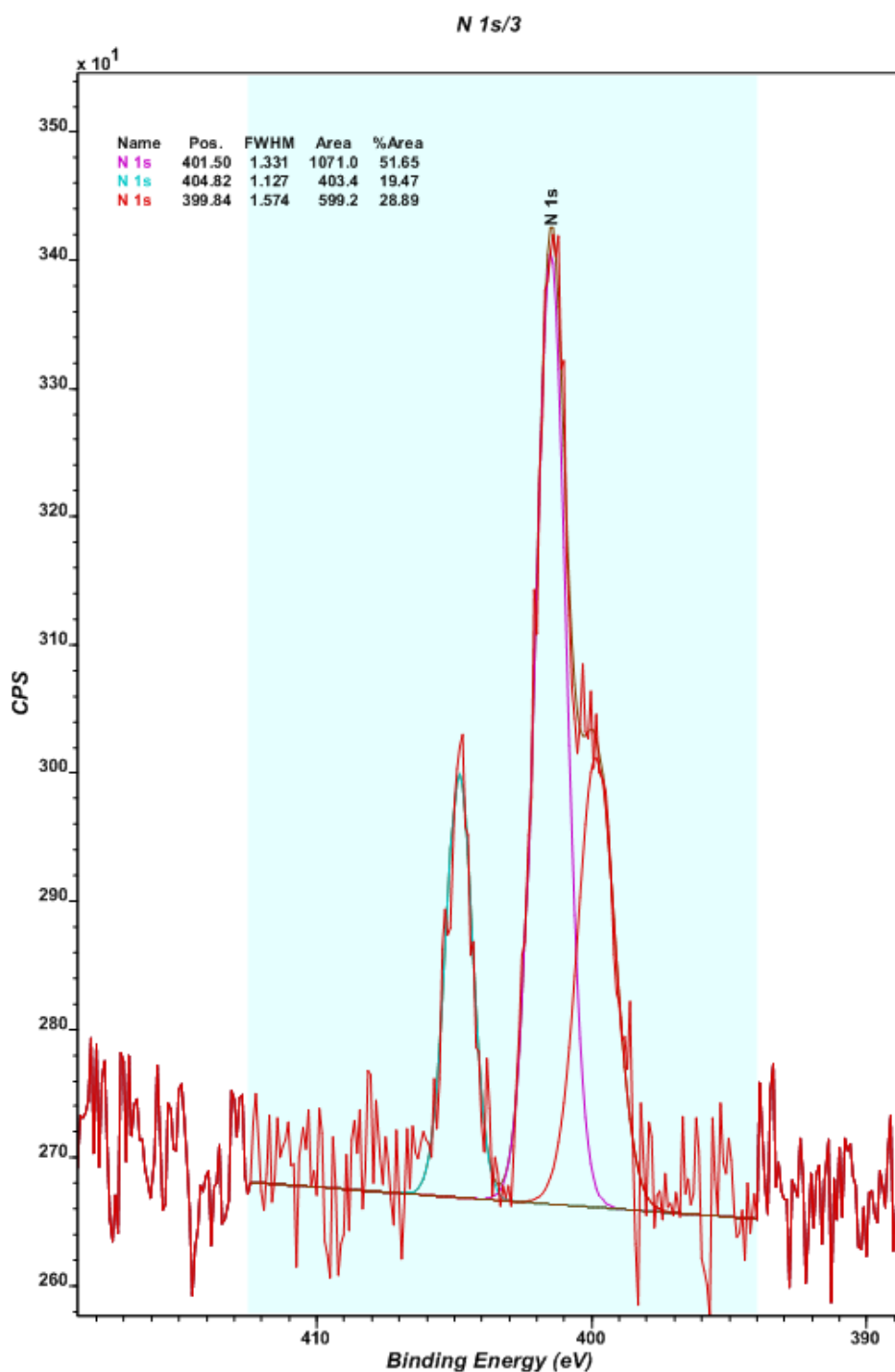


Figure D-22 Expanded X-ray photoelectron spectra peaks from likely nitrogen moieties on NeutrAvidin conjugated glass surfaces. Surfaces were prepared and analysed using the methods described in §3.2.10.

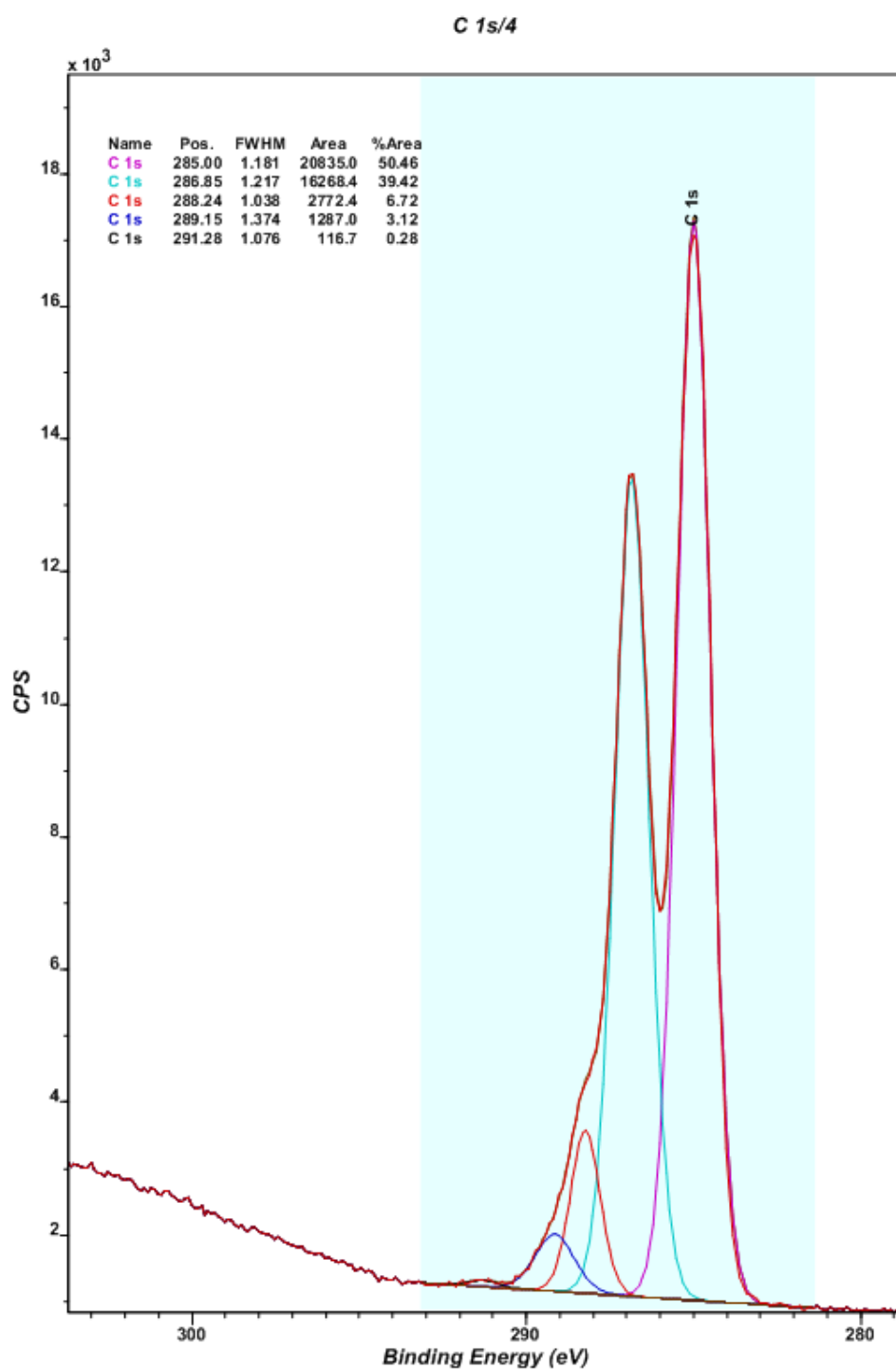


Figure D-23 Expanded X-ray photoelectron spectra peaks from likely carbon moieties on NeutrAvidin conjugated glass surfaces. Surfaces were prepared and analysed using the methods described in §3.2.10.

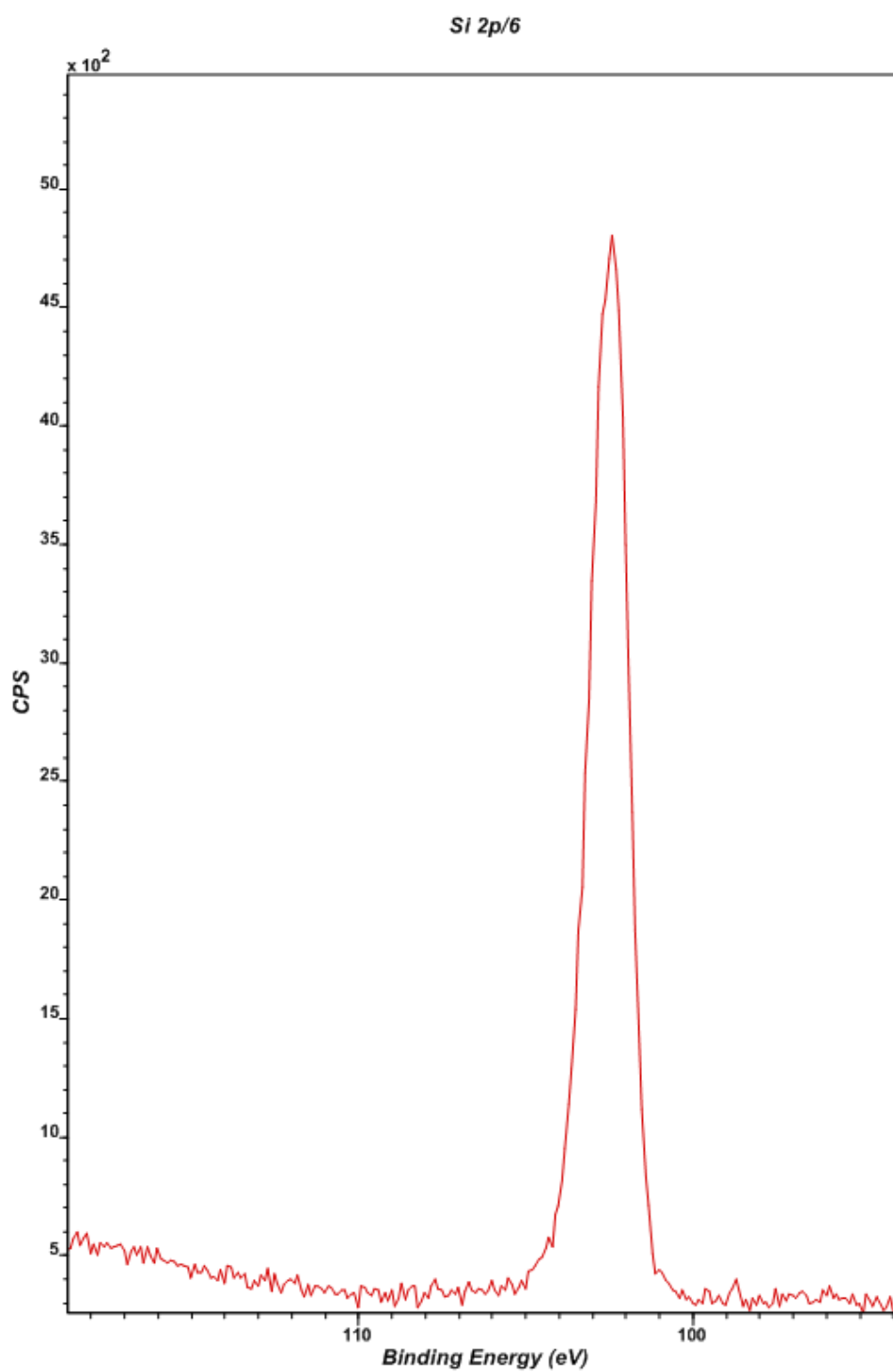


Figure D-24 Expanded X-ray photoelectron spectra peaks from likely silicon moieties on NeutrAvidin conjugated glass surfaces. Surfaces were prepared and analysed using the methods described in §3.2.10.

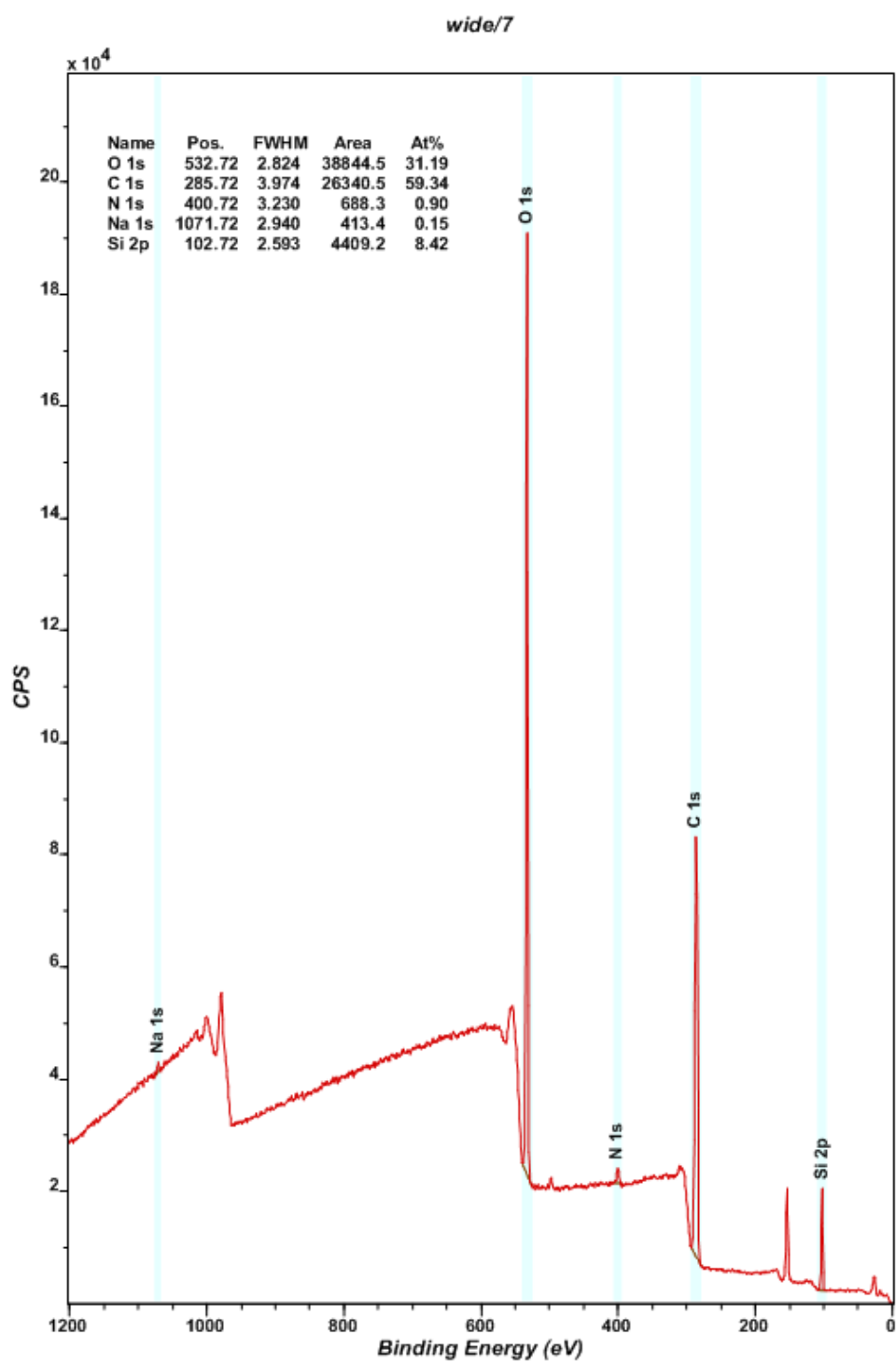


Figure D-25 Complete X-ray photoelectron spectra peaks from likely oxygen moieties on NeutrAvidin conjugated glass surfaces. Surfaces were prepared and analysed using the methods described in §3.2.10.

References

- [1] Di Nola J M and Neuberger M S 2007 Molecular mechanisms of antibody somatic hypermutation *Annual Review of Biochemistry* **76** 1-22
- [2] Quismori.Fp, Bland S L and Friou G J 1971 Autoimmunity in Thermal Injury - Occurrence of Rheumatoid Factors, Antinuclear Antibodies and Antiepithelial Antibodies *Clinical and Experimental Immunology* **8** 701-11
- [3] Arbuckle M R, McClain M T, Rubertone M V, Scofield R H, Dennis G J, James J A and Harley J B 2003 Development of autoantibodies before the clinical onset of systemic lupus erythematosus *New England Journal of Medicine* **349** 1526-33
- [4] Chapman C J, Murray A, McElveen J E, Sahin U, Luxemburger U, Tuereci O, Wiewrodt R, Barnes A C and Robertson J F 2008 Autoantibodies in lung cancer: possibilities for early detection and subsequent cure *Thorax* **63** 228-33
- [5] Fried A J and Bonilla F A 2009 Pathogenesis, Diagnosis, and Management of Primary Antibody Deficiencies and Infections *Clinical Microbiology Reviews* **22** 396-414
- [6] Rosen F S, Cooper M D and Wedgwood R J P 1995 Medical Progress - the Primary Immunodeficiencies *New England Journal of Medicine* **333** 431-40
- [7] Sparkes B G 1997 Immunological responses to thermal injury *Burns* **23** 106-13
- [8] Boddie D E, Currie D G, Eremin O and Heys S D 2003 Immune suppression and isolated severe head injury: a significant clinical problem *British Journal of Neurosurgery* **17** 405-17
- [9] Angele M K and Chaudry I H 2005 Surgical trauma and immunosuppression: pathophysiology and potential immunomodulatory approaches *Langenbecks Archives of Surgery* **390** 333-41
- [10] Lever A and Mackenzie I 2007 Sepsis: definition, epiderhiology, and diagnosis *British Medical Journal* **335** 879-83
- [11] Hotchkiss R S, Coopersmith C M and Karl I E 2005 Prevention of lymphocyte apoptosis - A potential treatment of sepsis? *Clinical Infectious Diseases* **41** S465-9
- [12] Hotchkiss R S, Coopersmith C M, McDunn J E and Ferguson T A 2009 Tilting toward immunosuppression *Nature Medicine* **15** 496-7
- [13] Monneret G, Lepape A, Voirin N, Bohe J, Venet F, Debard A L, Thizy H, Bienvenu J, Gueyffier F and Vanhems P 2006 Persisting low monocyte human leukocyte antigen-DR expression predicts mortality in septic shock *Intensive Care Medicine* **32** 1175-83
- [14] Rivers E P, McIntyre L, Morro D C and Rivers K K 2005 Early and innovative interventions for severe sepsis and septic shock: taking advantage of a window of opportunity *Canadian Medical Association Journal* **173** 1054-65
- [15] Raghavan M and Marik P E 2006 Management of sepsis during the early "golden hours" *Journal of Emergency Medicine* **31** 185-99

- [16] Rivers E, Nguyen B, Havstad S, Ressler J, Muzzin A, Knoblich B, Peterson E and Tomlanovich M 2001 Early goal-directed therapy in the treatment of severe sepsis and septic shock *The New England journal of medicine* **345** 1368-77
- [17] Berlot G and Dimastromatteo G 2004 Use of IgM and IgA-enriched immunoglobulins in the treatment of severe sepsis and septic shock. Clinical experience *Minerva anesthesiologica* **70** 739-43; 43-5
- [18] Marshall J C 2008 Sepsis: rethinking the approach to clinical research *Journal of Leukocyte Biology* **83** 471-82
- [19] Dahlback B and Villoutreix B O 2005 Regulation of blood coagulation by the protein C anticoagulant pathway: novel insights into structure-function relationships and molecular recognition *Arteriosclerosis, thrombosis, and vascular biology* **25** 1311-20
- [20] Parrillo J E 2005 Severe sepsis and therapy with activated protein C *New England Journal of Medicine* **353** 1398-400
- [21] Monneret G, Venet F, Pachot A and Lepape A 2008 Monitoring immune dysfunctions in the septic patient: A new skin for the old ceremony *Molecular Medicine* **14** 64-78
- [22] Hotchkiss R S and Karl I E 2003 Medical progress: The pathophysiology and treatment of sepsis. *New England Journal of Medicine* **348** 138-50
- [23] Hotchkiss R S, Osmon S B, Chang K C, Wagner T H, Coopersmith C M and Karl I E 2005 Accelerated lymphocyte death in sepsis occurs by both the death receptor and mitochondrial pathways *Journal of Immunology* **174** 5110-8
- [24] Parrino J, Hotchkiss R S and Bray M 2007 Prevention of immune cell apoptosis as potential therapeutic strategy for severe infections *Emerging Infectious Diseases* **13** 191-8
- [25] Heideman M and Bengtsson A 1992 The immunologic response to thermal injury *World journal of surgery* **16** 53-6
- [26] Munster A M, Hoagland H C and Pruitt B A 1970 Effect of Thermal Injury on Serum Immunoglobulins *Annals of Surgery* **172** 965-9
- [27] DiPiro J T, Howdieshell T R, Hamilton R G, Adkinson F and Mansberger A R 1996 Increased plasma IgE levels in patients with sepsis after traumatic injury *Journal of Allergy and Clinical Immunology* **97** 135-6
- [28] Pollack M, Huang A I, Prescott R K, Young L S, Hunter K W, Cruess D F and Tsai C M 1983 Enhanced Survival in Pseudomonas-Aeruginosa Septicemia Associated with High-Levels of Circulating Antibody to Escherichia-Coli Endotoxin Core *Journal of Clinical Investigation* **72** 1874-81
- [29] Laupland K B, Kirkpatrick A W and Delaney A 2007 Polyclonal intravenous immunoglobulin for the treatment of severe sepsis and septic shock in critically ill adults: A systematic review and meta-analysis *Critical Care Medicine* **35** 2686-92
- [30] Norrby-Teglund A, Haque K N and Hammarstrom L 2006 Intravenous polyclonal IgM-enriched immunoglobulin therapy in sepsis: a review of clinical efficacy in relation to microbiological aetiology and severity of sepsis *Journal of Internal Medicine* **260** 509-16
- [31] Barrette R W, Urbonas J and Silbart L K 2006 Quantifying specific antibody concentrations by enzyme-linked immunosorbent assay using slope correction *Clinical and Vaccine Immunology* **13** 802-5

- [32] Vidal J 2002 Improvements to the enzyme-developed radial immunodiffusion technique *Journal of Immunological Methods* **270** 163-70
- [33] Sista R, Hua Z S, Thwar P, Sudarsan A, Srinivasan V, Eckhardt A, Pollack M and Pamula V 2008 Development of a digital microfluidic platform for point of care testing *Lab on a Chip* **8** 2091-104
- [34] Sorger P K 2008 Microfluidics closes in on point-of-care assays *Nature Biotechnology* **26** 1345-6
- [35] Tudos A J, Besselink G A J and Schasfoort R B M 2001 Trends in miniaturized total analysis systems for point-of-care testing in clinical chemistry *Lab on a Chip* **1** 83-95
- [36] Warsinke A 2009 Point-of-care testing of proteins *Analytical and Bioanalytical Chemistry* **393** 1393-405
- [37] Bange A, Halsall H B and Heineman W R 2005 Microfluidic immunosensor systems *Biosensors & Bioelectronics* **20** 2488-503
- [38] Hober S, Nord K and Linhult M 2007 Protein A chromatography for antibody purification *Journal of Chromatography B-Analytical Technologies in the Biomedical and Life Sciences* **848** 40-7
- [39] Ngo T T, Jogie-Brahim S and Narinesingh D 2007 Affinity chromatographic purification of antibodies *Analytical Letters* **40** 2799-820
- [40] Guerreiro A R, Chianella I, Piletska E, Whitcombe M J and Piletsky S A 2009 Selection of imprinted nanoparticles by affinity chromatography *Biosensors & Bioelectronics* **24** 2740-3
- [41] Snowden M E, King P H, Covington J A, Macpherson J V and Unwin P R 2010 Fabrication of versatile channel flow cells for quantitative electroanalysis using prototyping *Anal Chem* **82** 3124-31
- [42] Gervais T and Jensen K F 2006 Mass transport and surface reactions in microfluidic systems *Chemical Engineering Science* **61** 1102-21
- [43] Goddard J M and Erickson D 2009 Bioconjugation techniques for microfluidic biosensors *Analytical and Bioanalytical Chemistry* **394** 469-79
- [44] Jonkheijm P, Weinrich D, Schroder H, Niemeyer C M and Waldmann H 2008 Chemical Strategies for Generating Protein Biochips *Angewandte Chemie-International Edition* **47** 9618-47
- [45] Muck A and Svatos A 2007 Chemical modification of polymeric microchip devices *Talanta* **74** 333-41
- [46] Park E J, Carroll G T, Turro N J and Koberstein J T 2009 Shedding light on surfaces- using photons to transform and pattern material surfaces *Soft Matter* **5** 36-50
- [47] Rusmini F, Zhong Z Y and Feijen J 2007 Protein immobilization strategies for protein biochips *Biomacromolecules* **8** 1775-89
- [48] Tomizaki K Y, Usui K and Mihara H 2005 Protein-detecting microarrays: Current accomplishments and requirements *ChemBiochem* **6** 783-99
- [49] Thaler M, Buhl A, Welter H, Schreiegg A, Kehrel M, Alber B, Metzger J and Lippa P 2009 Biosensor analyses of serum autoantibodies: application to antiphospholipid syndrome and systemic lupus erythematosus *Analytical and Bioanalytical Chemistry* **393** 1417-29

- [50] Delamarche E, Juncker D and Schmid H 2005 Microfluidics for processing surfaces and miniaturizing biological assays *Advanced Materials* **17** 2911-33
- [51] Verpoorte E and De Rooij N F 2003 Microfluidics meets MEMS *Proceedings of the Ieee* **91** 930-53
- [52] Beebe D J, Mensing G A and Walker G M 2002 Physics and applications of microfluidics in biology *Annual Review of Biomedical Engineering* **4** 261-86
- [53] Swensen J S, Xiao Y, Ferguson B S, Lubin A A, Lai R Y, Heeger A J, Plaxco K W and Soh H T 2009 Continuous, Real-Time Monitoring of Cocaine in Undiluted Blood Serum via a Microfluidic, Electrochemical Aptamer-Based Sensor *Journal of the American Chemical Society* **131** 4262-6
- [54] Marle L and Greenway G M 2005 Microfluidic devices for environmental monitoring *Trends in Analytical Chemistry* **24** 795-802
- [55] Kang L F, Chung B G, Langer R and Khademhosseini A 2008 Microfluidics for drug discovery and development: From target selection to product lifecycle management *Drug Discovery Today* **13** 1-13
- [56] Metzker M L 2005 Emerging technologies in DNA sequencing *Genome Research* **15** 1767-76
- [57] Lion N, Rohner T C, Dayon L, Arnaud I L, Damoc E, Youhnovski N, Wu Z Y, Roussel C, Josserand J, Jensen H, Rossier J S, Przybylski M and Girault H H 2003 Microfluidic systems in proteomics *Electrophoresis* **24** 3533-62
- [58] Henares T G, Mizutani F and Hisamoto H 2008 Current development in microfluidic immunosensing chip *Analytica Chimica Acta* **611** 17-30
- [59] Herr A E, Hatch A V, Throckmorton D J, Tran H M, Brennan J S, Giannobile W V and Singh A K 2007 Microfluidic immunoassays as rapid saliva-based clinical diagnostics *Proceedings of the National Academy of Sciences of the United States of America* **104** 5268-73
- [60] Mattos C and Ringe D 2001 Proteins in organic solvents *Current Opinion in Structural Biology* **11** 761-4
- [61] Dill K A and Shortle D 1991 Denatured States of Proteins *Annual Review of Biochemistry* **60** 795-825
- [62] Davies M J 2003 Singlet oxygen-mediated damage to proteins and its consequences *Biochemical and Biophysical Research Communications* **305** 761-70
- [63] Dankbar D M and Gauglitz G 2006 A study on photolinkers used for biomolecule attachment to polymer surfaces *Analytical and Bioanalytical Chemistry* **386** 1967-74
- [64] Kusnezow W, Jacob A, Walijew A, Diehl F and Hoheisel J D 2003 Antibody microarrays: An evaluation of production parameters *Proteomics* **3** 254-64
- [65] Delves P J and Roitt I M 2000 The immune system - First of two parts *New England Journal of Medicine* **343** 37-49
- [66] Manz R A, Hauser A E, Hiepe F and Radbruch A 2005 Maintenance of serum antibody levels *Annual Review of Immunology* **23** 367-86

- [67] Peer D, Karp J M, Hong S, Farokhzad O C, Margalit R and Langer R 2007 Nanocarriers as an emerging platform for cancer therapy *Nature Nanotechnology* **2** 751-60
- [68] Rojas R and Apodaca G 2002 Immunoglobulin transport across polarized epithelial cells *Nature Reviews Molecular Cell Biology* **3** 944-55
- [69] Navarre W W and Schneewind O 1999 Surface proteins of gram-positive bacteria and mechanisms of their targeting to the cell wall envelope *Microbiology and Molecular Biology Reviews* **63** 174-229
- [70] Foster T J and Mcdevitt D 1994 Surface-Associated Proteins of Staphylococcus-Aureus - Their Possible Roles in Virulence *Fems Microbiology Letters* **118** 199-205
- [71] Schudel B R, Choi C J, Cunningham B T and Kenis P J A 2009 Microfluidic chip for combinatorial mixing and screening of assays *Lab on a Chip* **9** 1676-80
- [72] Movitz J 1976 Formation of Extracellular Protein-a by Staphylococcus-Aureus *European Journal of Biochemistry* **68** 291-9
- [73] Verwey W F 1940 A Type-Specific Antigenic Protein Derived from the Staphylococcus *The Journal of experimental medicine* **71** 635-44
- [74] Lofdahl S, Guss B, Uhlen M, Philipson L and Lindberg M 1983 Gene for Staphylococcal Protein-A *Proceedings of the National Academy of Sciences of the United States of America-Biological Sciences* **80** 697-701
- [75] Moks T, Abrahmsen L, Nilsson B, Hellman U, Sjoquist J and Uhlen M 1986 Staphylococcal Protein-a Consists of 5 Igg-Binding Domains *European Journal of Biochemistry* **156** 637-43
- [76] Guss B, Uhlen M, Nilsson B, Lindberg M, Sjoquist J and Sjodahl J 1984 Region-X, the Cell-Wall-Attachment Part of Staphylococcal Protein-A *European Journal of Biochemistry* **138** 413-20
- [77] Lindmark R, Thorentolling K and Sjoquist J 1983 Binding of Immunoglobulins to Protein-a and Immunoglobulin Levels in Mammalian Sera *Journal of Immunological Methods* **62** 1-13
- [78] Deisenhofer J 1981 Crystallographic Refinement and Atomic Models of a Human Fc Fragment and Its Complex with Fragment-B of Protein-a from Staphylococcus-Aureus at 2.9-a and 2.8-a Resolution *Biochemistry* **20** 2361-70
- [79] Gouda H, Torigoe H, Saito A, Sato M, Arata Y and Shimada I 1992 3-Dimensional Solution Structure of the B-Domain of Staphylococcal Protein-a - Comparisons of the Solution and Crystal-Structures *Biochemistry* **31** 9665-72
- [80] Gouda H, Shiraishi M, Takahashi H, Kato K, Torigoe H, Arata Y and Shimada I 1998 NMR study of the interaction between the B domain of staphylococcal protein A and the Fc portion of immunoglobulin G *Biochemistry* **37** 129-36
- [81] Ingnas M 1981 Comparison of Mechanisms of Interaction between Protein-a from Staphylococcus-Aureus and Human Monoclonal Igg, Iga and Igm in Relation to the Classical Fc-Gamma and the Alternative F(Ab')₂-Epsilon Protein-a Interactions *Scandinavian Journal of Immunology* **13** 343-52
- [82] Vidal M A and Conde F P 1985 Alternative Mechanism of Protein a-Immunoglobulin Interaction - the Vh-Associated Reactivity of a Monoclonal Human-Igm *Journal of Immunology* **135** 1232-8

- [83] Sasso E H, Silverman G J and Mannik M 1991 Human-Iga and Igg F(Ab')₂ That Bind to Staphylococcal Protein-a Belong to the Vhiii-Subgroup *Journal of Immunology* **147** 1877-83
- [84] Roben P W, Salem A N and Silverman G J 1995 V(H)₃ Family Antibodies Bind Domain-D of Staphylococcal Protein-A *Journal of Immunology* **154** 6437-45
- [85] Ibrahim S 1993 Immunoglobulin Binding Specificities of the Homology Regions (Domains) of Protein-A *Scandinavian Journal of Immunology* **38** 368-74
- [86] Jansson B, Uhlen M and Nygren P A 1998 All individual domains of staphylococcal protein A show Fab binding *Fems Immunology and Medical Microbiology* **20** 69-78
- [87] Graille M, Stura E A, Corper A L, Sutton B J, Taussig M J, Charbonnier J B and Silverman G J 2000 Crystal structure of a Staphylococcus aureus protein A domain complexed with the Fab fragment of a human IgM antibody: Structural basis for recognition of B-cell receptors and superantigen activity *Proceedings of the National Academy of Sciences of the United States of America* **97** 5399-404
- [88] Meininger D P, Rance M, Starovasnik M A, Fairbrother W J and Skelton N J 2000 Characterization of the binding interface between the E-domain of Staphylococcal protein A and an antibody Fv-fragment (vol 39, pg 26, 2000) *Biochemistry* **39** 26-36
- [89] Sjobring U, Bjorck L and Kastern W 1991 Streptococcal Protein-G - Gene Structure and Protein-Binding Properties *Journal of Biological Chemistry* **266** 399-405
- [90] Bjorck L and Kronvall G 1984 Purification and Some Properties of Streptococcal Protein-G, Protein-a Novel Igg-Binding Reagent *Journal of Immunology* **133** 969-74
- [91] Akerstrom B, Brodin T, Reis K and Bjorck L 1985 Protein-G - a Powerful Tool for Binding and Detection of Monoclonal and Polyclonal Antibodies *Journal of Immunology* **135** 2589-92
- [92] Guss B, Eliasson M, Olsson A, Uhlen M, Frej A K, Jornvall H, Flock J I and Lindberg M 1986 Structure of the Igg-Binding Regions of Streptococcal Protein-G *Embo Journal* **5** 1567-75
- [93] Achari A, Hale S P, Howard A J, Clore G M, Gronenborn A M, Hardman K D and Whitlow M 1992 1.67-Angstrom X-Ray Structure of the B2 Immunoglobulin-Binding Domain of Streptococcal Protein-G and Comparison to the Nmr Structure of the B1 Domain *Biochemistry* **31** 10449-57
- [94] Gallagher T, Alexander P, Bryan P and Gilliland G L 1994 2 Crystal-Structures of the B1 Immunoglobulin-Binding Domain of Streptococcal Protein-G and Comparison with Nmr *Biochemistry* **33** 4721-9
- [95] Sauereriksson A E, Kleywegt G J, Uhl M and Jones T A 1995 Crystal-Structure of the C2 Fragment of Streptococcal Protein-G in Complex with the Fc Domain of Human-Igg *Structure* **3** 265-78
- [96] Gronenborn A M, Filpula D R, Essig N Z, Achari A, Whitlow M, Wingfield P T and Clore G M 1991 A Novel, Highly Stable Fold of the Immunoglobulin Binding Domain of Streptococcal Protein-G *Science* **253** 657-61
- [97] Kato K, Lian L Y, Barsukov I L, Derrick J P, Kim H H, Tanaka R, Yoshino A, Shiraishi M, Shimada I, Arata Y and Roberts G C K 1995 Model for the Complex between Protein-G and an Antibody Fc Fragment in Solution *Structure* **3** 79-85
- [98] Murdoch D A 1998 Gram-positive anaerobic cocci *Clin Microbiol Rev* **11** 81-120

- [99] Kastern W, Holst E, Nielsen E, Sjobring U and Bjorck L 1990 Protein L, a bacterial immunoglobulin-binding protein and possible virulence determinant *Infect Immun* **58** 1217-22
- [100] Myhre E B and Erntell M 1985 A non-immune interaction between the light chain of human immunoglobulin and a surface component of a *Peptococcus magnus* strain *Mol Immunol* **22** 879-85
- [101] Bjorck L 1988 Protein L. A novel bacterial cell wall protein with affinity for Ig L chains *J Immunol* **140** 1194-7
- [102] Muzard J, Adi-Bessalem S, Juste M, Laraba-Djebari F, Aubrey N and Billiald P 2009 Grafting of protein L-binding activity onto recombinant antibody fragments *Analytical Biochemistry* **388** 331-8
- [103] Kastern W, Sjobring U and Bjorck L 1992 Structure of peptostreptococcal protein L and identification of a repeated immunoglobulin light chain-binding domain *The Journal of biological chemistry* **267** 12820-5
- [104] Murphy J P, Duggleby C J, Atkinson M A, Trowern A R, Atkinson T and Goward C R 1994 The functional units of a peptostreptococcal protein L *Mol Microbiol* **12** 911-20
- [105] Nilson B H, Solomon A, Bjorck L and Akerstrom B 1992 Protein L from *Peptostreptococcus magnus* binds to the kappa light chain variable domain *The Journal of biological chemistry* **267** 2234-9
- [106] De Chateau M, Nilson B H, Erntell M, Myhre E, Magnusson C G, Akerstrom B and Bjorck L 1993 On the interaction between protein L and immunoglobulins of various mammalian species *Scandinavian journal of immunology* **37** 399-405
- [107] Enokizono J, Wikstrom M, Sjobring U, Bjorck L, Forsen S, Arata Y, Kato K and Shimada I 1997 NMR analysis of the interaction between protein L and Ig light chains *J Mol Biol* **270** 8-13
- [108] Janeway C 2005 *Immunobiology : the immune system in health and disease* (New York ; London: Garland Science)
- [109] Akerstrom B and Bjorck L 1989 Protein L: an immunoglobulin light chain-binding bacterial protein. Characterization of binding and physicochemical properties *J Biol Chem* **264** 19740-6
- [110] Graille M, Stura E A, Housden N G, Beckingham J A, Bottomley S P, Beale D, Taussig M J, Sutton B J, Gore M G and Charbonnier J B 2001 Complex between *Peptostreptococcus magnus* protein L and a human antibody reveals structural convergence in the interaction modes of Fab binding proteins *Structure* **9** 679-87
- [111] Wikstrom M, Sjobring U, Kastern W, Bjorck L, Drakenberg T and Forsen S 1993 Proton nuclear magnetic resonance sequential assignments and secondary structure of an immunoglobulin light chain-binding domain of protein L *Biochemistry* **32** 3381-6
- [112] Graille M, Stura E A, Housden N G, Beckingham J A, Bottomley S P, Beale D, Taussig M J, Sutton B J, Gore M G and Charbonnier J B 2001 Complex between *Peptostreptococcus magnus* protein L and a human antibody reveals structural convergence in the interaction modes of Fab binding proteins *Structure (Camb)* **9** 679-87
- [113] Beckingham J A, Bottomley S P, Hinton R, Sutton B J and Gore M G 1999 Interactions between a single immunoglobulin-binding domain of protein L from *Peptostreptococcus magnus* and a human kappa light chain *The Biochemical journal* **340** (Pt 1) 193-9

- [114] Housden N G, Harrison S, Housden H R, Thomas K A, Beckingham J A, Roberts S E, Bottomley S P, Graille M, Stura E and Gore M G 2004 Observation and characterization of the interaction between a single immunoglobulin binding domain of protein L and two equivalents of human kappa light chains *The Journal of biological chemistry* **279** 9370-8
- [115] Peoples M C and Karnes H T 2008 Microfluidic immunoaffinity separations for bioanalysis *Journal of Chromatography B-Analytical Technologies in the Biomedical and Life Sciences* **866** 14-25
- [116] Bonanno L M and DeLouise L A 2007 Whole blood optical biosensor *Biosensors & Bioelectronics* **23** 444-8
- [117] Wang W U, Chen C, Lin K H, Fang Y and Lieber C M 2005 Label-free detection of small-molecule-protein interactions by using nanowire nanosensors *Proceedings of the National Academy of Sciences of the United States of America* **102** 3208-12
- [118] Bilitewski U, Genrich M, Kadow S and Mersal G 2003 Biochemical analysis with microfluidic systems *Analytical and Bioanalytical Chemistry* **377** 556-69
- [119] Kurosawa S, Park J W, Aizawa H, Wakida S I, Tao H and Ishihara K 2006 Quartz crystal microbalance immunosensors for environmental monitoring *Biosensors & Bioelectronics* **22** 473-81
- [120] Krishnamoorthy G, Carlen E T, Kohlheyer D, Schasfoort R B M and van den Berg A 2009 Integrated Electrokinetic Sample Focusing and Surface Plasmon Resonance Imaging System for Measuring Biomolecular Interactions *Analytical Chemistry* **81** 1957-63
- [121] Pu Q S, Oyesanya O, Thompson B, Liu S T and Alvarez J C 2007 On-chip micropatterning of plastic (cyclic olefin copolymer, COC) microfluidic channels for the fabrication of biomolecule microarrays using photografting methods *Langmuir* **23** 1577-83
- [122] Morita M, Ohmi T, Hasegawa E, Kawakami M and Ohwada M 1990 Growth of Native Oxide on a Silicon Surface *Journal of Applied Physics* **68** 1272-81
- [123] Buriak J M 2002 Organometallic chemistry on silicon and germanium surfaces *Chemical Reviews* **102** 1271-308
- [124] Leftwich T R and Teplyakov A V 2008 Chemical manipulation of multifunctional hydrocarbons on silicon surfaces *Surface Science Reports* **63** 1-71
- [125] Linford M R and Chidsey C E D 1993 Alkyl Monolayers Covalently Bonded to Silicon Surfaces *Journal of the American Chemical Society* **115** 12631-2
- [126] Cicero R L, Linford M R and Chidsey C E D 2000 Photoreactivity of unsaturated compounds with hydrogen-terminated silicon(111) *Langmuir* **16** 5688-95
- [127] Yam C M, Lopez-Romero J M, Gu J H and Cai C Z 2004 Protein-resistant monolayers prepared by hydrosilylation of alpha-oligo(ethylene glycol)-omega-alkenes on hydrogen-terminated silicon (111) surfaces *Chemical Communications* 2510-1
- [128] Yin H B, Brown T, Wilkinson J S, Eason R W and Melvin T 2004 Submicron patterning of DNA oligonucleotides on silicon *Nucleic Acids Research* **32** p.e118
- [129] Frutos A G, Smith L M and Corn R M 1998 Enzymatic ligation reactions of DNA "words" on surfaces for DNA computing *Journal of the American Chemical Society* **120** 10277-82
- [130] Boman F C, Musorrafiti M J, Gibbs J M, Stepp B R, Salazar A M, Nguyen S B T and Geiger F M 2005 DNA single strands tethered to fused quartz/water interfaces studied by second harmonic generation *Journal of the American Chemical Society* **127** 15368-9

- [131] Yin H B, Brown T, Greef R, Wilkinson J S and Melvin T 2004 Chemical modification and micropatterning of Si(100) with oligonucleotides *Microelectronic Engineering* **73-74** 830-6
- [132] Sieval A B, Demirel A L, Nissink J W M, Linford M R, van der Maas J H, de Jeu W H, Zuilhof H and Sudholter E J R 1998 Highly stable Si-C linked functionalized monolayers on the silicon (100) surface *Langmuir* **14** 1759-68
- [133] Strother T, Cai W, Zhao X S, Hamers R J and Smith L M 2000 Synthesis and characterization of DNA-modified silicon (111) surfaces *Journal of the American Chemical Society* **122** 1205-9
- [134] Linford M R, Fenter P, Eisenberger P M and Chidsey C E D 1995 Alkyl Monolayers on Silicon Prepared from 1-Alkenes and Hydrogen-Terminated Silicon *Journal of the American Chemical Society* **117** 3145-55
- [135] Bocking T, James M, Coster H G L, Chilcott T C and Barrow K D 2004 Structural characterization of organic multilayers on silicon(111) formed by immobilization of molecular films on functionalized Si-C linked monolayers *Langmuir* **20** 9227-35
- [136] Sieval A B, Linke R, Zuilhof H and Sudholter E J R 2000 High-quality alkyl monolayers on silicon surfaces *Advanced Materials* **12** 1457-60
- [137] Yang M, Teeuwen R L M, Giesbers M, Baggerman J, Arafat A, de Wolf F A, van Hest J C M and Zuilhof H 2008 One-step photochemical attachment of NHS-terminated monolayers onto silicon surfaces and subsequent functionalization *Langmuir* **24** 7931-8
- [138] Sieval A B, Linke R, Heij G, Meijer G, Zuilhof H and Sudholter E J R 2001 Amino-terminated organic monolayers on hydrogen-terminated silicon surfaces *Langmuir* **17** 7554-9
- [139] Boukherroub R, Wojtyk J T C, Wayner D D M and Lockwood D J 2002 Thermal hydrosilylation of undecylenic acid with porous silicon *Journal of the Electrochemical Society* **149** H59-H63
- [140] Hoheisel J D 2006 Microarray technology: beyond transcript profiling and genotype analysis *Nature Reviews Genetics* **7** 200-10
- [141] Cha T, Guo A, Jun Y, Pei D Q and Zhu X Y 2004 Immobilization of oriented protein molecules on poly(ethylene glycol)-coated Si(111) *Proteomics* **4** 1965-76
- [142] Liao W, Wei F, Qian M X and Zhao X S 2004 Characterization of protein immobilization on alkyl monolayer modified silicon(111) surface *Sensors and Actuators B-Chemical* **101** 361-7
- [143] Ozkumur E, Yalcin A, Cretich M, Lopez C A, Bergstein D A, Goldberg B B, Chiari M and Unlu M S 2009 Quantification of DNA and protein adsorption by optical phase shift *Biosensors & Bioelectronics* **25** 167-72
- [144] Teramura Y, Arima Y and Iwata H 2006 Surface plasmon resonance-based highly sensitive immunosensing for brain natriuretic peptide using nanobeads for signal amplification *Analytical Biochemistry* **357** 208-15
- [145] Vaisocherova H, Faca V M, Taylor A D, Hanash S and Jiang S Y 2009 Comparative study of SPR and ELISA methods based on analysis of CD166/ALCAM levels in cancer and control human sera *Biosensors & Bioelectronics* **24** 2143-8
- [146] Lee Y, Lee E K, Cho Y W, Matsui T, Kang I C, Kim T S and Han M H 2003 ProteoChip: A highly sensitive protein microarray prepared by a novel method of protein, immobilization for application of protein-protein interaction studies *Proteomics* **3** 2289-304

- [147] Onclin S, Ravoo B J and Reinhoudt D N 2005 Engineering silicon oxide surfaces using self-assembled monolayers *Angewandte Chemie-International Edition* **44** 6282-304
- [148] Wang Y L and Lieberman M 2003 Growth of ultrasmooth octadecyltrichlorosilane self-assembled monolayers on SiO₂ *Langmuir* **19** 1159-67
- [149] Silberzan P, Leger L, Ausserre D and Benattar J J 1991 Silanation of Silica Surfaces - a New Method of Constructing Pure or Mixed Monolayers *Langmuir* **7** 1647-51
- [150] Dinh D H, Vellutini L, Bennetau B, Dejous C, Rebiere D, Pascal E, Moynet D, Belin C, Desbat B, Labrugere C and Pillot J P 2009 Route to Smooth Silica-Based Surfaces Decorated with Novel Self-Assembled Monolayers (SAMs) Containing Glycidyl-Terminated Very Long Hydrocarbon Chains *Langmuir* **25** 5526-35
- [151] Wasserman S R, Tao Y T and Whitesides G M 1989 Structure and Reactivity of Alkylsiloxane Monolayers Formed by Reaction of Alkyltrichlorosilanes on Silicon Substrates *Langmuir* **5** 1074-87
- [152] Halliwell C M and Cass A E G 2001 A factorial analysis of silanization conditions for the immobilization of oligonucleotides on glass surfaces *Analytical Chemistry* **73** 2476-83
- [153] Marchenko A, Katsonis N, Fichou D, Aubert C and Malacria M 2002 Long-range self-assembly of a polyunsaturated linear organosilane at the n-Tetradecane/Au(111) interface studied by STM *Journal of the American Chemical Society* **124** 9998-9
- [154] Raj J, Herzog G, Manning M, Volcke C, MacCraith B D, Ballantyne S, Thompson M and Arrigan D W M 2009 Surface immobilisation of antibody on cyclic olefin copolymer for sandwich immunoassay *Biosensors & Bioelectronics* **24** 2654-8
- [155] Sui G D, Wang J Y, Lee C C, Lu W X, Lee S P, Leyton J V, Wu A M and Tseng H R 2006 Solution-phase surface modification in intact poly(dimethylsiloxane) microfluidic channels *Analytical Chemistry* **78** 5543-51
- [156] Fadeev A Y, Helmy R and Marcinko S 2002 Self-assembled monolayers of organosilicon hydrides supported on titanium, zirconium, and hafnium dioxides *Langmuir* **18** 7521-9
- [157] Becker H and Gartner C 2008 Polymer microfabrication technologies for microfluidic systems *Analytical and Bioanalytical Chemistry* **390** 89-111
- [158] Xia Y N and Whitesides G M 1998 Soft lithography *Annual Review of Materials Science* **28** 153-84
- [159] Makamba H, Kim J H, Lim K, Park N and Hahn J H 2003 Surface modification of poly(dimethylsiloxane) microchannels *Electrophoresis* **24** 3607-19
- [160] Diaz-Quijada G A and Wayner D D M 2004 A simple approach to micropatterning and surface modification of poly(dimethylsiloxane) *Langmuir* **20** 9607-11
- [161] Efimenko K, Wallace W E and Genzer J 2002 Surface modification of Sylgard-184 poly(dimethyl siloxane) networks by ultraviolet and ultraviolet/ozone treatment *Journal of Colloid and Interface Science* **254** 306-15
- [162] Wang B, Chen L, Abdulali-Kanji Z, Horton J H and Oleschuk R D 2003 Aging effects on oxidized and amine-modified poly(dimethylsiloxane) surfaces studied with chemical forced titrations: Effects on electroosmotic flow rate in microfluidic channels *Langmuir* **19** 9792-8
- [163] Hu S W, Ren X Q, Bachman M, Sims C E, Li G P and Allbritton N 2002 Surface modification of poly(dimethylsiloxane) microfluidic devices by ultraviolet polymer grafting *Analytical Chemistry* **74** 4117-23

- [164] Malmsten M 1998 Formation of adsorbed protein layers *Journal of Colloid and Interface Science* **207** 186-99
- [165] Perkins T W, Mak D S, Root T W and Lightfoot E N 1997 Protein retention in hydrophobic interaction chromatography: Modeling variation with buffer ionic strength and column hydrophobicity *Journal of Chromatography A* **766** 1-14
- [166] Nnebe I M, Tilton R D and Schneider J W 2004 Direct force measurement of the stability of poly(ethylene glycol)-polyethylenimine graft films *Journal of Colloid and Interface Science* **276** 306-16
- [167] van der Veen M, Norde W and Stuart M C 2004 Electrostatic interactions in protein adsorption probed by comparing lysozyme and succinylated lysozyme *Colloids and Surfaces B-Biointerfaces* **35** 33-40
- [168] Cole M A, Voelcker N H, Thissen H and Griesser H J 2009 Stimuli-responsive interfaces and systems for the control of protein-surface and cell-surface interactions *Biomaterials* **30** 1827-50
- [169] Mendes P M 2008 Stimuli-responsive surfaces for bio-applications *Chemical Society Reviews* **37** 2512-29
- [170] Chen H, Song W, Zhou F, Wu Z K, Huang H, Zhang J H, Lin Q and Yang B 2009 The effect of surface microtopography of poly(dimethylsiloxane) on protein adsorption, platelet and cell adhesion *Colloids and Surfaces B-Biointerfaces* **71** 275-81
- [171] Han M, Sethuraman A, Kane R S and Belfort G 2003 Nanometer-scale roughness having little effect on the amount or structure of adsorbed protein *Langmuir* **19** 9868-72
- [172] Rechendorff K, Hovgaard M B, Foss M, Zhdanov V P and Besenbacher F 2006 Enhancement of protein adsorption induced by surface roughness *Langmuir* **22** 10885-8
- [173] Denis F A, Hanarp P, Sutherland D S, Gold J, Mustin C, Rouxhet P G and Dufrene Y F 2002 Protein adsorption on model surfaces with controlled nanotopography and chemistry *Langmuir* **18** 819-28
- [174] Chapman R G, Ostuni E, Takayama S, Holmlin R E, Yan L and Whitesides G M 2000 Surveying for surfaces that resist the adsorption of proteins *Journal of the American Chemical Society* **122** 8303-4
- [175] Bodas D S and Khan-Malek C 2007 Fabrication of long-term hydrophilic surfaces of poly(dimethyl siloxane) using 2-hydroxy ethyl methacrylate *Sensors and Actuators B-Chemical* **120** 719-23
- [176] Xiao D Q, Van Le T and Wirth M J 2004 Surface modification of the channels of poly(dimethylsiloxane) microfluidic chips with polyacrylamide for fast electrophoretic separations of proteins *Analytical Chemistry* **76** 2055-61
- [177] Jonsson C, Aronsson M, Rundstrom G, Pettersson C, Mendel-Hartvig I, Bakker J, Martinsson E, Liedberg B, MacCraith B, Ohman O and Melin J 2008 Silane-dextran chemistry on lateral flow polymer chips for immunoassays *Lab on a Chip* **8** 1191-7
- [178] Hasuda H, Kwon O H, Kang I K and Ito Y 2005 Synthesis of photoreactive pullulan for surface modification *Biomaterials* **26** 2401-6
- [179] Vanderah D J, Vierling R J and Walkers M L 2009 Oligo(ethylene oxide) Self-Assembled Monolayers, with Self-Limiting Packing Densities for the Inhibition of Nonspecific Protein Adsorption *Langmuir* **25** 5026-30

- [180] Halperin A, Fragneto G, Schollier A and Sferrazza M 2007 Primary versus ternary adsorption of proteins onto PEG brushes *Langmuir* **23** 10603-17
- [181] Halperin A 1999 Polymer brushes that resist adsorption of model proteins: Design parameters *Langmuir* **15** 2525-33
- [182] Bosker W T E, Patzsch K, Stuart M A C and Norde W 2007 Sweet brushes and dirty proteins *Soft Matter* **3** 754-62
- [183] Martwiset S, Koh A E and Chen W 2006 Nonfouling characteristics of dextran-containing surfaces *Langmuir* **22** 8192-6
- [184] Ratner B D and Bryant S J 2004 Biomaterials: Where we have been and where we are going *Annual Review of Biomedical Engineering* **6** 41-75
- [185] Sharma S, Johnson R W and Desai T A 2004 XPS and AFM analysis of antifouling PEG interfaces for microfabricated silicon biosensors *Biosensors & Bioelectronics* **20** 227-39
- [186] Bi H Y, Meng S, Li Y, Guo K, Chen Y P, Kong J L, Yang P Y, Zhong W and Liu B H 2006 Deposition of PEG onto PMMA microchannel surface to minimize nonspecific adsorption *Lab on a Chip* **6** 769-75
- [187] Heyes C D, Groll J, Moller M and Nienhaus G U 2007 Synthesis, patterning and applications of star-shaped poly(ethylene glycol) biofunctionalized surfaces *Molecular Biosystems* **3** 419-30
- [188] Johnsson B, Lofas S and Lindquist G 1991 Immobilization of Proteins to a Carboxymethyl-dextran-Modified Gold Surface for Biospecific Interaction Analysis in Surface-Plasmon Resonance Sensors *Analytical Biochemistry* **198** 268-77
- [189] Xu F, Persson B, Lofas S and Knoll W 2006 Surface plasmon optical studies of carboxymethyl dextran brushes versus networks *Langmuir* **22** 3352-7
- [190] Lange K, Grimm S and Rapp M 2007 Chemical modification of parylene C coatings for SAW biosensors *Sensors and Actuators B-Chemical* **125** 441-6
- [191] Yu F, Persson B, Lofas S and Knoll W 2004 Surface plasmon fluorescence immunoassay of free prostate-specific antigen in human plasma at the femtomolar level *Analytical Chemistry* **76** 6765-70
- [192] Unsworth L D, Sheardown H and Brash J L 2008 Protein-resistant poly(ethylene oxide)-grafted surfaces: Chain density-dependent multiple mechanisms of action *Langmuir* **24** 1924-9
- [193] de Sainte Claire P 2009 Degradation of PEO in the Solid State: A Theoretical Kinetic Model *Macromolecules* **42** 3469-82
- [194] Han S, Kim C and Kwon D 1997 Thermal/oxidative degradation and stabilization of polyethylene glycol *Polymer* **38** 317-23
- [195] Hermanson G T 1996 *Bioconjugate Techniques* p. 785
- [196] Pan F, Zhao X B, Waigh T A, Lu J R and Miano F 2008 Interfacial adsorption and denaturation of human milk and recombinant rice lactoferrin *Biointerphases* **3** Fb36-Fb43

- [197] Bayiati P, Malainou A, Matrozos E, Tserepi A, Petrou P S, Kakabakos S E and Gogolides E 2009 High-density protein patterning through selective plasma-induced fluorocarbon deposition on Si substrates *Biosensors & Bioelectronics* **24** 2979-84
- [198] Kannan B, Castelino K, Chen F F and Majumdar A 2006 Lithographic techniques and surface chemistries for the fabrication of PEG-passivated protein microarrays *Biosensors & Bioelectronics* **21** 1960-7
- [199] Pei R J, Cui X Q, Yang X R and Wang E K 2000 Real-time immunoassay of antibody activity in serum by surface plasmon resonance biosensor *Talanta* **53** 481-8
- [200] Rao S V, Anderson K W and Bachas L G 1998 Oriented immobilization of proteins *Mikrochimica Acta* **128** 127-43
- [201] Parker M C, Patel N, Davies M C, Roberts C J, Tendler S J B and Williams P M 1996 A novel organic solvent-based coupling method for the preparation of covalently immobilized proteins on gold *Protein Science* **5** 2329-32
- [202] MacBeath G and Schreiber S L 2000 Printing proteins as microarrays for high-throughput function determination *Science* **289** 1760-3
- [203] Elender G, Kuhner M and Sackmann E 1996 Functionalisation of Si/SiO₂ and glass surfaces with ultrathin dextran films and deposition of lipid bilayers *Biosensors & Bioelectronics* **11** 565-77
- [204] Iwata R, Satoh R, Iwasaki Y and Akiyoshi K 2008 Covalent immobilization of antibody fragments on well-defined polymer brushes via site-directed method *Colloids and Surfaces B-Biointerfaces* **62** 288-98
- [205] Partis M D, Griffiths D G, Roberts G C and Beechey R B 1983 Cross-Linking of Protein by Omega-Maleimido Alkanoyl N-Hydroxysuccinimido Esters *Journal of Protein Chemistry* **2** 263-77
- [206] Lee Y W, Reedmundell J, Sukenik C N and Zull J E 1993 Electrophilic Siloxane-Based Self-Assembled Monolayers for Thiol-Mediated Anchoring of Peptides and Proteins *Langmuir* **9** 3009-14
- [207] Wetzel R, Halualani R, Stults J T and Quan C 1990 A General Method for Highly Selective Cross-Linking of Unprotected Polypeptides via pH-Controlled Modification of N-Terminal alpha-Amino Groups *Bioconjugate Chemistry* **1** 114-22
- [208] Brase S, Gil C, Knepper K and Zimmermann V 2005 Organic azides: An exploding diversity of a unique class of compounds *Angewandte Chemie-International Edition* **44** 5188-240
- [209] Budyka M F 2008 Photodissociation of Aromatic Azides *Uspekhi Khimii* **77** 757-72
- [210] Gritsan N P and Platz M S 2006 Kinetics, spectroscopy, and computational chemistry of aryl nitrenes *Chemical Reviews* **106** 3844-67
- [211] Bhat V T, James N R and Jayakrishnan A 2008 A photochemical method for immobilization of azidated dextran onto aminated poly(ethylene terephthalate) surfaces *Polymer International* **57** 124-32
- [212] Karrasch S, Dolder M, Schabert F, Ramsden J and Engel A 1993 Covalent Binding of Biological Samples to Solid Supports for Scanning Probe Microscopy in Buffer Solution *Biophysical Journal* **65** 2437-46

- [213] Leyva E, Sagredo R and Moctezuma E 2004 Photochemistry of fluorophenyl azides in aniline asymmetric fluoroazobenzenes by N-H singlet nitrene insertion *Journal of Fluorine Chemistry* **125** 741-7
- [214] Shao L, Samseth J and Hagg M B 2008 Crosslinking and stabilization of high fractional free volume polymers for gas separation *International Journal of Greenhouse Gas Control* **2** 492-501
- [215] Chang I N, Lin J N, Andrade J D and Herron J N 1995 Photoaffinity-Labeling of Antibodies for Applications in Homogeneous Fluoroimmunoassays *Analytical Chemistry* **67** 959-66
- [216] Monsathaporn S and Effenberger F 2004 Preparation and photoinduced patterning of azidoformate-terminated self-assembled monolayers *Langmuir* **20** 10375-8
- [217] Dillmore W S, Yousaf M N and Mrksich M 2004 A photochemical method for patterning the immobilization of ligands and cells to self-assembled monolayers *Langmuir* **20** 7223-31
- [218] Houseman B T and Mrksich M 2002 Carbohydrate arrays for the evaluation of protein binding and enzymatic modification *Chemistry & Biology* **9** 443-54
- [219] Kiick K L, Saxon E, Tirrell D A and Bertozzi C R 2002 Incorporation of azides into recombinant proteins for chemoselective modification by the Staudinger ligation *Proceedings of the National Academy of Sciences of the United States of America* **99** 19-24
- [220] Gitlin G, Bayer E A and Wilchek M 1987 Studies on the Biotin-Binding Site of Avidin - Lysine Residues Involved in the Active-Site *Biochemical Journal* **242** 923-6
- [221] Tan L P, Lue R Y, Chen G Y and Yao S Q 2004 Improving the intein-mediated, site-specific protein biotinylation strategies both in vitro and in vivo *Bioorg Med Chem Lett* **14** 6067-70
- [222] Yeo D S, Panicker R C, Tan L P and Yao S Q 2004 Strategies for immobilization of biomolecules in a microarray *Comb Chem High Throughput Screen* **7** 213-21
- [223] Zhu H, Bilgin M, Bangham R, Hall D, Casamayor A, Bertone P, Lan N, Jansen R, Bidlingmaier S, Houfek T, Mitchell T, Miller P, Dean R A, Gerstein M and Snyder M 2001 Global analysis of protein activities using proteome chips *Science* **293** 2101-5
- [224] Barbulovic-Nad I, Lucente M, Sun Y, Zhang M J, Wheeler A R and Bussmann M 2006 Bio-microarray fabrication techniques - A review *Critical Reviews in Biotechnology* **26** 237-59
- [225] Christman K L, Enriquez-Rios V D and Maynard H D 2006 Nanopatterning proteins and peptides *Soft Matter* **2** 928-39
- [226] Yap F L and Zhang Y 2007 Protein and cell micropatterning and its integration with micro/nanoparticles assembly *Biosensors & Bioelectronics* **22** 775-88
- [227] Bernard A, Renault J P, Michel B, Bosshard H R and Delamarche E 2000 Microcontact printing of proteins *Advanced Materials* **12** 1067-70
- [228] Betancourt T and Brannon-Peppas L 2006 Micro- and nanofabrication methods in nanotechnological medical and pharmaceutical devices *International Journal of Nanomedicine* **1** 483-95
- [229] Weibel D B, DiLuzio W R and Whitesides G M 2007 Microfabrication meets microbiology *Nature Reviews Microbiology* **5** 209-18

- [230] Ginger D S, Zhang H and Mirkin C A 2004 The evolution of dip-pen nanolithography *Angew Chem Int Ed Engl* **43** 30-45
- [231] Shi J, Guo S S, Sun M H, Baigl D and Chen Y 2007 Fabrication of integrated patterns using lithography and particles assembling techniques *Microelectronic Engineering* **84** 1471-5
- [232] Choi D G, Yu H K, Jang S G and Yang S M 2004 Colloidal lithographic nanopatterning via reactive ion etching *Journal of the American Chemical Society* **126** 7019-25
- [233] Salaita K, Wang Y H and Mirkin C A 2007 Applications of dip-pen nanolithography *Nature Nanotechnology* **2** 145-55
- [234] Li H W, Muir B V O, Fichet G and Huck W T S 2003 Nanocontact printing: A route to sub-50-nm-scale chemical and biological patterning *Langmuir* **19** 1963-5
- [235] Ruiz S A and Chen C S 2007 Microcontact printing: A tool to pattern *Soft Matter* **3** 168-77
- [236] Hong J M, Ozkeskin F M and Zou J 2008 A micromachined elastomeric tip array for contact printing with variable dot size and density *Journal of Micromechanics and Microengineering* **18** 015003 (6pp)
- [237] Rozkiewicz D I, Gierlich J, Burley G A, Gutschmiedl K, Carell T, Ravoo B J and Reinhoudt D N 2007 Transfer printing of DNA by "Click" chemistry *Chembiochem* **8** 1997-2002
- [238] Pla-Roca M, Fernandez J G, Mills C A, Martinez E and Samitier J 2007 Micro/nanopatterning of proteins via contact printing using high aspect ratio PMMA stamps and NanoImprint apparatus *Langmuir* **23** 8614-8
- [239] Coq N, van Bommel T, Hikmet R A, Stapert H R and Dittmer W U 2007 Self-supporting hydrogel stamps for the microcontact printing of proteins *Langmuir* **23** 5154-60
- [240] Pagliara S, Persano L, Camposeo A, Cingolani R and Pisignano D 2007 Registration accuracy in multilevel soft lithography *Nanotechnology* **18** 175302 (6pp)
- [241] Delamarche E, Bernard A, Schmid H, Bietsch A, Michel B and Biebuyck H 1998 Microfluidic networks for chemical patterning of substrate: Design and application to bioassays *Journal of the American Chemical Society* **120** 500-8
- [242] Delamarche E, Bernard A, Schmid H, Michel B and Biebuyck H 1997 Patterned delivery of immunoglobulins to surfaces using microfluidic networks *Science* **276** 779-81
- [243] Fosser K A and Nuzzo R G 2003 Fabrication of patterned multicomponent protein gradients and gradient arrays using microfluidic depletion *Analytical Chemistry* **75** 5775-82
- [244] Crozatier C, Le Berre M and Chen Y 2006 Multi-colour micro-contact printing based on microfluidic network inking *Microelectronic Engineering* **83** 910-3
- [245] Bernard A, Michel B and Delamarche E 2001 Micromosaic immunoassays *Analytical Chemistry* **73** 8-12
- [246] Ziegler J, Zimmermann M, Hunziker P and Delamarche E 2008 High-performance immunoassays based on through-stencil patterned antibodies and capillary systems *Analytical Chemistry* **80** 1763-9

- [247] He X, Dandy D S and Henry C S 2008 Microfluidic protein patterning on silicon nitride using solvent-extracted poly(dimethylsiloxane) channels *Sensors and Actuators B-Chemical* **129** 811-7
- [248] Yoshida Y, Yokokawa R, Suzuki H, Atsuta K, Fujita H and Takeuchi S 2006 Biomolecular linear motors confined to move upon micro-patterns on glass *Journal of Micromechanics and Microengineering* **16** 1550-4
- [249] Atsuta K, Noji H and Takeuchi S 2004 Micro patterning of active proteins with perforated PDMS sheets (PDMS sheets) *Lab on a Chip* **4** 333-6
- [250] Atsuta K, Suzuki H and Takeuchi S 2007 A parylene lift-off process with microfluidic channels for selective protein patterning *Journal of Micromechanics and Microengineering* **17** 496-500
- [251] Wright D, Rajalingam B, Selvarasah S, Dokmeci M R and Khademhosseini A 2007 Generation of static and dynamic patterned co-cultures using microfabricated parylene-C stencils *Lab on a Chip* **7** 1272-9
- [252] Pal R, Sung K E and Burns M A 2006 Microstencils for the patterning of nontraditional materials *Langmuir* **22** 5392-7
- [253] Wood M A 2007 Colloidal lithography and current fabrication techniques producing in-plane nanotopography for biological applications *Journal of the Royal Society Interface* **4** 1-17
- [254] Blattler T M, Binkert A, Zimmermann M, Textor M, Voros J and Reimhult E 2008 From particle self-assembly to functionalized sub-micron protein patterns *Nanotechnology* **19** 075301 (10pp.)
- [255] Ruiz A, Valsesia A, Bretagnol F, Colpo P and Rossi F 2007 Large-area protein nano-arrays patterned by soft lithography *Nanotechnology* **18** 505306 (6pp.)
- [256] Valsesia A, Meziani T, Bretagnol F, Colpo P, Ceccone G and Rossi F 2007 Plasma assisted production of chemical nano-patterns by nano-sphere lithography: application to bio-interfaces *Journal of Physics D-Applied Physics* **40** 2341-7
- [257] Kim K H, Sanedrin R G, Ho A M, Lee S W, Moldovan N, Mirkin C A and Espinosa H D 2008 Direct delivery and submicrometer Patterning of DNA by a nanofountain probe *Advanced Materials* **20** 330-34
- [258] Tinazli A, Piehler J, Beuttler M, Guckenberger R and Tampe R 2007 Native protein nanolithography that can write, read and erase *Nature Nanotechnology* **2** 220-5
- [259] Larsson A, Du C X and Liedberg B 2007 UV-patterned poly(ethylene glycol) matrix for microarray applications *Biomacromolecules* **8** 3511-8
- [260] Oshikane Y, Kataoka T, Okuda M, Hara S, Inoue H and Nakano M 2007 Observation of nanostructure by scanning near-field optical microscope with small sphere probe *Science and Technology of Advanced Materials* **8** 181-5
- [261] Leggett G J 2006 Scanning near-field photolithography-surface photochemistry with nanoscale spatial resolution *Chemical Society Reviews* **35** 1150-61
- [262] Reynolds N P, Janusz S, Escalante-Marun M, Timney J, Ducker R E, Olsen J D, Otto C, Subramaniam V, Leggett G J and Hunter C N 2007 Directed formation of micro- and nanoscale patterns of functional light-harvesting LH2 complexes *Journal of the American Chemical Society* **129** 14625-31

- [263] Sun S Q and Leggett G J 2007 Micrometer and nanometer scale photopatterning of self-assembled monolayers of phosphonic acids on aluminum oxide *Nano Letters* **7** 3753-8
- [264] Ducker R E, Janusz S, Sun S Q and Leggett G J 2007 One-step photochemical introduction of nanopatterned protein-binding functionalities to oligo(ethylene glycol)-terminated self-assembled monolayers *Journal of the American Chemical Society* **129** 14842-43
- [265] Reynolds N P, Tucker J D, Davison P A, Timney J A, Hunter C N and Leggett G J 2009 Site-Specific Immobilization and Micrometer and Nanometer Scale Photopatterning of Yellow Fluorescent Protein on Glass Surfaces *Journal of the American Chemical Society* **131** 896-7
- [266] Dong R, Krishnan S, Baird B A, Lindau M and Ober C K 2007 Patterned biofunctional poly(acrylic acid) brushes on silicon surfaces *Biomacromolecules* **8** 3082-92
- [267] Lee L M, Heimark R L, Guzman R, Baygents J C and Zohar Y 2006 Low melting point agarose as a protection layer in photolithographic patterning of aligned binary proteins *Lab on a Chip* **6** 1080-5
- [268] Jiang J, Li X M, Mak W C and Trau D 2008 Integrated direct DNA/protein patterning and microfabrication by focused ion beam milling *Advanced Materials* **20** 1636-43
- [269] Petrou P S, Chatzichristidi M, Douvas A A, Argitis P, Misiakos K and Kakabakos S E 2007 A biomolecule friendly photolithographic process for fabrication of protein microarrays on polymeric films coated on silicon chips *Biosensors & Bioelectronics* **22** 1994-2002
- [270] Kaplan J H, Forbush B and Hoffman J F 1978 Rapid Photolytic Release of Adenosine 5'-Triphosphate from a Protected Analog - Utilization by Na-K Pump of Human Red Blood-Cell Ghosts *Biochemistry* **17** 1929-35
- [271] del Campo A, Boos D, Spiess H W and Jonas U 2005 Surface modification with orthogonal photosensitive silanes for sequential chemical lithography and site-selective particle deposition *Angewandte Chemie-International Edition* **44** 4707-12
- [272] Alonso J M, Reichel A, Piehler J and del Campo A 2008 Photopatterned surfaces for site-specific and functional immobilization of proteins *Langmuir* **24** 448-57
- [273] Christman K L, Requa M V, Enriquez-Rios V D, Ward S C, Bradley K A, Turner K L and Maynard H D 2006 Submicron streptavidin patterns for protein assembly *Langmuir* **22** 7444-50
- [274] Kim D N, Lee W and Koh W G 2009 Preparation of protein microarrays on non-fouling and hydrated poly(ethylene glycol) hydrogel substrates using photochemical surface modification *Journal of Chemical Technology and Biotechnology* **84** 279-84
- [275] Leyva E and Sagredo R 1998 Photochemistry of fluorophenyl azides in diethylamine. Nitrene reaction versus ring expansion *Tetrahedron* **54** 7367-74
- [276] Choi H J, Kim N H, Chung B H and Seong G H 2005 Micropatterning of biomolecules on glass surfaces modified with various functional groups using photoactivatable biotin *Analytical Biochemistry* **347** 60-6
- [277] Rozsnyai L F, Benson D R, Fodor S P A and Schultz P G 1992 Photolithographic Immobilization of Biopolymers on Solid Supports *Angewandte Chemie-International Edition in English* **31** 759-61

- [278] Toh C R, Fraterman T A, Walker D A and Bailey R C 2009 Direct Biophotolithographic Method for Generating Substrates with Multiple Overlapping Biomolecular Patterns and Gradients *Langmuir* **25** 8894-8
- [279] Hong Y, Krsko P and Libera M 2004 Protein surface patterning using nanoscale PEG hydrogels *Langmuir* **20** 11123-6
- [280] Zhang G J, Tanii T, Funatsu T and Ohdomari I 2004 Patterning of DNA nanostructures on silicon surface by electron beam lithography of self-assembled monolayer *Chemical Communications* 786-7
- [281] Miyake T, Tanii T, Kato K, Zako T, Funatsu T and Ohdomari I 2007 Selectivity improvement in protein nanopatterning with a hydroxy-terminated self-assembled monolayer template *Nanotechnology* **18** 305304 (6pp)
- [282] Christman K L, Schopf E, Broyer R M, Li R C, Chen Y and Maynard H D 2009 Positioning Multiple Proteins at the Nanoscale with Electron Beam Cross-Linked Functional Polymers *Journal of the American Chemical Society* **131** 521-7
- [283] Colina M, Duocastella M, Fernandez-Pradas J M, Serra P and Morenza J L 2006 Laser-induced forward transfer of liquids: Study of the droplet ejection process *Journal of Applied Physics* **99** 084909
- [284] Barron J A, Young H D, Dlott D D, Darfler M M, Krizman D B and Ringeisen B R 2005 Printing of protein microarrays via a capillary-free fluid jetting mechanism *Proteomics* **5** 4138-44
- [285] Duocastella M, Colina M, Fernandez-Pradas J M, Serra P and Morenza J L 2007 Study of the laser-induced forward transfer of liquids for laser bioprinting *Applied Surface Science* **253** 7855-9
- [286] Saunders R E, Gough J E and Derby B 2008 Delivery of human fibroblast cells by piezoelectric drop-on-demand inkjet printing *Biomaterials* **29** 193-203
- [287] Singh B K and Hillier A C 2007 Multicolor surface plasmon resonance imaging of ink jet-printed protein microarrays *Analytical Chemistry* **79** 5124-32
- [288] Natarajan S, Katsamba P S, Miles A, Eckman J, Papalia G A, Rich R L, Gale B K and Myszkka D G 2008 Continuous-flow microfluidic printing of proteins for array-based applications including surface plasmon resonance imaging *Analytical Biochemistry* **373** 141-6
- [289] Xu J T, Lynch M, Nettikadan S, Mosher C, Vegasandra S and Henderson E 2006 Microfabricated "Biomolecular Ink Cartridges" - Surface patterning tools (SPTs) for the printing of multiplexed biomolecular arrays *Sensors and Actuators B-Chemical* **113** 1034-41
- [290] Fan R, Vermesh O, Srivastava A, Yen B K H, Qin L D, Ahmad H, Kwong G A, Liu C C, Gould J, Hood L and Heath J R 2008 Integrated barcode chips for rapid, multiplexed analysis of proteins in microliter quantities of blood *Nature Biotechnology* **26** 1373-8
- [291] Kim J, Surapaneni R and Gale B K 2009 Rapid prototyping of microfluidic systems using a PDMS/polymer tape composite *Lab on a Chip* **9** 1290-3
- [292] Osterberg E, Bergstrom K, Holmberg K, Riggs J A, Vanalstine J M, Schuman T P, Burns N L and Harris J M 1993 Comparison of Polysaccharide and Poly(Ethylene Glycol) Coatings for Reduction of Protein Adsorption on Polystyrene Surfaces *Colloids and Surfaces a-Physicochemical and Engineering Aspects* **77** 159-69

- [293] Emoto K, Van Alstine J M and Harris J M 1998 Stability of poly(ethylene glycol) graft coatings *Langmuir* **14** 2722-9
- [294] Holden M A, Jung S Y and Cremer P S 2004 Patterning enzymes inside microfluidic channels via photoattachment chemistry *Analytical Chemistry* **76** 1838-43
- [295] Bottomley S P, Beckingham J A, Murphy J P, Atkinson M, Atkinson T, Hinton R J and Gore M G 1995 Cloning, expression and purification of Ppl-1, a kappa-chain binding protein, based upon protein L from *Peptostreptococcus magnus* *Bioseparation* **5** 359-67
- [296] Jang L S and Keng H K 2008 Modified fabrication process of protein chips using a short-chain self-assembled monolayer *Biomedical Microdevices* **10** 203-11
- [297] Nijdam A J, Zianni M R, Herderick E E, Cheng M M C, Prospero J R, Robertson F A, Petricoin E F, Liotta L A and Ferrari M 2009 Application of Physicochemically Modified Silicon Substrates as Reverse-Phase Protein Microarrays *Journal of Proteome Research* **8** 1247-54
- [298] Nordberg R, Albridge R G, Bergmark T, Ericson U, Fahlman A, Hamrin K, Hedman J, Johansson G, Nordling C, Siegbahn K and Lindberg B 1967 Shifts in Electron Spectra of Nitrogen in Organic Molecules *Nature* **214** 481-2
- [299] Siegbahn K, Barnett E F, Fellnerf.H and Hammond D 1972 Electron Spectroscopy with Monochromatized X-Rays *Science* **176** 245-52
- [300] Gergely G 2002 Elastic backscattering of electrons: determination of physical parameters of electron transport processes by elastic peak electron spectroscopy *Progress in Surface Science* **71** 31-88
- [301] Beamson G B D ed 1992 *High Resolution XPS of Organic Polymers* (Chichester: Wiley)
- [302] Vermette P, Gengenbach T, Divisekera U, Kambouris P A, Griesser H J and Meagher L 2003 Immobilization and surface characterization of NeutrAvidin biotin-binding protein on different hydrogel interlayers *Journal of Colloid and Interface Science* **259** 13-26
- [303] Ghosh M, Alves C, Tong Z, Tettey K, Konstantopoulos K and Stebe K J 2008 Multifunctional surfaces with discrete functionalized regions for biological applications *Langmuir* **24** 8134-42
- [304] Cras J J, Rowe-Taitt C A, Nivens D A and Ligler F S 1999 Comparison of chemical cleaning methods of glass in preparation for silanization *Biosensors & Bioelectronics* **14** 683-8
- [305] DeRosa R L, Cardinale J A and Cooper A 2007 Functionalized glass substrate for microarray analysis *Thin Solid Films* **515** 4024-31
- [306] Yu L, Li C M, Liu Y S, Gao J, Wang W and Gan Y 2009 Flow-through functionalized PDMS microfluidic channels with dextran derivative for ELISAs *Lab on a Chip* **9** 1243-7
- [307] Zammattéo N, Jeanmart L, Hamels S, Courtois S, Louette P, Hevesi L and Remacle J 2000 Comparison between different strategies of covalent attachment of DNA to glass surfaces to build DNA microarrays *Analytical Biochemistry* **280** 143-50
- [308] Seuryneck-Servoss S L, White A M, Baird C L, Rodland K D and Zangar R C 2007 Evaluation of surface chemistries for antibody microarrays *Analytical Biochemistry* **371** 105-15

- [309] Gibbs-Davis J M, Hayes P L, Scheidt K A and Geiger F M 2007 Anion chelation by amido acid functionalized fused quartz/water interfaces studied by nonlinear optics *Journal of the American Chemical Society* **129** 7175-84
- [310] Faucheux N, Schweiss R, Lutzow K, Werner C and Groth T 2004 Self-assembled monolayers with different terminating groups as model substrates for cell adhesion studies *Biomaterials* **25** 2721-30
- [311] Xia B, Xiao S J, Guo D J, Wang J, Chao M, Liu H B, Pei J, Chen Y Q, Tang Y C and Liu J N 2006 Biofunctionalisation of porous silicon (PS) surfaces by using homobifunctional cross-linkers *Journal of Materials Chemistry* **16** 570-8
- [312] Jo S and Park K 2000 Surface modification using silanated poly(ethylene glycol)s *Biomaterials* **21** 605-16
- [313] Jang L S and Liu H J 2009 Fabrication of protein chips based on 3-aminopropyltriethoxysilane as a monolayer *Biomedical Microdevices* **11** 331-8
- [314] Lee L M, Heimark R L, Baygents J C and Zohar Y 2006 Self-aligned immobilization of proteins utilizing PEG patterns *Nanotechnology* **17** S29-S33
- [315] McGovern M E, Kallury K M R and Thompson M 1994 Role of Solvent on the Silanization of Glass with Octadecyltrichlorosilane *Langmuir* **10** 3607-14
- [316] Heinze T, Liebert T, Heublein B and Hornig S 2006 *Polysaccharides II*, (Berlin: Springer-Verlag Berlin) pp 199-291
- [317] Sandblad P, Arnell R, Samuelsson J and Fornstedt T 2009 Approach for Reliable Evaluation of Drug Proteins Interactions Using Surface Plasmon Resonance Technology *Analytical Chemistry* **81** 3551-9
- [318] Skottrup P D, Nicolaisen M and Justesen A F 2008 Towards on-site pathogen detection using antibody-based sensors *Biosensors & Bioelectronics* **24** 339-48
- [319] Lofas S, Johnsson B, Edstrom A, Hansson A, Lindquist G, Hillgren R M M and Stigh L 1995 Methods for Site Controlled Coupling to Carboxymethyl-dextran Surfaces in Surface-Plasmon Resonance Sensors *Biosensors & Bioelectronics* **10** 813-22
- [320] Reis A V, Fajardo A R, Schuquel I T A, Guilherme M R, Vidotti G J, Rubira A F and Muniz E C 2009 Reaction of Glycidyl Methacrylate at the Hydroxyl and Carboxylic Groups of Poly(vinyl alcohol) and Poly(acrylic acid): Is This Reaction Mechanism Still Unclear? *Journal of Organic Chemistry* **74** 3750-7
- [321] Markovic G, Mutschler T, Wollner K and Gauglitz G 2006 Application of surface acoustic waves for optimisation of biocompatibility of carboxymethylated dextran surfaces *Surface & Coatings Technology* **201** 1282-8
- [322] Masson J F, Barnhart M, Battaglia T M, Morris G E, Nieman R A, Young P J, Lorson C L and Booksh K S 2004 Monitoring of recombinant survival motor neuron protein using fiber-optic surface plasmon resonance *Analyst* **129** 855-9
- [323] Lofas S and Johnsson B 1990 A Novel Hydrogel Matrix on Gold Surfaces in Surface-Plasmon Resonance Sensors for Fast and Efficient Covalent Immobilization of Ligands *Journal of the Chemical Society-Chemical Communications* 1526-8
- [324] Pritchard D J, Morgan H and Cooper J M 1995 Patterning and Regeneration of Surfaces with Antibodies *Analytical Chemistry* **67** 3605-7

- [325] Kuhner M and Sackmann E 1996 Ultrathin hydrated dextran films grafted on glass: Preparation and characterization of structural, viscous, and elastic properties by quantitative microinterferometry *Langmuir* **12** 4866-76
- [326] Tedeschi L, Domenici C, Ahluwalia A, Baldini F and Mencaglia A 2003 Antibody immobilisation on fibre optic TIRF sensors *Biosensors & Bioelectronics* **19** 85-93
- [327] Liu C H, Lin Q X, Gao Y, Ye L, Xing Y Y and Xi T 2007 Characterization and antitumor activity of a polysaccharide from *Strongylocentrotus nudus* eggs *Carbohydrate Polymers* **67** 313-8
- [328] Purama R K, Goswami P, Khan A T and Goyal A 2009 Structural analysis and properties of dextran produced by *Leuconostoc mesenteroides* NRRL B-640 *Carbohydrate Polymers* **76** 30-5
- [329] Shingel K I 2002 Determination of structural peculiarities of dextran, pullulan and gamma-irradiated pullulan by Fourier-transform IR spectroscopy *Carbohydrate Research* **337** 1445-51
- [330] Zhu A P, Zhang M, Wu J and Shen J 2002 Covalent immobilization of chitosan/heparin complex with a photosensitive hetero-bifunctional crosslinking reagent on PLA surface *Biomaterials* **23** 4657-65
- [331] Zhu A P, Zhang M and Zhang Z 2004 Surface modification of ePTFE vascular grafts with O-carboxymethylchitosan *Polymer International* **53** 15-9
- [332] Ito Y, Hasuda H, Yamauchi T, Komatsu N and Ikebuchi K 2004 Immobilization of erythropoietin to culture erythropoietin-dependent human leukemia cell line *Biomaterials* **25** 2293-8
- [333] Collman J P, Devaraj N K, Eberspacher T P A and Chidsey C E D 2006 Mixed azide-terminated monolayers: A platform for modifying electrode surfaces *Langmuir* **22** 2457-64
- [334] Wong A K Y and Krull U J 2005 Surface characterization of 3-glycidoxypropyltrimethoxysilane films on silicon-based substrates *Analytical and Bioanalytical Chemistry* **383** 187-200
- [335] Cloarec J P, Deligianis N, Martin J R, Lawrence I, Souteyrand E, Polychronakos C and Lawrence M F 2002 Immobilization of homooligonucleotide probe layers onto Si/SiO₂ substrates: characterization by electrochemical impedance measurements and radiolabelling *Biosensors & Bioelectronics* **17** 405-12
- [336] Wollman E W, Kang D, Frisbie C D, Lorkovic I M and Wrighton M S 1994 Photosensitive Self-Assembled Monolayers on Gold - Photochemistry of Surface-Confined Aryl Azide and Cyclopentadienylmanganese Tricarbonyl *Journal of the American Chemical Society* **116** 4395-404
- [337] Burdzinski G T, Gustafson T L, Hackett J C, Hadad C M and Platz M S 2005 The direct detection of an aryl azide excited state: An ultrafast study of the photochemistry of para- and ortho-biphenyl azide *Journal of the American Chemical Society* **127** 13764-5
- [338] Ladd J, Boozer C, Yu Q M, Chen S F, Homola J and Jiang S 2004 DNA-directed protein immobilization on mixed self-assembled monolayers via a Streptavidin bridge *Langmuir* **20** 8090-5
- [339] Peluso P, Wilson D S, Do D, Tran H, Venkatasubbaiah M, Quincy D, Heidecker B, Poindexter K, Tolani N, Phelan M, Witte K, Jung L S, Wagner P and Nock S 2003 Optimizing antibody immobilization strategies for the construction of protein microarrays *Analytical Biochemistry* **312** 113-24

- [340] Zubtsov D A, Savvateeva E N, Rubina A Y, Pan'kov S V, Konovalova E V, Moiseeva O V, Chechetkin V R and Zasedatelev A S 2007 Comparison of surface and hydrogel-based protein microchips *Analytical Biochemistry* **368** 205-13
- [341] Svensson H G, Wedemeyer W J, Ekstrom J L, Callender D R, Kortemme T, Kim D E, Sjobring U and Baker D 2004 Contributions of amino acid side chains to the kinetics and thermodynamics of the bivalent binding of protein L to Ig K light chain *Biochemistry* **43** 2445-57
- [342] Friedrich D, Please C and Melvin T 2008 Optimisation of analyte transport in integrated microfluidic affinity sensors for the quantification of low levels of analyte *Sensors and Actuators B-Chemical* **131** 323-32
- [343] Beckingham J A, Housden N G, Muir N M, Bottomley S P and Gore M G 2001 Studies on a single immunoglobulin-binding domain of protein L from *Peptostreptococcus magnus*: the role of tyrosine-53 in the reaction with human IgG *Biochemical Journal* **353** 395-401
- [344] Housden N G, Harrison S, Roberts S E, Beckingham J A, Graille M, Stura E and Gore M G 2003 Immunoglobulin-binding domains: Protein L from *Peptostreptococcus magnus* *Biochemical Society Transactions* **31** 716-8